Rehan Naqvi

Analysis of Natural Gas-Fired Power Cycles with Chemical Looping Combustion for CO_2 Capture

Doctoral thesis
for the degree of doctor philosophiae

Trondheim, July 2006

Norwegian University of
Science and Technology
Faculty of Engineering Science and Technology
Department of Energy and Process Engineering

NTNU
Innovation and Creativity

NTNU
Norwegian University of Science and Technology

Doctoral thesis
for the degree of doctor philosophiae

Faculty of Engineering Science and Technology
Department of Energy and Process Engineering

ISBN ISBN 82-471-8039-1 (printed ver.)
ISBN ISBN 82-471-8038-3 (electronic ver.)
ISSN 1503-8181

Doctoral Theses at NTNU, 2006:138

Printed by Tapir Uttrykk

Preface

This thesis is submitted in partial fulfilment of the requirements for the degree “Doctor of Philosophy” at the Norwegian University of Science and Technology (NTNU).

The work was carried out at the Department of Energy and Process Engineering at the Faculty of Engineering Science and Technology, with Professor Olav Bolland as supervisor.

The research was funded by The Norwegian Research Council.

Acknowledgements

I owe my gratitude to Prof. Olav Bolland for being a kind and sincere, caring and cooperative, rational and practical, appreciative and friendly supervisor. I find myself exceptionally fortunate to have a supervisor like Olav. I thank him for always being there when I needed his guidance, inciting professional thoughts in me and making me utilise my capabilities in the best possible ways. Olav not only guided me through to achieve PhD but also inspired me as a professional and human being that will help me throughout my career.

As the saying goes, 'Money makes the mare go'; many thanks go to the Norwegian Research Council for funding this project.

I thank my former colleague Øyvind Brandvoll for moral and professional support in the beginning of my PhD, interesting project-related ideas and for being a witty office mate. I would also like to thank my former colleagues Maria Jonsson and Ragnhild Ulfsnes for assistance in modelling and simulation. My friends and colleagues Rahul Anantharaman and Christoph Stiller are thanked for technical discussions and sharing social activities with me.

I thank all the people who used to regularly turn up for the 10'O clock coffee break in my office. Their presence and appreciation for the coffee was refreshing. I also thank Michael Koch for being a friendly and cooperative office mate.

I ought to mention the beautiful city, beautiful people and cheerful places in Trondheim that made my stay here full of nice experiences. Trondheim is an ideal city to carry out research work and fun to live in. Tusen Takk Trondheim!

I acknowledge and recognise all the love and care I received from my dearest friends Michaël Becidan, Maria Holing, Per Sigurd, Gry Ulfeng and Marianne Skjæran. I thank them for being like a family to me, for cheering me up during the murky periods of PhD and for never turning me down when I needed them.

Last but not the least; I thank my family back home in Pakistan for backing me up during all my endeavours of life. Without their moral support it would have been very difficult to accomplish this task. I thank my family for always encouraging me, being interested in my career aspirations and helping me attain everything I wished for. Above all, I thank my parents who brought me into this world, raised me, educated me and loved me; my father (late) for always being my guardian angel and my mother for all her prayers. I dedicate this thesis to both of them.

Rehan Naqvi

Trondheim, July 2006

Summary

Chemical Looping Combustion (CLC) is a rather novel concept of hydrocarbon fuel energy conversion with inherent CO_2 separation. In CLC, a solid oxygen carrier transports oxygen from air to the fuel; hence air and fuel remain in separate environments and the combustion exhaust mainly consists of CO_2 and water vapour. CLC can be applied in a circulating fluidised bed reactor system. The main objectives of this work have been the sensitivity study of CLC-reactor system in combination with different oxygen carriers, design of different CLC-combined and CLC-steam cycle configurations, off-design behaviour analysis of CLC-combined cycles and investigation of the possibility to use conventional machinery in CLC-power plants. The main efforts have been directed towards cycle design including parameter optimisation and cycle performance including off-design operation of combined cycles. The comparison of CLC-cycles with conventional natural gas-fired combined cycles has been presented at all the stages of this work.

Energy and mass balance models for CLC based on the oxides of Fe, Cu and Ni in combination with inert supports of Al_2O_3 and $NiAl_2O_4$ have been developed. The results of study on different oxygen carriers in natural gas-based CLC indicate that NiO supported on $NiAl_2O_4$ is the most suitable oxygen carrier for achieving a conceivable reactor system. In order to be applicable in CLC-combined cycles, the reactor system and the oxygen carrier must stand a temperature of at least 1000°C and pressure of 10-26 bar.

Various configurations of natural gas-fired CLC-combined cycles with $NiO/NiAl_2O_4$ oxygen carrier have been studied in this work. The results show that different designs of CLC-combined cycles consisting of single reactor system operating up to 1200°C can achieve 50-52% net plant efficiency including CO_2 compression to 110 bar. Different CLC-combined cycle configurations employing multi-CLC-reactors and reheat air turbine have also been analysed. CLC-combined cycle with two reactor systems and single reheat air turbine can achieve above 51% net plant efficiency at 1000°C oxidation temperature. At the same oxidation temperature, a cycle with three CLC-reactors and double reheat air turbine achieves about 52% net plant efficiency. At 1200°C oxidation temperature, single reheat cycle achieves above 53% net plant efficiency, while double reheat results in marginal efficiency improvement. All the CLC-combined cycles proposed in this work exhibit higher net plant efficiencies with close to 100% CO_2 capture compared to a conventional combined cycle with 90% post-combustion CO_2 capture. The off-design analysis of CLC-combined cycles shows that a CLC-combined cycle exhibits better relative net plant efficiency at part-load, compared to conventional combined cycles with and without CO_2 capture. However, the CLC-combined cycles need more advanced control strategies, especially if a CO_2/H_2O-turbine is included. The cycles demand advanced air flow control strategies during the start-up, shut-down and at part-load below 60%.

Two designs of ultra-supercritical natural gas-fired CLC-steam cycles based on $NiO/NiAl_2O_4$ oxygen carrier have also been proposed and analysed in this work. The single reheat CLC-steam cycle can achieve net plant efficiency of about 43% while the double reheat CLC-steam cycle achieves 44% net plant efficiency with close to 100% CO_2 capture.

This work suggests that CLC has a high potential for efficient power generation with CO_2 capture. However, there are some technological barriers discussed in this thesis, which need to be overcome in order to successfully realise CLC application in power plants.

Table of Contents

Nomenclature

Latin Symbols

A	Area	m^2
C_D	Drag coefficient	-
C_P	Specific heat capacity	kJ/molK
CF	Coolant fraction	-
d_p	Particles diameter	μm
F	Configuration correction factor	-
g	Acceleration due to gravity	m/s^2
h	Specific enthalpy	kJ/mol
I	Internal recirculation ratio	-
$\overset{\circ}{h}_f$	Standard enthalpy of formation	kJ/mol
H	Height	m
$\dot{H}$	Enthalpy	kJ/s
LHV	Lower heating value	kJ/kg
LMTD	Log mean temperature difference	-
$\dot{m}$	Flow rate	kg/s
M	Hold-up	kg
MW	Molecular weight	kg/mol
$\dot{n}$	Molar flow rate	mol/s
q	Heat of reaction	kJ/mol
P	Pressure	bar
$\dot{Q}$	Heat	kW
R	Entrainment ratio	-
Re	Reynolds number	-
s	Entropy	kJ/kg-K
T	temperature	K or °C
TIT	turbine inlet temperature	-
u	Velocity	m/s
U	Overall heat transfer coefficient	W/m^2K
$\dot{W}$	Power	KW
w	Specific work	kJ/kg
x	Molar fraction	-
X	Degree of reaction	-

Greek Symbols

α	Lower limit of VGV	-
ε	Average solids fraction	-
ϕ	Degree of fuel conversion	-
η	Efficiency	-
ρ	Density	kg/m^3
μ	Dynamic viscosity	$N\text{-}s/m^2$
π	Pressure ratio	-
λ	Split ratio	-

Abbreviations

ASU	Air Separation Unit
CF	Coolant Fraction
CFB	Circulating Fluidised Bed
CLC	Chemical Looping Combustion
CLCCC	CLC-Combined Cycle
CLC-SC	CLC-Steam Cycle
CPR	Compressor Pressure Ratio
DFR	Direct Fuel Reduction
GT	Gas Turbine
HRSG	Heat Recovery Steam Generator
HP	High Pressure
IAPWS	The International Association for the Properties of Water and Steam
IFBR	Interconnected Fluidised Bed Reactors
IP	Intermediate Pressure
LP	Low Pressure
Me	Metal
MeO	Metal Oxide
OX	Oxidation Reactor
PR	Pressure Ratio
RED	Reduction Reactor
SMR	Steam Methane Reforming
SRK	Soave-Redlich-Kwong (Equation of State)
ST	Steam Turbine
TIT	Turbine Inlet Temperature
TET	Turbine Exit Temperature
VGV	Variable Guide Vanes

1 Introduction

This chapter starts with motivation for this thesis and proceeds with introduction to Chemical Looping Combustion. The competing technologies for CO_2 capture are then briefly discussed followed by the objectives and methodology of this work. The chapter also summarises the thesis organisation in the form of a comprehensive description of each of the chapters and appendices.

1.1 Motivation

The global warming effect is allegedly leading to frequent hurricanes, melting of ice on the North Pole endangering animal species, floods and droughts around the world. The increased global warming may be a consequence of the steadily increasing greenhouse gases emissions into the earth's atmosphere due to human activities. CO_2 is the most significant anthropogenic greenhouse gas and the manmade CO_2 accumulates in the earth's upper atmosphere and enhances the greenhouse effect. The extensive use of fossil fuels to meet the world's energy demand inevitably results in CO_2 emissions, the power sector having the largest share. Since the world reliance on fossil fuels in the future cannot be undermined, it is the need of time to take necessary measures to reduce the CO_2 emissions for saving the earth from the above-said threats. The world has responded to this problem and research and development are being carried out around the world to develop technologies for capturing CO_2 from power plants. Although CO_2 cannot be completely eradicated, it can be captured from power plants and stored away from the atmosphere at some appropriate location.

The governments around the world have to play an important role in the CO_2 emissions reduction perspective. The countries which have signed the Kyoto protocol have undertaken the binding obligation to cut their emissions of carbon dioxide and five other greenhouse gases, or engage in emissions trading if they maintain or increase emissions of these gases. But unfortunately, most of these countries are not moving forward with the appropriate pace on the course of greenhouse gases emissions reductions so that they could meet this objective. A recent report by the European Union Commission revealed that within the EU member states, only Great Britain and Sweden will be able to meet the Kyoto-objectives by 2012. This may be due to extensive nuclear power generation in these two countries, which although does not result in greenhouse gas emissions but is an issue of conflict regarding the radioactivity related hazards. Since this topic is beyond the scope of this thesis it is not discussed further.

As a matter of fact nearly all the developing and developed countries, to a large extent, are relying on fossil fuels to power their economies. The developed countries have been combusting fossil fuels to reach their current level of industrialisation and economy; and therefore it is their moral obligation to take initiatives and invest in all forms to develop technology for power generation with CO_2 capture. The developing countries, on the other hand, are going through the process of industrialisation and using all means to keep up with the increasing energy requirements. The result is that these countries are releasing large amounts of CO_2 into the atmosphere at present, even if the world's awareness of the CO_2-problem is rather high. While the developing countries might consider it their right to combust fossil fuels without taking energy-intensive and expensive measures for CO_2 emissions reduction; the developed countries should still be heading in the direction of a

future of power generation with CO_2 capture. Many developed countries have been involved in CO_2 emissions reductions related activities in one form or other.

Norway is a small yet important Scandinavian country supplying energy to continental Europe in the form of natural gas. Despite its small population and CO_2-free hydro power plants making up for over 99% of on-shore electricity production; Norway is keen on the issue of CO_2 emissions reduction in a long term perspective. Therefore, Norway has actively been involved in the research and development related to CO_2 capture and storage. Regarding the CO_2 capture from power plants, Norway's efforts are recognisable by national research projects and its participation in international projects. Norwegian universities, research organisations and industry are key players in the international forums and consortia of CO_2-related projects. This work has been sponsored by the Norwegian Research Council as part of the CLIMIT Program. The main aim of this work is to provide an insight into the possibilities of using Chemical Looping Combustion for power generation with CO_2 capture in a long-term perspective.

1.2 Chemical Looping Combustion

Chemical Looping Combustion (CLC) is an ingenious concept of CO_2 capture from combustion of fossil fuels in power plants. CLC is closely related to oxy-fuel combustion as the chemically bound oxygen reacts in a stoichiometric ratio with the fuel. In CLC, the overall combustion takes place in two steps, while air and fuel are kept away from each other in two separate reactors. The necessary oxygen is supplied to the fuel by a metal oxide that is referred to as the oxygen carrier. In a reduction reactor, the fuel reacts with the metal oxide, reduces it by taking up the needed amount of oxygen from it and in turn giving away its chemical energy. The reduced metal oxide circulates to an oxidation reactor where it reacts with the air and gives away the fuel chemical energy to the air. In return, it takes up the needed oxygen and gets oxidised back to metal oxide. The metal oxide keeps circulating between the two reactors in a loop while taking part in the successive chemical reactions. Hence the process is named as 'Chemical Looping Combustion'. Both the reactors' product streams are available at high temperature and can be used in energy conversion plants. The oxidation reactor product is only the oxygen-depleted air while the reduction reactor exhaust consists of CO_2 and steam. Steam can be separated by condensing the exhaust stream and pure CO_2 can be compressed. In this way energy penalty for CO_2 capture is very low as compared to other energy intensive CO_2 capture techniques. Therefore, if CLC is applied in power plants, CO_2-free electricity can be generated without substantial energy penalty.

1.3 Competing Technologies for CO_2 Capture

At present, mainly three technologies for CO_2 capture from power plants are under consideration; pre-combustion decarbonisation, oxy-fuel combustion and post-combustion CO_2 capture. All three options are energy-intensive and result in considerable plant efficiency drop. Pre-combustion decarbonisation needs energy to remove carbon from the fuel, oxy-fuel process demands for energy to separate oxygen from air and post-combustion capture demands for energy to strip off CO_2 which is diluted with other gases in the power plant exhaust. A detailed description of these technologies is given in section 2.5. The use of the above-said energy-intensive technologies will result in efficiency reduction thereby leading to increased energy prices. Chemical Looping Combustion on the other hand, separates CO_2 inherently by using an oxygen carrier and can prove to be a technology for highly efficient power generation with CO_2 capture.

1.4 Objectives and Methodology of this Work

The novel concept of using a metal oxide for combustion, leading to a compact system with the feature of no need for oxygen separation plant, along with high system efficiency, almost no formation of NOx, and inherently facilitated separation of CO_2 without considerable energy expenditure make CLC worth of being analysed. This work lays emphasis on implementation of Chemical Looping Combustion in power cycles. In a broader view, the main objectives of this work are sensitivity study of CLC-reactor system in combination with different oxygen carriers, design of different CLC-combined and CLC-steam cycle configurations, off-design behaviour analysis of CLC-combined cycles and investigation of the possibility to use conventional machinery in CLC-power plants. A reactor system design involving reactors' geometry and hydrodynamic behaviour of solids inside the reactors has also been part of this work to meet the objectives. The working methodology has been to carry out a thermodynamic analysis of CLC systems with emphasis to establish the basic understanding of split reactor system as well as establishing knowledge of thermo-physical properties of the various oxygen carriers. Further, the main efforts have been directed towards cycle design including parameter optimisation and cycle performance including off-design operation of combined cycles. The comparison of the CLC-cycles with conventional cycles has been presented at all the stages of this work.

1.5 Thesis Organisation

This thesis comprises of 9 chapters and 3 appendices. In the following, a brief description of each element of this thesis will be given.

Following this introductory chapter, chapter 2 discusses the issue of greenhouse effect and man-made greenhouse gases. In the chapter, CO_2 is identified as the major greenhouse gas and its increase in atmosphere due to anthropological activities is discussed. Energy related CO_2 emissions and the technologies for CO_2 capture from power plants are briefly reviewed.

Chapter 3 presents the basic principle of Chemical Looping Combustion (CLC) and presents the chemistry involved in CLC. The chapter then presents a concise review of the CLC-research world wide covering all the aspects of CLC.

Chapter 4 presents the modelling and simulation basis and presents the CLC-models in detail. The other conventional unit operations models are also presented. The chapter also presents definitions of efficiency and specific work which are kept consistent throughout this thesis.

Chapter 5 presents the sensitivity study on CLC-reactor system. The study is categorised into three parts; oxygen carriers, adiabatic reactors and non-adiabatic reactors.

Chapter 6 presents implementation of CLC in combined cycles. Various combined cycle configurations are presented and sensitivity studies results presented. Each cycle is described in detail and the results in terms of efficiency and specific work are compared for all the cycles and to the reference conventional natural gas-fired combined cycle with post-combustion CO_2 capture. The chapter also presents the sensitivity study of the CLC-reactors. The environmental behaviour of CLC-oxygen carrier used for this work is also discussed to a slight extent.

Chapter 7 discusses the issue of the off-design of CLC. Two CLC-combined cycle configurations are chosen for part-load evaluation. The results are compared to a conventional combined cycle with and without CO_2 capture operating at part-load.

Chapter 8 presents CLC application in conventional steam cycles. The chapter discusses single reheat and double reheat steam cycle and the results for each cycle and its major components are presented for the optimum efficiency condition.

Chapter 9 concludes this work and gives recommendations for the future work.

Appendix A contains the set of computational assumptions used throughout this work.

Appendix B contains the design-point stream data for all the CLC-combined cycles and steam cycles presented in chapter 6 and chapter 8, respectively.

Appendix C contains the papers published during thesis work.

1.5.1 Papers Published During Thesis Work

Paper I

> Naqvi R., Bolland O., Brandvoll Ø., Helle K., "*Chemical Looping Combustion-Analysis of Natural Gas Fired Power Cycles with Inherent CO_2 Capture"*, GT2004-53359, Proceedings of ASME Turbo Expo 2004, June 14-17, 2004, Vienna, Austria

The paper presents CLC implementation in natural gas fired combined cycle and steam cycle. The paper includes energy and mass balances for the adiabatic and non-adiabatic CLC-reactor systems, implementation of a cooling model in the air turbine, incomplete reaction of fuel, and oxygen carrier flowrates dependency on the solids conversion in the two CLC-reactors. The paper concludes that the CLC-combined cycle can achieve about 50% net plant efficiency at the oxidation temperature of 1200 °C while the CLC-steam cycle can achieve about 40% net plant efficiency at the oxidation temperature of 850°C.

The author of this thesis contributed to this paper by co-advising modelling of the CLC-reactor systems. The air turbine cooling model implementation, cycles design, simulations, interpretation, documentation and presentation of the paper were solely done by the author.

Paper II

> Naqvi R., Bolland O., Wolf J., "Part-load *Evaluation of a Chemical Looping Combustion Combined Cycle with CO_2 Capture*, Accepted for publication in 'Energy-The International Journal'

The paper is the very first publication of a CLC-cycle in off-design mode. The paper presents part-load behaviour of a natural gas-fired CLC-combined cycle including an air turbine, a CO_2-turbine and a steam cycle. The paper presents a mathematical model involving the CLC-reactors geometry and the hydrodynamic behaviour of the solids. The paper also discusses the off-design models used in the work. The thermodynamic analysis of the combined cycle is presented in order to establish a design point and the component data at the selected design point is also given. The control strategy presented in the paper is the

use of variable guide vane angles at the air compressor inlet in order to control the air flow rate. In this way the pressure at the two CLC-reactors exit can be balanced, which is inevitable in order to avoid any gas leakage between the two reactors. The paper also compares the CLC-combined cycle part-load behaviour with two conventional combined cycles. The paper concludes that the CLC-combined cycle exhibits better relative net plant efficiency at part-load. The paper also concludes that the proposed cycle needs advanced control strategies at part-load below 60% as well as start-up and shut-down.

The author worked in collaboration with Jens Wolf (KTH and Vattenfall, Stockholm-Sweden) to develop the mathematical model involving CLC-reactors geometry. Furthermore, the author together with Prof. Olav Bolland derived and presented the correlations defining solids internal recirculation ratio and solids entrainment ratio in a pneumatic transport reactor, serving as the oxidation reactor in CLC. The modelling, simulation and writing of this paper were solely done by the author.

Paper III

> Naqvi, R., Bolland, O., *"Multi-stage Chemical Looping Combustion for Combined Cycles with CO_2 Capture"*, Presented at GHGT8 2006, Trondheim-Norway, invited for publication in 'International Journal of Greenhouse Gas Control'

The paper presents implementation of multi-CLC-reactors in natural gas-fired combined cycles including reheat air turbine. The paper presents single reheat CLC-combined cycle based on two CLC-reactors and double reheat CLC-combined cycle including three CLC-reactors. Furthermore, the paper also compares the cycles with a conventional natural gas-fired combined cycle with and without post-combustion CO_2 capture. The paper concludes that reheat CLC-combined cycles can achieve comparable efficiencies at lower oxidation temperatures compared to a non-reheat air turbine CLC-combined cycle. The paper also concludes that the CLC-combined cycles have substantially higher efficiency with close to 100% CO_2 capture, compared to a conventional natural gas-fired combined cycle with 90% post-combustion CO_2 capture.

The author performed modelling and simulation, writing and presenting of this paper.

2 CO_2 Mitigation and Capture

This chapter addresses the issue of anthropological addition to the greenhouse effect and the consequences of increased CO_2 concentration in the atmosphere. The chapter also briefly discusses global economic trends and their relevance to increase in CO_2 emissions. The global response towards the CO_2 problem has been pointed out briefly. Furthermore, the chapter presents a concise review of major CO_2 capture technologies.

2.1 The Greenhouse Effect

The greenhouse effect is warming up of the earth because of the presence of greenhouse gases in the atmosphere. The major greenhouse gases are water vapour, carbon dioxide, nitrous oxide, and methane. Most of the solar radiation that reaches the earth is absorbed by its surface and re-emitted at different wavelengths. The greenhouse gases in the atmosphere are opaque to long wavelength radiation. That is why some of the radiation emitted by the earth passes back into the space and some is absorbed by the greenhouse gases and re-emitted in all directions. The effect of this is to warm the earth's surface and the lower atmosphere. Figure 2.1 presents the natural greenhouse effect.

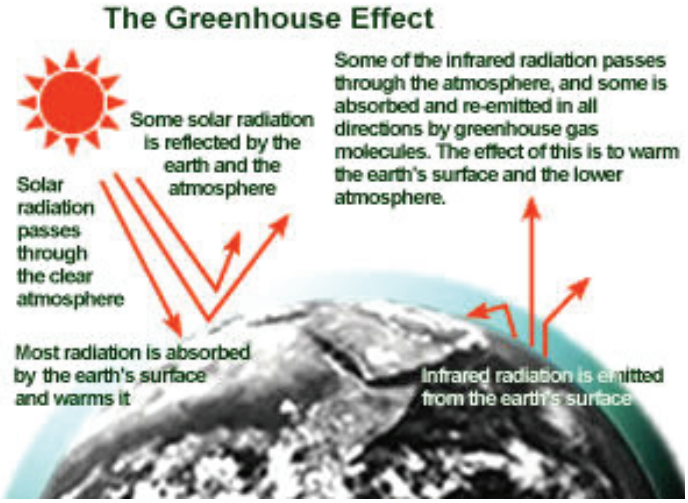

Figure 2.1 The greenhouse effect
[Source: US Environmental Protection Agency: http://yosemite.epa.gov]

Quite mistakenly, the greenhouse effect to most people is an undesirable phenomenon that occurs to our world. Atmospheric scientists first used the term 'greenhouse effect' in the beginning of 19th century. In those days, the term was used to express the naturally occurring function of trace gases in the atmosphere and did not have any negative implications. As a matter of fact, the natural greenhouse effect is essential for the earth. Without this effect, the earth would not be warm enough for humans and animal species to live, plants to grow and flora and fauna to flourish. The term greenhouse effect was attached with concern over climate change in the mid of 20th century. In recent decades, the term greenhouse effect has been used in somewhat negative terms. The negative concerns are related to the possible impacts of an enhanced greenhouse effect, which will make the earth warmer than usual thereby disturbing the natural course of meteorological phenomena and creating troubles for the living beings. This additional and undesirable man-made effect,

which is the major cause of global warming, is usually referred to as the greenhouse effect in general terms. The greenhouse gases exist naturally in the atmosphere in certain concentrations. The human activities on earth do however result in additional formation of greenhouse gases that are released into the atmosphere thereby adding to the overall concentrations of the gases. Table 2-1 presents comparison of the concentrations of the most significant greenhouse gases from the year 1750 until the present (2005).

Table 2-1 Most important greenhouse gases
[Source: Carbon Dioxide Information Analysis Centre: http://cdiac.esd.ornl.gov]

Greenhouse gases	Concentration (1750 AD)	Concentration (Present)
Carbon dioxide	280 ppm	373 ppm
Methane	730 ppb	1843 ppb
Nitrous Oxide	270 ppb	318 ppb
Chlorofluorocarbons (CFC)	0	~1000 ppt

The numerical values of the concentration of individual species vary depending on source and location of measurement. Three greenhouse gases account for the widely held human induced global warming effects; carbon dioxide (CO_2), methane (CH4), and nitrous oxide (N_2O). CO_2 is the most dominant man-made greenhouse gas and according to the figures provided by OECD it accounts for 75% of global man-made emissions followed by methane and nitrous oxide. About 90% of the greenhouse effect is due to the accumulative contribution by H_2O and CO_2. The remaining 10% comes from ozone, methane and nitrous oxide altogether. The present value for total concentration of chlorofluorocarbons is the sum of several compounds with a similar potential for global warming. With these figures, it becomes quite evident that CO_2 is the most prevalent man-made greenhouse gas.

2.2 CO_2 Emissions and Climate Change

The abundant presence of carbon dioxide in the atmosphere is justifiable in two terms; natural concentration of CO_2 in atmosphere and the extensively increasing human activities on earth, the latter being held responsible for the increase in total CO_2 concentration. The concentration of CO_2 in the atmosphere has significantly increased in the last decades. Figure 2.2 presents the year by year comparison of CO_2 concentrations in the atmosphere. It can be seen in Figure 2.2 that the level of CO_2 in the atmosphere has increased by about 60 ppm during the period 1958 and 2002. The increased concentrations of CO_2 thereby add up to the overall negative impact of the greenhouse effect and the average temperature at the earth's surface increases. It is believed that the mean global temperature has considerably increased over the past 100 years due to the growing manmade greenhouse effect. In order to have a further understanding of the cause of such a rise in average global temperature due to the rapidly increasing CO_2 emissions; it is important to discuss the world's economic trends in the recent decades that led to increased human activities producing CO_2 emissions.

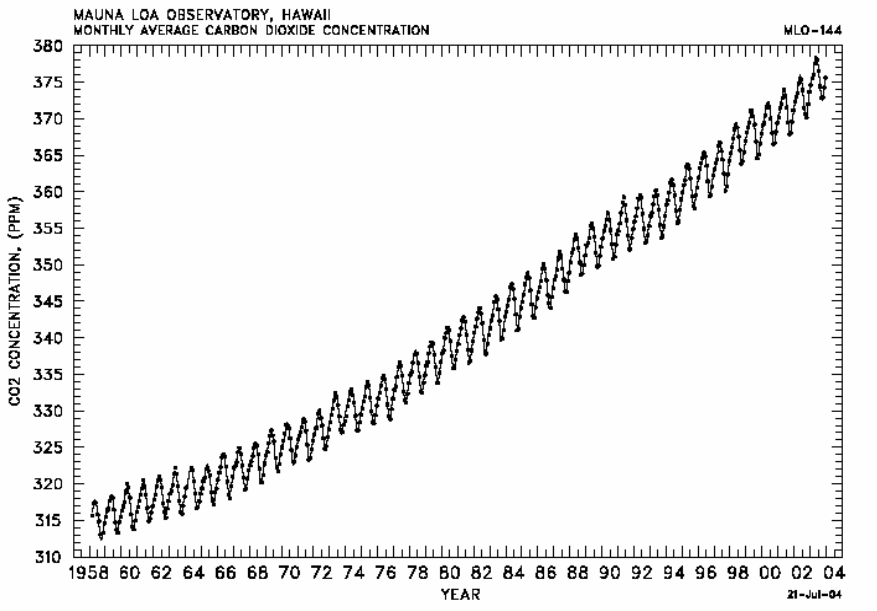

Figure 2.2 CO_2-concentration measured at Mauna Loa
[Source: CICERO Policy note 1998:3]

2.3 World's Economic Trends and CO_2 Emissions

CO_2 emissions are directly related to the economic trends of the world. The world's economy to a large extent relies on fossil fuels and their combustion results in large amounts of CO_2 emitted into the atmosphere each year. The energy related CO_2 emissions include power plants, transport and residential and commercial sectors. The figures provided by OECD show that energy production accounted for 34%, industry 17%, transport 27% and residential and commercial sectors accounted for 13% of world total CO_2 emissions; with other sectors contributing 9% in the year 1998. The major focus of this work has been the CO_2 emissions from power plants which are included in the so called 'Stationary Sources' of CO_2 emissions, together with process plants and other energy-intensive industry. It is of interest here to have an overview of the share of CO_2 emissions coming from different industrial sectors. Such a comparison is presented in Figure 2.3.

Figure 2.3 indicates that power plants dominate the data by having the highest share of 54 % of all identified stationary CO_2 emissions sources. This is quite justifiable considering the role of electricity that drives the industrial and commercial sectors; and even various means of transportation in many countries, for instance city trams, electricity driven buses, subways and domestic railways. The world electricity demand has increased over 50% since 1980. The increased demand has been most remarkable in developing countries.

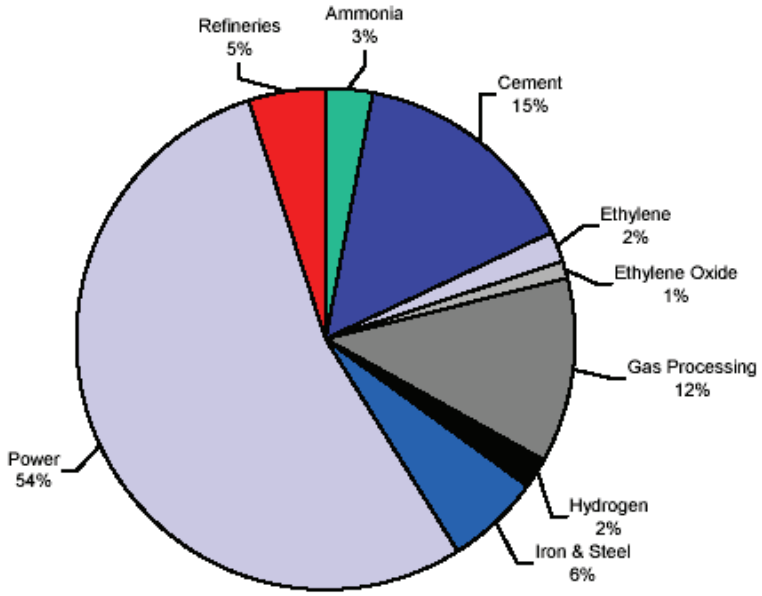

Figure 2.3 Distribution of CO_2 emission sources by industry sector in 2000 [Gale, 2002]

Figure 2.4 presents the electricity demand for different world economies from the year 1970 until present and projects it over to 2030.

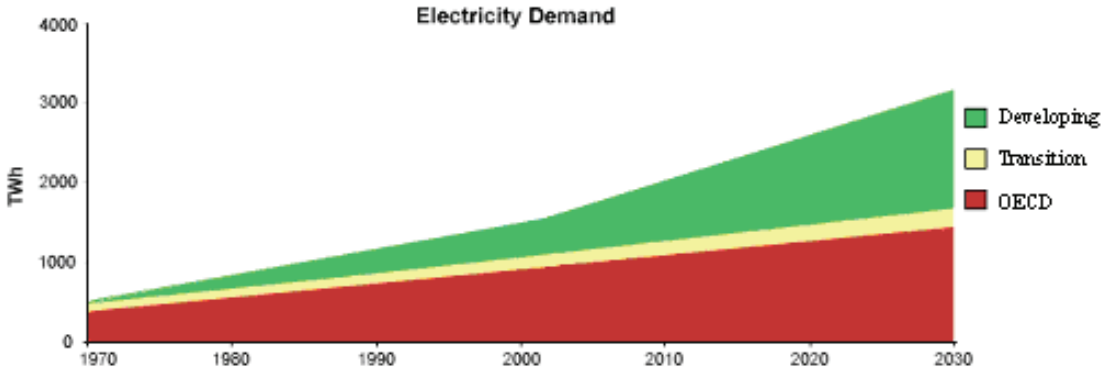

Figure 2.4 The world's electricity demand trends [OECD/IEA, 2005a]

In Figure 2.4 it can be seen that the most noteworthy electricity demand is in the developing countries after the start of the new millennium. OECD countries show a constantly increasing demand in order to keep up with their living standards while the transition economies have a small but consistent electricity demand. Nevertheless, the overall world electricity demand tends to increase sharply in the 21st century. For a detailed description of the world future energy trends, share of different energy sources in power generation and CO_2 emissions data, readers are referred to IPCC [www.ipcc.ch] and OECD/IEA [2005b].

Since the power generation sector has a major share in the global CO_2 emissions, measures should be taken in order to mitigate CO_2 in power plants. Since CO_2 can not be eradicated completely, its emissions can be reduced to a somewhat 'acceptable' level. The remedies to this problem largely depend on the world's awareness to this problem and willingness to take action in this regard.

2.4 Global Response to the CO_2 Problem

The indication of global mean temperature rise and the rational relation between CO_2 concentration and climate change calls the need to control worldwide CO_2 emissions, in particular those associated with power plants.

There can be four fundamental approaches to accomplish this goal, given in the following:

- Reduction in fossil fuels consumption through ; increased efficiency of power plants, reducing primary energy demand and increased usage of non-fossil energy sources like hydro power, wind energy, solar energy, nuclear power and biomass

- Using fossil fuels with lower Carbon/Hydrogen ratio; for instance replacing coal and oil with natural gas

- Nuclear power generation

- Capturing CO_2 from fossil fuels based power plants and storing it in aquifers or already used up empty gas reservoirs, using it for enhanced oil recovery or simply store it away from the atmosphere in some appropriate location

Due to the world's ever increasing energy demand, the lack of viable alternate clean energy sources, unavailability of clean energy conversion techniques and the relatively high abundance of fossil fuels on earth; reduced energy consumption is not a pragmatic approach to reducing carbon emissions. Substituting natural gas with coal or oil is somewhat a realistic and pragmatic approach, however abundant reserves of coal suggest that there must also be other means to control CO_2 emissions. Although nuclear power plants are CO_2-free, the radioactivity related concerns may be a hindrance in further development of nuclear power in several countries. Therefore, achieving reduction in CO_2 emissions by capture and storage is the only remaining option.

The most significant decision regarding the issue of greenhouse gas emissions took place at the famous 'Kyoto Conference' in 1997 where more than 160 nations met in Kyoto, Japan to negotiate required limitations on greenhouse gases. The outcome of the meeting was the 'Kyoto Protocol' in which the developed nations agreed to reduce their overall emission of greenhouse gases by at least 5% below 1990 levels in the commitment period of 2008 to 2012. This protocol manifested the concerns about CO_2 emissions despite the disinclination of countries like USA and Russia at that time, Russia having ratified the protocol in 2004. It is important in this regard, to mention the European Union's objectives to reduce CO_2 emissions within its boundaries. The EU Kyoto objectives imply to reduce total EU greenhouse gas emissions by 8% between 1990 and 2008-2012. Power generation is the prevalent sector in EU contributing approximately one third of the CO_2 emissions. The total EU emissions of CO_2 from thermal power generation including Norway were about 950 million tonnes in 1990.

The world's response to the call of technology development for CO_2 capture has been quite promising and numerous research and development projects have been commenced. In order to exemplify the types of CO_2 capture projects, some of the international programmes and forums for CO_2 capture, as of the year 2006, are mentioned in the following:

CO_2 Capture Project: Started in 2000 and it is a joint project comprising eight of the world's leading energy companies. The project aims to reduce the cost of CO_2 capture from combustion sources and developing methods for safely storing CO_2 underground.

CSI: The Carbon Sequestration Initiative: This is an industrial consortium formed to investigate carbon capture and storage technologies. The consortium began in July 2000. Currently there are twelve sponsors: Alstom Power, American Electric Power, American Petroleum Institute, Aramco Services, ChevronTexaco, Electricité de France (EDF), EPRI, ExxonMobil, Ford Motor Company, General Motors, Marathon Oil and Peabody Energy.

ENCAP: Enhanced Capture of CO_2: The project objective is to develop new pre-combustion CO_2 capture technologies and processes for power generation. It aims at technologies which meet a target of at least a 90 % CO_2 capture rate and a reduction in the cost of capture of 50 % compared to present. ENCAP is organised as an integrated project and has structured its research activities in order to have an impact in the medium to longer term. The project is supported by the European Commission under the 6th Framework Programme.

GESTCO: This project has the principal objective of making a major contribution to the reduction in CO_2 emissions to the atmosphere and so ensuring Europe a continued stable supply of affordable and environmentally acceptable energy. The GESTCO project intends to provide the first documentation that, for emission sources within selected key areas, sufficient geological storage capacity is available. Cost of energy will obviously increase, but it is anticipated that it will be comparable to that of renewables.

IEA-GHG: International Energy Agency Greenhouse Gas R&D Programme: It was founded in 1991 and is a major international research collaboration that assesses technologies capable of achieving deep reductions in greenhouse gas emissions.

RECOPOL: Reduction of CO_2 emission by means of CO_2 storage in coal seams in the Silesian Coal Basin of Poland: At a selected location in Poland a pilot installation is developed for methane gas production from coal beds while simultaneously storing CO_2 underground.

DYNAMIS: Started in 2006 and is a European Commission project under the 6th Framework Programme. It aims at development of viable technology for co-production of hydrogen and electricity with integrated CO_2 management using natural gas and coal as fuel.

There are several other projects of national and international level and certainly of the equal significance as of those mentioned above, in different regions of the world that focus on CO_2-related data, CO_2 mitigation and technology development for CO_2 capture and storage. The above-mentioned projects are selected for the sole purpose of exemplification of the types of CO_2-mitigation related activities being carrying out around the world.

2.5 CO_2 Capture from Power Plants

Over the course of last decades there have been significant efforts for research in the field of CO_2 capture and some technologies have emerged as possible solutions. It is ahead of the scope of this thesis to give a detailed and in-depth assessment of all those technologies, whether developed or under research and development. Nonetheless, a brief overview of the

main options is presented here in order to give the readers an idea of main processes and challenges involved in CO_2 capture. Approach-wise, there are three major types of CO_2 capture technologies given in the following:

- Post-combustion technologies
- Pre-combustion technologies
- Oxy-fuel combustion

The above-said technologies are discussed one by one in the following section.

2.5.1 Post-combustion Separation of CO_2

CO_2 separation (or capture) from the flue gases produced as a result of fossil fuels combustion processes is referred to as post-combustion capture. Post-combustion methods can further be categorised as follows:

Absorption-based separation: CO_2 is removed from flue gas by selective absorption in a liquid phase, either by exploiting solubility differences (physical solvent process) or by chemical interaction with the solvent.

Adsorption-based separation: CO_2 is removed by adsorption onto a solid medium, (molecular sieves or activated carbon) and subsequently removed by pressure swing operation (PSA) or temperature swing operation (TSA).

Membrane separation (with absorption): Used primarily to remove CO_2 from natural gas, as flue gas CO_2 concentration is to low to provide sufficient driving force (concentration difference across a permeable membrane). Membrane separation can be coupled with absorption, the membrane then acts as a permeable barrier between gas/liquid phases.

Regenerable solid solvent: Flue gas is put in contact with an alkali- or earth alkali metal oxide that reacts with the flue gas components to form carbonates. Regeneration of solids in a different reactor facilitates the release of CO_2 in a controllable way.

At present, economics and technical development suggest that amine absorption cane be a feasible means of capturing CO_2 from power plants. The technology can be incorporated in large scale power plants whether already existing or yet to be built. Since the absorption processes are the most mature technology, it is of interest to have a brief overview of these processes which is given in the following.

The basic principle of amine absorption is to convert specific gas components to a liquid phase where they are selectively soluble or captured by chemical interactions between solvent and solute. An example of the latter is selective amine absorption which is, at present, state-of-the-art technology in CO_2 separation by absorption. A schematic sketch of an absorption process for removal of CO_2 from flue gas is shown in Figure 2.5.

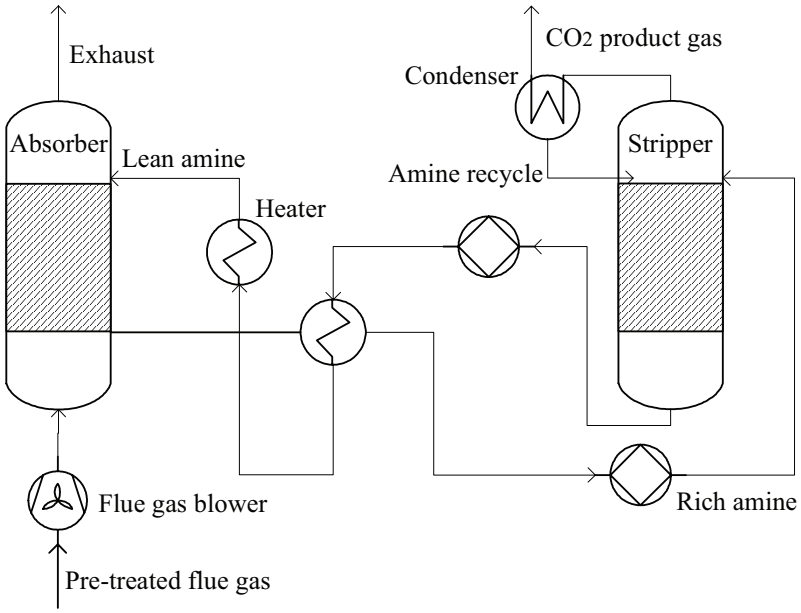

Figure 2.5 The amine absorption process

The process is based on the interaction between an aqueous (basic) amine and a CO_2 containing flue gas. The acidic nature of CO_2 leads to the formation of a loosely bonded acid-base complex which is not thermally stable. When the solvent is heated up, it results in CO_2 stripping or release with subsequent regeneration of the solvent. The absorption process is vulnerable to clogging of the reactor by particulate matter and solvent-detrimental acidic components (SOx, NOx) that form thermally stable amine complexes. Pre-treatment of the flue gas is therefore a requirement. Flue gases from coal-fired power plants typically have CO_2-concentration in the range of 12-15%, while natural-gas fired boiler exhausts contain about 8% CO_2 by volume. In natural gas fired combined cycles the concentration of CO_2 is even lower (3-4%).

The solubility of gas components in a liquid is temperature dependent and heating the solvent after CO_2 saturation in the absorber (generally to around 100-140 °C) leads to a release of gas components in a subsequent stripper. The most important current drawback of the technology is the energy penalty associated with solvent recirculation and the heat required to heat up large quantities of solvent. There are also a number of other obstacles to be overcome. Long term amine stability, improved pre-absorption treatment of flue gas in order to remove solvent-detrimental components and development of new solvents with improved CO_2 selectivity and capacity are the most important challenges.

2.5.2 Pre-combustion Decarbonisation (PCDC)

As the name implies, the pre-combustion decarbonisation concept involves carbon removal from the fuel. The process involves fuel conversion into hydrogen and CO_2 followed by CO_2-capture by physical solvent processes prior to hydrogen combustion. The basic principle of PCDC is depicted in Figure 2.6. As it can be seen in Figure 2.6 that the foremost step in pre-combustion decarbonisation is to produce syngas that subsequently undergoes the water-gas shift reaction thereby converting the remaining CO to CO_2.

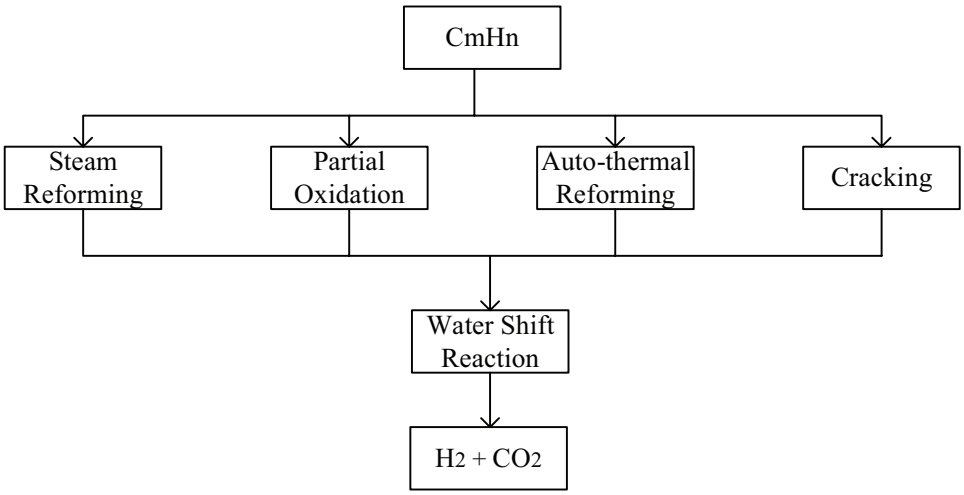

Figure 2.6 Overview of pre-combustion decarbonisation pathway

Syngas can be produced in the following ways:

- Steam reforming
- Partial oxidation
- Auto-thermal reforming
- Cracking

S**team reforming** is an endothermic process which is commercially important and can be regarded as a mature industrial process. Equation 2.1 formulates the steam reforming process for a light weight hydrocarbon with a low tendency of coke formation.

$$C_m H_n + mH_2O \Leftrightarrow mCO + \left(m + \frac{n}{2} \right) H_2 \qquad (2.1)$$

When the process involves converting natural gas it is referred to as steam-methane reforming (SMR). SMR is a highly endothermic catalytic process, and is carried out in reaction tubes at 800-900°C. A portion of natural gas, which can be regarded as the secondary fuel, is burnt outside the reaction tubes for supplying the necessary heat of reaction.

Partial oxidation, contrary to steam reforming, is an exothermal process taking place at 1250-1400°C. Fuel is oxidised to CO and hydrogen by supplying pure oxygen. Equation 2.2 symbolises a partial-oxidation process.

$$C_m H_n + \frac{m}{2} O_2 \Leftrightarrow mCO + \frac{n}{2} H_2 \qquad (2.2)$$

The need for a cryogenic air separation unit (ASU) for oxygen production leads to high investment costs and energy demands. However, this energy demand is compensated by the

higher reforming efficiency and the elimination of nitrogen from the syngas. These two factors significantly reduce the cost associated with the subsequent separation of CO_2.

Auto-thermal reforming is carried out at 950-1050°C and can be viewed as a combination of steam reforming and partial oxidation, as both processes take place within different sections of the reactor. Secondary fuel is not required in this case because fuel is first partially oxidised by air or oxygen in a POX burner. SMR is carried out in a downstream catalytic reactor by the introduction of steam.

Thermal cracking, or methane pyrolysis, is the decomposition of methane into hydrogen and carbon as represented by Equation 2.3.

$$CH_4 \Leftrightarrow C + 2H_2 \tag{2.3}$$

Thermal cracking is a very common and widely used technique in the process industry. The main objective of thermal cracking is the endothermic conversion of fuel into carbon and hydrogen. This approach results in yielding a clean product gas, which is free of oxides. The chemical energy associated with carbon oxidation is not released during this process and consequently only 60% of the heating value of methane may ideally be utilised by later combustion of the hydrogen. There are several methods of cracking which employ the pyrolysis principle, out of which the most important include: thermal catalytic, thermal non-catalytic and plasma cracking. Plasma cracking represents a promising option for hydrogen production where plasma arc supplies the necessary heat of reaction. In all pre-combustion capture process schemes, the final step is to cool down the reforming gas and convert CO to CO_2 resulting in even more hydrogen production by the so-called water gas-shift reaction. This is given by Equation 2.4.

$$CO + H_2O \Leftrightarrow CO_2 + H_2 \tag{2.4}$$

In order to yield a carbon-free fuel for combustion, the CO_2 is separated by physical absorption processes. By virtue of the higher partial pressures of CO_2 in the syngas, pre-combustion separation can be carried out with relatively less effort as compared to post-combustion of CO_2 in atmospheric flue gases.

2.5.3 Oxy-fuel Combustion

In the oxy-fuel combustion, as the name implies, fuel reacts with pure oxygen instead of air. In flue gases of conventional combustion processes, CO_2 is diluted with other combustion products and has a lower partial pressure (typically in the range of 0.03-0.15 bar). The lower partial pressure of CO_2 results in high demands of energy to separate it from other combustion products. Using concentrated O_2 instead of air as oxidiser yields a flue gas that ideally constitutes only of CO_2 and water vapour. The result is that CO_2 is available at a high partial pressure and can easily be separated from the exhaust by cooling down the CO_2-steam mixture. The oxy-fuel process can be presented in the form of the chemical reaction given in Equation 2.5.

$$CH_4 + 2O_2 \Leftrightarrow CO_2 + 2H_2O \tag{2.5}$$

The oxy-fuel process allows for the use of simpler post-combustion separation techniques, such as condensation, in order to cool down the exhaust stream and separate CO_2. This will significantly reduce the energy demand and capital cost needed for CO_2 capture and the only energy penalty will be associated with CO_2 compression prior to its sequestration. Nevertheless the stoichiometric combustion of fuel leads to combustion temperatures quite higher than those which current materials can withstand. There are two ways to avoid excessively high temperatures; either by recycling the flue gas or steam injection into the combustor. Oxy-fuel combustion can be implemented in different power cycles; the mainstream oxy-fuel combustion based cycles are described here briefly.

Direct heating - Brayton cycle (O_2/CO_2 recycling)

Flue gas is recycled, compressed and the resulting CO_2-rich fluid is subsequently expanded in a gas turbine. Remaining heat in exhaust is utilised in a Rankine steam cycle (Figure 2.7). Proposed variants of this principle include MATIANT cycle [Mathieu 2003], AZEP-cycle [Griffin 2002] and Graz-cycle [Heitmer 2003]. Main technical obstacle is the complete redesign of turbo machinery components and combustor, compatible with a CO_2-rich working fluid.

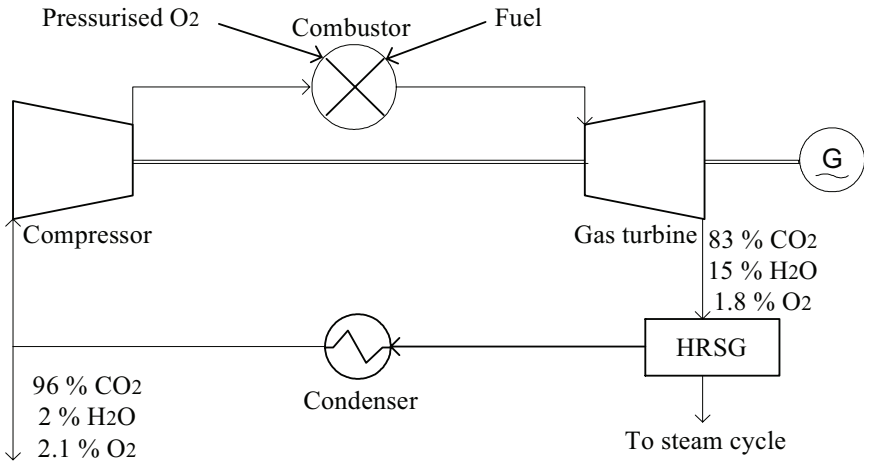

Figure 2.7 Schematics of direct heating oxy-fuel Brayton cycle combined with steam cycle

Direct heating - Rankine cycle (O_2/H_2O recycling)

Combustion temperature is regulated by direct injection of water, and the resulting fluid is expanded in turbines followed by condensation of water. Example cycle is that proposed by Clean Air Systems (CES) [Anderson et al. 2003]. The main technical obstacle is the design of high-temperature (TIT=1300°C) steam turbines.

Indirect Heating (O_2/CO_2 recycling)

Combustion temperature is moderated by recycling of flue gas and heat is transferred from an oxy-fuel process to a separate fluid which is used for process heating or in a Rankine steam cycle. Method is sensitive to fouling (reduced heat transfer) and requires the design of high temperature-tolerant boilers. The use of pure oxygen does necessarily imply the use of

an Air Separation Unit (ASU) using cryogenic, membrane or adsorption principles. The ASU is the major source of cost and energy penalty in the oxy-fuel combustion.

Apart from the three main CO_2 capture techniques; there exist some other concepts of CO_2 capture from power plants; '**Chemical Looping Combustion (CLC)'** being one of the most **promising** alternate concepts. This thesis focuses on Chemical Looping Combustion and its implementation in power cycles; and the rest of this thesis will deal with several facets of the CLC-technology.

3 Chemical Looping Combustion

This chapter illustrates the principle of Chemical Looping Combustion (CLC) and reviews the literature available on various aspects of CLC. The characterisation of vital CLC-components is also presented. The literature review covers a time period of over two decades starting from the year 1983 when the CLC concept was conceived.

3.1 The CLC Principle

Chemical Looping Combustion (CLC), proposed by Richter and Knoche [1983], is a novel concept of the hydrocarbon fuels energy conversion with inherent CO_2 capture. The term 'inherent' implies that CO_2 is readily available in rich form by virtue of the process itself. In CLC, the so-called 'combustion' is unlike a conventional combustion process because the combustion air and the fuel remain in separate environments and have no direct contact with each other. The CLC can be regarded as an alternative to oxy-fuel combustion while achieving the combustion product in the form of a CO_2/steam mixture.

Figure 3.1 depicts the principle of Chemical Looping Combustion. The fuel conversion is accomplished by virtue of the two intermediary reactions; oxidation and reduction. The oxygen needed by the fuel is supplied by employing an intermediate agent; which is a certain metal oxide (MeO). In a reduction reactor (RED), the metal oxide reacts with the fuel. As a result of the reduction reaction, the fuel reacts with the oxygen in the metal oxide thereby reducing the metal oxide to metal (Me), as given by Equation 3.1. The reduced metal then circulates to a separate oxidation reactor (OX), transports the chemical energy of the fuel to the air in the form of sensible heat, reacts with oxygen in the air, and gets regenerated to MeO, as given by Equation 3.2. The metal oxide then circulates back to the reduction reactor to react with the fuel. The metal oxide keeps circulating in a cyclic regenerative fashion or a loop and hence Ishida et al. [1987] named the process as Chemical Looping Combustion.

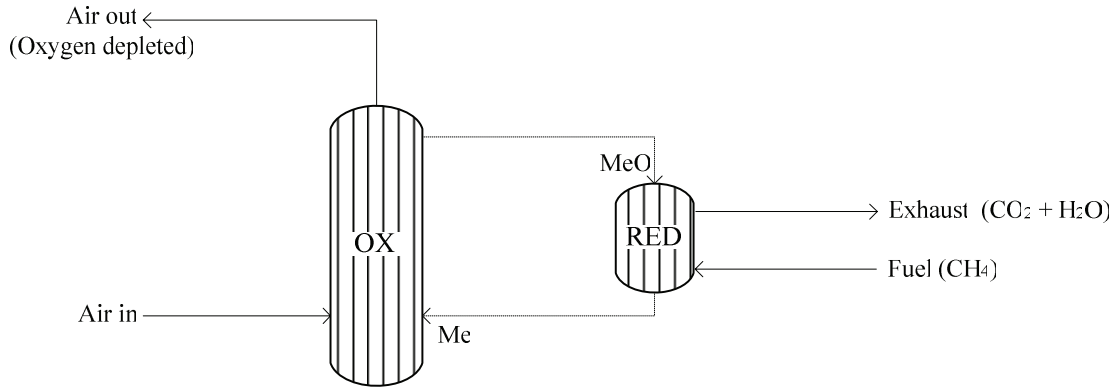

Figure 3.1 The Chemical Looping Combustion principle

In order to elaborate the concept of Chemical Looping Combustion and to comprehend how it can be implemented in power cycles, it is essential to have an understanding of the heterogeneous solid-gas reactions simultaneously taking place in the two reactors in continuous operation.

In the reduction reactor, fuel reacts with oxygen in the metal oxide in a stoichiometric ratio thereby reducing the metal oxide to metal. This is given by Equation 3.1.

$$C_nH_{2n+2} + mMeO \rightarrow nCO_2 + [n+1]H_2O + mMe \quad (3.1)$$

The reduced metal oxide circulates to the oxidation reactor where it reacts with air. The metal oxide also transports the chemical energy in the fuel to the air in the form of sensible heat. In the oxidation reactor, oxygen in the air oxidises the metal to metal oxide. The oxidation reaction is given by Equation 3.2.

$$mMe + \left(\frac{m}{2}\right)O_2 \rightarrow mMeO \quad (3.2)$$

The metal oxide circulates back into the reduction reactor and transports oxygen as well as sensible heat to the fuel.

The net heat of reaction of the fuel conversion is the same as in a direct, conventional combustion and is the sum of the heats of reaction of oxidation and reduction reactions. Equation 3.3 gives the net exothermic reaction.

$$C_nH_{2n+2} + \left[\frac{3n+1}{2}\right]O_2 \rightarrow nCO_2 + [n+1]H_2O \quad (3.3)$$

In Equations 3.1, 3.2 and 3.3, MeO is metal oxide, Me is metal and C_nH_{2n+2} is a hydrocarbon fuel molecule. While m and n are stoichiometric factors.

The metal oxide which is referred to as the 'oxygen carrier' is bound with an inert solid substance that does not take part in the chemical reactions yet provides mechanical stability and enhances the heat carrying capacity of the solids.

The oxidation reaction for a metal is exothermic and results in heat release thereby making the oxygen depleted air available at high temperature. If the reactors are pressurised the oxygen depleted air can be expanded in a gas turbine to generate power. The reduction reaction of solids can either be exothermic or endothermic, depending on the nature of the metal oxide employed. If the reduction is endothermic, the heat needed for the reaction is supplied by the hot metal oxide from the oxidation reaction. The CO_2-rich exhaust stream is also available at high temperature (and pressure in case of pressurised reactors) and can also be utilised for power generation, either by expansion in a turbine or steam generation in a heat recovery steam generator. If the reactors are not pressurised (atmospheric reactors), the available heat can be extracted to produce steam which can further be employed for power generation in a Rankine cycle.

The CO_2 in the exhaust stream is available at a high partial pressure thanks to its higher concentration in the mixture. After extracting the heat available in the exhaust, the stream can be condensed to separate water. The stream is then left with pure CO_2 which can then be compressed and converted to liquid CO_2 which can further be transported for storage. In this way the energy penalty for CO_2 separation and compression is lower as compared to CO_2-

capture penalty in a conventional power plant where CO_2 is diluted with other combustion products and is available at lower partial pressure as compared to that in CLC.

3.2 Chemical Reactions of CLC

Thermo-chemical data from Barrow [1988] is used throughout this section for calculation of standard heats of reaction at STP (298 K, 1 atmos). The nickel oxide/nickel is chosen as the oxygen carrier while pure methane is chosen as the reducing agent for exemplification purpose.

3.2.1 Oxidation

During the oxidation reaction, nickel metal embedded with the spinel matrix is converted exothermically to nickel oxide (ΔH^0=-488.7 kJ/mol O_2). This is given by Equation 3.4.

$$2Ni(s) + O_2(g) \Leftrightarrow 2NiO(s) \qquad (3.4)$$

The earlier experimental evaluations (as pointed out in the CLC-research review) suggest that the oxidation to NiO is rapid at high temperatures. The carrier's re-oxidation is vital to CLC feasibility, since it symbolises the source of thermal energy within the reactor system.

3.2.2 Reduction

In contrast to the oxidation reaction, reduction of NiO is not that straightforward and can be further classified into two distinct sets of reactions:

- Direct Fuel Reduction (DFR)
- Reforming reactions

DFR using methane and nickel oxide (ΔH^0 = 175.0 kJ / mol CH_4), can be formulated as in Equation 3.5.

$$4NiO(s) + CH_4(g) \Leftrightarrow 4Ni(s) + CO_2(g) + 2H_2O(g) \qquad (3.5)$$

Multiplication of Equation 3.4 by 2 and subtraction of Equation 3.5 gives the net reaction for the combustion of methane (ΔH^0 = -801.3 kJ / mol CH_4).

$$CH_4(g) + 2O_2(g) \Leftrightarrow CO_2(g) + 2H_2O(g) \qquad (3.6)$$

Coking is a possible problem whenever carbonaceous fuels are exposed to high temperatures and reducing conditions. According to Lødeng et al. [2000] and Brandvoll [2005], the existence of elementary nickel generated in direct fuel reduction poses additional problems by virtue of its tendency to catalyse the formation of coke. In order to suppress coke formation, studies by Ishida et al. [1998b] indicate that steam addition can effectively hold back coke to form on the solids.

In the presence of water vapour, however, methane is converted to carbon monoxide, carbon dioxide, carbon and hydrogen by a composite set of reactions commonly known as reforming reactions. The literature associated with experimental studies of methane reforming is vast and it is beyond the scope of this thesis to give a thorough discussion of the topic. Table 3-1 gives a brief overview of the reactions that are likely to occur.

Table 3-1 Methane reforming reactions

	Reaction	ΔH^0_{298} [kJ/mol]
Reforming reactions (strongly endothermic)	$CH_4(g) + H_2O(g) \Leftrightarrow CO(g) + 3H_2(g)$	206.1
	$CH_4(g) + CO_2(g) \Leftrightarrow 2CO(g) + 2H_2(g)$	247.3
Water shift reaction (weakly exothermic)	$CO(g) + H_2O(g) \Leftrightarrow CO_2(g) + H_2(g)$	-41.1
Methane decomposition	$CH_4(g) \Leftrightarrow C(s) + 2H_2(g)$	74.8
Boudouard reaction	$2CO(g) \Leftrightarrow C(s) + CO_2(g)$	-172.5
	$CO(g) + H_2(g) \Leftrightarrow C(s) + H_2O(g)$	-131.3

In addition to the reactions in the above table there are numerous mechanisms of minor importance that will not be considered. A complete listing of reforming reactions and equilibrium constants is given by Hou and Hughes [2001].

The hydrogen produced in the steam reforming is a complicating factor as it might participate in reduction of nickel oxide (ΔH^0 = 2.5 kJ/mol H_2) as given by Equation 3.7.

$$NiO(s) + H_2(g) \Leftrightarrow Ni(s) + H_2O(g) \qquad (3.7)$$

3.3 CLC-Research Review

Although the CLC-concept may have caught the attention of scientists and environmentalists as early as its idea was conceived, yet it did not stimulate the researchers for almost one decade to commence any full-fledged research projects on CLC. It was not before early 1990s that the growing awareness related to global warming, greenhouse effect and CO_2 emissions made the scientific community to look in different directions and envision some long-term solution to the CO_2 problem. It was first then the interest for the CLC-concept inspired some research organisations and engineers around the world to the extent that a few research projects were initiated for evaluating CLC as a potential candidate for power generation with CO_2 capture. Since then, the research on various aspects of CLC

has been going on with an increasing pace; nevertheless CLC can be regarded as the 'technology' in its youth. Therefore, the literature on CLC is still sparse as compared to other fields of research related to combustion or power generation with CO_2 capture. The CLC development can be categorised into the following main areas:

- Oxygen Carriers
- CLC-Reactors
- Modelling and simulation/Cycle studies

In the coming sections, each of the three areas is discussed and the literature review for each is briefly presented.

3.3.1 Oxygen Carriers

An oxygen carrier is a certain metal oxide that transfers oxygen in the air to the fuel. Oxygen carrier is considered the most vital component in a CLC-system. The three core criteria that an oxygen carrier ought to meet for being applicable in CLC are the following:

- The reduction and oxidation reaction rates must be sufficient over time to ensure high conversion of fuel and rapid regeneration of oxide
- The mechanical properties of the carrier solids must be such that material breakdown and sintering/agglomeration is minimised
- Carrier solids should also be economically viable and environmentally safe during production and operation

It is a challenge to fulfil the first two criteria at the same time, as the requirements on mechanical strength and chemical activity are generally incompatible. A rigid and dense particle will although possess a high crush strength yet it will lack the porosity that is crucial for achieving sufficient reactivity for reduction and oxidation.

Over the course of the last decade, there has been a considerably immense research done in the field of development of various oxygen carriers and evaluating their performance in CLC. Realising the early stage of CLC-development, to most of the researchers the area of foremost priority has been methodology development for analysing and benchmarking various potential oxygen carriers. The experimental work has been mainly focussing on the following aspects:

- Determination of reaction rates of several oxygen carriers
- Fuel conversion
- Study of durability characteristics of potential oxygen carriers

The experimental work related to the oxygen carriers does in fact lay the foundations of the CLC-related research, by not only providing the results concerning the materials but also

providing realistic assumptions for carrying out cycle studies. As stated earlier, developing a suitable and reliable oxygen carrier is the top priority in the concept development; therefore a considerable number of articles have been published that address this issue. The oxygen carrier-related literature is presented in Table 3-2. The table includes the authors and their countries, years of publications in a chronological order, the studied materials, the oxidising and reducing agents (gases), and the main issues or findings of each study.

Table 3-2 Oxygen carrier development in chronological order

Authors (Country)	Year	Carriers/ stabilisers	Reactant gases	Issues / Results
Nakano et al. (Japan)	1986	Fe_2O_3 Fe_2O_3- Ni Fe_2O_3/Al_2O_3	H_2 H_2O/H_2	Reduction and Oxidation characteristics
Ishida, Jin (Japan)	1994a	NiO NiO/YSZ Fe_2O_3/YSZ	H_2/Air	Effect of inert binder composition and reaction temperature
Ishida, Jin (Japan)	1996	NiO NiO/YSZ	H_2/Air	Zero NO_X emissions Comparative study of the solids
Ishida, Jin, Okamoto (Japan)	1996	NiO/YSZ	H_2/Air	Preparation methods Effect of cycling Effect of gas composition and temperature
Hatanaka, Matsuda, Hatano (Japan)	1997	NiO	CH_4/Air	Reduction and oxidation kinetics of pure Ni/NiO Carbon deposition in a small fixed bed
Ishida, Jin, Okamoto (Japan)	1997	NiO/YSZ NiO/Al_2O_3 Fe_2O_3/YSZ	H_2/Air	Iron-solids unsuitable due to crust formation Carbon formation can be controlled by water vapour
Ishida, Jin, Okamoto (Japan)	1998a	NiO/YSZ, Al_2O_3, TiO_2 Fe_2O_3/YSZ, Al_2O_3, TiO_2	CH_4/H_2O	Effect of material on reduction rate Effect of the composition- H_2O/CO_2 on carbon deposition Model for carbon deposition

Jin, Okamoto, Ishida (Japan)	1998b	NiO/YSZ CoO-NiO/YSZ CoO/YSZ Fe_2O_3/YSZ	CH_4/Air H_2/Air	Reactivity of single and double oxide Regenerability of materials (with Hydrogen) Carbon deposition
Ishida, Jin (Japan)	1999	NiO/YSZ, Al_2O_3, TiO_2 CoO-NiO/ YSZ, Al_2O_3, TiO_2 CoO/YSZ, Al_2O_3, TiO_2 Fe_2O_3/YSZ, Al_2O_3, TiO_2	CH_4/Air H_2/Air	Summary of previous results
Jin, Okamoto, Ishida (Japan)	1999	NiO/Al_2O_3, TiO_2, MgO CoO/Al_2O_3, TiO_2, MgO Fe_2O_3/Al_2O_3, TiO_2, MgO	CH_4/H_2O Air	Effect of solid reactant and binder on reactivity Suppression of carbon deposition Increase in pressure reduces necessary reaction temperature
Jin, Ishida (Japan)	2001	NiO NiO/YSZ and $NiAl_2O_4$	H_2/Air	Effect of pressure Investigation of regenerability The potential of NiO/$NiAl_2O_4$ pointed out
Ishida, Jin (Japan)	2001	NiO NiO/YSZ, Al_2O_3, TiO_2, MgO CoO/YSZ, Al_2O_3, TiO_2, MgO Fe_2O_3/YSZ, Al_2O_3, TiO_2, MgO	H_2/Air CH_4/H_2O Air	Summary of previous results (effect of solid reactant and binder, carbon deposition, regenerability, effect of pressure and use of simulated gasified coal)
Ryu et al. (S. Korea)	2001	NiO/Bentonite	CH_4 (5%) in Ar/Air	Effect of particle composition on rate Un-reacted shrinking core model

Mattisson, Lyngfelt, Cho (Sweden)	2001	Fe_2O_3	CH_4 Synthetic Air	Impact of bed mass and reaction time Effect of cycling on reduction and oxidation reactions Proposals for reactor design
Cho, Mattisson, Lyngfelt (Sweden)	2002	Fe_2O_3/Al_2O_3 Fe_2O_3/MgO	CH_4/H_2O 5 % O_2 in Nitrogen	Effect of solid reactant and cycling on reaction rates Agglomeration characteristics Physical characterisation
Ishida, Yamamoto, Ohba (Japan)	2002	$NiO/NiAl_2O_4$	H_2/Ar	Circulation characteristics Circulation rates Solid conversion rates Particle durability
Copeland et al. (USA)	2002	Iron based sorbents and NiO/Al_2O_3	Simulated syngas/Air	Effect of cycling on rates Estimation of carrier attrition Testing in pilot scale fluidised bed
Jin, Ishida (Japan)	2002	$NiO/NiAl_2O_4$ CoO-NiO/ YSZ	CH_4/H_2O Air	Effect of material, temperature and pressure on reduction rates Carbon deposition
Jeong et al. (S. Korea)	2003	$CoO/CoAl_2O_4$ $NiO/NiAl_2O_4$	H_2/Ar CH_4/Ar/ He	Characteristics of the studied material in oxidation and reduction
Brandvoll et al. (Norway)	2003	$NiO/NiAl_2O_4$	H_2/Air	Effect of particle size Temperature and composition on reaction rates Rate limiting mechanism
Song et al. (S. Korea)	2003	NiO/ Hexaaluminate	H_2/Ar	Characteristics of the studied material and the new type of binder
Mattisson, Järdnäs, Lyngfelt (Sweden)	2003	Cu/ Al_2O_3 Co/Al_2O_3 Mn/Al_2O_3 Ni/Al_2O_3	10%CH_4 5% CO_2 10% H_2O 10% O_2	Effect of material, temperature and cycling on reaction rates Estimation of mechanical properties Application of design criteria

Villa R. et al (Italy)	2003	Ni-Al-O and Ni-Mg-Al-O mixed oxides	H_2 CH_4/Air	Materials synthesis and characterisation
Adánez et al. (Spain)	2004a	Various combinations	CH_4/ N_2 Air	Selection of oxygen carriers
Adánez et al. (Spain)	2004b	Various combinations	CH_4/H_2O Air	Characterisation of oxygen carriers
de Diego et al. (Spain)	2004	CuO/Al_2O_3, SiO_2, TiO_2, ZrO_2 and sepiolite	CH_4, H_2 or CO, H_2 in H_2O Air	Effect of solid binder and gross composition Gas concentration
Jin, Ishida (Japan)	2004	$NiO/NiAl_2O_4$ CoO-NiO/YSZ	Simulated coal gasification syngas	Comparative study of the carriers $NiO/NiAl_2O_4$ found to be better Coal gas found to be more suitable than natural gas
Garcia-Labiano et al.	2004	CuO/Al_2O_3	CH_4, H_2, CO O_2	Preparation of the carrier Reduction and oxidation kinetics
Lee et al. (S. Korea)	2004	$NiO/AlPO_4$, ZrO_2, YSZ and $NiAl_2O_4$	CH_4/H_2O	Characteristics of redox reactions of the studied material in combination with several stabilisers
Mattisson, Johansson, Lyngfelt (Sweden)	2004	Fe_2O_3/Al_2O_3, ZrO_2, TiO_2 and $MgAl_2O_4$	CH_4/H_2O/ 5 % O_2	Carrier synthesis and comparative study of reaction rates at 950 °C Study of agglomeration characteristics
Johansson, Mattisson, Lyngfelt (Sweden)	2004	Fe_2O_3/ $MgAl_2O_4$	CH_4/H_2O/ 5 % O_2	Carrier synthesis Oxide/inert ratio and sintering temperature variation for finding optimal solids properties 60% Fe_2O_3 on 40% $MgAl_2O_4$

Brandvoll (Norway)	2005	$NiO/NiAl_2O_4$ and Perovskite	CH_4 CH_4/H_2O H_2	Doctoral Thesis Various issues covered in detail
Cho et al. (Sweden)	2005a	Fe_2O_3/Al_2O_3, $NiO/NiAl_2O_4$	CH_4 CH_4/H_2O	Investigation of the Carbon formation conditions High fuel conversion necessary to avoid carbon formation
Cho et al. (Sweden)	2005b	Fe_2O_3/Al_2O_3, $NiO/NiAl_2O_4$	CH_4 CH_4/H_2O	Investigation of defluidisation conditions in fluidised beds of the selected carriers
Cho (Sweden)	2005c	Natural iron ore, and synthetic carriers based on Fe, Ni, Cu and Mn	CH_4 CH_4/H_2O	Doctoral Thesis Covering several issues including solids synthesis, reactivity study, testing procedures, evaluation and comparison
Corbella, et al. (Spain)	2005	CuO/TiO_2	CH_4	Investigation of the oxygen carrier performance in a fixed reactor
Lee et al. (S. Korea)	2005	CoO/YSZ NiO NiO/ZrO_2, YSZ, $AlPO_4$ and $NiAl_2O_4$	H_2	Investigation of the reduction and oxidation characteristics of the selected carriers
Zafar, Mattisson, Gevert (Sweden)	2005a	CuO/SiO_2 Mn_2O_3/SiO_2 NiO/SiO_2 Fe_2O_3/SiO_2	CH_4/H_2O O_2	Investigation of CLC potential for integrated hydrogen and power production NiO found out to be the most suitable oxygen carrier Temperatures exceeding 800 °C should be avoided with NiO
Zafar Mattisson, Gevert (Sweden)	2005b	NiO/SiO_2, $MgAl_2O_4$ CuO/SiO_2, $MgAl_2O_4$ Mn_2O_3/SiO_2, $MgAl_2O_4$	10%CH_4 5% CO_2 10% H_2O 75% N_2 5% O_2 in Nitrogen	Preparation of the carriers Reactivity studies The carriers performance in redox cycles NiO and CuO showed high reactivity

Zafar (Sweden)	2005c	Ni, Cu, Mg, Fe and Mn based carriers	Various gases	Licentiate Thesis Covering various aspects of oxygen carriers
Mattisson et al. (Sweden)	2005	NiO/ SiO_2 CuO/ SiO_2	CH_4/H_2O O_2	Integrated hydrogen and power production potential Selectivity studies NiO gives high H_2 selectivity
Johansson (Sweden)	2005	90 different oxygen carriers based on Ni, Mn	50% CH_4 and 50%H_2O 5% O_2 in	Doctoral Thesis Diversity of issues covered in detail
Garcia-Labiano et al. (Spain)	2005	CuO, Fe_2O_3, NiO with Al_2O_3, MgO, SiO_2, TiO_2, ZrO_2	CH_4/CO_2 CH_4/H_2O	Simulation Temperature variations in the solids during oxidation and reduction reactions The highest temperature variations reached for oxidation of all solids with Ni having the maximum

It can be seen from Table 3-2 that it did not take long after the CLC-concept was proposed (although the process was not quite yet given the name Chemical Looping Combustion) that Nakano et al. [1986] carried out experiments on iron oxide as a potential oxygen carrier. However, no more contribution to the oxygen carrier development was seen until early 1990s. The research group headed by Masaru Ishida at the Laboratory of Resource Utilization at the Tokyo Institute of Technology can undoubtedly be designated as the initiator of the oxygen carrier development and has a major contribution to research in this aspect of CLC. The research effort initiated in the early 1990s and the early experiments by Ishida & Jin [1994b] focussed on the reactivity of pure nickel oxide (NiO) and solids of NiO and iron oxide (Fe_2O_3) mixed with yttrium stabilised zirconia (YSZ). The outcome of this study was that the pure NiO solids were not suitable for CLC. The reason behind this conclusion was the formation of dense layers of elementary metal after a few cycles of reduction and oxidation. The result of this effect was that the reactant gases faced a limitation at the solids surface and the metal layers blocked the gases off and consequently stopped them to diffuse into the solids interior. The elementary metal layer formation on the solids also contributed to the mechanical stability loss. Solids containing a mixture of metal oxide and an inert stabiliser (or binder) such as YSZ or alumina improved reaction rates, regenerability (i.e. consistency of reaction rates after repeated reduction and oxidation cycles) and mechanical durability. Ishida et al. [1998b] also investigated the well known issue of carbon deposition on the solids at high temperature and low oxygen partial pressures when using a carbonaceous fuel. It was found that a steam-carbon ratio (S/C) of 2 was needed to effectively suppress carbon formation in the reduction.

During the years from 1994 to 1998, the oxygen carrier development was more of a field of research confined in Japan and the experimental work focussed mainly on the NiO and Fe_2O_3 in combination with various reducing agents (reactant gases). Although these experiments did not result in a major breakthrough; they added value to the proof of concept as well as laid a foundation for the forth-coming series of experiments and the later experiments benefited from their outcome.

It was in 1999 that Jin et al. conducted a series of experiments on the reactivity of NiO, CoO and Fe_2O_3 in combination with different supports (Al_2O_3, TiO_2 and MgO). It was found that NiO supported on alumina produced nickel-aluminate ($NiAl_2O_4$) at high temperatures. $NiAl_2O_4$ belongs to a class of compounds more generally referred to as 'spinels', and the 'new' binder showed very promising reaction rates and robustness in combination with NiO. A variety of stabilisers have been tested so far, but none of them showed appreciably better results than those achieved using nickel-aluminate.

The beginning of 21st century brought about an ever increasing concern of CO_2 emissions and the need to develop a long-term solution to this problem. Consequently, the CLC-concept was paid more serious attention in many parts of the world other than Japan (although cycle studies were also carried out in rest of the world during 1990s, which will be reviewed later) and research projects were kicked off in some European countries and experimental facilities were set up to investigate potential oxygen carriers. Another research group that was inspired by the CLC-concept is the one headed by Anders Lyngfelt at Chalmers University of Technology, Sweden. The group can be designated as the second largest contributor to the experimental data on the oxygen carriers. The early studies [Mattisson et al., 2001] focussed on iron oxide (Fe_2O_3, hematite) mainly because it is an inexpensive substance and also due to promising results.

There are other research groups as well, which have come forward as contributors to the accumulated experimental data on oxygen carriers, e.g. Corbella et al., Lee et al., Garcia-Labiano et al., Jeong et al., Ryu et al., Song et al., Adanez et al., Villa et al. and Copeland and co-workers. All of the groups have contributed to the oxygen carrier development and introduced new concepts. Copeland et al. however came up with a different approach of the Sorbent Energy Transfer System (SETS) which is quite identical to the CLC apart from the feature that SETS focuses on CuO as the metal oxide. The reason for it is that both reduction and oxidation reactions for CuO are exothermic. A mixture of oxides (Fe_2O_3 –CuO) supported on alumina is thus chosen to yield an oxygen carrier where both reactions are exothermic. This also has some significant implications on the gases and solids flowrates, reactors design and cycle efficiency.

Although the research community involved in oxygen carrier development for CLC is still limited, the prospects of finding suitable materials for large-scale and long term CLC-operation have become brighter during recent years. The number of publications per year has risen, especially since 2003. Although the mainstream publications involve experimental set-up based on thermogravimetric methods, nevertheless there is a quite apparent trend towards more realistic experimental set-ups using fixed and fluidised beds.

Oxygen Carriers' Characterisation

For a thorough comparison of oxygen carrier materials on the basis of experimental findings, the reader is referred to Lyngfelt et al. [2001]. Based on the literature cited earlier,

the most promising candidate materials for use in CLC are NiO, CuO, CoO and Fe_2O_3 (converted to Fe_3O_4 (magnetite)). Based on findings by Cho et al. [2004], other conversions of iron-based materials are not considered. Brandvoll [2005] presented a comparison of the standard heats of reaction (oxidation per mol of oxygen and reduction per mole of methane) and the theoretical oxygen carrying capacity of the above mentioned oxides.

Iron-based oxygen carriers have an advantage in the economical terms; as the raw material is relatively inexpensive compared to other metals. Moreover, Brandvoll [2005] emphasised on the oxygen carrying capacity of various oxygen carriers and suggested that the iron-based oxygen carriers have lower oxygen carrying capacity compared to that of NiO, CoO and CuO. Regarding the heats of reaction of the aforementioned oxides, all the oxides except CuO, have exothermic oxidation and endothermic reduction reaction. CuO has quite a unique feature that both of its reduction and oxidation reactions are exothermic. It can be argued that oxygen carriers with a slightly endothermic reduction are preferable. This will result in a higher heat of reaction for oxidation than that for the net combustion of fuel. Consequently, the thermal potential can be retrieved from one large process stream (oxidation air exhaust) and one small stream (CO_2-rich exhaust). At present, it is unclear if copper based oxides are suitable in high temperature CLC operation, due to a reported tendency towards sintering [Cho et al., 2004]. However, the work by Garcia-Labiano et al. [2004] reports no such sintering tendency. Nevertheless, more research on copper oxides is required before a sound conclusion can be reached on their usage as oxygen carriers in CLC.

In search of candidates to be employed as oxygen carriers, an interesting class of compounds is the perovskites. Brandvoll [2005] experimentally investigated this material. This class of oxides includes a wide variety of compounds with the similar crystal structure and composition as that of mineral Perovskite, $CaTiO_3$. Ideal perovskites have the general formula ABO_3; where A is an alkali, alkaline earth or rare earth metal, and the B atom is an element in the transition series or in the main groups III, IV or V. The most interesting property of perovskites in this context is the ability of the structure to accommodate any oxygen deficiency without major structural change [Olafsen, 1999].

Perovskites are easily re-oxidised by air at high temperatures. The experimental work related to perovskites, has mainly focussed on determination of oxygen carrying capacity and its comparison with $NiO/NiAl_2O_4$. One limitation of such systems is that the temperature stability generally is low. For example perovskites of the general type $La_nCo_nO_{3n-1}$ are known to undergo decomposition at temperatures above 650°C:

$$LaCoO_{3-\delta} \rightarrow La_{m+1}C_mO_{3m+1} + La_2O_3 + Co \qquad (3.8)$$

In order to increase the temperature stability, elements such as Sr and Fe can be added to the structure. This will result in compounds with general formula $La_xSr_{1-x}Co_{1-y}Fe_yO_{3\delta}$, [Brandvoll, 2005]. Brandvoll [2005] concluded, on the basis of experimental findings, that perovskite is not competitive to $NiO/NiAl_2O_4$ as oxygen carrier in CLC.

3.3.2 CLC-Reactors

A CLC reactor system should fulfil the following three requirements:

- Achieve a high gas-solid mass transfer to guarantee a high conversion of the fuel in the reduction reactor and oxidisation of metal in the oxidation reactor

- Achieve a high solid-gas heat transfer in order to transport the required heat of reaction from the hot oxygen carrier solids to the fuel for endothermic reduction reaction

- Establish continuous circulation of the needed amount of solids between the two reactors in order to maintain an uninterrupted oxygen supply to the fuel; and exhibit minimal gas leakage and energy requirements

In contrast with the oxygen carrier development, experimental data on reactor systems suitable for CLC applications in power cycles are virtually non-existent. The paper by Johansson et al. [2003] provides experimental data for a cold, scaled model of two interconnected fluidised beds. Gas leakages are simulated by tracking helium and air within the reactors. It was shown that although controllable by means of steam injection, gas leakage between different components of the reactor system, might be a significant problem. The nature of CLC demands that gas leaks be kept at a minimum. It was also demonstrated that solids circulation is relatively easily controllable. The first experimental data on continuous CLC are given by Ishida et al. [2002]. For short term operation (<300 minutes) conversions of 100- and 70% were found for oxidation and reduction, respectively.

The research related to CLC-reactors consists of two main issues; experiments to test reactor system designs and study of operational aspects of CLC. The latter includes oxygen carrier deactivation, agglomeration and mechanical breakdown, solids transport, gas-solid separation and determination of optimal process parameters (mainly temperature and pressure) in large scale operation.

Table 3-3 reviews the CLC-reactor system related literature.

Table 3-3 Literature related to reactor system design

Authors	Year	Issue	Results/Rationale
Lyngfelt, Leckner, Mattisson (Sweden)	2001	General discussion of concept	Literature survey on oxygen carriers Reactor design equations Cycle considerations
Ishida, Yamamoto, Ohba (Japan)	2002	Circulation of solids Material: $NiO/NiAl_2O_4$ Gases: H_2/Air	100% hydrogen conversion and 70% air conversion found for continuous operation with circulation

Johansson et al. (Sweden)	2003	Gas leakage measurements in interconnected fluidized beds, scaled cold model Material: Sand Gases: He/Air	Reactor leaks are in the area of 2-15% of reactor inlet flowrates Gas leakage can be controlled by using steam
Adánez et al. (Spain)	2003	Simulation Material: CuO-SiO_2 Gases: CH_4	Mathematical model developed for fuel reactor optimisation Operating conditions set and effect of operation variables studied
Lyngfelt et al. (Sweden)	2004	10 kW pilot plant operation Nickel based oxygen carrier Gases: NG/Air	First operational CLC-prototype 99.5 % fuel conversion achieved Gas leakages not detectable No deactivation observed Small attrition rates indicate long particle lifetime
Wolf (Sweden)	2004	(Simulation) Interconnected pressurised circulating fluidised bed reactor system Solids transport Pressure drops	Doctoral Thesis Various reactor system configurations proposed and designed The operation modes of various reactor system concepts discussed
Jin, Ishida (China & Japan)	2004	High pressure fixed-bed Material: $NiO/NiAl_2O_4$ CoO-NiO/YSZ Gases: Simulated Coal Gas	Coal- gas fueled CLC Investigation of kinetic behaviour of the solids with coal gas Coal gas combustors found better than natural gas combustor for CLC
Kronberger et al. (Austria & Sweden)	2005	A Two-compartment fluidised bed reactor for CLC	Design and development of a two-compartment CLC-reactor system Parameter variation to measure gas leakage and solids circulation rate Suitable operating conditions defined

Johansson (Sweden)	2005	Experimental work covering a broad range of the aspects related to CLC-reactors design, development and operation and testing of different	Doctoral Thesis Design and construction of two types of cold-flow models of CLC-reactors Design and construction of one 300 W CLC reactor system Testing of nickel-based carriers with natural gas and syngas in the developed reactor systems Long operation hours testing
Pavone (France)	2005	(Simulation) Innovative Reactor Concept Monolith CLC-reactor with alternate feeding of air and natural gas	Monolith CLC-reactor model development by considering one channel and assuming the reactor as consisting of a bundle of identical channels Scaling for mesh number reduction Flowrates, concentrations and temperature calculation Optimisation with respect to volumetric flowrate of air to extract maximum work from the gas turbine
Naqvi, Bolland, Wolf (Norway & Sweden)	2006	(Simulation) Pressurised circulating fluidised bed reactor system	Reactor system design and implementation in a combined cycle for off-design evaluation
Rydén, Lyngfelt (Sweden)	2006a	(Simulation) Hydrogen production using steam reforming of natural gas in CLC Material: NiO/Al_2O_3 Gases: CH_4/H_2O/Air	Process, reformer tube, reactors and heat exchanger network design Reformer efficiency comparable to the conventional steam reformers Higher selectivity towards H_2 can be achieved as compared to the conventional steam reforming plants
Rydén, Lyngfelt, Mattisson (Sweden)	2006b	Continuous natural gas reforming with $NiO/MgAl_2O_4$ as oxygen carrier Synthesis gas generation for production of pure H_2 through water-gas shift	Complete conversion of natural gas achieved High selectivity towards H_2 and CO 41 hours of reforming recorded Formation of solid carbon recorded in some cases Adding 25% steam to the natural gas reduced or eliminated the solid carbon formation

The work by Lyngfelt et al. [2004] stands for a major advancement in the development of CLC. This is the first demonstration of all the fundamental facets of CLC and the experimental findings of this work can be regarded as greatly promising. Moreover, the Lyngfelt and co-workers have also accomplished the task of constructing the world's first functional CLC-prototype and no serious problems have been observed as per documented by Lyngfelt et al. Therefore, there exists a great incentive for continuing CLC development.

Characterisation of Reactor Systems

The two reactors in CLC are of different types as regards their operations and must meet certain requirements depending on the nature of the gases present and the reactions taking place inside each of the two. The reduction reactor should ideally achieve a very high degree of fuel conversion and selectivity towards CO_2 so that it can be assured that the exhaust stream is reasonably pure and constitutes of CO_2 and water vapour in high concentrations. Also, the rate of oxidation must be high enough to transfer heat to large amounts of air in the oxidation reactor. In addition, the desired solids amounts must be transported between the reactors without the solids being undergone excessive mechanical stresses.

The state-of-the-art reactor technology can be employed in order to realise CLC in operation. The solids circulation in CLC is very much alike that taking place in the process of fluid catalytic cracking (FCC) that is a widely used process of major commercial importance. However, CLC differs from FCC that the CLC oxygen carriers undergo chemical reactions, but FCC solids act as catalyser. In general, fluidised beds offer several appealing advantages to an application such as CLC. One of the most tempting advantages is that the fluidised beds can provide an outstanding gas-solid heat and mass transfer. Another advantage is the liquid-like behaviour of the fluidised solids thereby simplifying the handling and transportation of large amounts of solids within the system. Moreover, the bulk of solids present inside the reactors provide a thermal reservoir that defies any rapid temperature changes thus maintaining a stable temperature of the gases leaving the reactors. This property is advantageous not only in terms of a stable operation but also when CLC is implemented in power cycles and incorporated with the standard power plant machinery.

Bubbling fluidised beds offer high gas conversion rates and are suitable for large-scale operations with a diversity of solids. The reactor interior also provides favourable conditions for heat. The reactor temperature can be maintained and controlled through solids recirculation rates. One of the drawbacks of such a reactor is the problems associated with erosion of pipes and immersed objects. Also there may be high particle attrition rates. Moreover, deep beds usually have high pressure drops that will certainly result in an efficiency penalty for CLC implemented in power cycles.

Fast fluidised beds with pneumatic transport of solids are appropriate for fast reactions and fine solids. The co-current nature of the reactor allows achieving high conversion rates of solids. The pressure drop in such a reactor is particle size-dependant and large solids generally result in higher pressure drop. Therefore, use of fine solids will result in a low pressure drop thereby making it suitable for CLC implementation in power cycles. But as far as erosion and particle attrition are concerned, they cannot be avoided completely and are still experienced in this reactor regime; mainly due to the high local velocities within a transport reactor. The internal heat exchange is not as good as that in bubbling beds but heat transport to and from the reactor can be facilitated with circulation of solids.

By virtue of its well documented suitability as a gas-solid reaction system [Kunii and Levenspiel, 1991], the concept of interconnected fluidised beds as the reactor system of choice is assumed in virtually all publications on CLC. There are, however some alternatives, of which two will be discussed here.

In order to realise a practical, feasible and operable working solution for CLC, a combination of two fluidised beds operating in different flow regimes can be provided. Such a configuration is presented in Figure 3.2. The oxidation reactor is a pneumatic transport reactor where solids are lifted by the air entering the reactor at a certain superficial velocity. The solids are separated from the hot oxidation air in a cyclone system and are lead to a buffer-tank before being transported into the reduction vessel in a controlled manner. The reduced solids flow back to the air reactor under the action of gravity. The two reactors are separated by a system of valves providing a steady and controllable flow of oxygen carrier with a minimum of gas leakage. Recent studies of gas leakage between reactors by Johansson et al. [2003] indicate that this problem can be controlled by relatively simple means. This reactor system regime can be applied in CLC with modifications and adaptations with respect to controlling the solids flowrate between the two reactors.

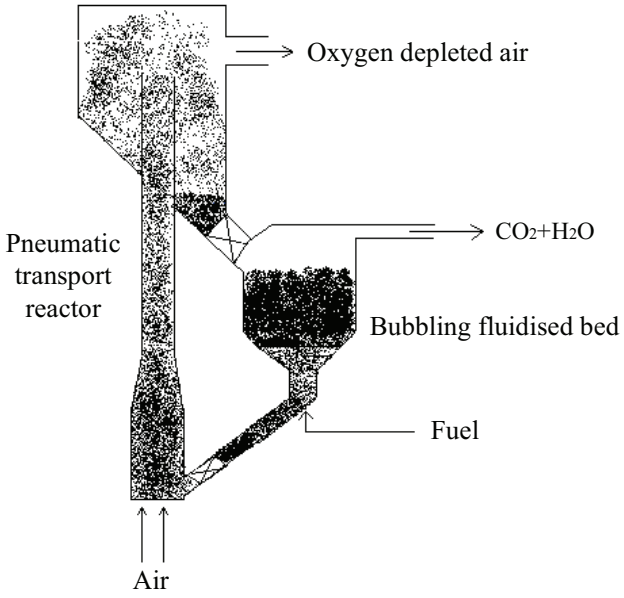

Figure 3.2 Schematic sketch of reactor system without gas/solid separation equipment

Although the cyclic regenerative operation in the CLC implies that a conventional circulating fluidised bed reactor system for solids circulation is a suitable set-up, yet innovative concepts of reactor system also exist. An alternative is the rotating CLC-reactor system resembling the 'CO_2 wheel' proposed by Shimomura [2003]. The idea of rotating reactor system is to absorb CO_2 by formation of lithium carbonate and is based on the principle that the oxygen carrier is immobilised in a rotary reactor where fuel and air are introduced into separated compartments as shown in Figure 3.3. The rotary CLC-reactors concept is currently in the early phase of research and concept development at Alstom [Jukkola et al. 2003]. This concept has not been evaluated and implemented in this thesis; however its principle and operation are briefly described here. The cylindrical reactor is comparable to a fixed bed and needs to be divided into channels running longitudinally along the vessel in order to prevent any mixing of gases within the cylinder. The oxygen

carrier has to be provided in the form of channels with active surfaces. When channels with small hydraulic diameters are used, the gases flow is laminar. This approach results in low pressure drop across the reactor. With rotary reactor scheme, the gases entry and exit requires separate gas-handling units at the both ends of the reactor. The gas-handling units feed the reactant gases, the inert gas for air and fuel purging, and the exhaust gases.

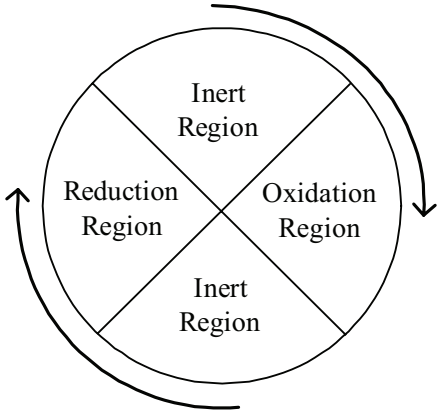

Figure 3.3 Rotary CLC-reactor schematic

The gas-handling units have to be stationary in order to incorporate the reactor with other unit operations when applied in a power cycle. This means that the reactor itself will rotate (either continuously or in discrete steps) with respect to the gas handling units and potentially lead to some gas leaks. The same chemistry as that for conventional CLC outlined in section 3.2 will apply and there will in principle be two effluent streams; a stream rich in CO_2 and a stream of oxygen depleted air. The carrier is reduced with fuel/steam in the reduction region whereas hot air regenerates the carrier in the oxidation region. Oxygen depleted air may be used as fluid in the inert regions.

Pavone [2005] presented implementation of CLC in monolith structures where the oxygen carrier is immobilised and is present in the form of a thin washcoat on the walls of narrow channels running along the axis of the reactor. The concept is very interesting and can prove to be a ground breaking technology if successfully realised in CLC. This type of reactor has many advantages over the conventional reactor systems, low pressure drops in particular. The gases can diffuse into the oxygen carrier material quite easily by virtue of very thin layer of the oxygen carrier. Such a reactor system can also be made very compact by increasing the number of cells per square inch along the diameter of the reactor. Nevertheless, the reactor poses a very high degree of novelty. If single reactor design is applied, it essentially requires injection of some inert gas, preferably steam, between the successive runs of oxidation and reduction reaction. When applied in real applications in conjunction with compressor and gas turbine, such an arrangement may result in time delays thereby introducing in the system instabilities. Therefore, in order to apply monolith CLC-reactor concept in power plants, multi-monolith-reactors would be a better and pragmatic approach where the reactors are based on a batch process. However, such an arrangement also demands for advanced control strategies with a series of valves and ducting arrangement. This concept is at an early stage of its development and requires further development on various aspects.

3.3.3 Modelling and Simulation/Cycle Studies

Apart from the research on oxygen carriers and reactor system for CLC, it is also important to investigate the power producing potential of CLC. Concept development and cycle evaluation are two indispensable features for development of innovative technologies like CLC. The CLC-reactors are modelled and incorporated into different power cycles for carrying out simulations. Parameters sensitivity studies are carried out for various suitable plant configurations in order to estimate net plant efficiency. Simulations of this type are, to a large extent, dependent on the choice of assumptions made for the cycle studies. When simulating a CLC power cycle, the assumptions regarding oxygen carrier and reactor system performance should be fairly realistic. In this way a CLC power cycle can be compared to a conventional cycle. Thermodynamic analysis of the power producing potential of CLC is essential in all phases of CLC research & development. First of all, the goal is to establish a theoretical basis for the potential of the process, and secondly to investigate the characteristics of CLC implemented in already existing power cycles.

The sparse availability of real experimental data on long term operation of continuous CLC systems may result in unrealistic assumptions. That may result in simulations becoming prone to errors, unrealistic and idealised with regard to the possible downsides of CLC. Nevertheless, simulation results help setting 'benchmarks' for oxygen carrier development; as they indicate reaction temperatures and conversion rates of solids at which reasonable cycle efficiencies can be achieved. Moreover, they add value to the CLC-research by indicating the challenges in tailoring CLC towards state-of-the-art power plants machinery. Since 1983, there has been a continuous contribution by different research groups to CLC power cycle studies. Table 3-4 provides an overview of the literature related to modelling and simulation including CLC-cycles studies.

Table 3-4 Literature related to cycle studies

Authors (Country)	Year	Carrier Fuel/oxidiser	Cycles Issues	Results
Richter, Knoche	1983	Generalised	Concept introduction and thermodynamic analysis of CLC potential	Increased exergetic efficiency as compared to conventional combustion
Ishida et al. (Japan)	1987	NiO Saturated CH_4/Air	CLC-GT Brayton cycle Exergy analysis	CLC-GT: 50.2% efficiency (LHV) Reactants preheating reduces exergy losses
Harvey, Richter (USA)	1994	Fe_2O_3/FeO CH_4	CLC-SOFC with reforming of fuel	Maximum theoretical efficiency 78.4% (LHV) and 69% with losses

Ishida, Jin (Japan)	1994b	NiO CH_4/Air	Study of CLC power cycle with air saturation (CLSA) and steam injected gas turbine (STIG) with exergy diagrams	Efficiency (LHV): CLSA: 55.1%) STIG: 48.4% Exergy losses reduced in CLC
Anheden, Näsholm, Svedberg (Sweden)	1995	NiO CH_4/Air	CLC comparison with a conventional GT cycle	CLC has less combustion irreversibilities as compared to a conventional GT CLC has the advantage of easy CO_2 separation despite a lower thermal efficiency
Anheden, Svedberg (Sweden)	1996	NiO Fe_2O_3 Mn_3O_4 CH_4/Air Simulated coal gasification syngas	CLC in combination with integrated coal gasification	CLC with integrated coal gasification compared with a conventional IGCC system The studied systems have the same efficiencies as the conventional IGCC but CLC systems have easy CO_2 separation
Jin, Ishida (Japan)	1998	NiO, Fe_2O_3 CH_4/Air and simulated coal gasification syngas	CLC-GT cycles compared with conventional GT cycles	Efficiencies for CLC-GT cycles similar or higher than conventional GT cycles Exergy losses are lower in CLC-GT
Anheden, Svedberg (Sweden)	1998	NiO Fe_2O_3 CH_4/Air Fuel gas from simulated coal gasification	CLC in combination with gas turbine systems simulated with methane and NiO CLC in combination with fuel gas simulated with NiO and Fe_2O_3	Reduced exergy losses in CLC-processes Thermal efficiency of CLC systems is comparable or less to the conventional systems but CLC has the advantage of easy CO_2 separation

Anheden, (Sweden)	2000	NiO Fe_2O_3 Mn_3O_4 CH_4/Air Simulated coal gasification syngas	CLC-GT Brayton cycles comparison with the conventional GT cycle CLC in combination with integrated coal gasification Exergy analysis of CLC systems	Doctoral Thesis Reduced exergy losses in CLC-processes Thermal efficiency of CLC systems is comparable or less to the conventional systems but CLC has the advantage of easy CO_2 separation
Wolf, Anheden, Yan (Sweden)	2001	Fe_2O_3 Methane/Air	CLC-Combined Cycle Sensitivity study of two cycles and comparison with a conventional combined cycle	Thermal efficiency of conventional cycle 56.4% without CO_2 capture Both CLC-CC achieve efficiency of about 52% with CO_2 capture
Wolf, Yan (Sweden)	2004	NiO CaO for CO_2 separation in a calcination reactor Methane/Air	Cogeneration of Hydrogen and electricity with extended CLC and its comparison with classical CLC	The extended CLC is feasible from the thermodynamic point of view and has potential for hydrogen and electricity
Brandvoll, Bolland (Norway)	2004	NiO/YSZ Methane/ Humid air	CLC-HAT Parameter variation Exergy analysis	Cycle efficiency: 55.9% With CO_2 compression cycle efficiency is 52%
Consonni et al. (Italy)	2004	Fe_2O_3 Natural gas/Air	CLC-Combined Cycle with and without supplementary firing Cost estimation	Unfired and fired cycles efficiency 48% and 52%, respectively, cost of avoided CO_2: 50-60 €/ton
Naqvi et al. (Norway)	2004	$NiO/NiAl_2O_4$ Natural gas/Air	CLC-Combined Cycle CLC-Steam Cycle Turbine Cooling Sensitivity study: Efficiency Cooling penalty Exhaust recirculation Solids flowrates Degree of fuel	CLC Combined Cycle: Efficiency: 52.3% (PR=18, Tox=1200 C) CLC-Steam Cycle: efficiency 41% with CO_2 compression 0.5%-point loss in efficiency for each %-point decrease in fuel conversion

Wolf (Sweden)	2004	Fe and Ni based carriers Natural gas/Air	Reactors sensitivity study Study on some combined cycle configurations Hydrogen production in combination with CLC	Doctoral Thesis The CLC-combined cycles can achieve net plant efficiency of above 50% while cogeneration with hydrogen production may result in a thermal efficiency of about 54%
Wolf, Anheden, Yan (Sweden)	2005	$NiO/NiAl_2O_4$ Fe_2O_3/Al_2O_4 Methane/Air	CLC-Combined Cycle Comparison of the oxygen carriers Reactor system layout	No significant difference in cycle efficiency if both oxygen carriers operate at the same temperature
Kronberger Löffler, Hofbauer (Austria)	2005	Mn, Ni, Cu, Fe-oxides on SiO_2 $CH_4/CO/H_2/$ Air	Simulations of mass and energy balances of a CLC system	Model developed for selection of oxygen carriers; the model allows identification of operating ranges for different carriers
Naqvi, Wolf, Bolland (Norway & Sweden)	2006	$NiO/NiAl_2O_4$ Natural gas/Air	Part-load evaluation of a CLC-Combined Cycle Reactors design Solids internal recirculation Pressure drops	CLC-CC relative efficiency at part load is better than a conventional CC CO_2 turbine should be avoided to balance pressure at reactors' exit
Naqvi, Bolland (Norway)	2006	$NiO/NiAl_2O_4$ Natural gas/Air	Multi-stage CLC for combined cycles with reheat air turbine	Above 51% efficiency at oxidation temperature of 1000°C with reheat

Two main topics of investigation can be recognised from Table 3-4 and; cycle analyses that have mainly focused on comparative studies of different variants of CLC, and secondly, exergy analyses of CLC and its comparison with a conventional combustion processes. Generally, all simulations of CLC-power cycles show promising results in terms of high efficiency and high degree of CO_2 capture. However, there may be some uncertainties associated with the CLC-cycles due to lack of consistent and established data for long term operation of CLC-reactors. Even so, the potential of CLC has been found to be promising when applied to a number of cycles, including simple GT cycles, combined cycles, conventional steam cycles, and humid air turbine cycles and even with integrated coal

gasification. Important requirements on reactor temperatures and pressures have also been revealed, providing goals for materials development. Furthermore, all exergy analyses performed on the CLC concept show reduced losses as compared to conventional combustion. Considering the early stage of CLC development, not many efforts have been made towards dimensioning and sizing of a CLC power plant and its evaluation in off-design mode or transient behaviour prediction. This is due to many unresolved issues regarding the CLC-reactors and lack of experimental data especially for pressurised reactors. The only work on CLC-reactors sizing and its implementation in a combined cycle to perform part-load evaluation has been presented by Naqvi et al [2006]. Considering the high potential of CLC and the pace of CLC-research, more contribution to this issue can be expected in the future.

4 Modelling and Simulation Basis

This chapter describes mathematical models of different unit-operation components used in various CLC-power cycles. The core components are the CLC-reactors which are developed as a lumped model in a single unit. All other components are state of the art unit-operations which are extensively used in conventional power cycles. These include compressor, gas turbine, steam turbine, heat recovery steam generator, gas-to-gas heat exchanger, gas-to-steam-heat exchanger, steam-to-steam heat exchanger, pump and valve. Each of these components is modelled as an individual unit so that a component-model library is formed. This approach provides the flexibility that the individual models can also be altered and modified according to the specific requirements, whether CLC-specific or cycle-specific. Hence, all the cycle configurations that will be presented in the forthcoming chapters are set up by joining the individual component models in a hierarchical fashion. The methodology to analyse and benchmarking various power cycle concepts is to keep a similar and consistent definition of work and efficiency which are defined in this chapter. Most of the models are implemented in the simulation tool gPROMS [PSE, Inc.]; if not, the simulation tools are mentioned otherwise. In gPROMS, the thermodynamic properties for all streams except pure steam/water were calculated with the software Multiflash [PSE, Inc.], using the SRK equation of state. For steam and water, the IAPWS-IF97 steam table was used. A common basis for the cycle analysis is established in the form of computational assumptions included in Appendix A; which enables a transparent comparison between different cycle concepts and their comparison with the reference cases.

4.1 CLC-Reactors

The section contains the description of reactor system modelling in Chemical Looping Combustion (CLC). In order to study various CLC-power cycles, it is essential to provide a heat and mass balance for the heterogeneous solid-gas reactions taking place in the CLC-oxidation and reduction reactors. In addition, a model involving the reactors' geometry is required that takes into account the reactors dimensions, solids residence times and transport between the two reactors as well as pressure drops in connection with the proposed reactors concept. Such a model can be incorporated with the heat and mass balance model for the sake of dimensioning and sizing a certain CLC-power plant for further off-design evaluation. The two mathematical models are described in the following sections.

4.1.1 Heat and Mass Balance Model

In the following, the heat and mass balance will be given in accordance with the CLC-reactor system schematic in Figure 4.1. Based on the co-current nature of transport reactors, it can be a reasonable assumption that solids at the two reactors exit are in thermal equilibrium with the gaseous streams leaving their corresponding reactors. The CLC-reactors may operate as an adiabatic system or a non-adiabatic system; and heat balance for both the states will be presented in the following.

Considering the CLC-reactors schematics in Figure 4.1, separate boundary conditions can be applied around the oxidation reactor (OX), the reduction reactor (RED) and for the overall reactor system. Therefore in the following, the heat and mass balance is given for the two

reactors as well as for the overall reactor system. The terms oxidation and reduction refer to the conversion of metal to metal oxide; and metal oxide to metal, respectively.

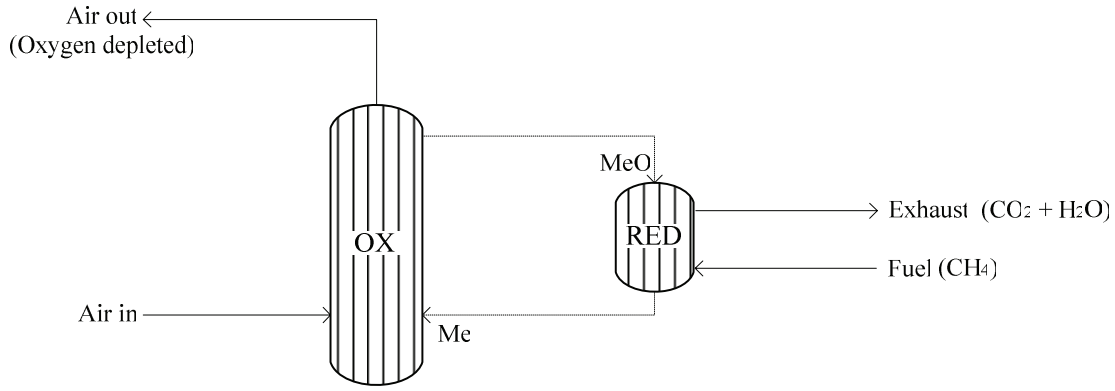

Figure 4.1 Schematics of a CLC-reactor system

When treating the reactors as an adiabatic system, the oxidation reactor heat balance can be written as follows:

$$\dot{H}_{MeO} = \dot{H}_{air,in} + \dot{H}_{Red} - \dot{H}_{air,out} - \dot{Q}_{OX} \quad (4.1)$$

The heat balance over the reduction reactor is given by the following:

$$\dot{H}_{Me} = \dot{H}_{fuel} + \dot{H}_{MeO} + \dot{Q}_{RED} - \dot{H}_{exhaust} \quad (4.2)$$

In Equation 4.1 and 4.2;

$\dot{H}_{Meo}$ = Enthalpy in the solid stream leaving the oxidation reactor and entering the reduction reactor

$\dot{H}_{air,in}$ = Enthalpy in the air stream at the oxidation reactor inlet

$\dot{H}_{Me}$ = Enthalpy in the solid stream leaving the reduction reactor and entering the oxidation reactor

$\dot{H}_{air,out}$ = Enthalpy in the oxygen-depleted air stream leaving the oxidation reactor

$\dot{Q}_{OX}$ = Heat of the oxidation reaction (defined as negative)

$\dot{H}_{fuel}$ = Enthalpy in the fuel at the reduction reactor inlet

$\dot{Q}_{RED}$ = Heat of the reduction reaction (defined as positive)

$\dot{H}_{exhaust}$ = Enthalpy in the exhaust stream leaving the reduction reactor

Although none of the components taking part in the heterogeneous reactions undergo phase change; in this work it has been chosen to calculate the enthalpy in each stream as enthalpy difference with respect to the reference state using SRK equation of state. This can be done by utilising the commercially available physical properties calculation packages; Multiflash [PSE, Inc.] being used in this work. The sensible heat in each of the gaseous streams is thus retrieved by the following expression:

$$\dot{H}_j = \dot{n}_j \cdot h_j \left(T_j, P_j, x_j \right) \tag{4.3}$$

In Equation 4.3, j corresponds to a certain gaseous stream; while $\dot{n}$ is molar flowrate, h is specific enthalpy at the temperature T, pressure P and molar composition x.

Regarding the solid streams, the enthalpy in each stream has to be calculated on the basis of specific heat capacity and temperature difference, since Multiflash does not provide the solids' properties. Since a number of metal oxide and inert supports have been evaluated in the CLC-reactors sensitivity study, the specific heat capacity of each material is calculated according to its respective polynomial equation.

The specific heat capacity of a solid stream is thus calculated by the following expression:

$$c_{p,x} = \sum_{i=1}^{n} \left(c_{p,i} \right) \tag{4.4}$$

It is important to consider that each solid stream may contain metal, metal oxide and the inert stabiliser. In Equation 4.4, i corresponds to the solid species and therefore the specific heat capacity of a solid stream is the summation of all the solid species contained in it. Similarly the flow rate of each solid stream is the summation of flow rate of all the species.

Heat of oxidation and reduction is calculated using the standard enthalpy of formation of reacting components at the corresponding reference temperature. Equations 4.5 and 4.6 give the heat of oxidation and reduction, respectively.

$$\dot{Q}_{OX} = \dot{n}_{MeO} \cdot \overset{\circ}{h}_{f,MeO} \tag{4.5}$$

$$\dot{Q}_{RED} = \dot{n}_{MeO} \cdot \overset{\circ}{h}_{f,MeO} + \sum_{i=1}^{n} \left(\dot{n}_i \cdot \overset{\circ}{h}_{f,i} \right)_{fuel} - \sum_{i=1}^{n} \left(\dot{n}_i \cdot \overset{\circ}{h}_{f,i} \right)_{exhaust} \quad (4.6)$$

In Equations 4.5 and 4.6;

$\dot{n}_{MeO}$ = Molar flowrate of the metal oxide

$\overset{\circ}{h}_f$ = Standard enthalpy of formation

Also, the subscript 'fuel' corresponds to the reacting components in the fuel and the subscript 'exhaust' corresponds to the exhaust products as a result of the reduction reaction.

The overall heat balance for an adiabatic reactor system can thus be written as follows:

$$\dot{H}_{air,in} + \dot{H}_{fuel} = \dot{H}_{air,out} + \dot{H}_{exhaust} - \dot{Q}_{LHV} \quad (4.7)$$

When CLC is applied in non-adiabatic air reactor, the overall heat balance becomes:

$$\dot{H}_{air,in} + \dot{H}_{fuel} = \dot{H}_{air,out} + \dot{H}_{exhaust} - \dot{Q}_B - \dot{Q}_{LHV} \quad (4.8)$$

In Equation 4.8, $\dot{Q}_B$ is the heat that crosses the boundary of the oxidation reactor. This heat can be utilised in any side process, for instance it can be used to generate steam.

In Equations 4.7and 4.8, $\dot{Q}_{LHV}$ is the sensible heat given off by the fuel as a result of combined intermediate oxidation and reduction reactions, given by the following:

$$\dot{Q}_{LHV} = \dot{Q}_{OX} - \dot{Q}_{RED} \quad (4.9)$$

The molar specific heat of reaction (q_{rx}) per mole of a given fuel can be calculated as follows:

$$q_{rx} = \frac{\left(\dot{Q}_{OX} - \dot{Q}_{RED} \right)}{\sum_{i=1}^{n} \left(\dot{n}_i \right)_{fuel}} \quad (4.10)$$

The oxidation and reduction temperature are calculated by Equation 4.11.

$$T_x = \frac{\dot{Q}_x + \left\{ \dot{n}_x \cdot Cp_0\left(T_0\right) \cdot T_0 \right\}}{\dot{n}_x \cdot Cp_x\left(T_x\right)} \tag{4.11}$$

In Equation 4.10, 'i' correspond to the solid (metal, metal oxide or inert stabiliser). Whereas, in Equation 4.11, 'x' corresponds to either reduction or oxidation and '0' corresponds to the reference state.

Since the model is based on the assumption that the solids at each reactor's exit are in thermal equilibrium with their corresponding gaseous stream leaving the reactors exit, therefore it can be written that:

$T_{ox} = T_{air,\,out}$ and $T_{red} = T_{exhaust}$

Mass balance over the reduction and oxidation reactor is given by Equation 4.12 and 4.13, respectively.

$$\dot{m}_{air,\,in} + \dot{m}_{total,\,red} - \dot{m}_{air,\,out} - \dot{m}_{total,\,ox} = 0 \tag{4.12}$$

$$\dot{m}_{fuel} + \dot{m}_{total,\,ox} - \dot{m}_{exhaust} - \dot{m}_{total,\,red} = 0 \tag{4.13}$$

In Equation 4.12 and 4.13;

$\dot{m}_{total,red}$ = Total mass flowrate of the solid stream leaving the reduction reactor

$\dot{m}_{total,red}$ is given by Equation 4.14.

$$\dot{m}_{total,\,red} = X_{red} \cdot \dot{m}_{ox} + \left(1 - X_{red}\right)\dot{m}_{red} + \dot{m}_{inert} \tag{4.14}$$

$\dot{m}_{total,ox}$ = Total mass flowrate of the solid stream leaving the oxidation reactor

$\dot{m}_{total,ox}$ is given by Equation 4.15.

$$\dot{m}_{total,\,ox} = X_{ox} \cdot \dot{m}_{ox} + \left(1 - X_{ox}\right)\dot{m}_{red} + \dot{m}_{inert} \tag{4.15}$$

In Equation 4.14 and 4.15;

$\dot{m}_{ox}$ = Mass flowrate of metal oxide in a solid stream; i.e. converted metal in the oxidation reactor or unconverted metal oxide in the reduction reactor

$\dot{m}_{red}$ = Mass flowrate of metal in a solid stream; i.e. converted metal oxide in the reduction reactor or unconverted metal in the oxidation reactor

$\dot{m}_{inert}$ = Mass flowrate of the inert stabiliser in a solid stream

X is degree of reaction in both the oxidation and reduction reactor and is defined by Equation 4.16.

$$X = \frac{m - m_{red}}{m_{ox} - m_{red}} \tag{4.16}$$

In Equation 4.16, m_{red} is mass of metal oxide when it is fully reduced and m_{ox} is its mass when it is fully oxidised; while m stands for mass of metal oxide at a certain time. Hence:

$X_{red} = 0.0$ For complete reduction of metal oxide to metal

$X_{ox} = 1.0$ For complete oxidation of metal to metal oxide

It is of significance to mention the oxygen consumption in the air reactor and its transfer to the fuel reactor. Equations 4.17 and 4.18 reflect the function of the oxygen carrier in the oxidation and reduction reactor, respectively.

$$\dot{m}_{air,out} = \dot{m}_{air,in} - \dot{m}_{oxygen,rx} \tag{4.17}$$

$$\dot{m}_{exhaust} = \dot{m}_{fuel} + \dot{m}_{oxygen,rx} \tag{4.18}$$

In Equation 4.17 and 4.18, $\dot{m}_{oxygen,rx}$ is the mass flowrate of the oxygen that is extracted by the oxygen carrier thereby making the air oxygen-depleted. The same oxygen is then supplied to the fuel by the oxygen carrier in the reduction reactor and hence the exhaust flowrate is the sum of the fuel supplied and the oxygen supplied by oxygen carrier.

The overall mass balance can thus be written as:

$$\dot{m}_{air,in} + \dot{m}_{fuel} = \dot{m}_{air,out} + \dot{m}_{exhaust} \tag{4.19}$$

The mass flowrate of each stream is calculated according to the following:

$$\dot{m}_j = \dot{n}_j \cdot MW_j \tag{4.20}$$

In Equation 4.20, $\dot{n}$ is the total molar flowrate of a stream and is summation of the molar flowrates of constituent components of each stream, while MW is the total molecular weight of stream j.

The oxygen consumption in the reactor system is based on the stoichiometry of the combustion reaction i.e. reaction of metal with oxygen in the air, in case of CLC. The amount of oxygen needed can be formulated as follows:

$$\dot{n}_{oxygen} = \sum_{i=1}^{n} \left(S_i \cdot \dot{n}_i \right)_{fuel} \tag{4.21}$$

In Equation 4.21, 'i' corresponds to the hydrocarbon constituents of the fuel while S corresponds to the stoichiometric coefficient.

In order to accomplish a proper mass balance on the basis of stoichiometry of the chemical reactions taking place in the reactors, all the streams are defined on molar basis (index 'n'). Figure 4.2 exemplifies the overall molar balance for the reactor system with complete conversion of the fuel (natural gas) and the oxygen carrier ($NiO/NiAl_2O_4$). This work does not take into account incomplete reaction of fuel resulting in CO and H_2. The heat and mass balance model is based on complete stoichiometric conversion of fuel i.e. 1 mole of methane reacts with 2 moles of oxygen to form 1 mole of CO_2 and 2 moles of H_2O and the same holds for other components of natural gas. However, the model does consider the extent of fuel conversion. Despite complete stoichiometric conversion, some portion of fuel may not react with the solids due to insufficient residence time or design limitations of the reduction reactor. Under such a condition, there can be some unreacted fuel components in the exhaust stream as shown in Figure 4.2.

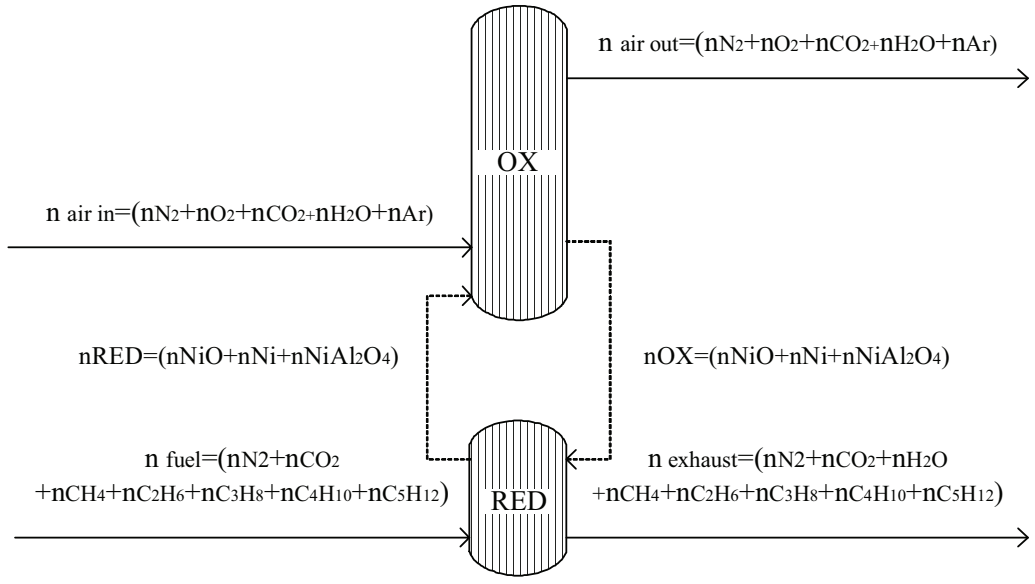

Figure 4.2 Molar balance for the CLC-reactor system

In order to analyse CLC at such a condition, a factor 'degree of fuel conversion' is defined, which is given by Equation 4.22.

$$\varphi = \frac{n_{rx,fuel}}{n_{fuel}} \qquad (4.22)$$

In Equation 4.22, $n_{rx,fuel}$ is the number of moles of fuel actually reacting with the oxygen carrier and n_{fuel} is the number of moles of fuel supplied. Therefore, according to Equation 4.23, at φ=1, all the fuel reacts with the solids and is converted into CO_2 and H_2O, while at φ=0, no fuel reacts with the solids at all.

4.1.2 Model Involving Reactors' Geometry

A circulating fluidised bed (CFB) reactor is considered to be the most appropriate system for a regenerative cyclic process like Chemical Looping Combustion [Lyngfelt et al., 2001]. This section describes the reactor system modelling for an interconnected fluidised bed reactor (IFBR) system. Figure 4.3 shows the reactor design with two interconnected pressurised fluidised bed reactors (IFBR), where the fuel reactor is a bubbling bed and the air reactor is essentially a pneumatic transport reactor. The solids (metal oxide and inert oxygen carrier) are separated from the hot air by a cyclone system similar to the one in a pressurised fluidised bed combustion (PFBC) system.

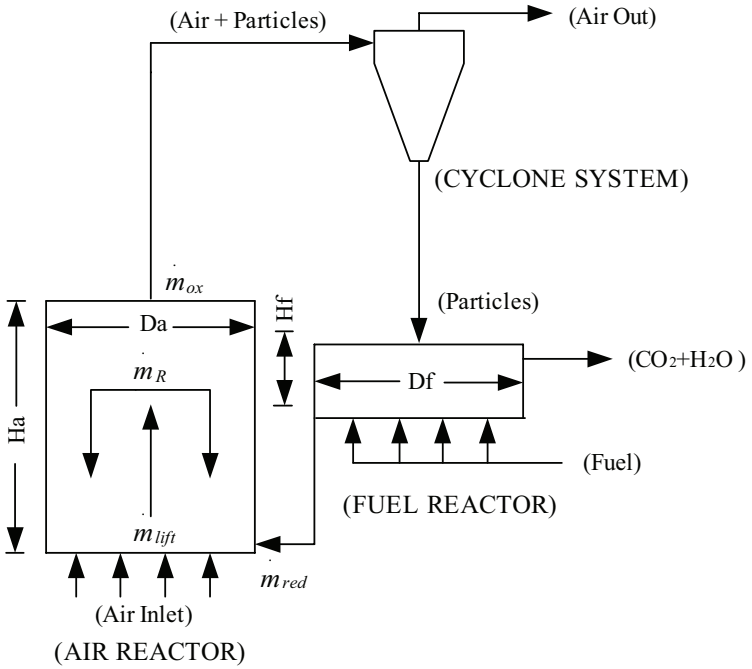

Figure 4.3 Schematics of interconnected fluidised bed reactor system for CLC

The system shown in Figure 4.3 is an interconnected fluidised bed reactor (IFBR) system where the riser is a pneumatic transport reactor. The air velocity controls the flowrate of solids between the reactors. The faster the air flows through the air reactor, the more solids will be entrained. The amount of the solids that can be transported from the riser into the cyclone is influenced by a number of parameters. In order to comprehend the phenomenon of pneumatic transport of solids, it is important to have an overview of different parameters that influence the solids transport.

The solids transport is a function of the superficial air velocity at the reactor inlet and air density while the air density is a function of temperature and pressure in the air reactor. Also, the amount of solids transported by the air depends on the solids density and diameter, since the terminal falling velocity of solids is a function of these parameters. In addition, the terminal falling velocity is a function of drag coefficient and the density ratio between the solids and air. The drag coefficient is further a function of the Reynolds number which in turn is a function of solids terminal falling velocity, density of air, solids diameter and dynamic viscosity of the air lifting the solids. In addition, there is internal recirculation of solids in the air reactor that affects the solids residence time as well as pressure drop in the air reactor. In this section, all these parameters are used to establish expressions to predict the behaviour of the CLC-reactor system applied in CFB reactor system.

The reduced (fully or partially) solids along with the inert material are transported from the fuel reactor to the air reactor under gravity. At this point air has a certain solids lifting capacity, assumed as in Equation 4.23.

$$\dot{m}_l = A_a \cdot \rho_s \cdot \varepsilon \cdot \left(u_0 - u_T\right) \tag{4.23}$$

In Equation 4.23, $\dot{m}_l$ is the maximum flowrate of solids or the lifting capacity of air, A_a is the cross-sectional area of the air reactor, ρ_s is the average density of solids and ε is the average solids fraction in the air reactor, while u_0 and u_T are the superficial air velocity at the reactor inlet and terminal falling velocity of solids, respectively.

The superficial air velocity is calculated by Equation 4.24.

$$u_0 = \frac{\dot{m}_{air}}{A_a \cdot \rho_{air}} \tag{4.24}$$

In Equation 4.24, ρ_{air} is the density of air at the oxidation (reactor exit) temperature.

The terminal falling velocity of solids is calculated by Equation 4.25.

$$u_T = \left[\frac{4 \cdot g \cdot d_p}{3 \cdot C_D} \cdot \left(\frac{\rho_s}{\rho_{air}} - 1\right)\right]^{1/2} \tag{4.25}$$

In Equation 4.25, g is acceleration due to gravity, d_p is the average diameter of solids and C_D is the drag coefficient, which is calculated by Equation 4.26.

$$C_D = \frac{a_1}{Re_T{}^b} \tag{4.26}$$

In Equation 4.26, Re_T is Reynolds Number of solids at terminal falling velocity and is given by Equation 4.27.

$$Re_T = \frac{u_T \cdot d_p \cdot \rho_{air}}{\mu} \quad (4.27)$$

The constants a_1 and b can be approximated as Howard [1989], given in Table 4-1.

Table 4-1 Constants a_1 and b for calculation of the drag coefficient

Range of Re_T	**Region**	**a_1**	**b**
$0 < Re_T < 0.4$	Stoke's Law	24	1
$0.4 < Re_T < 500$	Intermediate	10	0.5
$500 < Re_T$	Newton's Law	0.43	0

In the riser (air reactor), there is certain internal recirculation of solids, which also affects solids transport out of the reactor. The internal recirculation ratio 'I' is here defined by Equation 4.28.

$$I = 1 - R \quad (4.28)$$

In Equation 4.28, R is the entrainment ratio of the solids in the air reactor, defined in Equation 4.29. The objective of defining the entrainment ratio of solids in the air reactor is to determine the solids residence time and air pressure drop. Therefore, entrainment ratio is a significant parameter in this regard and it is quite rational to define it in the following way:

$$R = \frac{\dot{m}_{ox}}{\dot{m}_{lift}} \quad (4.29)$$

In Equation 4.29, $\dot{m}_{lift}$ is the flowrate of solids lifted by the air at the air reactor inlet; while $\dot{m}_{ox}$ is the flowrate of solids eventually transported out of the air reactor. So that; When R=0, the reactor behaves as a steady-state fluidised bed and when R=, $\dot{m}_{ox} = \dot{m}_{lift}$, i.e. there is no internal recirculation of solids and all the solids are transported out of the reactor in a single pass and hence there is no internal recirculation of solids.

The internal recirculation results in an increased overall solid fraction in the riser. The overall solid fraction in the air reactor can be defined in terms of solids entrainment ratio and solid fraction at the exit of a pneumatic transport reactor, as given in Equation 4.30.

$$\varepsilon = \frac{(2 - R) \cdot \varepsilon_{se}}{R} \quad (4.30)$$

In Equation 4.30, ε_{se} is the solid fraction at the exit of a pneumatic transport reactor and is typically is in the range of 0.001-0.003. Hence, ε_{se} is here assumed to be 0.0015.

Entrainment ratio (R) determines flowrate of solids eventually transported out of the air reactor ($\dot{m}_{ox}$) after the conversion (oxidation). R is here defined a function of the difference in superficial air velocity and solids terminal velocity Δu (Equation 4.31).

$$\Delta u = u_0 - u_T \tag{4.31}$$

The internal recirculation of solids decreases with an increase in superficial velocity (which means that R increases), since the terminal falling velocity remains constant at a certain temperature and pressure, until a threshold point is reached where all the solids are blown out of the reactor without any recirculation. The difference in the two velocities at the threshold point can be denoted as Δu_{TH} and be set equal to a real number. After the threshold point, an increase in the superficial air velocity has no effect on the internal recirculation and the continuous pneumatic transport prevails. Entrainment ratio can then be defined by Equation 4.32.

$$R = \begin{cases} \dfrac{1}{\Delta u_{TH}} \Delta u & \Delta u - \Delta u_{TH} < 0 \\ 1 & \Delta u \geq \Delta u_{TH} \end{cases} \tag{4.32}$$

Figure 4.4 represents the outcome of Equation 4.32. This work assumes that that threshold point occurs at Δu_{TH}=2.5 where all the solids are transported out of the air reactor and thus there is no internal recirculation of solids.

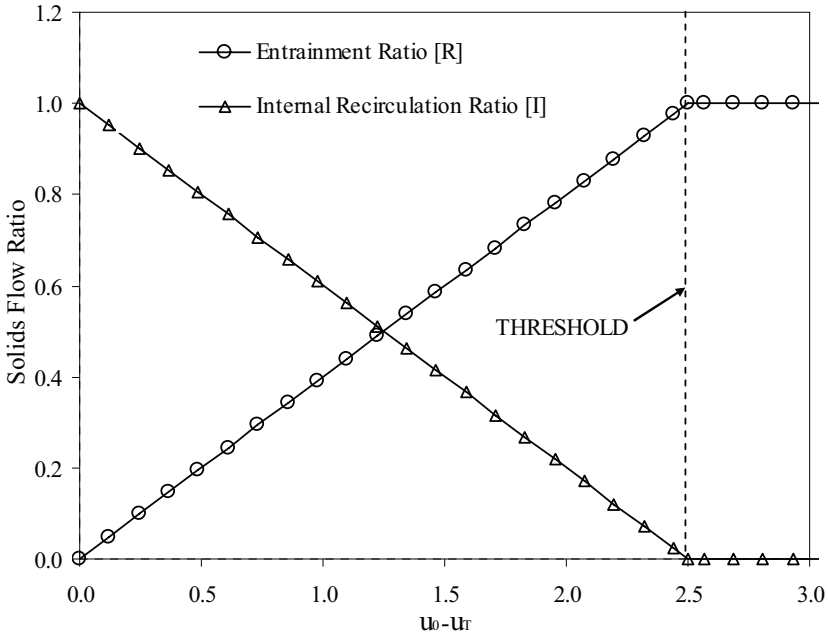

Figure 4.4 Solids flow ratios in the air reactor

The hold up of solids (M_a) or the mass of solids present in the air reactor can then be calculated by Equation 4.33.

$$M_a = A_a \cdot H_a \cdot \rho_s \cdot \varepsilon \quad (4.33)$$

In Equation 4.33, A_a and H_a are the area and height of the riser, respectively.

The average residence time of the solids in the air reactor (τ_a) is then calculated by Equation 4.34.

$$\tau_a = \frac{M_a}{\dot{m}_{lift}} \quad (4.34)$$

The average solids residence time in the fuel reactor (τ_f) is given by Equation 4.35.

$$\tau_f = \frac{2 \cdot M_f}{\dot{m}_{red} + \dot{m}_{ox}} \quad (4.35)$$

In Equation 4.35, $\dot{m}_{red}$ are the solids flowing out of the fuel reactor and M_f is the hold up of solids in the fuel reactor and is given by Equation 4.36.

$$M_f = A_f \cdot H_f \cdot \rho_s \cdot \varepsilon_f \quad (4.36)$$

In Equation 4.36, A_f and H_f are the area and height of fuel reactor, respectively. The term ε_f corresponds to the average solids fraction in the fuel reactor and is assumed to be 0.4, considering that the fuel reactor is a bubbling bed reactor.

Various variables associated with the fuel reactor can be calculated by making use of the equations described for the air reactor calculations by replacing the variables and parameters for the air reactor with those for the fuel reactor.

Pressure Drop in Air and Fuel Reactor

The pressure drop ΔP in the air and fuel reactor is calculated by Equation 4.37.

$$\Delta P = \Delta P_B + \Delta P_D \quad (4.37)$$

In Equation 4.37, ΔP_B is pressure drop in the fluidised bed and ΔP_D is pressure drop caused by the gas distributor.

The pressure drop over the fluidised bed (ΔP_B) is calculated by using Equation 4.38, which is derived from the hydrodynamics described by Carberry and Varma [1986], and Kunii and Levenspiel [1991].

$$\Delta P_B = 1.2 \cdot \frac{M \cdot g}{A} \quad (4.38)$$

In Equation 4.38, M is hold up of solids in the reactor (air or fuel), g is acceleration due to gravity and A is cross-sectional area of the reactor (air or fuel reactor).

The pressure drop due to the gas distribution is given by Equation 4.39.

$$\Delta P_D = 0.4 \cdot \Delta P_B \tag{4.39}$$

4.2 Compressor

The model is used for air compression before the air reactor. The compressor model calculates the temperature and pressure at the compressor discharge by using the physical properties of the incoming gas. The enthalpy change during the compression process is used to calculate the compressor work as well as the temperature and pressure at the compressor discharge.

Considering isentropic compression, $\Delta s=0$. But also:

$$\Delta s_c = s\left(T_{is,out}, P_{out}, x\right) - s\left(T_{in}, P_{in}, x\right) \tag{4.40}$$

In Equation 4.40, x corresponds to the molar composition of gas. The isentropic outlet temperature can be calculated with Equation 4.40. The isentropic enthalpy change can be calculated with the following equation:

$$\Delta h_{is,c} = h\left(T_{is,out}, P_{out}, x\right) - h\left(T_{in}, P_{in}, x\right) \tag{4.41}$$

In order to calculate the real enthalpy change, the isentropic efficiency of compressor ($\eta_{is,c}$) is used as given by Equation 4.42.

$$\Delta h_c = \frac{\Delta h_{is,c}}{\eta_{is,c}} \tag{4.42}$$

In Equation 4.42, Δh_c is the real enthalpy change, which is used to further calculate the outlet condition of the gas and is given by the following equation:

$$\Delta h_c = h\left(T_{out}, P_{out}, x\right) - h\left(T_{in}, P_{in}, x\right) \tag{4.43}$$

The real enthalpy change is then used to calculate the compressor work provided that the gas flowrate is known, as given by Equation 4.44.

$$\dot{W}_{comp} = -\dot{m} \cdot \Delta h_c \tag{4.44}$$

The minus sign in Equation 4.44 shows that the compressor work is negative, since the real enthalpy change calculated according to Equation 4.43 is positive. Therefore, this work is based on the convention of negative input work, which is also mentioned in section 4.10, ‘Definitions of Work and Efficiency’.

4.2.1 Off-design Model for Compressor

A compressor characteristic map for a large axial compressor was implemented in the generic compressor model to evaluate compressor performance in the off-design mode. Dimensional analysis shows that for a given compressor, the performance is determined from the following quantities:

Reduced speed:

$$N_{red} = \frac{N}{\sqrt{T_{in}\gamma_{in}R}} \tag{4.45}$$

Reduced flowrate:

$$\dot{m}_{red} = \frac{\dot{m}\sqrt{T_{in}}}{P_{in}}\sqrt{\frac{R}{\gamma_{in}}} \tag{4.46}$$

Pressure ratio: π_c

Isentropic efficiency: η_{is}

In order to facilitate a potential alternation of the design point, the variables used for describing the compressor map are divided by the values of the variables at the compressor design point, thus making a set of normalised variables. The set of normalised variables required for establishing the compressor characteristics in the off-design mode are given in the following:

Normalised reduced speed:

$$\bar{N}_{red} = \frac{N_{red}}{N_{red,0}} \tag{4.47}$$

Normalised reduced mass flow:

$$\bar{\dot{m}}_{red} = \frac{\dot{m}_{red}}{\dot{m}_{red,0}} \tag{4.48}$$

Normalised pressure ratio:

$$\bar{\pi}_c = \frac{\pi_c}{\pi_0} \tag{4.49}$$

Normalised isentropic efficiency:

$$\bar{\eta}_{is} = \frac{\eta_{is}}{\eta_{is,0}} \tag{4.50}$$

Other quantities describing compressor behaviour can be represented in the same fashion.

Representation of Normal Speed Characteristics

The mathematical model representing the normal speed characteristics is developed from a compressor map in Thermoflex [Thermoflow Inc.]. The Thermoflex map covers normalised reduced speeds from 0.3 to 1.2; however the mathematical model used in this work includes the reduced speed lines only from 0.5 to 1.2. This range of reduced speed lines covers the normal operating range of a compressor. The given data is for a compressor that operates with fully open inlet guide vanes (IGV).

The Ellipse Approach

As a means to represent the relationship between reduced speed, reduced flowrate and pressure ratio; the ellipse approach has been used. Each line for constant reduced speed can be described using the ellipse equation, which is given in the following:

$$\left(\frac{\bar{\dot{m}}_{red}}{a}\right)^z + \left(\frac{\bar{\pi}_c}{b}\right)^z = 1 \tag{4.51}$$

In Equation 4.51; a, b and z are functions of reduced speed. The ellipse approach can be used to generate a compressor map. Figure 4.5 shows the map generated with the help of the ellipse equation and its comparison with a map generated from Thermoflex. The data from Thermoflex is used to find parameters a, b and z in Equation 4.51.

Figure 4.5 presents the agreement between the Thermoflex map and the map generated in this work. With the ellipse approach, three of the four quantities determining the compressor behaviour i.e. normalised reduced speed, reduced flowrate and reduced pressure ratio, are related. In order to also include the isentropic efficiency, points are found on the compressor map giving the isentropic efficiency as a function of reduced speed and pressure ratio. These points are the basis of the black lines shown in Figure 4.6, where the isentropic efficiency is shown as a function of pressure ratio with constant reduced speed lines. The efficiency for a certain speed and pressure ratio is calculated in two steps. First of all, an expression for the maximum efficiency and the pressure ratio at that point is developed as a function of reduced speed. Maximum efficiency and the related pressure ratio are expressed as a function of reduced speed using polynomials. The second step is to define a pressure ratio correction factor (PRCF). PRCF is needed in order to account for the deviation in pressure ratio between the maximum efficiency point and the actual pressure ratio at the operating reduced speed. PRCF is calculated by Equation 4.52.

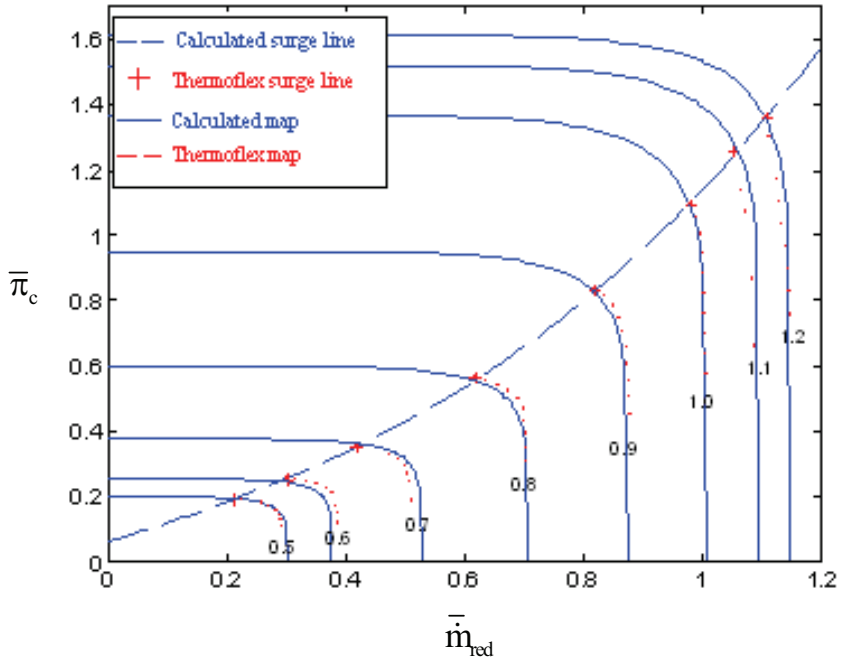

Figure 4.5 Comparison of the Thermoflex compressor map and the compressor map calculated with the ellipse approach.

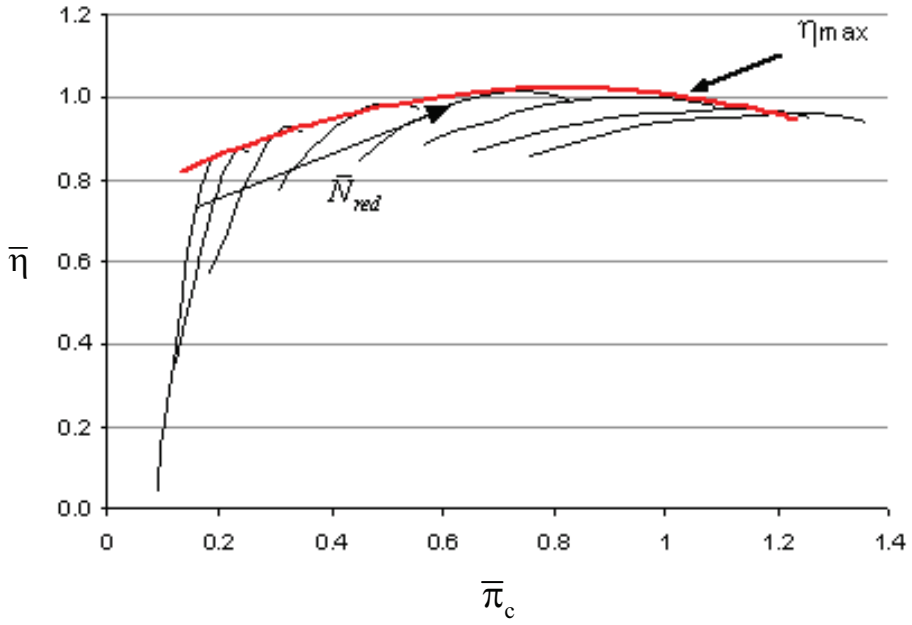

Figure 4.6 The Thermoflex efficiency data shown in black. The red line shows a polynomial fitting to the maximum efficiency vs. reduced speed.

$$PRCF = PolyA(\overline{N}_{dim}) \cdot \overline{\pi}_{norm}^2 + PolyB(\overline{N}_{dim}) \cdot \overline{\pi}_{norm} + PolyC(\overline{N}_{dim}) \qquad (4.52)$$

In Equation 4.52, PolyA, PolyB and PolyC are third degree polynomial functions of the reduced speed. The efficiency at the operating point is then given by:

$$\bar{\eta} = \eta_{max} \cdot PRCF \tag{4.53}$$

In Equation 4.53, η_{max} is the maximum efficiency as a function of speed, given as:

$$\eta_{max} = e1 \cdot \bar{N}_{dim}^3 + e2 \cdot \bar{N}_{dim}^2 + e3 \cdot \bar{N}_{dim} + e4 \tag{4.54}$$

A comparison between the efficiency data from the compressor map and the calculated efficiency is shown in Figure 4.7.

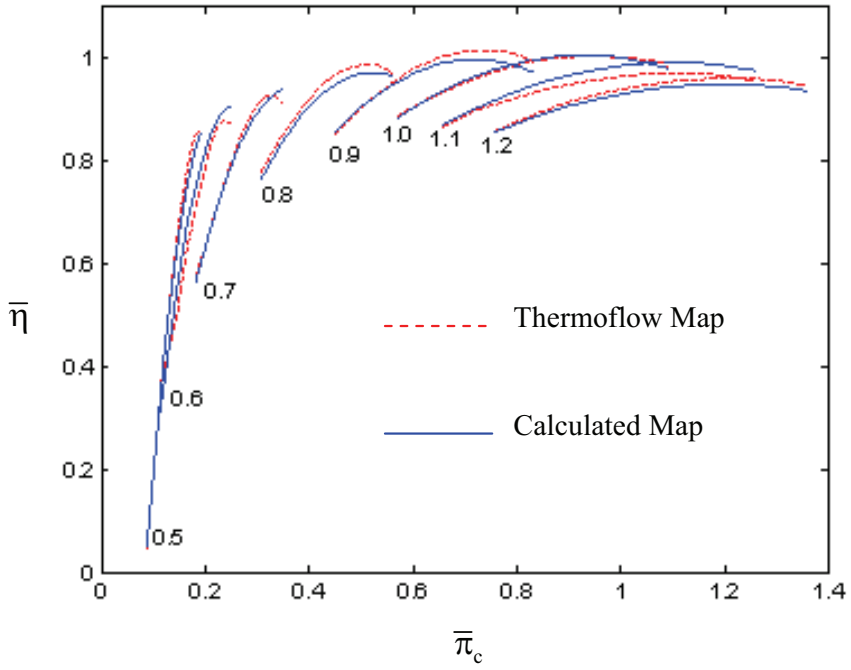

Figure 4.7 Comparison between Thermoflex efficiency and calculated efficiency

4.2.2 Implementation of VGV-Calculation Method

A reduced compressor mass flow can be achieved by using variable guide vanes (VGVs) at the compressor inlet. Closing the guide vanes does in fact impose a geometry change on to the compressor, which implies that the compressor map compressor map yielding fully open VGVs becomes no longer valid. Instead of introducing new compressor maps for the new compressor geometries arising as a result of VGVs implementation, a modification to the existing map can be performed. A compressor map with the speed line at the design point is shown in Figure 4.8. When the VGVs are closed down, the compressor mass flow will be reduced thus moving this speed line to the left on the map. The more the VGVs are closed, the further to the left the speed line will move. The design speed line for the fully closed VGVs is also shown in the figure. The line is horizontally moved to the left, giving the same surge pressure ratio for the total range of VGV angles. In order to be able to model the VGVs effect on the compressor parameters, two variables are introduced; (1) VGVRelax and (2) Relax. VGVRelax as a function of load is shown in Figure 4.8, where Relax is the gradient in Equation 4.55.

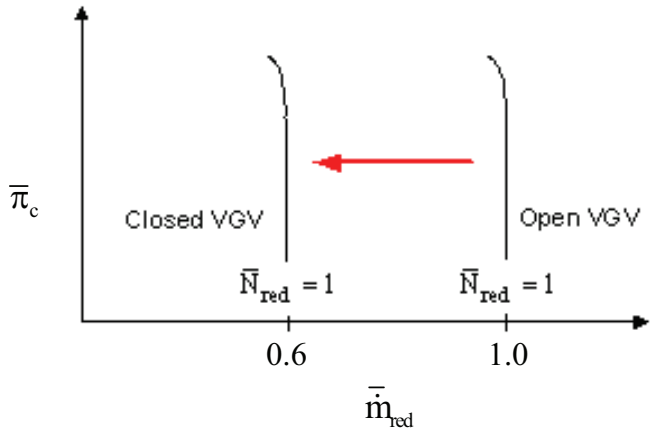

Figure 4.8 Influence on a constant reduced speed line in a compressor map introducing VGV-closing

$$\mathrm{VGV}Relax = 1 + Relax \cdot (\mathrm{Load} - 1) \tag{4.55}$$

The term Load in Equation 4.55 is defined by the following:

$$\mathrm{Load} = \frac{\dot{W}_{GT}}{\dot{W}_{GT,Design}} \tag{4.56}$$

Relax equal to zero will give 'VGVRelax' equal to 1 throughout the total load area, representing the compressor map for a system without VGVs. A value of 'Relax' greater than zero implies that the VGVs are closing at part load. The greater the value of 'Relax', the greater the mass flow reduction is for a given part load.

Reduced flow rate for fully open VGVs is calculated with the compressor map. The VGV-effect is calculated in the following way:

For VGVRelax > 1 (VGVs are fully open for VGVRelax = 1):

$$\bar{\dot{m}}_{red} = \bar{\dot{m}}_{red,\ NoVGV} \tag{4.57}$$

For 0.7 < VGVRelax ≤ 1:

$$\bar{\dot{m}}_{red} = \mathrm{VGV}Relax \cdot \bar{\dot{m}}_{red,\ NoVGV} \tag{4.58}$$

For VGVRelax < λ (VGVs are fully closed):

$$\bar{\dot{m}}_{red} = \alpha \cdot \bar{\dot{m}}_{red,NoVGV} \tag{4.59}$$

In Equation 4.59, λ is the lower limit of VGVs, i.e., below that VGVs cannot be closed further and is assumed a value of 0.6.

The compressor map is incorporated in the generic compressor model when needed to evaluate a cycle in the off-design mode.

4.3 Turbine

The turbine is modelled in the same way as compressor. Considering isentropic expansion, $\Delta s=0$. But also:

$$\Delta s_t = s\left(T_{in}, P_{in}, x\right) - s\left(T_{is,out}, P_{out}, x\right) \tag{4.60}$$

In Equation 4.60, x corresponds to the molar composition of gas. The isentropic outlet temperature can be calculated with Equation 4.60. The isentropic enthalpy change can be calculated with the following equation:

$$\Delta h_{is,t} = h\left(T_{in}, P_{in}, x\right) - h\left(T_{is,out}, P_{out}, x\right) \tag{4.61}$$

In order to calculate the real enthalpy change, the isentropic efficiency of turbine ($\eta_{is,t}$) is used as given by Equation 4.62.

$$\Delta h_t = \Delta h_{is,t} \cdot \eta_{is,t} \tag{4.62}$$

In Equation 4.62, Δh is the real enthalpy change, which is used to further calculate the outlet condition of the gas and is given by the following equation:

$$\Delta h_t = h\left(T_{in}, P_{in}, x\right) - h\left(T_{out}, P_{out}, x\right) \tag{4.63}$$

The real enthalpy change is then used to calculate the turbine work provided that the gas flowrate is known, as given by Equation 4.64.

$$\dot{W}_{turbine} = \dot{m} \cdot \Delta h_t \tag{4.64}$$

The turbine work is positive because of the positive real enthalpy change calculated by Equation 4.63.

Throughout the different cycles presented in the chapters to follow, the turbine model is frequently used for the air turbine while some cycles also employ a 'CO_2-turbine' that operates on CO_2/steam mixture as the working fluid. The gas turbine model is applicable solely for an uncooled turbine unless a cooling model is incorporated to calculate the efficiency drop due to cooling. In this work, only the air turbine is considered to be cooled. The conventional cooling techniques cannot be applied to the CO_2-turbine because the working fluid is generated in a reactor before turbine, without any compression process of the working fluid prior to the reactor. Since the working fluid is CO_2/steam mixture therefore the compressed air can also be not used as the cooling media. One choice of cooling technique for the CO_2-turbine would be advanced closed loop steam cooling, but that is not evaluated in this work. Since the CO_2-turbine operates at relatively lower temperatures, so for the sake of simplicity, no cooling model is implemented for the CO_2-

turbine. The turbine cooling model described in the following section is therefore applied to the air turbine.

4.3.1 Turbine Cooling

The efficiency and specific work output of a gas turbine increase by raising turbine inlet temperature (TIT). The modern gas turbines operate at high inlet temperatures (TIT). The higher the TIT the higher is the net work; however, it leads to an increase in the cooling demand for the gas turbine. With the current gas turbine technology, the gas turbine cycle can achieve an efficiency as high as 40% or higher. In order to improve this efficiency, increased TIT and pressure ratio is inevitable that also results in an increased turbine cooling demand. The development in gas turbines has made it possible to operate the gas turbines at the turbine inlet temperatures of 1300-1400°C and a compressor pressure ratio of 30. The next generation gas turbines are expected to operate at TIT of about 1500°C. The increased TIT results in the demand for material that can withstand high temperatures; and cooling of the turbine components exposed to the hot gas i.e., blades, rotor and turbine housings. Surfaces of the gas turbine components exposed to hot gas need to be maintained below a certain safe working temperature at which they show mechanical stability and corrosion resistance. Typically, the maximum temperature that turbine metal can withstand without any cooling demands is 850°C. An increase in temperature results in the following impacts:

- Thermal fatigue
- Fractures formation
- Corrosion

The above-said wear and tear effects intensify if turbine load is frequently changed and frequent starting up and shutting down of the turbine. Consequently, the turbine efficiency will reduce over a certain period of time of operation. In order to avoid the strain on the turbine components, efforts are focussed on two major areas. One way is to employ highly thermal resistant components, for instance single crystal materials and ceramic coatings; while the other option is to utilise the coolant air as efficient as possible. The higher the TIT, the higher is the temperature difference between hot gas and blade surface. In cooled turbines, mixing of coolant with hot gas results in thermodynamic penalties due to stagnation temperature reduction and pressure losses, and aerodynamic losses. For a given level of cooling technology, raising TIT beyond a certain limit results in such cooling penalties that cycle efficiency drops. These penalties can be reduced by minimising the coolant flow. It is achieved by improving internal heat transfer between the coolant and the blade; and reducing the blade external heat transfer coefficient.

Turbine Cooling Model Implementation

The foremost objective of implementing a cooling model in CLC-combined cycle is to determine the amount of cooling air required over a range of turbine inlet temperature and compressor pressure ratio. There are different approaches for modelling turbine cooling; however, considering the implementation in a CLC-based gas turbine, the approach adopted for this work is given in Figure 4.9. The present model implies mixing of the combustor exit stream and the cooling air stream before the expansion in the turbine.

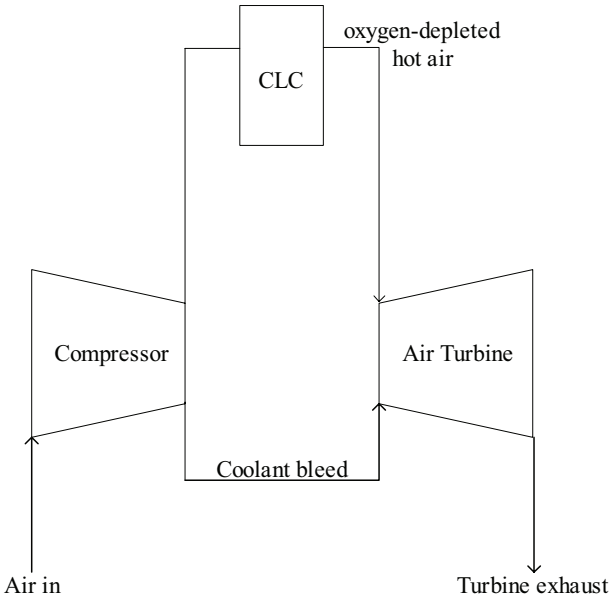

Figure 4.9 The turbine cooling approach

The air at the compressor discharge is split into two streams; one flows to the CLC-air reactor; while the other stream mixes with the hot air stream coming out of the CLC-air reactor. The cooling air penalties are assumed lumped together in the mixing of the two streams. This simplified approach is considered to be sufficient, because of the relatively low temperatures (900-1200°C) and small cooling air flowrates (0-9%) applied in the current work. This work is based on the turbine cooling model presented by Bolland and Stadaas [1995].

The Meta-modelling Approach

In order to consider a state-of-the-art gas turbine, the technology level was derived from data available for the gas turbine GE93519FA in GTPRO [Thermoflow, Inc.]. The cooling model produced the results in terms of coolant fraction as percent of turbine exhaust for different TIT and compressor pressure ratio values, as shown in Figure 4.10. There are two reasons for relating the cooling air demand to the exhaust gas flowrate; bleeding off the coolant air makes the flowrate at compressor discharge lower than that at the compressor inlet, and oxygen is consumed in the combustor (or CLC-reactor). Therefore, if presented as compressor flowrate fraction, the cooling air does not reflect the total flowrate through the system. However, since the turbine exhaust contains all the streams, i.e. coolant stream and the combustion products, therefore it is quite appropriate to present the coolant fraction as percentage of turbine exhaust. Figure 4.10 served as the basis for developing a meta-model for coolant fraction estimation. Based on the results from Bolland and Stadaas model [1995], a two-dimensional third order polynomial equation was generated that treats CF as a function of both and TIT, i.e.:

$$CF = f\left(\pi_c, TIT\right) \quad (8 \geq \pi_c \leq 26 \text{ and } 900°C \geq TIT \leq 1200°C) \qquad (4.65)$$

In Equation 4.65, π_c is the compressor pressure ratio. The term TIT refers to the combustor exit temperature and not the real turbine inlet temperature, which is lower due to the mixing of the hot and the cold streams.

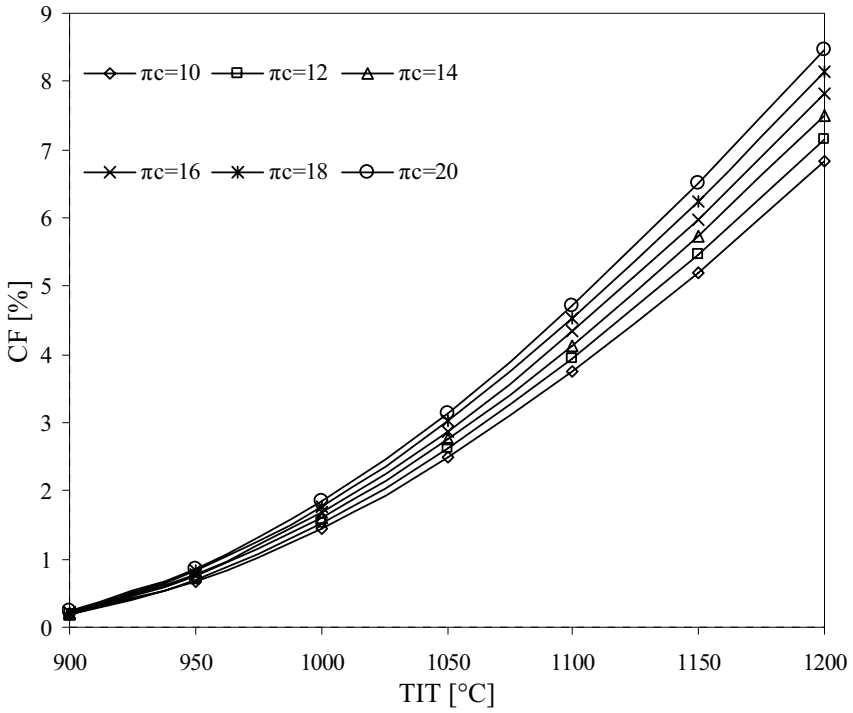

Figure 4.10 Coolant fraction as percent of turbine exhaust

The results generated with the polynomial equation were counterchecked against the data over a wide range of compressor pressure ratio and turbine inlet temperature. The equation was then incorporated in the cooled turbine model and the coolant demand was then calculated by Equation 4.66.

$$\dot{m}_{coolant} = CF \cdot \dot{m}_{exhaust,turbine} \tag{4.66}$$

However, this is somewhat a different scenario in a CLC-air turbine because oxygen is not only consumed in the air reactor but also not recovered back to the turbine. Also, Figure 5 holds for a gas turbine with 10 mbar back pressure turbine operating on air/methane combustion products while the working fluid in CLC-turbine is oxygen-depleted air.

4.3.2 Off-design Model of a Turbine

In order to estimate performance of a turbine in off-design mode, it is necessary to establish performance characteristics. In order to generalise this work, characteristic quantities are used for an axial flow turbine, which is choked at various load conditions. The characteristic quantities are then used in the standard choked nozzle equation [Saravanamuttoo et al., 2001], which is given by Equation 4.67.

$$\overline{FR}^2 = \frac{\left(\overline{P_{in}}^2\right)}{\overline{TIT}} \qquad (4.67)$$

In Equation 4.67, $\overline{FR}$ is dimensionless flowrate at the turbine inlet, $\overline{P_{in}}$ is the dimensionless turbine inlet pressure and $\overline{TIT}$ is dimensionless turbine inlet temperature. In this work, the working fluid molecular weight and the mean specific heat capacity ratio are assumed constant. Each dimensionless variable can be defined as the ratio between the variable at a certain operating point and its value at the design point. In all the equations to follow in this section, numerator corresponds to a certain operating point and denominator corresponds to the design point. The dimensionless variables are given in the following:

Dimensionless flowrate:

$$\overline{FR} = \frac{\dot{m}}{\dot{m}_0} \qquad (4.68)$$

Dimensionless turbine inlet pressure:

$$\overline{P_{in}} = \frac{P_{in}}{P_{in,0}} \qquad (4.69)$$

Dimensionless Turbine inlet temperature:

$$\overline{TIT} = \frac{TIT}{TIT_0} \qquad (4.70)$$

The simplicity and ease in implementation of choked nozzle equation lies in the fact that the equation suggests the same reduced mass flow at two different load-states. Moreover, with the help of this equation the turbine performance can be evaluated independent of the rotational speed. Since the turbine inlet temperature and pressure change in the off-design mode, the cooling demands also vary. Therefore, a suitable expression for the coolant air flowrate in the off-design mode is also needed to be formulated. There are two major strategies for determining the coolant fraction. It can either be assumed as the same as at full-load; or it can be assumed that the coolant flow is choked. The latter approach has been adopted for the present work. The off-design performance of the CO_2-turbine can also be evaluated with the help of the choked nozzle equation that was presented in Equation 4.67. Equation 4.67 presented choked nozzle equation for a typical turbine whose working fluid molecular weight and specific heat capacity changes at different operating conditions. The coolant air has constant molecular weight regardless of the operating condition and the CO_2-stream can also be assumed to have constant molecular weight provided that the fuel conversion rate is constant. The specific heat capacity of the air and the CO_2-stream can also be assumed constant over a range of temperature. Thus the dimensionless molecular weight and dimensionless mean specific heat capacity ratio can be omitted from the choked nozzle equation, presented in Equation 4.67.

Equations 4.71 and 4.72 present the governing equations for the coolant air flowrate and the CO_2-turbine at off-design, respectively. The equations are basically derived from the choked nozzle equation given by Equation 4.67; however they are based on the assumption of constant gas molecular weight and mean specific heat capacity ratio.

The coolant air flowrate at off-design is thus calculated by using the following variant of the choked nozzle equation:

$$\frac{P_{coolant}}{P_{coolant,0}} = \frac{\dot{m}_{coolant}}{\dot{m}_{coolant,0}} \cdot \sqrt{\frac{T_{coolant}}{T_{coolant,0}}} \tag{4.71}$$

The CO_2-turbine performance at off-design is governed according to the following equation:

$$\frac{P_{in,CO_2-turbine}}{P_{in0,CO_2-turbine}} = \frac{\dot{m}_{in,CO_2-turbine}}{\dot{m}_{0,CO_2-turbine}} \cdot \sqrt{\frac{TIT_{CO_2-turbine}}{TIT_{0,CO_2-turbine}}} \tag{4.72}$$

4.4 Heat Exchanger

The generic heat exchanger model is based on the following assumptions:

- Steady-state counter flow heat exchanger
- No heat transfer area calculation
- Pressure drops given as percentages of the inlet pressures
- Pressure and temperature profiles calculated by using distributed variables
- No heat loss

The model is based on the convention that the heat exchanger consists of 'n' number of segments, where the hot fluid enters at the segment '0' while the cold fluid enters at the segment 'n', as shown in Figure 4.11.

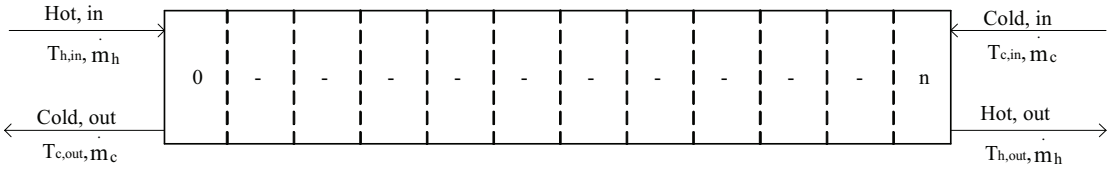

Figure 4.11 The counter-flow heat exchanger

Considering the energy balance around the heat exchanger, the overall duty Q is given by Equations 4.73 and 4.74, respectively.

$$Q = \dot{m}_c \cdot \left(h_{c,out} - h_{c,in} \right) \tag{4.73}$$

$$Q = \dot{m}_h \cdot \left(h_{h,in} - h_{h,out} \right) \tag{4.74}$$

Equations 4.73 and 4.74 imply that there is no heat loss since the hot-side duty is equal to the cold-side duty. The enthalpy 'h' of the hot and cold fluids in Equations 4.73 and 4.74 can thus be calculated at their corresponding temperatures and pressures.

The cold-end and the hot-end temperature difference defined according to Equation 4.75 and 4.76, respectively.

$$\Delta T_c = \Delta T_n = \left(T_{h,out} - T_{c,in} \right) \tag{4.75}$$

$$\Delta T_h = \Delta T_0 = \left(T_{h,in} - T_{c,out} \right) \tag{4.76}$$

For a heat exchanger consisting of 'n' number of segments with 'i' corresponding to a certain segment, the hot-side and cold-side pressure profile is calculated by Equation 4.77 and 4.78, respectively.

$$P_{h,i} = P_{h,0} \cdot \left(\frac{\left(1 - \left(PL_h \cdot i \right) \right)}{n} \right) \quad (0 \le i \le n) \tag{4.77}$$

$$P_{c,i} = P_{h,n} \cdot \left(\frac{\left(1 - PL_c \cdot \left(n - i \right) \right)}{n} \right) \quad (0 \le i \le n) \tag{4.78}$$

In Equations 4.77 and 4.78, PL is the fraction pressure loss over the hot side or the cold side.

The duty in one segment of heat exchanger is calculated according to the following:

$$\dot{Q}_i = \frac{i \cdot \dot{Q}}{n} \quad (0 \le i \le n) \tag{4.79}$$

In Equation 4.79, $\dot{Q}$ is the overall duty of heat exchanger. Since the model is based on the assumption of no heat loss, the overall duty is the same as the duty on the hot-side and the duty on the cold-side. Hence, the hot-side and the cold-side duty of heat exchanger are calculated according to Equation 4.80 and 4.81, respectively.

$$\dot{Q} = \frac{n \cdot \dot{m}_h \cdot \left(h_{hot,0} - h_{hot,i} \right)}{i} \quad (0 \le i \le n) \tag{4.80}$$

$$\dot{Q} = \frac{n \cdot \dot{m}_c \cdot \left(h_{cold,0} - h_{cold,i} \right)}{i} \quad (0 \leq i \leq n) \tag{4.81}$$

The model is applied for three heat exchanger types given in the following:

- Gas/Gas heat exchanger
- Gas/Steam heat exchanger
- Steam/Water heat exchanger

Each heat exchanger type is briefly discussed in the following section.

4.4.1 Gas/Gas Heat Exchanger

The model is applicable for pure gases and the gas mixtures except saturated pure water in two-phase. The reason is that enthalpy is calculated from temperature and pressure and not the steam quality as given in the following:

$$h = h\left(P, T\right) \tag{4.82}$$

Throughout this work, the model is extensively used where the heat exchange is between gas mixtures, i.e. as air preheater and fuel preheater.

4.4.2 Gas/Steam Heat Exchanger

The model is based on the following:

- Hot stream: Gas
- Cold stream: Steam/Water

This type of heat exchanger can further be categorised into two types:

- Heat Exchanger for latent heat transfer i.e. evaporator or boiler
- Heat Exchanger for sensible heat transfer i.e. economiser or superheater

When used as economiser or superheater the cold outlet condition is specified by giving the approach temperature (ΔT_{app}) given as follows:

$$\Delta T_{app} = T_{sat} - T_{cold,out} \tag{4.83}$$

In Equation 4.83, T_{sat} is the saturation temperature. The approach temperature is positive for subcooled liquid and negative for superheated vapour. For saturated conditions, i.e. when used as evaporator the steam quality is provided as the input data.

4.4.3 Steam/Water Heat Exchanger

The model is used for two components:

- Condenser
- Feedwater preheater

When used for condenser, the hot stream i.e. steam outlet condition is specified by giving the approach temperature for subcooled liquid, as given by Equation 4.84.

$$\Delta T_{app,hot} = T_{sat} - T_{out,hot} \quad (\Delta T_{app} > 0) \tag{4.84}$$

While for saturated conditions, the steam quality (x=0-1) is specified. The model calculates the temperature differences between saturated vapour and condensing steam and between saturated liquid and condensing steam.

When used in fed water preheater, there are certain constraints. Figure 4.12 depicts the approach used for feedwater preheaters in this work.

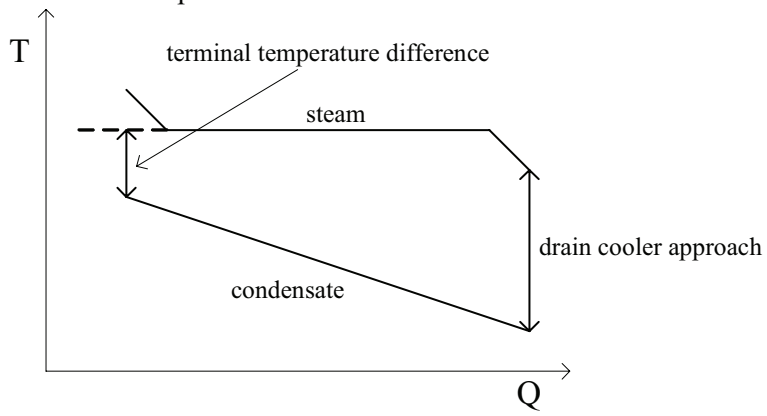

Figure 4.12 Temperature profiles of cold and hot fluid in a feed water preheater

One of the two approaches can be specified for performance calculation of feed water preheater. When it is desired to equally distribute the overall duty for water preheating between the numbers of preheater units, some of the units are equipped with desuperheater and subcooler. The two approaches shown in Figure 4.12 then serve the purpose to specify the conditions for desuperheater and the subcooler.

4.4.4 Off-design Model of Heat Exchanger

In order to evaluate the off-design performance of a heat exchanger the design point has to be established. It is common practice to formulate the design-point overall duty of a heat exchanger in the form of following equation:

$$Q = U \cdot A \cdot F \cdot (LMTD) \tag{4.85}$$

In Equation 4.85, Q is the total heat load to be transferred, U is the overall heat transfer coefficient referred to the overall heat transfer area A. F is the configuration correction factor and depends on the type of heat exchanger selected. In this work F has been assumed unity. LMTD is the logarithmic mean temperature difference for a purely counter-current flow configuration and is given by the following:

$$LMTD = \frac{\Delta T_h - \Delta T_c}{\ln \frac{\Delta T_h}{\Delta T_c}} \tag{4.86}$$

In Equation 4.86, ΔT_h and ΔT_c correspond to the hot-end and cold-end temperature difference of a heat exchanger, respectively.

Also, the hot side duty is equal to the cold side duty, i.e.:

$$Q = \dot{m}_c \cdot \Delta h_c \tag{4.87}$$

$$Q = \dot{m}_h \cdot \Delta h_h \tag{4.88}$$

During the off-design calculation, the hot fluid inlet temperature ($T_{h,in}$) and fluid inlet temperature ($T_{c,in}$) are known. Since the afore-described generic model does not take into account the overall area of heat transfer, therefore the design point data for a heat exchanger is provided to HYSYS [AspenTech, Inc.] to calculate the overall area of heat transfer. In the off-design mode, a heat exchanger with fixed area will undergo a varying overall heat transfer coefficient and a varying LMTD. At a certain off-design point, LMTD is calculated by Equation 4.85, while U is calculated according to Equation 4.89 [Bolland, 2003].

$$U = U_0 \left(\frac{\dot{m}_{hot}}{\dot{m}_{0,hot}} \right)^{\Omega} \tag{4.89}$$

In Equation 4.89, U_0 is the overall heat transfer coefficient at design point, $\dot{m}_{hot}$ is the hot fluid flowrate at off-design point and $\dot{m}_{0,hot}$ is the hot fluid flowrate at design point. The exponent Ω varies according to the way tubes are arranged in a heat exchanger. The constant Ω is typically 0.56-0.58 for parallel tubes and 0.59-0.65 for staggered tubes. In this work, parallel tubes arrangement has been assumed with a selected Ω value of 0.58. The pressure drops occurring at the hot and the cold side are given as percentage of the pressure in the incoming stream, at the design point. The off-design analysis is based on the assumption that the hot and the cold fluid undergo the same percentage of pressure drop in off-design as that at the design point. In this way, the temperatures of the hot and cold fluid at the outlet are calculated in the off-design calculation of the heat exchanger, and hence the off-design duty is determined.

4.5 Heat Recovery Steam Generator

This work consists of two different models of Heat Recovery Steam Generator. One type is the HRSG and steam turbine used in the combined cycles throughout this work; which have been simulated in GTPRO [Thermoflow, Inc.] in design calculations and GTMASTER [Thermoflow, Inc.] in the off-design calculations. The other HRSG model is applied mainly for heat recovery from the CO_2-rich exhaust and oxygen-depleted air; has been modelled in gPROMS [PSE, Inc.] by using the distributed heat exchanger models that were explained in section 4.4.

4.6 Steam Turbine

Apart from the steam turbine in the combined cycles, which has been simulated in GTPRO and GTMASTER, there are two basic models for steam turbines applied in steam cycles.

The two types are given in the following:

- Supercritical steam turbine with no extractions
- Sub-critical Steam turbine with extraction points

Supercritical Steam Turbine

The turbine operates at supercritical steam at the inlet and expands it down to a certain reheat pressure. There are no steam extractions along the expansion path. Also, the steam exit enthalpy loss is neglected. The turbine work is calculated from the steam enthalpy drop.

Sub-critical Steam Turbine with Extractions

It is common in steam power plants to extract steam from a number of points along the expansion path. The extractions are used for feed water preheating in order to improve the efficiency. However, this makes the turbine subject to variations in efficiency in each turbine stage i.e. different segments along the expansion path between two successive extraction points. In many thermodynamic problems, an overall efficiency can be assumed to be locally applicable to all those segments; for maintaining simplicity in the calculation procedure. In reality, each turbine stage or segment will have its own efficiency. In this work however, a model for steam turbine with extractions is developed that calculates efficiency for each segment. There are different approaches to achieve this goal; and this work is based on the 'Straight Line' method [Black and Veatch, 1996].

A steam turbine with 'n' number of extractions and 'n+1' segments (or turbine stages) is shown in Figure 4.13. Before establishing the model, it can be identified that the total isentropic efficiency for the whole steam turbine is known. The inlet pressure and temperature and hence enthalpy are also known. Moreover, pressure at each extraction point is already specified. In order to successfully evaluate performance of such a turbine, it is inevitable to determine the steam enthalpy at each extraction point.

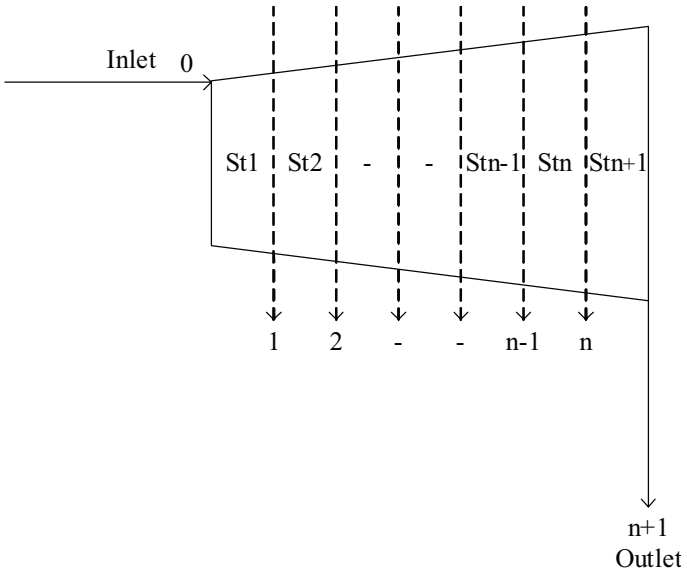

Figure 4.13 Sub-critical steam turbine with extractions

Apart from the aforementioned suppositions, the major assumptions for this model are given in the following:

- The straight expansion line method for enthalpy calculation
- No enthalpy loss at each extraction point through the expansion path
- No pressure losses at the extraction point
- Pressure loss in the extracted stream included as pressure loss in the component to which the extraction is lead

The model for calculation of total enthalpy, enthalpy for each segment (or stage) and work for the steam turbine is given in accordance with Figure 4.13.

Considering the inlet state (point 0), the inlet temperature is given as:

$$T_0 = T\left(P_0, h_0\right) \tag{4.90}$$

The entropy at inlet state is given as:

$$s_0 = s\left(P_0, h_0\right) \tag{4.91}$$

At the outlet state (point n+1):

The outlet entropy in case of isentropic expansion is given as:

$$s_{s,\,n+1} = s_0 = s\left(P_{n+1}, h_{s,\,n+1}\right) \tag{4.92}$$

The outlet temperature in case of isentropic expansion is:

$$T_{s,\,n+1} = T\left(P_{n+1}, h_{s,\,n+1}\right) \tag{4.93}$$

The outlet enthalpy can be calculated from the total isentropic efficiency, which is formulated as follows:

$$\eta_{is,\,tot} = \frac{h_0 - h_{n+1}}{h_0 - h_{s,\,n+1}} \tag{4.94}$$

In Equation 4.94, $h_{s,\,n+1}$ is the enthalpy in case of isentropic expansion and h_{n+1} is the real enthalpy at the outlet state.

The isentropic outlet enthalpy can be determined from the entropy, as given in the following:

$$s_{s,\,i-1} = s_i = s\left(P_i, h_{s,\,i}\right) \Rightarrow h_{s,\,i} \tag{4.95}$$

Since the outlet enthalpy and pressure are known, the real temperature and real entropy at the outlet can be calculated by Equation 4.96 and 4.97, respectively.

$$T_{n+1} = T\left(P_{n+1}, h_{n+1}\right) \tag{4.96}$$

$$s_{n+1} = s\left(P_{n+1}, h_{n+1}\right) \tag{4.97}$$

The total turbine work can thus be given by the following:

$$W_{turbine} = \sum_{i=0}^{n} \dot{m}_i \cdot \left(h_i - h_{i+1}\right) \tag{4.98}$$

In Equation 4.98, $\dot{m}_i$ is the steam mass flowrate through one turbine segment.

Assuming that the expansion line is a straight line between the inlet (point 0) and the outlet (point n+1) on an h-s-diagram, enthalpy and entropy at a certain point in the expansion path can be calculated by iteration since the extraction pressure (P_i) is known. Applying the equation for a straight line, the enthalpy at a given point 'h_i' can be calculated according to the following:

$$h_0 - h_i = \left(\frac{h_0 - h_{n+1}}{s_0 - s_{n+1}}\right) \cdot \left(s_0 - s_i\right) \;\; (1 \le i \le n) \tag{4.99}$$

So that enthalpy at a certain point becomes:

$$h_i = h_0 - \left(\frac{h_0 - h_{n+1}}{s_0 - s_{n+1}} \right) \cdot \left(s_1 - s_i \right) \ (1 \le i \le n) \tag{4.100}$$

The entropy at that point can be calculated by the following:

$$s_i = s\left(P_i, h_i \right) \tag{4.101}$$

The extraction temperature is then given by:

$$T_i = T\left(P_i, h_i \right) \tag{4.102}$$

Isentropic efficiency for each segment can then be formulated as follows:

$$\eta_{is,\,St,i} = \frac{h_{i-1} - h_i}{h_{i-1} - h_{s,\,i}} \ (1 \le i \le n) \tag{4.103}$$

The straight-line method is a fair approximation though; it gives low efficiencies at high pressures. However, the method is quite practical when considering its application in the models for simulating large steam power plants.

4.7 Valve

All the valve types used in this work are constant enthalpy, pressure reduction valves.

4.8 Pump

There are two types of water pumps used in the steam cycle; one that operates below critical pressure and the other that pumps the feed water up to the critical pressure or above. For each type, the temperature rise is neglected and the pump work is calculated by the following equation:

$$W_P = \frac{\dot{m}_{water} \cdot \nu_f \cdot \Delta P}{\eta_P} \tag{4.104}$$

In Equation 4.104;

ν_f = Specific volume of saturated liquid water at inlet temperature

ΔP = Pressure rise i.e. (P_{out} - P_{in}) and η_P = Pump efficiency

4.9 CO_2 Dehydration and Compression

Figure 4.14 presents the schematics of CO_2 dehydration and compression plant.

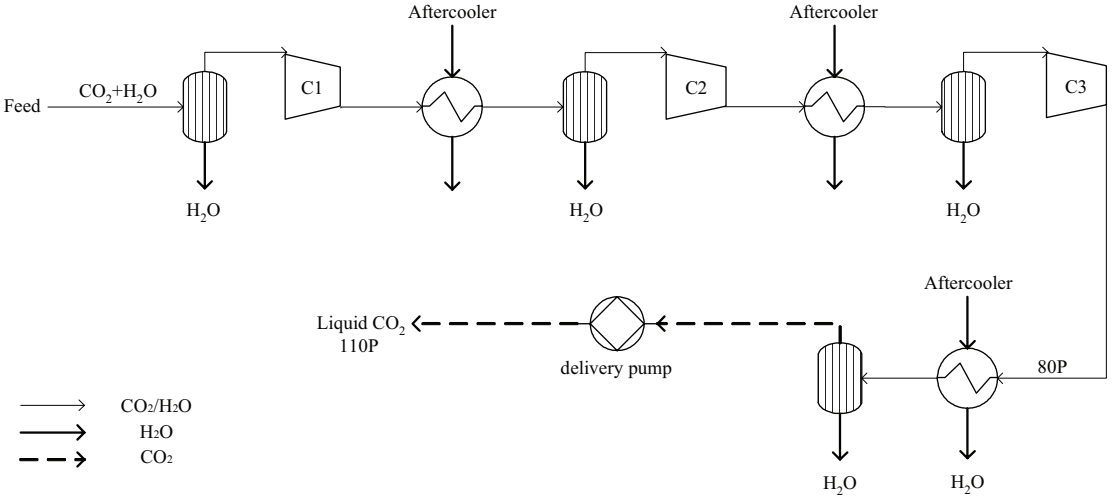

Figure 4.14 Flow sheet for CO_2 dehydration and compression process

The CO_2 compression plant is simulated in PRO/II version 6.0 [Simsci, Inc.]. Most of the power cycles integrated with CLC result in CO_2 at atmospheric pressure saturated with water vapour, while others do it at above-atmospheric pressure. The same CO_2 dehydration and compression model has been used in all the calculations; by changing the input at the inlet conditions in case of different pressure. The desired end pressure for CO_2 is assumed 110 bar at a temperature of 30°C. Three compressor stages including aftercoolers compress the CO_2 up to 80 bar, while water is removed simultaneously in between the compression stages. Finally the dense CO_2 is pumped up to the final pressure by the CO_2 delivery pump. The pressure ratio is equally distributed between the three compressor stages. The Soave-Redlich-Kwong equation of state is used in the compression process. The calculation includes water vapour in phase-equilibrium with the CO_2. The presence of non-condensable gases like N_2, H_2, Ar, and O_2 is not taken into account.

4.10 Definitions of Work and Efficiency

Figure 4.15 exemplifies the efficiency calculation method.

The net plant efficiency is calculated by the following equation:

$$\eta_{\text{Net Plant}} = \frac{\dot{W}_{\text{Net Plant}}}{\dot{m}_f \cdot \text{LHV}} \tag{4.105}$$

In Equation 4.105;

$\dot{W}_{\text{Net, Plant}}$ = Net plant work
$\eta_{\text{Net, Plant}}$ = Net plant efficiency
$\dot{m}_f$ = Fuel flow rate
LHV = Lower Heating Value

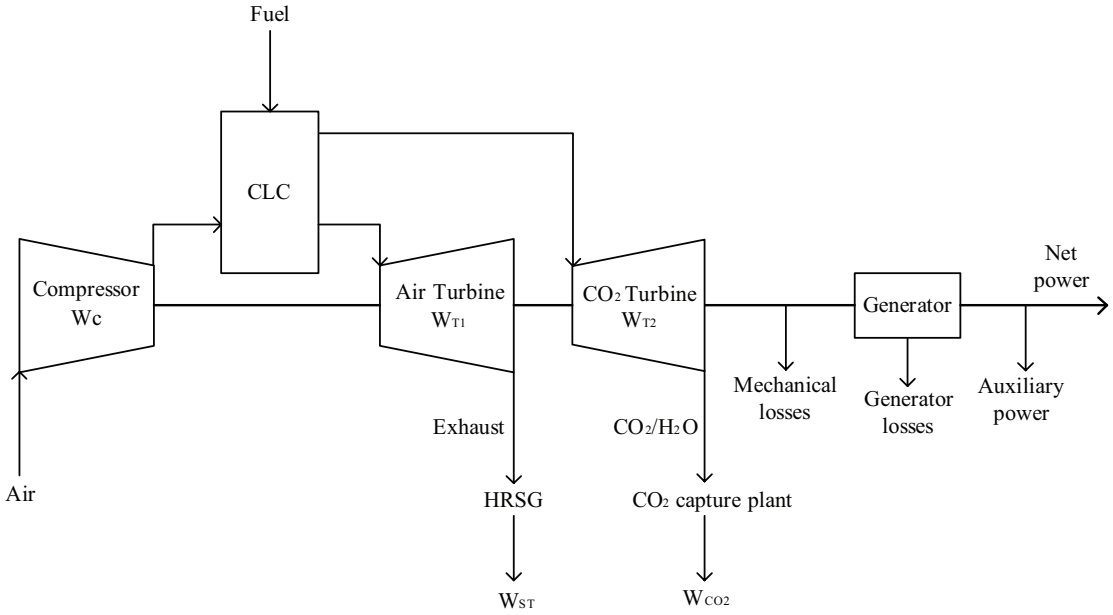

Figure 4.15 Example of net plant efficiency calculation for a CLC-combined cycle

The net plant work is calculated according to the following:

$$W_{\text{Net Plant}} = \left[\left(\sum \dot{W}_T + \dot{W}_C + \dot{W}_{ST} \right) \eta_m \, \eta_g + \sum \dot{W}_P \right] \eta_{aux} + \dot{W}_{CO_2} \qquad (4.106)$$

In Equation 4.106:

$\dot{W}_T$ = Gas turbine (s) work, calculated as fluid enthalpy change (positive)

$\dot{W}_C$ = Compressor work, calculated as fluid enthalpy change (negative)

$\dot{W}_{ST}$ = Steam turbine work, calculated as fluid enthalpy change (positive)

$\dot{W}_P$ = Pump work (negative)

$\dot{W}_{CO_2}$ = CO_2 compression work (negative)

η_m = Mechanical efficiency

η_g = Generator efficiency

η_{AUX} = Efficiency Auxiliary power efficiency

The specific work is calculated according to the following:

$$\omega = \frac{\dot{W}_{\text{Net Plant}}}{\dot{m}_{\text{comp. inlet}}} \tag{4.107}$$

In Equation 4.107;

ω = Specific work

$\dot{m}_{\text{comp. inlet}}$ = Air flowrate at compressor inlet

5 Sensitivity Study of CLC-Reactor System

This chapter presents sensitivity study of CLC-reactor system. The study takes into account three aspects; oxygen carrier, adiabatic reactors and non-adiabatic reactors. The significant parameters for the oxygen carriers and both types of reactor system are identified and parameter variation is carried out to study the system behaviour under varying conditions. The results of sensitivity study indicate the suitable oxygen carrier species and provide an overview of different operating conditions; mainly those related to air flowrate, solids flowrate, temperatures of various streams and degrees of solids conversion. The results also define the favourable operating conditions and operating limits when the reactors are integrated into power cycles.

5.1 The Scope of Sensitivity Study

The main scope of this sensitivity study is to analyse the effect of certain inlet and outlet streams' parameters on the overall performance of the CLC-reactor system. Also, the inter-dependency of various reactors' parameters is presented. There are in principle two approaches to carry out the sensitivity study of a component in a process. Sensitivity study may be carried out for the stand-alone component or it can be done for that component when it is integrated into a larger process system. The former approach has been adopted for the present work. The stand-alone analysis does in fact also reveal the behaviour of the component when it is integrated into a process. The parameters of significance are identified and varied within the same range as they would vary when integrated in a process or power cycle. There are however, some component-specific parameters which do not vary according to the conditions at the component boundary, for instance extent of reaction and degrees of conversion within CLC-reactors; which are purely dependent on the physical properties of the nature of oxygen carrier and mechanical design of the reactor system. These parameters quite oppositely though, affect the conditions at the reactors' boundaries. Such parameters are varied in order to assess the operating limits of the component and provide suitable operating conditions.

The literature review on oxygen carrier development presented in Chapter 3 covers a wide range of oxygen carriers and inert support substances that can be applied in CLC. When carrying out sensitivity study of the CLC-reactors with respect to the oxygen carriers, there can be two approaches. One approach can be to carry out the study and present the results in a generalised fashion so that the results are valid not for any specific oxygen carrier supported on a certain inert substance, rather they are valid for any kind of material used as the oxygen carrier. This approach may however lead to the results that are not very accurate because the physical properties of each substance are considerably different from other substances. Therefore, the physical properties cannot be set as the absolute values but in the form of non-dimensional relative values. The results produced in this way also need a number of correction factors and constants to relate the properties of one substance to another. Hence, it can be inferred that the generalised results for the CLC-reactors will not exhibit clarity and ease of comprehension and would therefore require a lot of effort in reproducing them for a given oxygen carrier. Hence, in this work, the sensitivity study is carried out by selecting a number of most commonly analysed oxygen carriers and their respective inert support materials, with pure methane (CH_4) as the fuel. Cho [2005c] presented the discussion on properties of most interesting pairs of metal oxide/reduced metal

oxide for CLC. The work by Cho [2005c] suggests that the relevant pairs of metal oxide/metal are CuO/Cu, NiO/Ni, Mn_3O_4/MnO and Fe_2O_3/Fe_3O_4. The present work considers these oxygen carriers except for Mn_3O_4/MnO, due to the low decomposition temperatures of Mn-based oxides. The other important task is to choose an appropriate inert support material for the selected oxygen carriers. In the present work the two most commonly used inert supports have been chosen i.e. Al_2O_3 and $NiAl_2O_4$.

Table 5-1 presents the selected oxygen carriers with their corresponding inert supports. The redox reactions for each metal oxide/metal and the respective heats of reaction are also shown in the table. The convention for the present work is that an exothermic reaction results in negative heat of reaction (-) sign while an endothermic reaction results in positive heat of reaction (+) sign. The solid oxides given in the following table are presented together with their inert supports which do not take part in the chemical reactions. The ΔH for the oxidation reaction is given as kJ/mol of oxygen consumed while for the reduction reaction it is kJ/mol of CH_4 reacting with the solid oxide.

Table 5-1 Reaction data for the selected oxygen carriers/inert supports

Carrier/Inert(s)	Redox reactions	ΔH
NiO/Al_2O_3, $NiAl_2O_4$	$2Ni + O_2 \Leftrightarrow 2NiO$	-479.4 (kJ/mol-O_2)
	$4NiO + CH_4 \Leftrightarrow 4Ni + CO_2 + 2H_2O$	156 (kJ/mol-CH_4)
Fe_2O_3/Al_2O_3	$4Fe_3O_4 + O_2 \Leftrightarrow 6Fe_2O_3$	-471.6 (kJ/mol-O_2)
	$12Fe_2O_3 + CH_4 \Leftrightarrow 8Fe_3O_4 + CO_2 + 2H_2O$	140.5 (kJ/mol-CH_4)
CuO/Al_2O_3	$2Cu + O_2 \Leftrightarrow 2CuO$	-314.6 (kJ/mol-O_2)
	$4CuO + CH_4 \Leftrightarrow 4Cu + CO_2 + 2H_2O$	-173.4 (kJ/mol-CH_4)

The sensitivity study of the CLC-reactors is categorised into three parts; parameter variation related to the oxygen carrier and inert, sensitivity study of adiabatic CLC-reactors by varying parameters that influence a combined cycle and the sensitivity of non-adiabatic CLC-reactors to be employed in a steam cycle. The physical properties of NiO/Ni have been calculated according to Knache et al. [1991]. The physical properties of Fe_2O_3/Fe_3O_4 and CuO/Cu have been calculated according to Çengel and Bole [2005]. Thermochemical data by Barin [1991] has been used to calculate the heat capacity of $NiAl_2O_4$ and Al_2O_3.

5.2 Study on Oxygen Carriers

The oxygen carrier is the most vital component of the CLC-process and successful realisation of CLC in power plant applications largely depends on the oxygen carrier properties. In order to study the selected oxygen carriers supported on their respective inert materials, it is important to identify the most significant parameters that can affect the

performance of an oxygen carrier and in turn the CLC-reactor system performance in the most drastic way. In the following, such parameters will be discussed one by one.

5.2.1 Inert to Carrier Ratio

A pure metal oxide used in CLC may not show mechanical stability and therefore it must be supported on an inert substance. The selection of an appropriate ratio between the inert and the oxygen carrier is a significant task as it influences the CLC-reactor system in several ways. In the present work, the inert to carrier ratio is defined as:

$$\chi = \frac{M_{inert}}{M_{MeO}}$$

In the above equation M_{inert} and M_{MeO} represent mass of the inert support and the metal oxide, respectively. When χ=0, there is no inert and the pure metal oxide circulates between the two reactors, at χ=1 the oxygen carrier and inert are in equal mass proportion and at χ=2, the mass of inert is double the mass of the oxygen carrier. The inert to carrier ratio is varied from 0 to 2 for the selected oxygen carriers and its effect on the significant parameters is discussed in the following sections. The results shown in the following are based on the assumption of complete conversion of solids in the oxidation and the reduction reactor i.e. X_{ox}=1 and X_{red}=0.

Solids Temperature

The temperature of the solids circulating between the two reactors is affected by the inert to carrier ratio as the solids flowrates change and hence the average heat capacity of solid streams at the reactors exit changes depending on the amount of reactive and inert material present in the stream. Figure 5.1, Figure 5.2, Figure 5.3 and Figure 5.4 present the solids temperature variation as a function of inert to carrier ratio for Fe_2O_3/Al_2O_3, NiO/Al_2O_3, $NiO/NiAl_2O_4$ and CuO/Al_2O_3, respectively. The primary temperature for all the oxygen carriers, except CuO is the solids temperature at the exit of the oxidation reactor ($T_{s,i}$) i.e. at the inlet of the reduction reactor. In the following figures, for all the oxygen carriers except for CuO, Ts,i and Ts,o are the solids temperature at the inlet and the outlet of the reduction reactor, respectively. In case of CuO, since there are exothermic reactions in both the reactors; the primary temperature is the solids temperature at the exit of the reduction reactor i.e. at the inlet of the oxidation reactor. Therefore, in Figure 5.4, Ts,i and Ts,o are the solids temperature at the inlet and the outlet of the oxidation reactor, respectively.

The increase in inert to carrier ratio (χ) means that the amount of the inert material circulating together with the reactive oxygen carrier goes on increasing. This means that the heat transport contribution of the inert also increases. It can be seen that variation in χ for iron oxide particles does not have much stronger impact on the solids temperature because of the very large flowrates of iron oxide particles, which is also evident from the stoichiometry of the reactions of iron oxide, shown in Table 5.1. Also, the molecular weight of iron oxide is much larger as compared to the other metal oxides thereby resulting in larger mass of Fe_2O_3/ Fe_3O_4 particles in the reactor system. At the same time the heat capacity of iron oxide particle is also higher than the rest of the selected oxygen carriers. The large amounts of solid with high heat capacity levels out the effect of increasing amounts of inert Al_2O_3 and hence the increasing inert to carrier ratio does not have a

prominent effect on the solids temperature and it varies to a slight degree with inert to carrier ratio variation. On the other hand, NiO-based carriers show a comparatively strong dependency on the inert to carrier ratio. That is mainly because of two reasons; lower molecular weight of the NiO resulting in smaller flowrates of NiO/Ni.

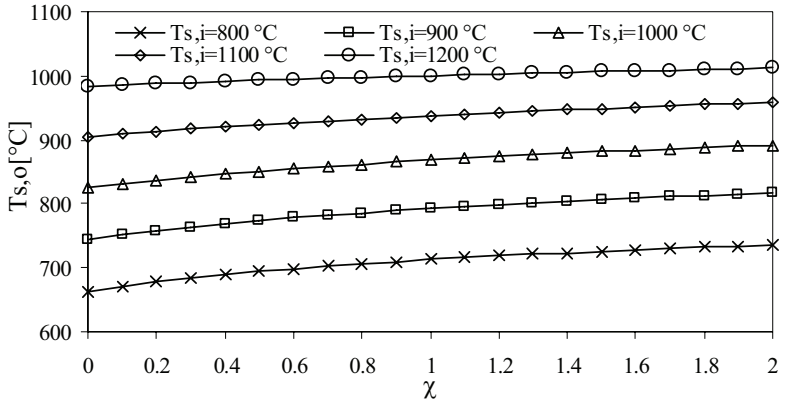

Figure 5.1 Solids temperature variation with χ for Fe_2O_3/Al_2O_3 as oxygen carrier

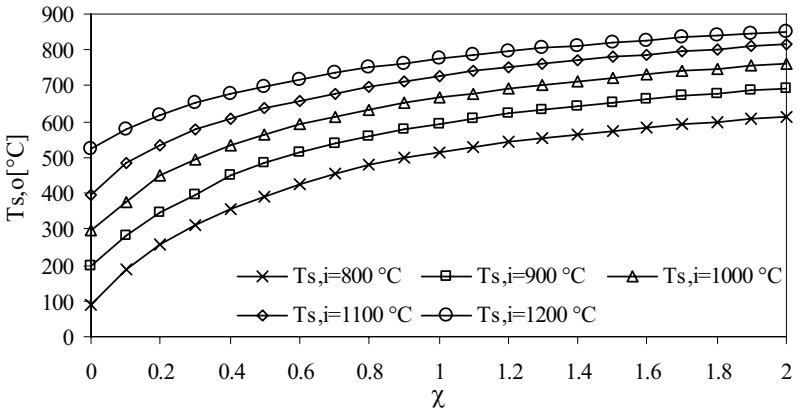

Figure 5.2 Solids temperature variation with χ for NiO/Al_2O_3 as oxygen carrier

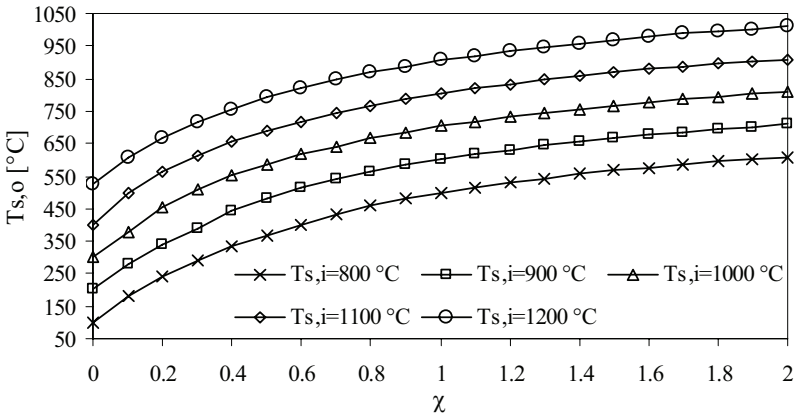

Figure 5.3 Solids temperature variation with χ for $NiO/NiAl_2O_4$ as oxygen carrier

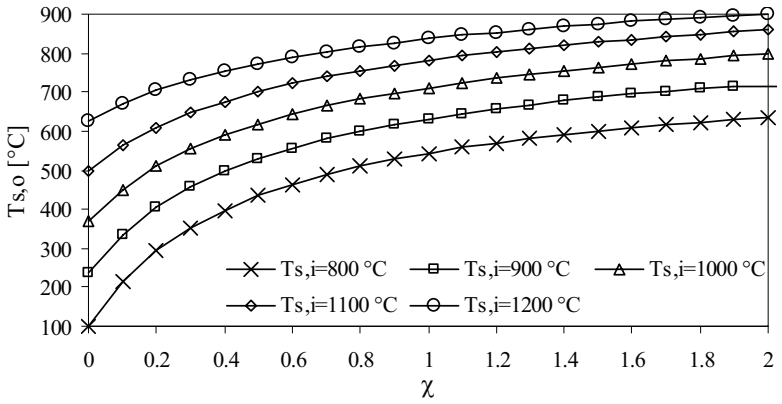

Figure 5.4 Solids temperature variation with χ for CuO/Al_2O_3 as oxygen carrier [$T_{s,i}$ & $T_{s,o}$ are the solids temperature at the oxidation reactor inlet and exit, respectively.]

The copper oxide particles also show a strong dependency on the inert to carrier ratio. Just like NiO particles, the CuO particles are also very light and therefore less mass of solids circulates between the two reactors and an increase in inert amount affects the solids temperature in a more outstanding way as compared to iron-based oxygen carrier.

Another feature of interest is the solids temperature at χ=1 i.e. the same amounts of inert and oxygen carrier. After this point the temperature variation is not very prominent and there is a linear increase in solids temperature. As the inert to carrier ratio (χ) approaches 2 i.e. when the amount of inert is double than that of the oxygen carrier, the solids temperature tend to become constant. It can be inferred that after the point of χ=2, there will be negligible variation in solids temperature. Although, the choice of a suitable inert to carrier ratio can be made with an intention to achieve suitable solids temperatures, its effect on the solids flowrates cannot be overlooked. The impact of varying inert to carrier ratio on the solids total flowrate between the reactors will be discussed in the following section.

Solids Flowrate

The inert to carrier ratio influences the total solids flowrate in the CLC-reactor system which in turn also changes the reactors' sizing requirements.

In order to present the solids flow a parameter fuel to solids ratio is defined given by the following:

$$R_{fs} = \frac{\dot{n}_{fuel}}{\dot{n}_{s}}$$

In the above equation, R_{fs} is the fuel-to-solids ratio; the numerator is molar flowrate of fuel while the denominator is the solids molar flowrate at the reduction reactor inlet. According to this equation; when R_{fs}=0, either there is no fuel supply at all, or there is infinite amount of solids. The former condition is not possible for an operating CLC-reactor system continuously being fed with the fuel; however the latter condition is virtually possible if despite the fuel supply there is no conversion of metal oxide particles in the reduction

reactor. This will be discussed in detail in the section 5.2.2, 'Degrees of Solids Conversion'. As per the definition of R_{fs}, the higher the fuel to solids ratio, the less are the solids required in the CLC-reactor system and vice-versa. Hence, a higher R_{fs} value should be desired in order to conceive feasible CLC-reactors dimensions. Figure 5.5 presents the fuel to solids ratio as a function of inert to carrier ratio for the selected oxygen carriers. The R_{fs} takes into account the total solid stream flowrate at the oxidation reactor exit consisting of pure metal oxide and inert based on the assumption of complete conversion of metal to metal oxide.

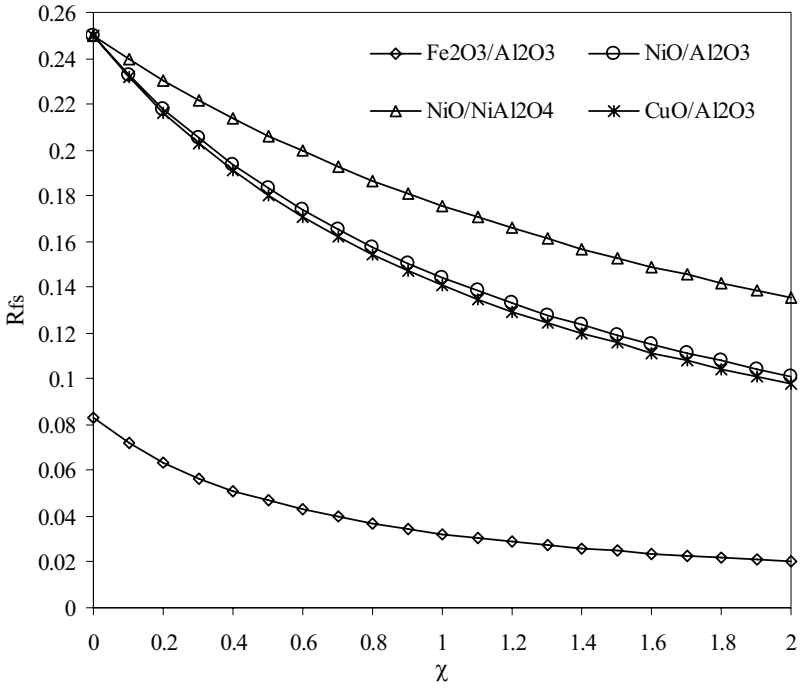

Figure 5.5 Fuel-to-solids ratio (R_{fs}) as a function of inert to carrier ratio (χ)

It can be seen that the iron oxide particles flowrate is the largest as compared to the rest of the three oxygen carriers. While CuO has the lowest flowrate because Cu-based particles are the lightest compared to iron- and nickel-based particles. The NiO based solids flowrate does not differ from each other appreciably, because the active component remains the same i.e. NiO and the only variation is the amounts of inert i.e. $NiAl_2O_4$ and Al_2O_3.

As per the definition of R_{fs}, the higher the value of R_{fs} the lower is the total solids flowrate and vice-versa. It can be seen that, regardless of the extent, the solids flowrate for all the oxygen carriers goes on decreasing with increase in inert to carrier ratio. An increase in inert to carrier ratio implies that the amounts of inert material are increasing relative to the amount of active metal oxide. Since, the amount of active material is a function of amount of fuel supplied, it is independent of the inert to carrier ratio. Hence, increasing the inert to carrier ratio just adds up the amount of inert material resulting in an increase in the total solids flowrate at the oxidation reactor exit.

Air Flowrate

The air flowrate required to maintain a certain temperature in the oxidation reactor is also largely dependent on the selection of the inert to carrier ratio. Since the air flowrate requirements are linked with the amounts of solids circulating between the two reactors, therefore, it is of interest to examine the impact of inert to carrier ratio on the air flow requirements. Figure 5.6 presents the air flowrate per mol of oxygen consumed as a function of inert to carrier ratio for the selected oxygen carriers; at the solids temperature of 800°C at the oxidation reactor exit. Based on the assumption of isothermal mixing in the oxidation reactor, temperature of the oxygen-depleted air stream is also 800°C. The solids te

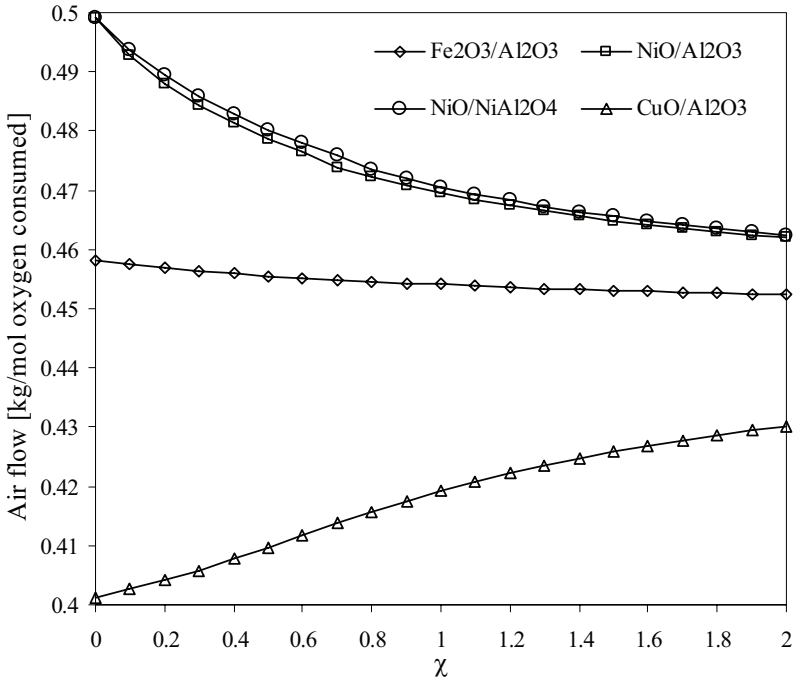

Figure 5.6 Air flowrate as a function of inert to carrier ratio for the selected oxygen carriers [$T_{s,i}$=800°C, i.e. solids temperature at the oxidation reactor exit. Air temperature at the oxidation reactor inlet is 15°C, while the solids temperature at the oxidation reactor inlet is different for each oxygen carrier.]

Since the solids flowrate depends on this ratio, the larger the amounts of solids at a fixed temperature, the lower the air flowrate will be to fulfil the heat balance. Although the nature of the heat balance around the CLC-reactor system is independent of the type of oxygen carrier, but nevertheless the extent of heat flow at the two reactors' boundaries is reliant on the type of carrier being circulated inside the reactor system. Since, the total amount of solids increases with increases in the inert to carrier ratio, it implies that the sensible heat carried away by the solid streams also increases. It can be seen in Figure 5.6 that in order to fulfil the overall heat balance around the oxidation reactor, the air flowrate decreases with increase in the inert to carrier ratio, in case of all the oxygen carriers except CuO. There is however, a different scenario in the oxidation reactor in case of CuO. The air flowrate depends on the solids temperature at the inlet and exit of the oxidation reactor. At the same time, the two temperatures are also inter-dependent. In case of exothermic oxidation and

endothermic reduction reactions, due to the heat consumption in the reduction reaction, the solids temperature at the reduction reactor exit i.e. oxidation reactor inlet is lower than that at the oxidation reactor exit. Due to the exothermic nature of both the oxidation and reduction reactions of CuO, the temperature of the solids entering the oxidation reactor is higher than that leaving the oxidation reactor. In principle, the higher the solids temperature at the oxidation reactor exit the lower is the air flowrate in order to fulfil the heat balance around the oxidation reactor. As the inert to carrier ratio in case of CuO/Al_2O_3 increases, the temperature of the solids leaving the reduction reactor and entering the oxidation reactor goes on increasing. Therefore, the air flowrate increases in order to satisfy the heat balance around the oxidation reactors with increase in the amounts of total solids flow.

5.2.2 Degrees of Solid Conversion

In order to study the effect of degrees of solid conversion in the two split-reactors of CLC-reactor system, the inert to carrier ratio must be fixed for the oxygen carriers. Based on the literature review of CLC as well as the findings presented in the previous section, all the oxygen carriers are based on a 3/2 metal oxide/inert ratio on the mass-basis i.e. an inert to carrier ratio-χ of 0.67. At this value of inert to carrier ratio, based on the results presented in the previous sections, it can be inferred that there is a reasonable air and solids flowrate at which a conceivable CLC-reactor system can be achieved.

The degrees of reduction and oxidation of solids are the key parameters in the CLC-reactor system and affect the reactors' design and performance, in terms of solids flowrate and temperatures. The oxidation reaction occurs more rapidly as compared to the reduction reactor. Experiments by Brandvoll [2005] suggest that the oxidation reaction is much more rapid as compared to the reduction reaction and also a very high degree of conversion in the oxidation reactor can be achieved. Therefore, it can be of interest to compare the selected oxygen carriers on the basis of complete degree of oxidation and varying degree of conversion. The degree of conversion, however, has a strong impact on the solids flowrate required by the fuel being fed to the reduction reactor, in order to maintain the circulation and uninterrupted operation of the reactor system. The solids flowrate was presented in the form of fuel to solids ratio R_{fs}, in the previous section. Figure 5.7 presents the R_{fs} as a function of degree of reduction (X_{red}) for the selected oxygen carriers. The solids flowrate is independent of the temperatures in the reactors and is solely a function of the fuel flowrate and the degrees of solids conversion in the two reactors. Examination of Figure 5.7 tells just at once that a higher degree of reduction is desired in order to realise a conceivable reactor design with realistic dimensions. The results show that solids flowrate increases exponentially with decrease in degree of reduction, which is although not presented in the form of figure here; nevertheless the R_{fs} reflects the amounts of solids needed at a particular operating condition. Since CLC is to be implemented in large power plants, a very low R_{fs} value means a very high solids flowrate between the reactors. Therefore, a lower X_{red} (or higher conversion) will make it possible to operate CLC-reactors with solids in a reasonable range of flowrates.

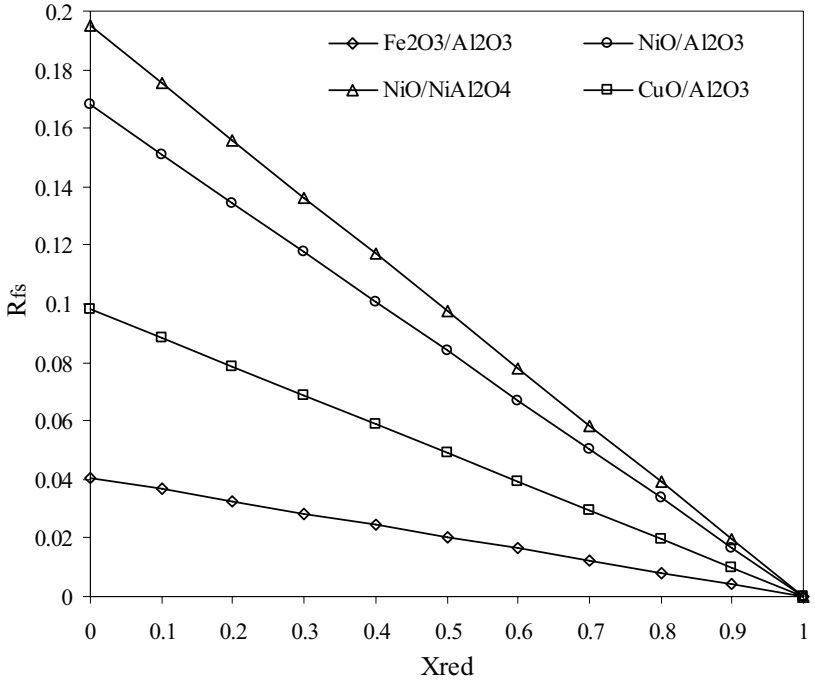

Figure 5.7 Fuel to Solids ratio at oxidation and reduction reactor exit as a function of degree of reduction (X_{red}). X_{ox}=1 i.e. complete oxidation, χ=0.67

The results presented so far are based on the assumption of complete conversion in the oxidation reactor (X_{ox}=1), which is quite a rational and reasonable assumption as oxidation reaction is much more rapid than the reduction of solid oxide with fuel. Although it can be argued that there may be an insignificant decrease in the degree of oxidation of solids; yet it is also of use to analyse the reactors over a range of degrees of oxidation with varying reduction degrees. The outcome of such an analysis can further be used to define the operating limits of the reactor system. The solids flowrate at exit of the oxidation reactor changes with degree of oxidation in the similar fashion as it changes at the exit of reduction reactor with change in degree of reduction. However, a so-called solids-flow map can be generated over a range of oxidation and reduction degrees to estimate the solids requirement, which is indicative of the requirements of the reactors dimensions. Such a flow-map will be different for different oxygen carrier species; however in the present work the most commonly used oxygen carrier i.e. $NiO/NiAl_2O_4$ is selected for the sole purpose of the presentation of operating conditions variations as a result of the interdependency of degrees of solids conversion in the two reactors. This interdependency remains the same regardless of the oxygen carrier type and therefore the elaboration of the phenomenon can very well be performed through presentation of any selected type of oxygen carrier specie.

Figure 5.8 presents the so-called solids flow map for $NiO/NiAl_2O_4$. A salient feature of the above-shown map is the restriction imposed on the degree of reduction by the degree of oxidation. In order to have a more elaborated discussion on this map, the definitions of X_{ox} and X_{red} used in this work are reiterated here. X_{ox}=1 in case of complete oxidation, while X_{red}=0 in case of complete reduction. At the condition of complete oxidation (X_{ox}=1), the degree of reduction must not decrease below 10% (X_{ox}=0.9). A further decrease in reduction would result in excessive solids flow requirement as the solids flow increases exponentially

with decrease in reduction. At the 'Operating Limit Line' shown in Figure 5.8, the solids flowrates are extremely large.

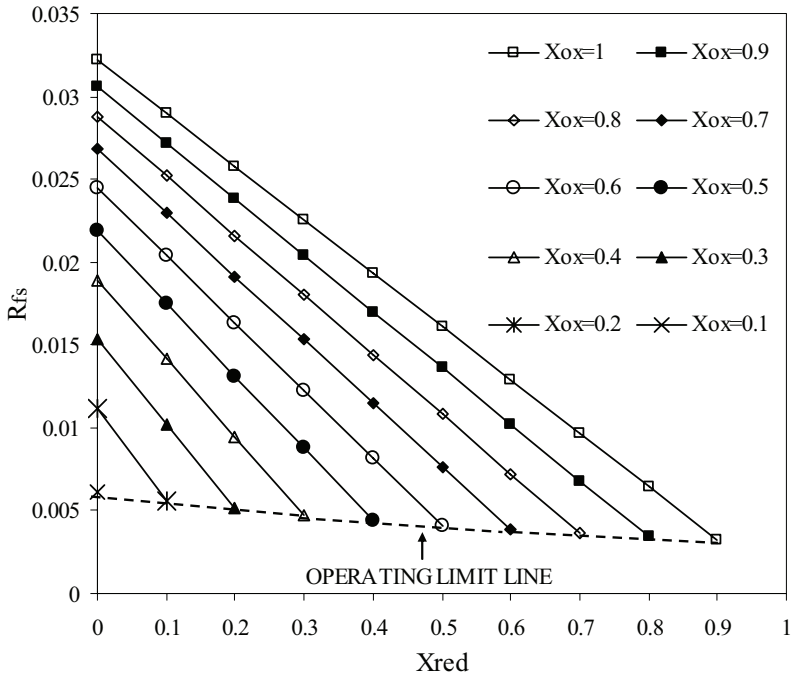

Figure 5.8 The so-called solids-flow map for $NiO/NiAl_2O_4$ in a 3:2 mass basis i.e. χ=0.67

The definition of fuel to solids ratio R_{fs} suggests that at such a large solids flow, R_{fs} approaches zero, which is undesirable. Decreasing the oxidation also demands for increase in reduction and X_{red} can never be equal to or higher than X_{ox}. For instance at a condition of X_{ox}=1, X_{red}=1 means that there is no reaction of metal with the fuel taking place at all and therefore there is no metal available to be converted to metal oxide in the oxidation reactor. This does virtually mean collapse of the reactor system. Such a condition is virtually impossible to occur within CLC; nevertheless the phenomenon is useful when looking at the other degrees of oxidation and reduction. Reducing the degree of oxidation down to 50% i.e. X_{ox}=0.5, the operating limit is to achieve a minimum of 60% reduction (X_{red}=0.4). If X_{red}=0.5, i.e. 50% of the solids are converted, there will become a mismatch of the oxygen demand by the fuel and the oxygen supplied to the fuel as a result of oxidation reaction. In other words, there would be less oxygen available for the fuel in the form of metal oxide, than what is required by the fuel. The same virtually impossible condition would occur as in the case of X_{ox}=1 and X_{red}=1 with the exception that the extra supply of oxygen would need to be provided by adding extra metal oxide at the commencement of each chemical loop with removal of the non-utilisable metal by the same quantity, thereby making the system an open system. Although the 'Operating Limit Line' sets the limits of degrees of oxidation and reduction; going beyond the points lying on this line does not necessarily result in open systems or reactor system collapse unless the two degrees of conversion (X_{ox} and X_{red}) are equal to each other. Nevertheless, beyond the 'Operating Limit Line', the solids flowrates are excessively large which will not match with any feasible and conceivable reactor system design. Although the solids-flow map presents the solids-flow scenario over a broad range of conversion degrees; even so, a CLC-reactor system is expected to operate in the upper

left region of the map shown in Figure 5.8 on the line for X_{ox}=1 and high degrees of reduction, preferably X_{red}=0.3.

At a certain operating condition with constant degrees of conversion in the two reactors, the solids flowrate at the oxidation and the reduction reactor exit is constant. However, there is a slight difference in the solids flowrate at the exits of the two reactors that is due to the oxygen consumption in the reduction reactor. The most influential parameter on the solids flowrate and solids temperature is the degree of conversion in the reduction reactor i.e. X_{red}. The X_{red} not only affects the total solids flowrate but also the ratio between the oxygen carrier and the total solids flowrate, δ, given in the following:

$$\delta_i = \frac{\dot{m}_{MeO}}{\dot{m}_i} \quad (i=ox, red)$$

In the above equation, the subscript 'i' represents the solid streams at the oxidation and the reduction reactor outlet. According to the equation, when δ_{ox}=0 means that there is no metal oxide at the oxidation reactor outlet, a condition that is virtually impossible to occur, as the oxidation reaction is rapid and takes place with high extent. At δ_{red}=0, there is complete conversion of metal oxide into metal i.e. X_{red}=0, a condition which is ideally possible to occur. Hence, the parameter of interest is the δ_{red} that varies with the degree of reduction and also affects the solids temperature. The temperature of the solids leaving the reduction reactor varies with variation in the ratio between oxygen carrier and total solids flow. The effect of this ratio on the solids temperature is different for each oxygen carrier and inert substance. In order to give an insight into the phenomenon, $NiO/NiAl_2O_4$ is chosen as an example. Assuming complete conversion of metal to metal oxide in the oxidation reactor i.e. X_{ox}=1, the solids at the oxidation reactor outlet contain only NiO and NiAl2O4 in the prefixed proportions. On the other hand, since it is established that a complete conversion is unlikely to happen in the reduction reactor, the solids at the reduction reactor outlet contain reduced Ni, unconverted NiO and $NiAl_2O_4$.Therefore the ratio between the metal oxide (NiO) and the total solids at the reduction reactor exit changes with each degree of reduction. Thereby, due to different heat capacities of all the three components (metal, metal oxide and inert) of the solid stream, the solids temperature also varies. An overview of the scenario in the reduction reactor, taking into account the solids temperature, X_{red} and δ can be of interest in this regard.

Figure 5.9 presents the solids temperature at the reduction reactor exit as a function of δ at the solids temperature ($T_{s,i}$) of 1000°C at the reduction reactor inlet. It can be seen from Figure 5.9 that the solids temperature remains constant at the reduction reactor exit at X_{red}=0 as all the metal oxide is converted to metal. However, this ratio decreases linearly with the decrease in degree of reduction (X_{red} increasing). The lower the degree of reduction the higher is the proportion of unconverted metal oxide in the solids leaving the reduction reactor. Hence, flowrate of the active components increases with decrease in reduction; since metal oxide has a higher molecular weight, while the inert substance remains unconverted thereby decreasing the inert to carrier ratio.

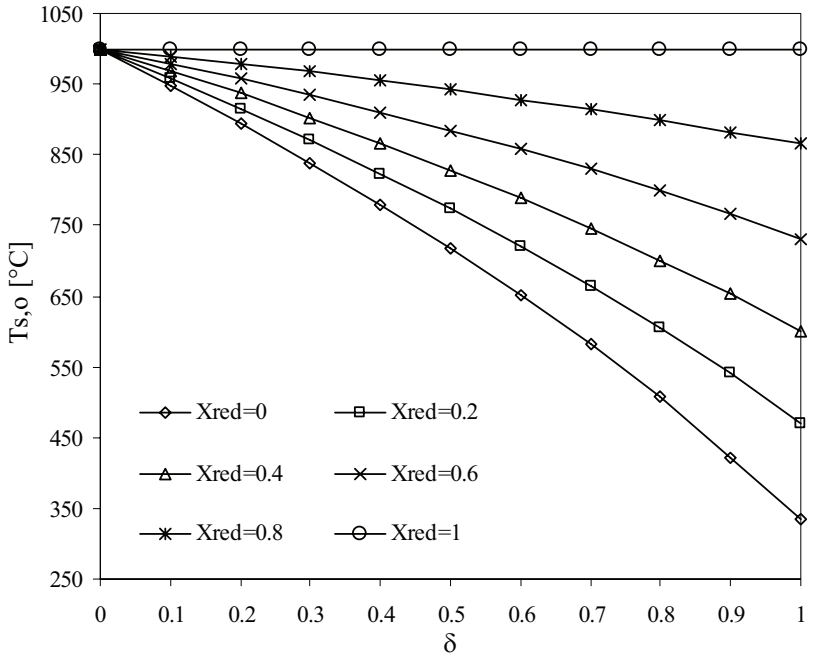

Figure 5.9 Solids temperature at the reduction reactor exit as a function of δ and X_{red} [X_{ox}=1, $T_{s,i}$=1000°C, oxygen carrier: $NiO/NiAl_2O_4$ with χ=0.67]

5.2.3 Solids Heat Capacity

The solids heat capacity is one of the major criteria in the CLC-reactors because it is purely dependent on the nature of the oxygen carrier employed. The effect of heat capacity variation on the reactors can be presented in the form of various parameters as a function of relative heat capacity can be defined as the following:

$$Cp_{rel,i} = \frac{Cp_i}{Cp_{air(STP)}} \quad (i=ox, red)$$

In the above equation, Cp_i is the specific heat capacity (kJ/kg-K) of the solid stream at the oxidation or reduction reactor exit. $Cp_{air,(STP)}$ is the heat capacity (kJ/kg-K) of air at the reference point i.e. standard temperature and pressure.

Figure 5.10 presents the relative heat capacity of the solid stream at the reduction reactor exit as a function of solids temperature at the reduction reactor outlet ($T_{s,o}$) for the selected oxygen carriers. Figure 5.10 is based on complete conversion of solids in the two reactors and thus the results hold for pure metal with the inert material coming out of the reduction reactor exit. It can be seen that Fe_2O_3/Al_2O_3 has the largest heat carrying capacity. NiO/Al_2O_3 has the heat capacity higher than that of $NiO/NiAl_2O_4$ while CuO/Al_2O_3 has the lowest of all heat carrying capacity. This should be emphasised here that the relative heat capacity takes into account the mass flowrate of the solids and air as it is based on the specific heat capacity (kJ/kg-K) of each stream relative to the specific heat capacity of air. That is why the heavier the metal oxide the higher is the flowrate of the solid particles and thus the higher is the heat carrying capacity. Therefore iron-based particles show the highest heat carrying capacity while Cu-based carriers exhibit the lowest.

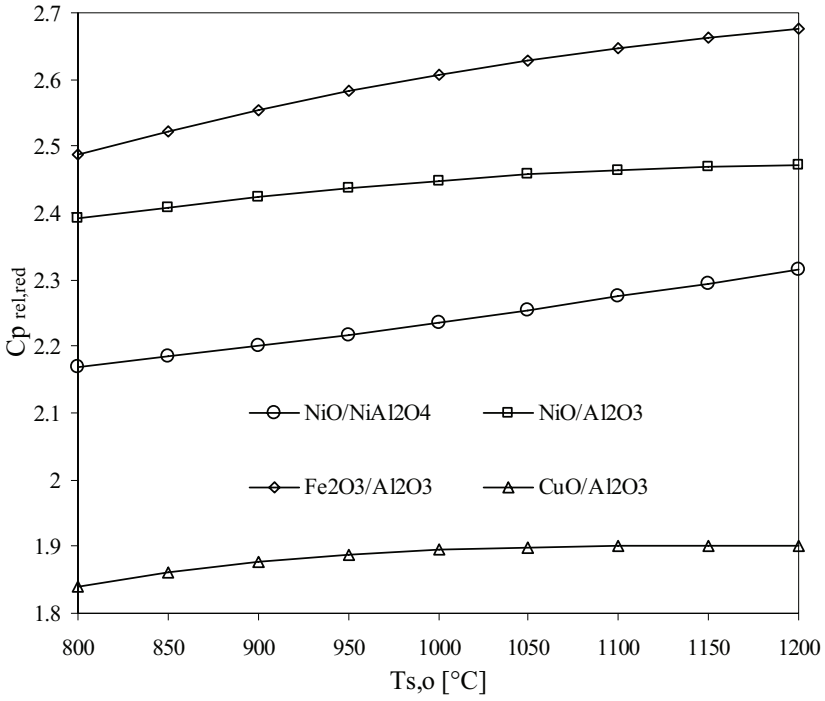

Figure 5.10 Relative heat capacity of the solid stream leaving the reduction reactor [X_{ox}=1, X_{red}=0, χ=0.67]

The relative heat capacity can also be correlated with the air flow as shown in Figure 5.11.

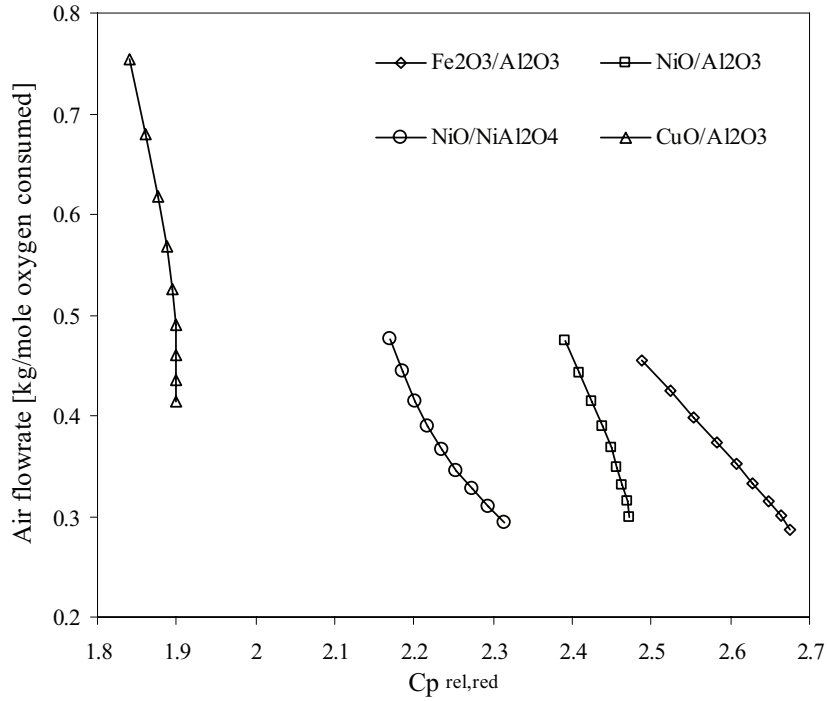

Figure 5.11 Air flowrate as a function of relative heat capacity of the solid stream leaving the reduction reactor

According to Figure 5.11, the higher the heat capacity of solids, the lower is the air flowrate. An increased specific heat capacity of solids results in an increased specific enthalpy of the solid stream entering the oxidation reactor. The total sensible heat thus also increases. The sensible heat does however also depend on the molecular weight of the solids. The net effect is an increase in air flowrate with a higher specific capacity and a decrease in air flowrate with a decreased heat capacity in order to fulfil the energy balance at a fixed oxidation temperature. Figure 5.11 indicates that the NiO-based oxygen carriers have moderately high heat carrying capacity resulting in moderate air flowrate. The Cu-based particles result in very high air flowrates; while in case of the iron-based particles the changes in heat capacity influence the air flowrate more strongly as compared to the other oxygen carriers.

5.3 Adiabatic Reactors Study

The adiabatic CLC-reactors are integrated into gas turbine combined cycles. Hence, in order to carry out the adiabatic CLC-reactors' sensitivity study, it is quite a rational approach to identify the parameters and the streams of significance that affect performance of a combined cycle. Figure 5.12 serves the basis for the sensitivity study of adiabatic reactors. The specific enthalpy (h) in this thesis is although assumed a function of temperature and pressure, the effect of temperature is much more influential. Therefore, in this section, only the temperature is taken into account. The approach to present the outcome of the study has been to show rather generalised results. In the previous section, it was found that the Ni-based oxygen carriers possess the most attractive thermodynamic properties, i.e. the highest air flowrate, highest heat carrying capacity and lowest solids requirements.

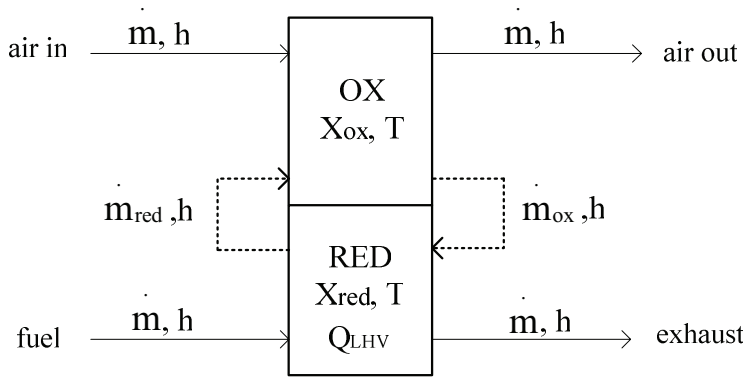

Figure 5.12 Schematics of adiabatic CLC-reactors with important stream and reactors parameters [T is the solids temperature in a reactor that is equal to the corresponding gaseous stream leaving that reactor, h is specific enthalpy of the solids and gaseous streams, Q is sensible heat]

Therefore, the adiabatic reactors sensitivity study is mainly based on $NiO/NiAl_2O_4$ as the oxygen carrier where the carrier to inert ratio is 3/2 (mass basis) or in other words χ=0.67. The same oxygen carrier will be applied in the advanced CLC-power cycles in the forthcoming chapters and therefore it is of significance to focus the study of CLC-reactors with this specific oxygen carrier. Nevertheless, some important parameters are also presented for the other oxygen carriers for the sake of comparison.

5.3.1 Oxidation Reactor Temperatures

The air and fuel inlet temperature play an important role in the overall heat balance of the reactor system and in turn affect the mass balance as well. These two parameters however, also depend on the cycle configuration into which CLC is integrated. For instance, temperature at the oxidation reactor inlet depends on the air compressor pressure ratio and on the performance of air preheater, if applied. Similarly the temperature at the reduction reactor inlet depends on the performance of fuel preheater, if present. The temperatures around the reactors determine the air flowrate required by the system to fulfil any specified oxidation temperature. Figure 5.13 exhibits the trends of air flowrate as kg per mole of oxygen consumed in the oxidation reactor as a function of air inlet temperature for different values of solids temperature at the oxidation reactor outlet ($T_{s,o}$). Figure 5.13 shows quite a strong dependency of air flowrate on the air inlet temperature and the dominance of this effect increases with oxidation temperature. For a fixed air inlet temperature, the higher the oxidation temperature, the lower is the air flowrate required to fulfil the heat balance. The increase in oxidation temperature while keeping the air inlet temperature constant, results in an increased specific enthalpy rise, which has to be compensated with by a decrease in the air flowrate. The air inlet temperature also plays a major part in determination of air flowrate. For a fixed oxidation temperature, the higher the air inlet temperature, the lower is the sensible heat in fuel required to reach the desired oxidation temperature and vice-versa. The air flowrate does inevitably increase with increase in air inlet temperature for a fixed oxidation temperature. The increase in air inlet temperature for a fixed oxidation temperature results in decrease in specific enthalpy rise that would occur by virtue of heat addition. In order to make up for the decreased enthalpy rise, the air flowrate increases at the oxidation reactor inlet.

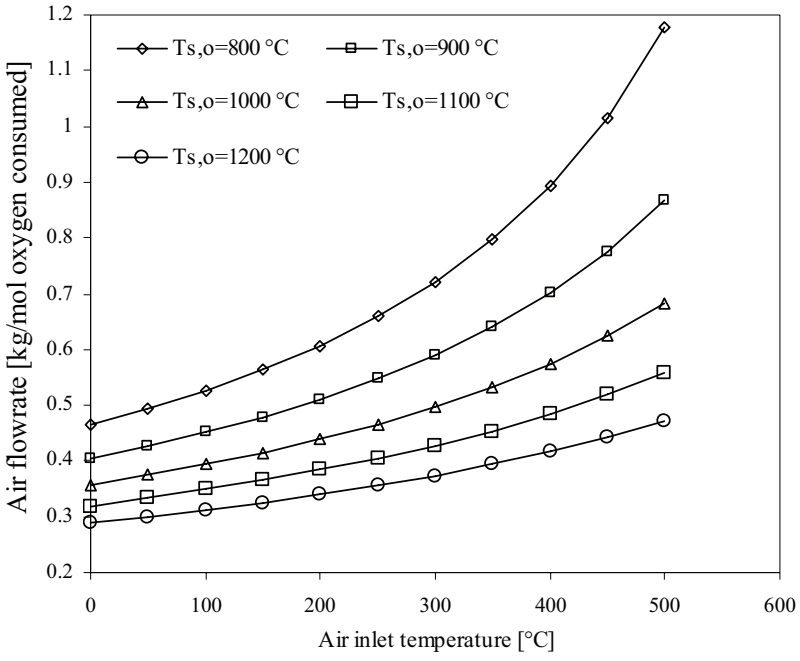

Figure 5.13 Air flowrate as a function of air inlet temperature and solids temperature at the oxidation reactor outlet. [X_{ox}=1, X_{red}=0, $NiO/NiAl_2O_4$, χ=0.67, The solids temperature at the oxidation reactor inlet is different for each value of $T_{s,o}$ and lower than $T_{s,o}$ due to endothermic reduction reaction]

The solids temperature at the reduction reactor exit may also vary with the air temperature inlet. Nevertheless, the results show that variation in the reduction temperature is not prominent with change in air inlet temperature at a certain oxidation temperature. Since, the air temperature at the inlet of the oxidation reactor results in an increased air flowrate in case of $NiO/NiAl_2O_4$, based on the nature of the heat balance around the oxidation reactor; it can be inferred that the same would be the effect of increase in the air inlet temperature in case of other oxygen carriers. The effect would however be to a different extent.

5.3.2 Degrees of Solids Conversion

Within the CLC-reactors, two parameters of foremost significance are degree of oxidation (X_{ox}) and degree of reduction (X_{red}). According to the definition of these two parameters given in Chapter 4, $X_{ox}=1$ for complete oxidation and $X_{red}=0$ for complete reduction. As mentioned previously, the experimental investigation by Brandvoll [2005] suggest that the solids oxidation reaction is much more rapid as compared to the reduction reaction and that all the solids are converted in the oxidation reactor. The degree of reduction is however, more of an issue of further investigation. The degree of reduction influences the reduction temperature as well as solids flowrates between the two reactors. Figure 5.14, Figure 5.15 and Figure 5.16 present the solids temperature at the reduction reactor outlet ($T_{s,o}$) as a function of degree of reduction and different oxidation temperature values for Fe_2O_3/Al_2O_3, NiO/Al_2O_3 and $NiO/NiAl_2O_4$, respectively. Due to the cyclic nature of CLC, the temperatures in two reactors are interdependent. As a matter of fact, the reduction reaction is a key reaction in this regard. The nature of the reduction reactor also plays an important role. In case of exothermic oxidation and endothermic reduction, the heat is consumed in the reduction reactor, thereby making the solids to leave the reduction reactor at a lower temperature relative to the temperature at the entry of the reduction reactor. On the other hand, when both the oxidation and reduction reactions are exothermic, as in case of CuO, the temperature of the solids at the reduction reactor exit is higher relative to that at the entry of the reduction reactor. This is due to the release of heat in the reduction reactor instead of heat consumption. In case of iron- and nickel-based oxygen carriers, the higher the degree of reduction the more is the heat utilised in the endothermic reaction and the lower is the temperature of the solids at the reduction reactor exit and vice-versa.

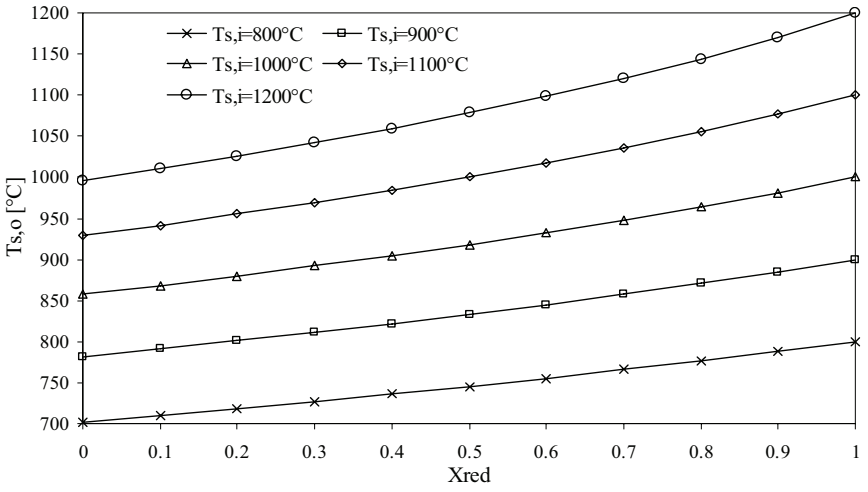

Figure 5.14 Variation in reduction reactor exit temperature ($T_{s,o}$) as a function of degree of reduction (X_{red}) for Fe_2O_3/Al_2O_3 particles [$\chi=0.67$, $X_{ox}=1$]

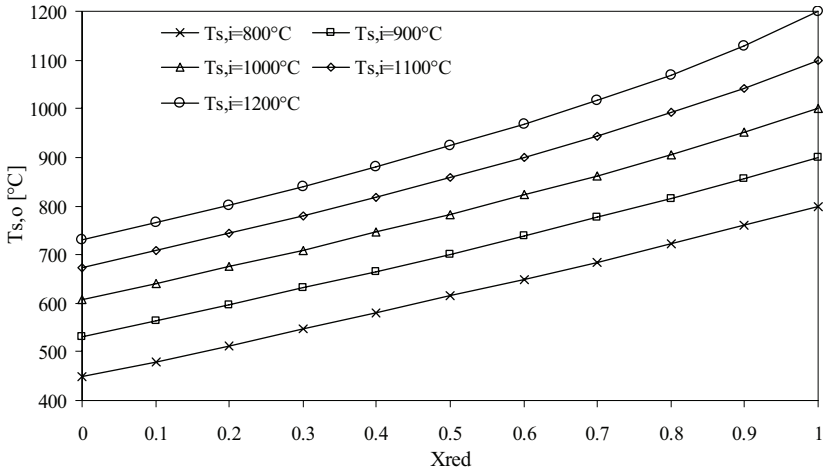

Figure 5.15 Variation in reduction reactor exit temperature ($T_{s,o}$) as a function of degree of reduction (X_{red}) for NiO/Al_2O_3 particles [χ=0.67, X_{ox}=1]

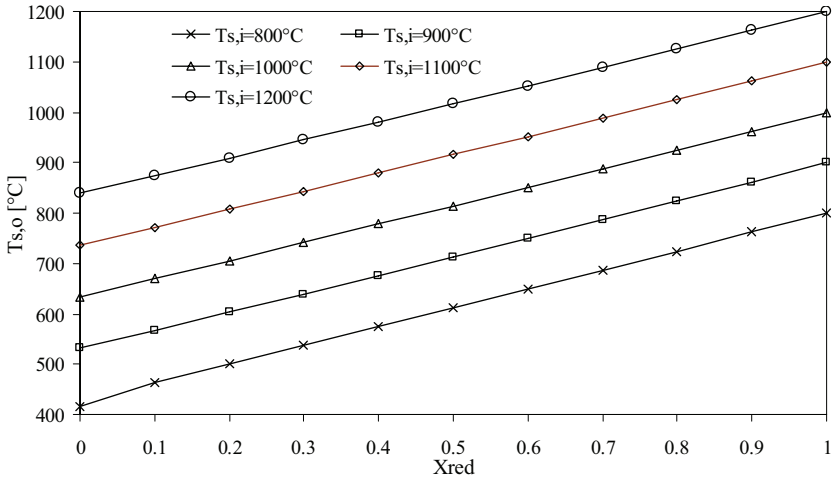

Figure 5.16 Variation in reduction reactor exit temperature ($T_{s,o}$) as a function of degree of reduction (X_{red}) for $NiO/NiAl_2O_4$ particles [χ=0.67, X_{ox}=1]

As the degree of reduction decreases (X_{red} increases), the less solids are converted. In other words, the extent of the reduction reaction decreases thereby resulting in declination of the heat requirements for the endothermic reduction reaction. The net result is that less energy is consumed in the reduction reactor and the temperature of the solids leaving the reduction reactor increases. When the reduction degree (X_{red}) approaches 1, i.e. no conversion at all, the solids do not take part in any reaction. Hence, they do not give away any heat and do not undergo any changes in the reduction reactor.

It can be seen in Figure 5.14, Figure 5.15 and Figure 5.16 that in case of the iron- and nickel-based oxygen carriers that the solids temperature at the reduction reactor exit ($T_{s,o}$) is equal to their temperature at the reduction reactor inlet ($T_{s,i}$), at the condition of X_{red}=1 i.e. no reduction at all.

Figure 5.17 shows the variation in the oxidation reactor exit temperature as a function of X_{red} at different values of oxidation reactor inlet temperature ($T_{s,i}$) for CuO/Al_2O_3.

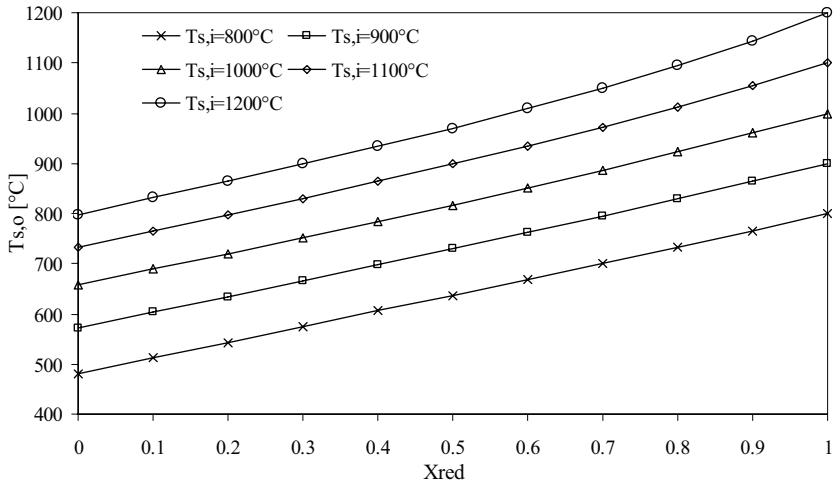

Figure 5.17 Variation in oxidation reactor exit temperature ($T_{s,o}$) as a function of degree of reduction (X_{red}) for CuO/Al_2O_3 particles [χ=0.67, X_{ox}=1]

The solids temperature at the reduction reactor exit is equal to the temperature at the reduction reactor inlet, at the condition of X_{red}=1 i.e. no reduction reaction at all. In case of CuO, with the decreasing degree of reduction (X_{red} increasing), less and less heat is released because of the declination in the extent of the exothermic reduction reaction. Hence, the temperature rise in the reduction reactor is lesser as compared to that at the higher degrees of reduction. When there is no reaction taking place in the reduction reactor, contrary to the other oxygen carriers, there is no heat release in the reduction reactor at all in case of CuO. Hence, the solids temperature rise is solely by virtue of the oxidation reaction.

The solids temperature at the reduction reactor exit is also influenced by the degree of oxidation together with degree of reduction. Although, very high degrees of oxidation can be expected to occur in CLC-reactor, regardless of the type of the oxygen carrier, yet it can be interesting to study the combined effect of varying X_{ox} and X_{red}. In order to study this effect, one oxygen carrier specie is selected i.e. $NiO/NiAl_2O_4$. Figure 5.18 presents reduction temperature variation as a function of X_{red} and X_{ox}, for a fixed oxidation temperature. It is evident from Figure 5.18 that for a fixed degree of reduction, the higher the degree of oxidation (high X_{ox}) the higher is the reduction temperature and vice-versa. Under such a condition, higher oxidation results in large amounts of metal oxide being transported to the reduction reactor which can convert only a fixed amount of solids to metal, since degree of reduction is fixed. Therefore, the heat consumption for the endothermic reaction remains the same while more and more heat is being transported along with the solid oxide. The result is an increased reduction temperature, in order to fulfil the energy balance over the reduction reactor. Analysing the condition of fixed X_{ox} and sliding X_{red} however, presents quite the opposite scenario. For such a condition, higher degree of reduction (low X_{red}) results in lower reduction temperatures, since the heat transported from the oxidation reactor remains the same while heat consumption for the endothermic reduction increases with increase in degree of reduction.

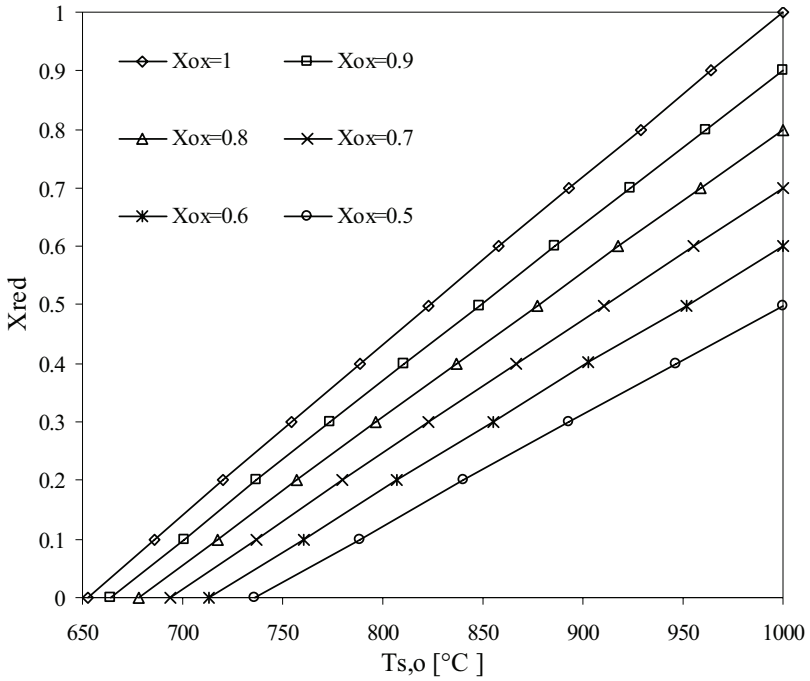

Figure 5.18 Reduction temperature as a function of X_{ox} and X_{red} at T_{ox}=1000°C [$NiO/NiAl_2O_4$, χ=0.67]

5.4 Non-Adiabatic Reactors

The non-adiabatic CLC-reactors can be used to provide heat to a side process. In this work, the oxidation reactor is assumed to be non-adiabatic that transfers heat to a certain side process from its interior; while the reduction reactor is adiabatic. However, when considering the overall reactor system, it can be considered as non-adiabatic. Figure 5.19 serves the basis for the sensitivity study of non-adiabatic reactors.

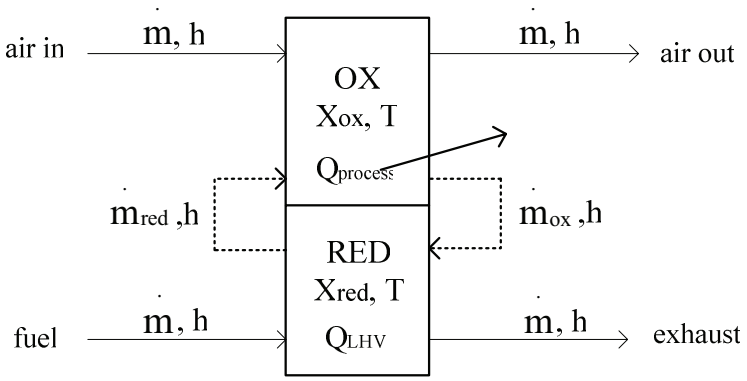

Figure 5.19 Schematics of non-adiabatic CLC-reactors with important stream and reactors parameters [T is the solids temperature in a reactor that is equal to the corresponding gaseous stream leaving that reactor, h is specific enthalpy of the solids and gaseous streams, Q is sensible heat]

The non-adiabatic CLC-reactor system is beneficial in the terms that it can be integrated with a side process; for instance steam can be produced in the heat exchangers provided at the interior of the oxidation reactor, which can further be supplied to a process or a steam cycle. The sensitivity study of the non-adiabatic reactors is carried out for a fixed oxidation temperature of 850°C. This is mainly due to the fact that in case of internal steam production, steam is produced at a fixed temperature which is lower than 850°C, even if ultra-supercritical steam is produced. Also, this temperature can be considered rather safe concerning the solids performance and the reactors material. On contrary to the approach adopted for studying adiabatic reactors; air flowrate is specified when carrying out parameter variation at a certain condition. This work designates the heat transferred to the side process ($Q_{process}$) as the parameter of foremost significance, with a viewpoint to integrate the non-adiabatic CLC-reactors in a steam cycle.

The sensitivity study results are presented in the form of a non-dimensional variable called, Relative Heat, defined by the following equation:

Relative Heat: $$Q_{rel,i} = \frac{Q_i}{Q_{LHV}}$$ (i= air out, exhaust, process)

In the above equation, Q_i is the sensible heat in a stream and Q_{LHV} is the heat supplied to the reactor system in the form of fuel.

This study does not present impact of varied parameters on solids flowrates, because they are in accordance with the results presented for the adiabatic reactors.

5.4.1 Air Flowrate

Air flowrate can be regarded as the most significant factor in non-adiabatic reactors when maximisation of the heat transferred to the side process is the foremost objective. When the reactors operate at a fixed oxidation temperature with a certain air inlet temperature, an increase in the air flowrate will result in the less heat transferred to the process and vice-versa. This can be of interest to compare the relative heat of the gaseous streams as a function of air flowrate. Figure 5.20 presents such a comparison for the selected oxygen carriers. It can be seen that the relative heat for the exhaust stream remains constant independent of the air flowrate as it depends on the amount of fuel and the exhaust temperature. The air flowrate however, affects the relative heat of the air stream leaving the oxidation reactor because the relative heat depends on the sensible heat in the stream which again is a function of the specific enthalpy of the stream and its flowrate. The heat transferred to the process is thus linked with the specific enthalpy of the air stream leaving the oxidation reactor. At the condition of constant temperature of air at the inlet and the outlet of the oxidation reactor, the specific enthalpy (h) rise for the air remains constant. For a constant fuel flowrate and constant degrees of oxidation and reduction of solids, the total solids flowrate of at the exit of each reactor remains constant. This means that at a fixed oxidation and reduction reactor exit temperature and constant degrees of solids conversion, the heat transported by the solids from one reactor to the other remains constant. Considering the heat balance over the oxidation reactor, an increase in air flowrate inevitably results in less heat available for the side process in order to maintain the enthalpy of the oxygen-depleted air at the oxidation reactor exit.

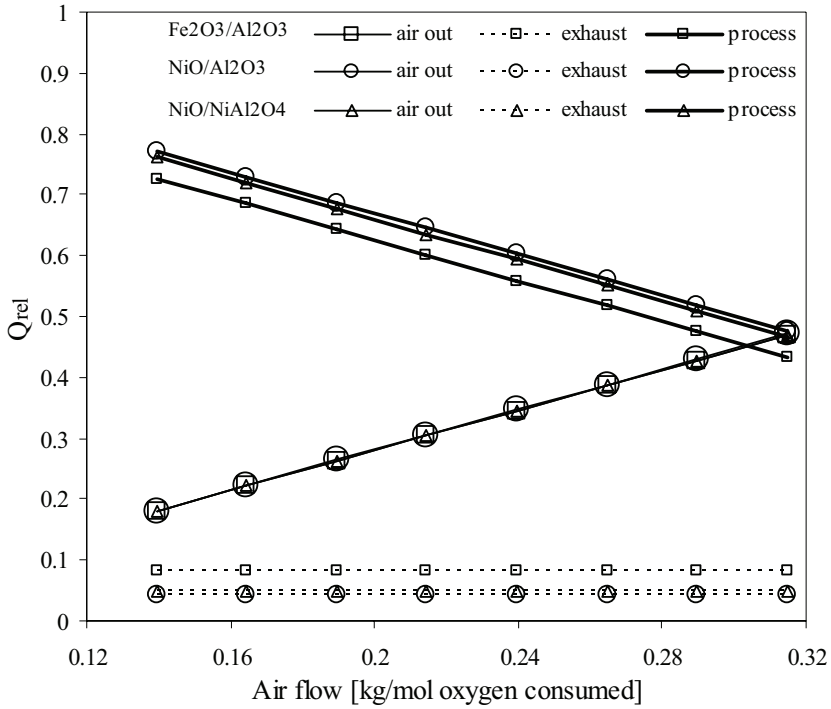

Figure 5.20 Relative heat as a function of air flowrate to the non-adiabatic CLC-reactors [Air inlet temperature=15°C, Air outlet temperature=850°C, Fuel inlet temperature=10°C, Exhaust temperature=602°C, X_{ox}=1, X_{red}=0.3, χ=0.6]

Figure 5.20 includes the lower limit of the air flowrate at which the maximum heat transferred to the side process is possible. Therefore, it can be seen in Figure 5.20 that the lowest air flowrate results in the highest heat availability for the process. Since, the main objective of non-adiabatic reactors is to maximise the heat available for the process (for instance produce steam at maximised level for a Rankine cycle); therefore the lowest possible air flowrate is an appropriate choice. Nonetheless, there is a lower limit of the air flowrate in connection with the fuel flowrate and the oxidation temperature.

5.4.2 Air Inlet Temperature

Air inlet temperature, as in adiabatic reactors; also plays significant role in the energy balance of non-adiabatic CLC-reactors. The higher the air inlet temperature, the higher is the enthalpy of the air stream entering the oxidation reactor. As it has been established in the previous section that the lowest possible air flowrate results in the maximum heat transferred to the process; therefore it can be of interest to analyse the reactors for different air to fuel ratios at various values of air and fuel inlet temperature. In this way a chart can be generated that exhibits the non-adiabatic reactors characteristics over a wide range of air temperature data. Such a chart can be helpful to find an operating range, considering the limitations associated with air preheating and maximum possible air inlet temperature. Such a chart is presented in Figure 5.21.

When non-adiabatic CLC-reactors are integrated into a larger process there are a number of streams available for the heat integration. However, the air inlet temperature cannot be increased beyond a certain value owing to the heat exchanger limitations.

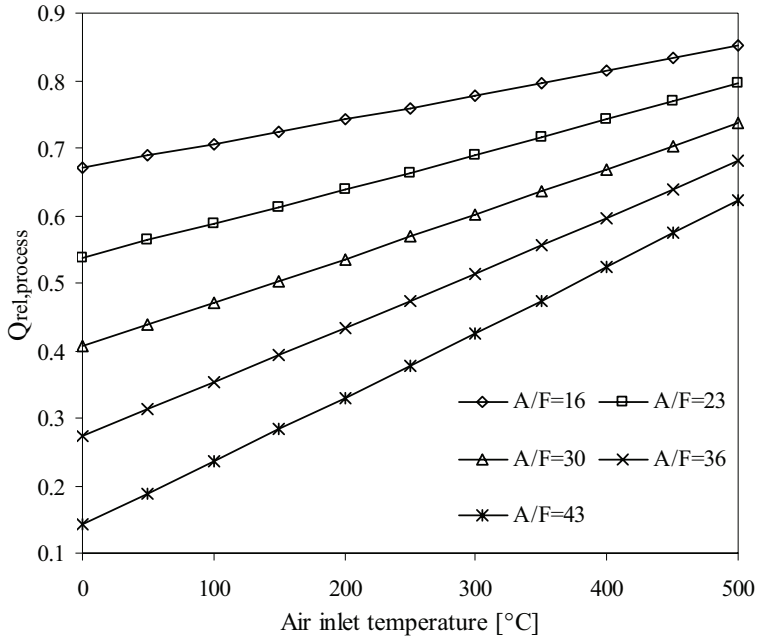

Figure 5.21 Relative heat (process) as a function of air inlet temperature [$NiO/NiAl_2O_4$, χ=0.67, X_{ox}=1, X_{red}=0, A/F: Air to fuel ratio (kg/kg)]

The trends in Figure 5.21 show that the heat available for the side process increases with an increase in air inlet temperature. That is due to the balancing off the energy around the oxidation reactor. At the condition of a fixed oxidation reactor exit temperature and a fixed air flowrate, an increase in air inlet temperature results in the air stream at a higher specific enthalpy (h) thereby the enthalpy rise decreases. The net result is that the heat transferred to the side process increases in order to fulfil the oxidation reactor energy balance.

5.4.3 Degrees of Solids Conversion

Figure 5.22 presents the heat transferred to process relative to the heat supplied by the fuel, as a function of degrees of solids conversion in the two reactors. The degrees of solids conversion in the two reactors play a major role in the heat balance over the reactor system. Therefore, the heat available for steam production will vary according to the conditions of solids conversion in the two reactors. The air to fuel ratio (A/F in kg/kg) is selected to be the minimum possible, i.e. 16. This can be seen in Figure 5.22 that although heat is transferred from the interior of the oxidation reactor, degree of oxidation has a small impact on the heat available to the process; while degree of reduction has a prominent effect. The revelation of this effect from Figure 5.22 is important because it is the degree of reduction which is an issue of concern in the CLC-research. A higher solids conversion in the reduction reactor is also desirable to obtain reasonable solids flowrates and realise a conceivable reactor system. A declination in degree of reduction (increase in X_{red}) inevitably results in an increased reduction temperature as well as increased amount of unconverted metal oxide, which also means that the solids entering the oxidation reactor carry more heat. A decreased rate of reduction of solids implies an increased solids flowrate and also the solids leaving the oxidation reactor are in thermal equilibrium with the oxygen-depleted air; therefore the energy and mass balance demand a higher consumption of heat in the process of heating up an increased supply of solids up to the oxidation reactor exit temperature.

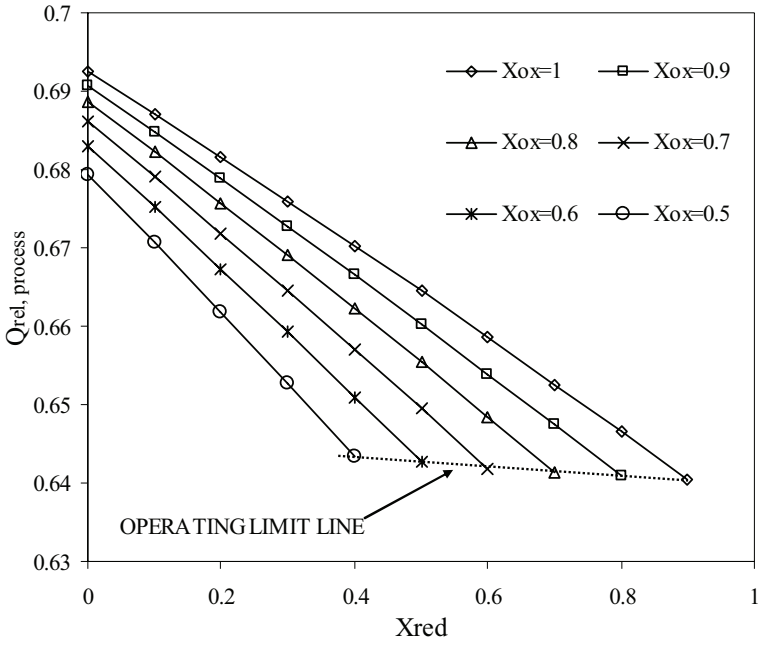

Figure 5.22 Relative heat (process) as a function of X_{ox} and X_{red} [$NiO/NiAl_2O_4$, χ=0.67]

In other words, a higher sensible heat in solids entering the oxidation reactor also results in a higher sensible heat in solids leaving it. The net effect is a decrease in heat available for steam consumption. The OPERATING LIMIT LINE shown in Figure 5.22 suggests that the reactor system should operate above this line in order to achieve a conceivable reactor system design. The CLC-reactors are however expected to operate in the upper left region of the above figure i.e. at very high degree of oxidation (X_{ox}) and at moderately high degree of reduction, i.e. low values of X_{red}, for instance X_{red}=0.3. The result shown in Figure 5.22 thus point out the significance of the extent of solids reduction in a non-adiabatic CLC-reactor system integrated with a side process. Therefore, if supply of heat to the side process is the primary objective of non-adiabatic CLC-reactors; the higher the reduction achieved the better the system will perform.

6 CLC Application in Combined Cycles

This chapter presents implementation of Chemical Looping Combustion in combined cycles. As a starting point, a conventional natural gas-fired combined cycle is presented as the reference cycle. Post combustion CO_2-capture to the conventional combined cycle is also applied and the efficiency drop due to CO_2 capture is calculated. A CLC-combined cycle is then designated as the base-case CLC cycle. Sensitivity results for the base-case CLC combined cycle are presented. Also, modifications to the base-case CLC-power cycle are presented and results for each cycle are discussed. Environmental aspects of nickel oxide in CLC operation is also dealt with in this chapter. Moreover, the challenges in applying conventional technology in CLC-combined cycles are briefly discussed. The chapter concludes the findings of the simulations by presenting a comparison of different options for CLC-combined cycle and their comparison with the reference conventional combined cycle.

6.1 CLC for Combined Cycles

The combined cycle (gas turbine cycle and steam turbine cycle) enjoys the status of having the highest fuel energy to power conversion efficiency. The high efficiency together with the possibility of its integration into process plants makes combined cycle an attractive option for the power industry. As regards CLC, being a relatively young field of research competing with other alternate contestants for efficient and clean power generation; combined cycle can be a choice for CLC-application. The CLC-reactors in this case, will replace combustion chamber of the gas turbine in combined cycle. This substitution however, if successful, will be quite a big step in the field of power plants, considering the nature of operation, the size of reactors, the nature of reactions and the working fluids, as compared to a conventional gas turbine. However, there are big challenges ahead which have to be met and overcome before CLC can be realised in combined cycles. Although there may exist arguments and doubts about the successful realisation of CLC in combined cycles at this stage; nevertheless CLC has quite a few features that make it a suitable option for efficient power generation with CO_2 capture. Unlike a conventional combined cycle, the different types of working fluids and availability of two streams available for power generation make CLC a flexible process as concerns different plant configurations as well as its integration with other processes. This availability of different streams on the other hand, also demands for smart and efficient plant configurations that are well-integrated and result in minimum exergy destruction through high degree of heat utilisation. Therefore, while the research on other aspects of CLC is going on, it is quite a rational approach to figure out the best combined cycle configurations or alternatives for CLC application. When the suitable plant configurations are achieved, CLC research can be directed towards and focussed on the specific aspects and challenges that arise when CLC operates in such configurations.

6.2 Selection of Fuel

Chemical Looping Combustion is in principle possible to use with any kind of hydrocarbon fuel whether oil, coal or natural gas. The energy trends predictions show that coal will be amongst the primary energy sources in the future [OECD/IEA, 2005b]; this has previously been discussed in chapter 2. Although coal is less expensive as compared to natural gas and oil, it is not an easy fuel to handle. Also it is very difficult to feed a solid fuel like coal directly into a gas turbine. However, coal can be converted into some other form of fuel

first. For instance, coal can be gasified into a synthesis gas, mainly consisting of hydrogen and carbon monoxide, which after cleaning up, can be separated into a carbon-rich gas and a hydrogen-rich gas. The hydrogen-rich gas can then be used as fuel in a conventional gas turbine. There has been some research concerning coal-based CLC, which has been reviewed in chapter 3; but nonetheless its realisation in combined cycles has yet not been presented. Also, reaction of coal with different oxygen carriers in CLC still remains an issue of deeper investigation. Natural gas on the other hand, possesses all the properties that make it a suitable and attractive option as a fuel for gas turbines, and in combination with CLC. The foremost distinguishing property of natural gas is its being clean in composition. Natural gas is cleaner than oil and coal in terms of carbon content; and also it contains no sulphur. As regards CLC, natural gas is very promising fuel for its reaction with solid oxides and most of the CLC-research is focussed on natural gas. Therefore, in this work, natural gas has been chosen as the fuel for CLC-combined cycles.

6.3 Methodology and Scope of Cycles Analysis

The methodology of analysing a power cycle basically consists of two parts; energy analysis and exergy analysis, where energy analysis is performance evaluation of energy conversion systems through thermodynamic analysis. The exergy analysis of CLC has previously been presented by some researchers; [Anheden and Svedberg, 1998], [Brandvoll and Bolland, 2004]. The results of the studies performed by these researchers are in agreement with each other that a CLC-system has exergy destruction of the order of about 2-3%-points less as compared to conventional combustion. Although the work by above-mentioned researchers as well as others (reviewed in chapter 3) presents thermodynamic analysis of some CLC-cycles; detailed sensitivity studies, comparison and benchmarking of several CLC-combined cycle designs still remains an unaccomplished task. One of the paramount objectives of this thesis is to come up with various options for CLC-combined cycles that can achieve a reasonable efficiency with CO_2 capture. Therefore, design and thermodynamic analysis for selection of reasonable operating conditions of various CLC-combined cycles form the major core of the research work presented in this chapter. The sensitivity study of each of the CLC-combined cycles is carried out in order to find the optimum design point. The methodology for studying the CLC-combined cycles has been to vary the TIT and CPR at a constant fuel flowrate. The term TIT refers to the temperature of the oxygen-depleted air at the oxidation reactor exit and CPR is the air compressor pressure ratio.

It is important to discuss the computational assumptions before the cycles are presented. The main set of assumptions is included in Appendix A. However, some of the CLC-specific assumptions used throughout the simulations are given here. The CLC-reactors are assumed to be adiabatic with isothermal mixing of solids and gases. The simulations are based on idealised behaviour of solid particles circulating between the two reactors; i.e. it is assumed that the solids exhibit mechanical and chemical stability over long periods of operation. The pressure drop in each reactor, including the ducting before and after the reactors as well as the cyclone, is assumed to be 5% of the incoming stream pressure. Based on the experiments by Brandvoll [2005], the present work uses NiO supported on $NiAl_2O_4$ (60% NiO by mass) as oxygen carrier. According to Lyngfelt et al. [2004], the theoretical thermodynamic limit of NiO to convert fuel is 99.5%. However, 100% fuel conversion was assumed for the present work. Nevertheless, the sensitivity of a CLC combined cycle with respect to the degree of fuel conversion is also presented in the section 6.5.1. Degree of oxidation is assumed 100% (Xox=1.0) which means that all Ni entering the air reactor undergoes a complete oxidation. Degree of reduction in the fuel reactor is assumed 70% (Xred=0.3)

which means that 70% of NiO entering the fuel reactor is converted into Ni. All the results are based on the assumption of complete stoichiometric conversion of fuel, for instance 1 mole of methane reacts with 2 moles of oxygen to form 1 mole of CO_2 and 2 moles of H_2O and the same holds for other components of natural gas. Definitions of all the parameters are in accordance with chapter 4.

6.4 Reference-Conventional Combined Cycle (CC-Ref)

In order to compare the efficiency of several natural gas-fired CLC-combined cycle configurations with a conventional natural gas-fired combined cycle, a generic combined cycle model was developed. Figure 6.1 presents schematics of the conventional combined cycle that is designated as the reference cycle. The assumptions for the reference-conventional combined cycle are included in Appendix A.

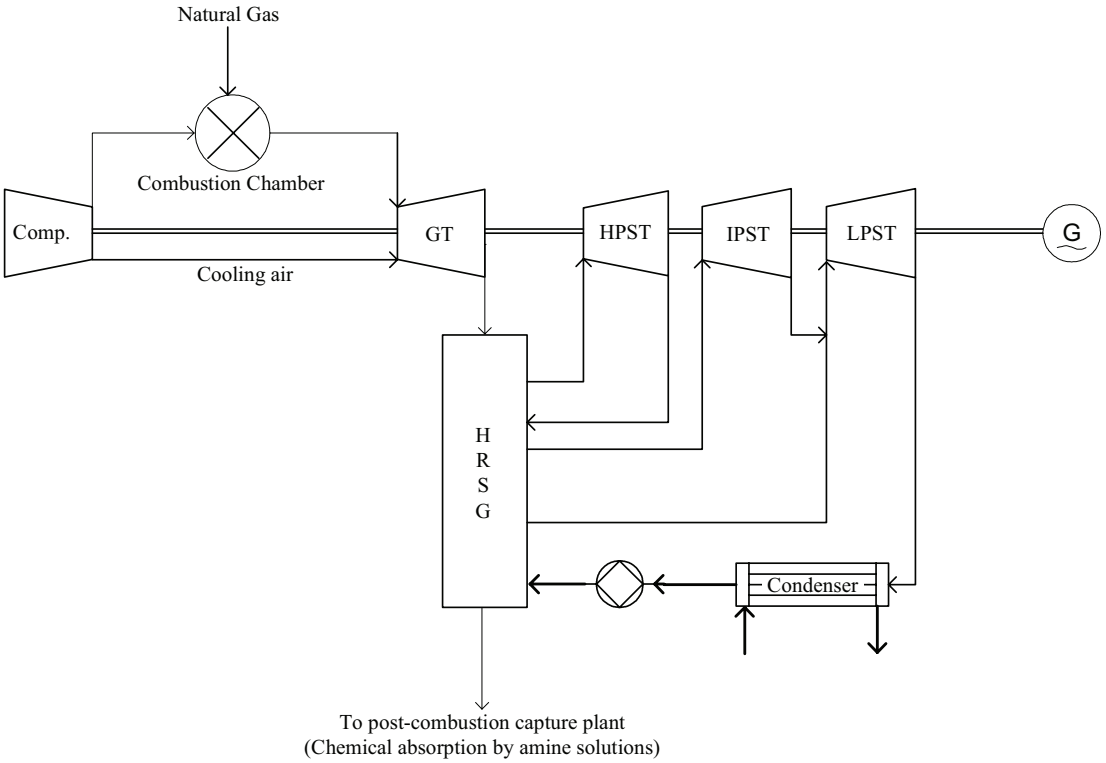

Figure 6.1 Schematics of the conventional natural gas-fired combined cycle set as reference

The combined cycle is based on compressor pressure ratio 17 and combustion chamber exit temperature 1425°C. The plant can achieve a net plant efficiency of 56.6% at these conditions. This efficiency does not include the penalty for CO_2 capture. Also, the efficiency has not been optimised by parameter variations (compressor pressure ratio, combustion chamber exit temperature or steam cycle parameters).

It can be seen in Figure 6.1 that the flue gas at the HRSG exit is led to the post combustion CO_2 capture plant. The chosen technique is chemical absorption of CO_2 by amine solution. Estimation of the CO_2 capture penalty based on this technique however, is not a straightforward procedure. The efficiency drop depends on the choices and assumptions on which the post combustion plant operates.

Undrum and Bolland [2003] presented a novel methodology for comparing CO_2 capture options for natural gas-fired combined cycle plants. The CO_2 capture penalty associated with the reference combined cycle has been calculated on the basis of the work presented by Undrum and Bolland. The efficiency drop due to CO_2 capture is calculated by the following equation.

$$\Delta\eta = \eta_{CC} - \eta_{CC-CO_2}$$

In the above equation, $\eta_{CC\text{-}CO2}$ and η_{CC} is the net plant efficiency of the combined cycle with and without CO_2 capture.

The efficiency drop $\Delta\eta$ is the sum of the penalties related to the CO_2 capture and compression and is given by the following equation:

$$\Delta\eta = \frac{E_{mf}^{CO_2} C}{LHV} + \frac{E_{hr}^{CO_2} \alpha Cf}{LHV} + \frac{E_{comp}^{CO_2} Cf}{LHV}$$

(1) (2) (3)

The term (1) in the above equation represents the mechanical work or electricity consumption in the absorption process, which is chiefly associated with the exhaust gas fan. Since there is pressure drop across the absorption tower, exhaust gas fan is used to overcome this pressure. In the absence of exhaust gas fan, the inducing of back pressure on the gas turbine would become inevitable to overcome this pressure drop, which in turn will result in further efficiency drop due to work reduction from the gas turbine. In term (2), E_{mf} describes the exhaust gas fan work consumption (MJ/kg CO_2) while C is the ratio between formed CO_2 and fuel (kg CO_2/kmol fuel).

The term (2) represents the efficiency drop concerned with the steam extraction from the steam turbine in order to provide heat for CO_2 stripping. In term (2), E_{hr} describes the heat consumption which has been selected as 3.8 MJ/kg CO_2 captured, based on the work by Undrum and Bolland. In term (2), α is the ratio of incremental power reduction to incremental heat output (MJ_{el}/MJ_{heat}) when extracting steam at given pressures from a steam turbine, while f is the fraction of CO_2 captured in the absorption process. The penalty represented by term (2) constitutes the major efficiency reduction in CO_2 capture process.

The term (3) represents the efficiency drop due to CO_2 compression, where E_{comp} describes the work consumption (MJ/kg CO_2) for CO_2 compression from atmospheric pressure to the desired end pressure.

Undrum and Bolland presented the outcome of their work in the form of several charts relating all the parameters involved in the equation. These charts have been utilised in the present work for calculating efficiency drop due to CO_2 capture from the reference conventional combined cycle. The same fuel composition has been used for the reference cycle as that in the CLC-cycles. Also, the fraction of CO_2 captured (f) is selected to be 90 %, which is very high, to make it comparable to CLC-cycles that can capture close to 100% CO_2. These assumptions make the comparison of CLC-cycles with the reference cycle to be at a higher degree of transparency. The detailed procedure of efficiency drop calculation is

not discussed here. However, for further insight into the post combustion amine-based capture, readers are referred to the work by Undrum and Bolland.

Figure 6.2 presents the results for the CO_2 capture penalty for the reference conventional combined cycle in the form of efficiency drop as a function of the heat requirements for CO_2 stripping for different values of pressure drop in the absorption tower at the end CO_2 pressure of 110 bar. It can be seen that the efficiency drop increases with the heat requirements for CO_2 stripping as well as the pressure drop in the absorption tower.

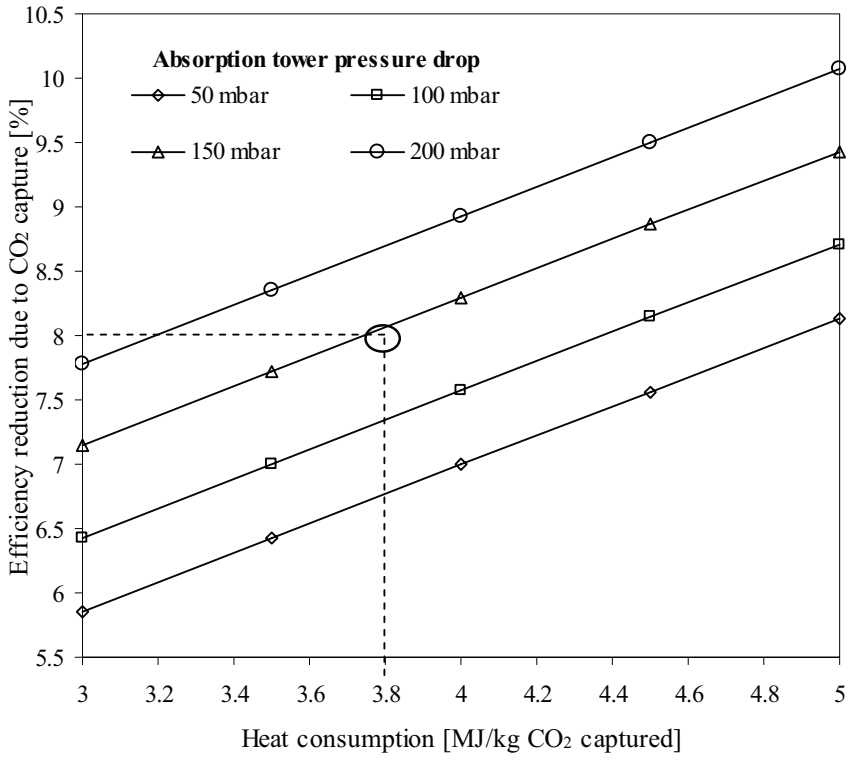

Figure 6.2 Conventional natural gas combined cycle efficiency drop due to CO_2 capture

However, the efficiency drop due to the CO_2 stripping is more prominent and constitutes for the major energy penalty in the CO_2 capture process. It can be seen in Figure 6.2 that the efficiency drop increases with the pressure drop in the absorption tower. The selection of an appropriate point in Figure 6.2 is significant here, when considering the comparison of the reference cycle with the CLC-cycles. Based on the work by Undrum and Bolland [2003], the absorption tower pressure drop is assumed to be 150 mbar, the heat requirements for CO_2 stripping is assumed to be 3.8 MJ/kg CO_2 captured. While, the CO_2 end pressure is assumed 110bar, which is the same as that for the CLC-cycles. With these assumptions, the penalty in mechanical work for exhaust gas fan is about 2%, the penalty due to heat for CO_2 stripping is 4.3% and the penalty related to CO_2 compression is 1.7%. Thus the total efficiency drop due to CO_2 capture is about 8% thereby reducing the net plant efficiency of the reference cycle from 56.6% down to 48.8%.

6.5 The Base-case CLC Combined Cycle (CLCCC)

Figure 6.3 shows schematics of the CLC-combined cycle designated as the base-case.

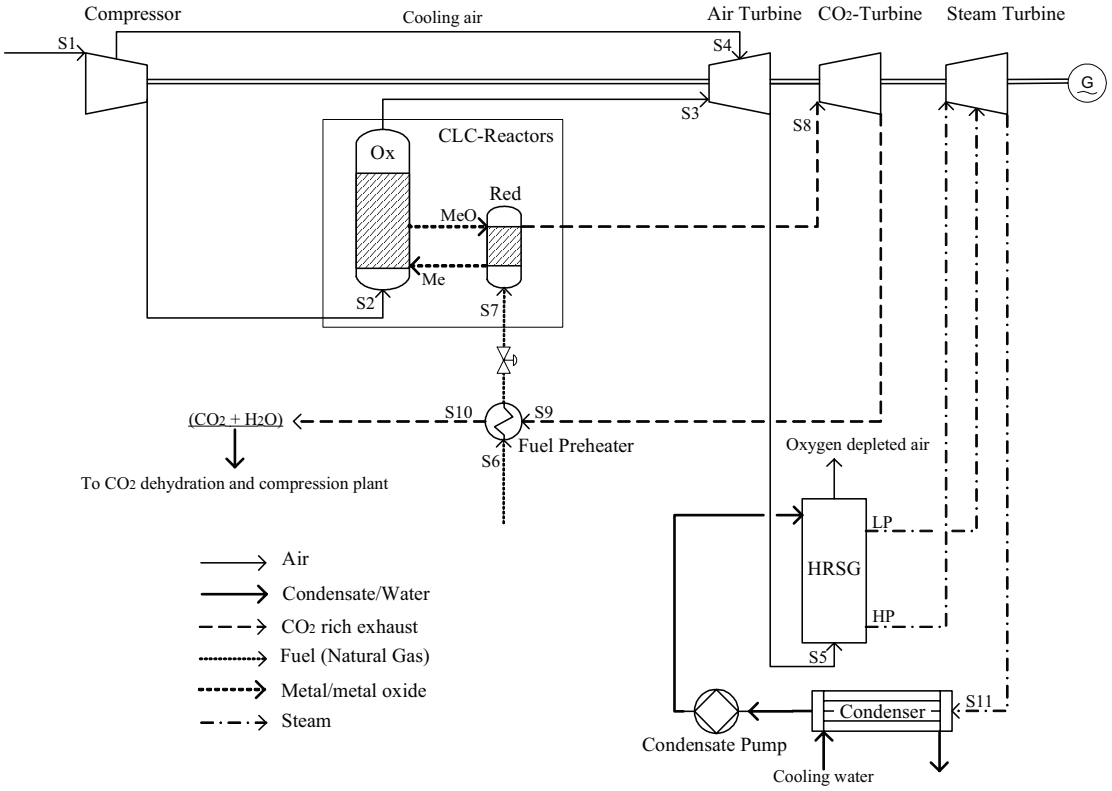

Figure 6.3 Schematics of the base-case CLC-combined cycle (CLCCC)

The combined cycle is different compared to a conventional combined cycle as the air and fuel streams are kept separate in two Brayton cycles; and with expansion in an air-based turbine and CO_2 turbine. The air compressor, air turbine and CO_2-turbine are assumed to be on the same shaft, while it can be assumed that the air turbine drives the compressor. The fuel is assumed to be pressurised, therefore no fuel compressor is included. Air at compressor exit enters the CLC-oxidation reactor (Ox) where it reacts with the reduced metal, while fuel reacts with the metal oxide in the reduction reactor (Red) at the same time, in a continuous operation. In order to avoid any gas leakages between the two reactors, it is very important to maintain the same pressure of the gases in the ducting that connects the CLC-reactors for solids transport. This duct is necessarily the one through which the solids separated from the oxygen-depleted air in the cyclone system fall down to the fuel reactor. In case of any pressure difference occurring in the ducting, gas may leak between the two reactors. Therefore, it is desirable to obtain the same pressure at the exit of oxidation and reduction reactors. This is done by controlling the pressure at the reduction reactor inlet by using a pressure control valve. The pressure is varied in accordance with the pressure at the oxidation reactor exit and the pressure drop through the reduction reactor. Hot and pressurised oxygen-depleted air flowing out of the oxidation reactor enters the air turbine where it mixes with the cooling air drawn from the compressor. The air expands down to slightly above atmospheric pressure, considering the pressure drop in the heat recovery steam generator (HRSG). The air turbine exhaust then passes through the HRSG to generate

steam at two pressure levels. The steam turbine is a condensing turbine as the combined cycle in the current work is solely for electricity production. High pressure steam is admitted to the steam turbine at 60 bar and expands down to 5 bar where the low pressure steam is admitted. The total steam then expands down to the condenser pressure. In the reduction reactor (Red), the reaction of fuel with metal oxide results in an exhaust comprising CO_2 and steam at the reduction reactor temperature and pressure. The exhaust expands in the CO_2-turbine to a pressure slightly above atmospheric pressure considering the pressure drop in the fuel preheater. The fuel preheater not only adds up to overall exergy loss minimisation but also cools down the exhaust stream, which also facilitates its subsequent dehydration. The hot stream temperature at the fuel preheater exit is selected in such a way that there is no risk of steam condensation. The exhaust is then fed to the CO_2 dehydration and recompression plant, which is described in chapter 4.

6.5.1 Results of the Cycle study

Since the cycle has been designated as the base-case, the cycle study covers certain aspects and parameter variations that will not be presented for all the other cycles. The main findings of the cycle study are presented in the form of efficiency as a function of specific work, as shown in Figure 6.4. The compressor pressure ratio and oxidation temperature are varied. The term TIT corresponds to the oxidation reactor exit temperature.

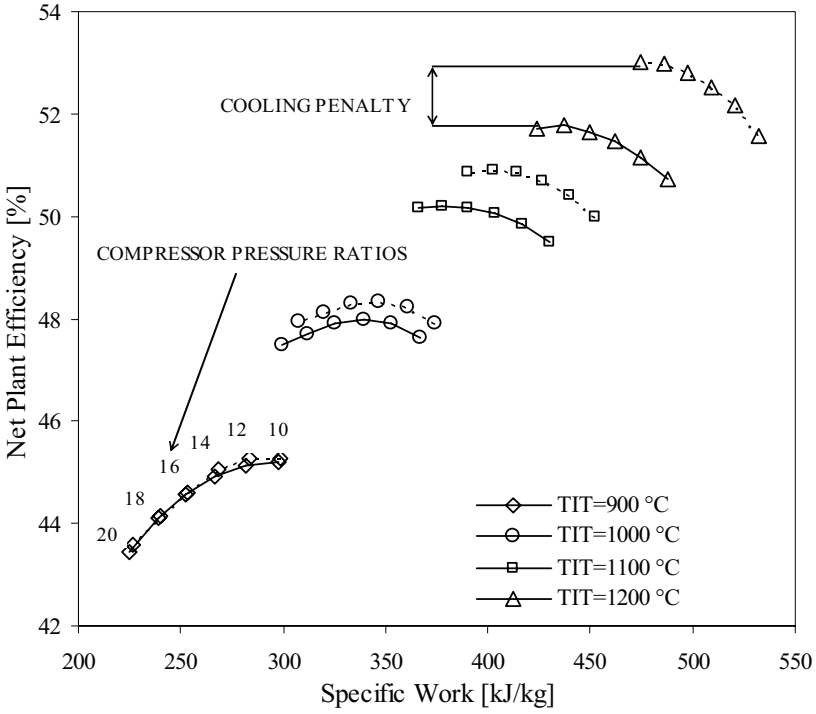

Figure 6.4 Net plant efficiency of CLCCC as a function of specific work
[The term TIT refers to the oxidation temperature.
The broken lines correspond to the cycle with uncooled air turbine.]

The figure also presents the efficiency drop due to the air turbine cooling penalty. The broken lines on the figure represent the cycle where the air turbine is uncooled. The air flow through the cycle decreases with an increase in desired TIT value in order to maintain the

reactor temperature. Therefore, the points of specific work move towards the right with increased TIT values and it can be seen that the maximum specific work is at TIT=1200°C and PR=10. At a certain TIT, increase in PR results in lower specific work. This is due to an increased air flow in order to maintain the reactor temperature when the compressor exit temperature increases with increased PR. Although efficiency is a function of TIT and the modern gas turbines can stand elevated temperatures (above 1200°C) because of advanced cooling technologies; yet the material constraints associated with the CLC reactor system still hinder the adoption of high temperatures. In general, turbine blades need to be cooled at TIT values higher than 850°C. Figure 6.4 also presents the efficiency drop due to cooling for different TIT's and PR's. At the optimum condition of TIT=1200 °C and PR=18, the cooling penalty results in an efficiency drop of 1.2% points and the net efficiency is 51.8%. This efficiency is slightly higher than that achieved at the condition of PR=10, TIT=1200°C with no turbine cooling. It is of interest to see a comparison of the cycle summary in terms of flow rates and power balance, for cooled and uncooled air turbine. Table 6-1 presents the combined cycle summary for uncooled and cooled air turbine at the optimum pressure ratio of 10 and different TIT values. It can be seen that the net efficiency for the combined cycle with cooled air turbine is lower compared to that with uncooled turbine, because of the cooling penalty on the turbine power output. When employing air turbine cooling, the airflow rate at the compressor inlet increases in the amount required for turbine cooling in turn increasing the power required to drive the compressor. The work extracted by the cooled air turbine is higher than that of the uncooled turbine due to the increased flow rate; however, the gross work is lower due to an increased compressor duty.

Table 6-1 Comparison of energy balances for the base-case CLC-combined cycle with cooled and uncooled air turbine
[The compressor pressure ratio is 10 for all the conditions.]

	Uncooled Air Turbine				Cooled Air Turbine			
TIT (°C)	900	1000	1100	1200	900	1000	1100	1200
Airflow at comp. exit (kg/s)	1058	893	771	676	1059.7	905.4	798.5	721.8
Coolant flow (kg/s)	0	0	0	0	1.7	12.4	27.5	45.8
	Power (MW)							
Fuel Input	697.5	697.5	697.5	697.5	697.5	697.5	697.5	697.5
Air Turbine	518.5	472.0	436.5	408.0	519.0	475.4	443.7	420.1
CO2-Turbine	32.7	36.6	40.5	44.4	32.7	36.6	40.5	44.4
Compressor	-322.9	-272.6	-235.2	-206.4	-323.5	-276.4	-243.9	-220.5
Steam Turbine	109.6	120.5	129.4	136.4	109.3	118.9	126.1	131.5
Gross Power	337.9	356.5	371.2	382.4	337.5	354.5	366.4	375.5
Auxiliaries + Losses	-7.7	-7.9	-8.1	-8.3	-7.7	-7.9	-8.1	-8.2
CO2-Compression	-14.5	-14.5	-14.5	-14.5	-14.5	-14.5	-14.5	-14.5
Net Power	315.7	334.1	348.6	359.6	315.3	332.1	343.8	352.8
Specific Work (kJ/kg)	298.4	374.1	452.1	532.0	297.5	366.8	430.6	488.7
Net Plant Efficiency (%)	45.3	47.9	50.0	51.6	45.2	47.6	49.3	50.6

As mentioned earlier, the term TIT refers to the oxidation reactor exit temperature and in case of cooled turbine the real turbine inlet temperature is lower than TIT due to mixing of hot air and coolant air streams. As the TIT increases, the cooling demands rise, and the real TIT becomes lower than the oxidation temperature. At a certain pressure ratio, a lower turbine inlet temperature also results in a lower turbine exit temperature in comparison with the uncooled turbine. The effect of lower turbine exit temperature is less heat available for steam generation in HRSG and hence a lower output power from the steam turbine as well. This effect together with the increased compressor work results in a lower net efficiency

compared to that of the cycle with uncooled air turbine. Since the air turbine cooling has no effect on the conditions in the reduction reactor, the reduction temperature and exhaust flowrate remain the same irrespective of the air-side of the cycle. Hence, the CO_2-turbine power output remains the same in both cases under the same conditions. Therefore the power requirements for CO_2 compression also remain the same. Another parameter of significance is the compressor pressure ratio. The selection of pressure ratio is in fact a trade-off between the output power from the gas turbine and the steam turbine. At low pressure ratios and high TITs, the work extraction from gas turbine is less so that the turbine exit temperature (TET) is comparatively high resulting in HP steam with a high degree of superheat and hence higher work extraction from the steam turbine. On the other hand, at high pressure ratios, gas turbine output power and efficiency increase due to higher difference in TIT and TET; i.e. the TET is comparatively lower, resulting in HP steam with a lower degree of superheat and lower output from the steam cycle. Although an increase in pressure ratio results in more work extracted from the gas turbine, it has an optimum value at which the gas turbine work and the steam turbine work altogether give the maximum work output. The results at this condition do not however reflect a fully optimised plant, unless all the significant parameters other than TIT and PR are also optimised. The results presented so far conclude that the most optimum operating condition for a CLC-combined cycle under the devised configuration is at the TIT of 1200°C and at a pressure ratio between 14 and 20. The specific work is of significance in this regard, when considering the selection of an efficiency point as the design point. For economical reasons, the higher the specific work the less expensive is the gas turbine. Therefore, when the efficiency improvement is not so prominent going from one value of pressure ratio to another, the lower pressure ratio should be selected as the design point, because it results in higher specific work at the cost of very little efficiency drop. Since the cycle has not been optimised, one pressure ratio can be chosen as the optimum condition, which can be selected to be 18. Under this condition, a net plant efficiency of 51.8% is achieved at near to zero CO_2 emissions level.

Exhaust Recirculation to the Reduction Reactor

One operational problem that may arise during CLC operation is carbon deposition (or coking) on the oxygen carrier particles in the reduction reactor. When hydrocarbon i.e. natural gas comes into a high temperature environment, as in the reduction reactor, carbon can be formed through a series of reactions. This may affect mass transfer between solids and fuel in the reduction reactor thereby reducing the rate of conversion of solids during the reduction reaction. Also, if formed, carbon will be carried away with the solid particles to the oxidation reactor and will come in direct contact with air. This is highly undesirable and must be avoided in order to prevent any CO_2 formation in the oxidation reactor. Although experiments by Mattisson et al. [2001] suggest that there is no carbon formation in the reduction reaction; nevertheless there may exist some risk of carbon formation, if operating conditions are varied as in the experiments by Ishida et al. [1998b] and Cho et al. [2005c]. One way to deal with this problem is use of steam in the reduction reactor. This practice is also carried out in different industrial processes. Jin et al. [1999] suggested that in CLC, an optimum steam to fuel ratio is 2:1. In CLC, steam is readily available in the form of the CO_2-rich exhaust and can be supplied by recycling a part of exhaust back to the reduction reactor through its mixing with fuel. Apart from coking, recycle may also be necessary to keep the reduction reactor fluidised at part-load. Figure 6.5 shows the principle of exhaust recirculation used in the present work.

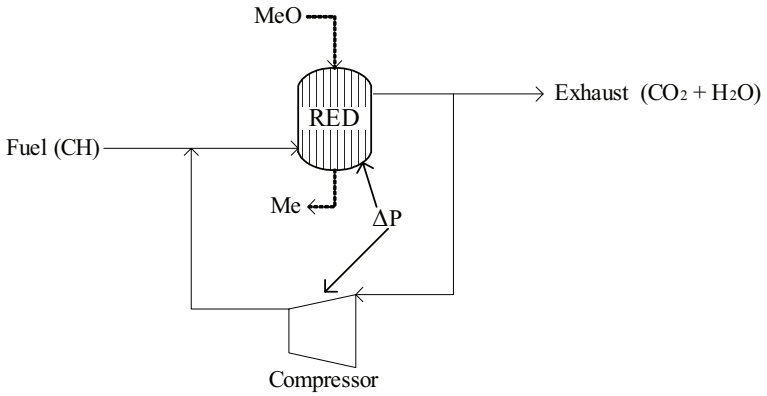

Figure 6.5 Recirculation of exhaust stream to the reduction reactor

The exhaust stream is split into two parts, one being recycled back to the fuel stream. This is beneficial in the terms that the exhaust stream also contains CO_2 which has the same effect as that of steam for avoiding coking. The cycle analysis with exhaust recirculation shows that recirculation has a very little effect on the efficiency which is related to the use of a light duty compressor in order to make up for the pressure loss through the reactor. The results show that the efficiency drop due to exhaust recirculation is negligible (0.04%). This must be mentioned here that the stoichiometry of the reaction of fuel with metal oxide is assumed to be the same regardless of exhaust recirculation. Therefore, the added CO_2 does not take part in any reaction and the combustion products remain the same as in the case of no exhaust recirculation.

Effect of Degree of Fuel Conversion

The results shown so far are based on the assumption of complete fuel conversion. In reality, the solid-gas reactions are likely to result in partial conversion due to the limitations associated with mass transfer. Therefore, it is of significance to analyse the cycle under the conditions of incomplete fuel conversion. The results show that there is a 0.6% efficiency drop for each 1% reduction in degree of fuel conversion. This should be considered as a significant efficiency drop and efforts should be made to achieve a maximum possible degree of fuel conversion. For the CLC reactors based on nickel oxide, ideal fuel conversion efficiency will of course be 99.5%, considering the thermodynamic limit of nickel oxide. This conversion efficiency can be achieved by designing a sophisticated reduction reactor that provides sufficient residence time of particles so that natural gas adsorption into the particles takes place; and providing an atmosphere that favours the solids-gas reaction. It is being reiterated here that the current work is based on stoichiometric reaction between fuel and solids with 100% fuel conversion resulting in pure CO_2/H_2O mixture. If the side reactions of metal oxide with natural gas are considered, the net plant efficiency of the cycle may vary to some extent but this is not presented here.

Power and Energy Balance

Table 6-2 presents the power and energy balance for the base-case CLC-combined cycle.

Table 6-2 Power and energy balance for CLCCC: CPR=18, TIT=1200°C, T_{red}=980°C

Fuel flow	kg/s	15	Share of LHV
Fuel LHV	MW	697.5	100.0 %
Air Turbine work	MW	575.9	82.6 %
CO_2 Turbine work	MW	53.4	7.7 %
Steam Turbine work	MW	105.0	15.1 %
Compressor work	MW	-349.2	-50.1 %
Turbomachinery shaft power	MW	385.1	55.2 %
Turbomachinery mechanical loss	MW	-1.1	-0.2 %
Turbomachinery generator loss	MW	-4.2	-0.6 %
Turbomachinery generator terminal output	**MW**	**379.8**	**54.5 %**
Plant auxiliary power		-4.1	-0.6 %
Net plant power island output	**MW**	**375.7**	**53.9 %**
Work CO_2 compression	MW	-13.9	-2.0 %
Net plant power output	**MW**	**361.8**	**51.9 %**

The stream data for the CLCCC at the condition of PR=18 and TIT=1200°C are included in Appendix B.

Note: *Paper I also presents results for the same cycle configuration but with a different fuel composition and different computational assumptions especially those related to the CO_2 dehydration and compression plant. The paper is based on a CO_2 end pressure of 200 bar compared to 110 bar assumed in this work. Moreover, the paper presents a typical 'proof of concept' study and therefore all the results concerning the base-case cycle (CLCCC) presented in the previous sections are not necessarily in conformity with those presented in Paper I. Nevertheless, the trends of net plant efficiency as a function of oxidation reactor exit temperature are the same. Also, the turbine cooling penalty is the same regardless of the computational assumptions.*

6.6 Modifications to the Base-case cycle

The base-case cycle (CLCCC) employs CO_2 turbine that gives additional power yet contributes little (about 14%) to the gross power output compared to the air turbine and steam turbine. The intricacy associated with the use of CO_2 turbine in a CLC combined cycle is worth mentioning here. It can be inferred from the configuration of the base-case CLC combined cycle that presence of CO_2 turbine will increase the complexity of the plant especially when in off-design operation. In order to avoid a direct contact between air and fuel, it is of utmost importance to achieve the same pressure at the air and fuel reactors exit under all conditions. However, in off-design mode, turbine flow conditions determine the turbine inlet pressure and presence of a secondary turbine other than the air turbine requires extra control mechanisms in order to balance the pressure between oxidation and reduction reactor. There are also concerns regarding the material of the CO_2-turbine and the high temperature at its inlet. At the design point, the CO_2 turbine operates at 980°C, which is the

reduction reactor exhaust temperature at the oxidation temperature of 1200°C. This means that the turbine needs to be cooled. Nonetheless, the cooling of such a turbine is a challenge in itself. Due to the CO_2/steam mixture as the working fluid, the conventional air cooling techniques cannot be applied. One possible solution will be advanced closed loop steam cooling, but that has not been applied in this work. This work presents the analysis of alternate cycles that utilise the CO_2 stream in a series of heat exchangers i.e. a combination of air and fuel recuperator as well as an additional CO_2-heat recovery steam generator.

6.6.1 CLCCC with Exhaust Recuperation (CLCCC-ER)

Figure 6.6 presents the CLC-combined cycle where no CO_2 turbine is applied; rather the exhaust is used for air and fuel preheating.

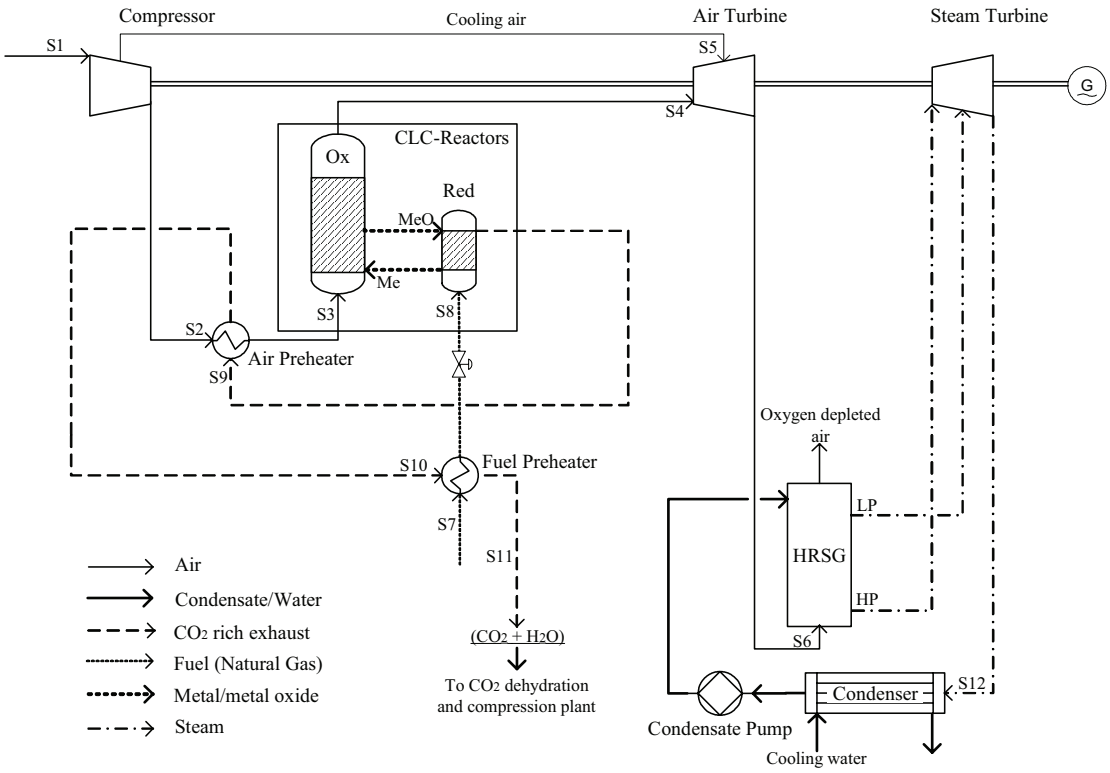

Figure 6.6 Schematics of CLCCC with exhaust recuperation (CLCCC-ER)

The cycle is quite similar to the base-case CLC-combined cycle, except for the way the reduction reactor exit stream is utilised. The exhaust at the reduction reactor outlet, instead of expanding through the turbine, is lead to the air preheater. The heat is added to the compressed air prior to its entry into the oxidation reactor. Due to a large difference in the flowrates of the cold fluid (compressed air) and the hot fluid (exhaust), the preheater specification is based on the cold end temperature difference. The exhaust at the air preheater exit is available at a sufficiently high temperature to pre-heat the fuel in the fuel preheater. The CO_2-rich exhaust at the fuel preheater exit enters the CO_2 dehydration and compression plant

CO_2 Compression Work Variation

One significant feature of not expanding the reduction reactor exit stream is that it is available at a higher pressure and thus the CO_2 compression work is reduced as compared to compression from atmospheric pressure. Figure 6.7 presents the change in CO_2 compression work as a function of the CO_2 pressure at the entry to the CO_2 dehydration and compression plant. It can be deduced from Figure 6.7 that a higher air compressor pressure ratio will not only result in a higher air turbine work but also lower CO_2 compression work. Since, the pressure at the exit of the two reactors has to be maintained equal, a higher air compressor pressure ratio results in a higher pressure of the CO_2/H_2O stream available at the entry to the CO_2 dehydration and compression plant. The CO_2 compression work variation makes the cycle to behave in quite a different way as compared to the base-case cycle where the CO_2 compression work is independent of the compressor pressure ratio and remains constant under different conditions. This is discussed in detail in the following section of sensitivity analysis results.

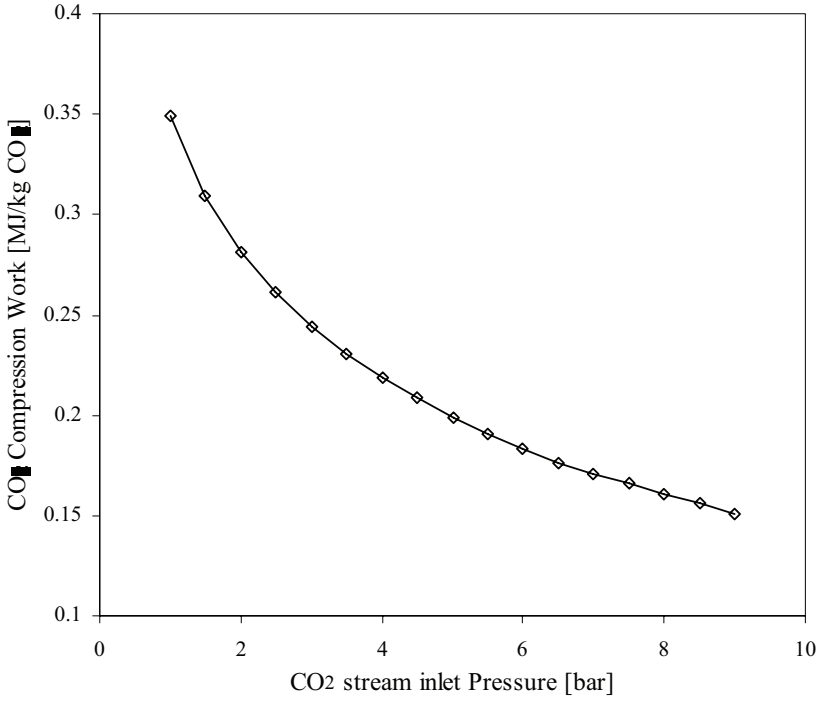

Figure 6.7 CO_2 compression work as a function of CO_2-stream inlet pressure to the dehydration and compression plant
[The figure is valid for the CLC-cycles and CO_2 end pressure of 110 bar.]

Cycle Sensitivity Study Results

Figure 6.8 presents the cycle study results in the form of net plant efficiency and specific work for different values of oxidation temperature. The cycle does not show a strong dependency on the compressor pressure ratio. This is due to the combined effect of the absence of the CO_2-turbine and appearance of the air preheater. In order to understand the behaviour of the cycle currently under study, it is important to briefly discuss the scenario when there is no air recuperator and the CO_2-turbine is present. When there is no air

recuperator, the increase in compressor pressure ratio results in increased air temperature at the oxidation reactor inlet and in turn an increased air flow rate through the system, when constant fuel flow is assumed. Therefore, at a certain TIT, an increased compressor ratio essentially results in increased extraction of work since the enthalpy drop remains the same regardless of the compressor pressure ratio. Also, the CO_2-turbine work increases with increased compressor pressure ratio, because the CO_2-turbine inlet pressure corresponds to the air turbine inlet pressure. Hence, the higher the compressor pressure ratio, the higher is the work extracted from the CO_2-turbine. In the cycle under study, there is no CO_2-turbine and the air inlet temperature does not vary to a large extent with the compressor pressure ratio because of the air recuperator presence downstream of the compressor. However, there is a sharp declination in net plant efficiency with pressure ratio rise at lower TIT values. At higher TIT values, the air turbine work and the steam turbine work balance each other out giving a net plant work that does not vary a lot with the compressor pressure ratio. Therefore, the sharp decrease in efficiency with compressor pressure ratio diminishes as the TIT increases. This can be explained in terms of the air preheater performance.

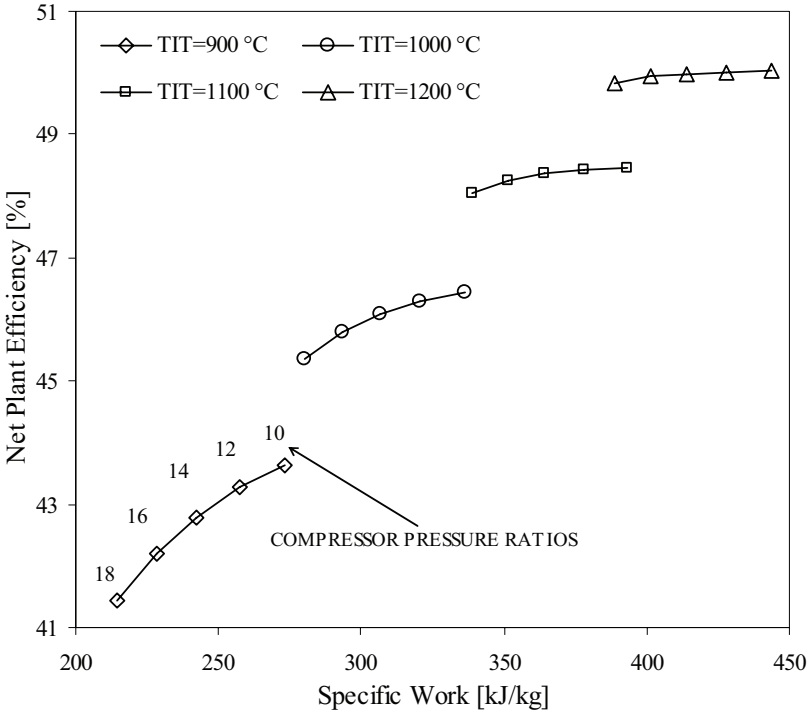

Figure 6.8 Net plant efficiency of CLCCC-ER as a function of specific work. [The term TIT refers to the oxidation temperature.]

The hot fluid is the CO_2-rich exhaust that flows at a constant rate regardless of the pressure ratio and TIT, assuming constant fuel flow. The exhaust temperature however varies with oxidation temperature but still it is constant for a constant oxidation temperature. At lower TIT values, the air flow rate is considerably large while the air temperature at the air preheater inlet is solely a function of compressor pressure ratio. At a certain oxidation temperature, increase in compressor pressure ratio also results in air flow rate increase. On the other hand, the higher compressor pressure ratio results in a higher air temperature at the air preheater inlet. With the constant oxidation temperature and fuel flow, the exhaust temperature and flowrate remain the same. Therefore, the net effect is that there is lesser

heat transfer in the air preheater, which leads to increased exhaust temperature at the air preheater exit. The exhaust is then fed to the fuel preheater that has its own limitations as regards the temperature to which it can heat up the fuel. The net result is that the exhaust temperature at the exit of fuel preheater increases with increase in compressor pressure ratio. However, as the TIT increases, the air flow rate decreases; nevertheless it increases a little with an increase in compressor pressure ratio at a fixed TIT. As the air flow rate decreases, the heat transfer in the air preheater improves. The overall effect is that for a certain compressor pressure ratio, the higher the TIT, the lower is the exhaust temperature at the entry to the CO_2 dehydration and compression plant. The lower the temperature at the entry of CO_2 dehydration and compression plant, the higher is the degree of heat integration within the cycle and thus the better is the net plant efficiency.

Another important feature of the cycle is the CO_2 compression work which is different from that in the base-case cycle. The higher the air compressor pressure ratio, the higher is the oxidation reactor outlet pressure. At the same time, the reduction reactor exit stream pressure is maintained equal to the oxidation reactor exit pressure in order to avoid any gas leakage between the reactors. Therefore, the higher the air compressor pressure ratio, the higher is the CO_2/H_2O stream pressure at the entry to the CO_2 dehydration and compression plant. The net effect is lesser work needed for CO_2 compression to the end pressure. However, it is observed that with increase in compressor pressure ratios, the net plant efficiency decreases. A comparison of energy and power balance for the cycle reveals that the gross power output i.e. total work excluding the work needed for CO_2 compression decreases with increase in the air compressor pressure ratio. This decrease is more prominent as compared to the decrease in the CO_2 compression work. Therefore, a declining trend of the net plant efficiency is observed. The maximum efficiency is achieved at the lowest compressor pressure ratio, over the chosen range of CPR, at all TIT values.

Power and Energy Balance

Table 6-3 presents the power and energy balance for the CLCCC-ER.

Table 6-3 Power and energy balance for CLCCC-ER: CPR=10, TIT=1200°C

Fuel flow	kg/s	15	Share of LHV
Fuel LHV	MW	697.5	100.0 %
Air Turbine work	MW	452.5	64.9 %
Steam Turbine work	MW	150.0	21.5 %
Compressor work	MW	-240.2	-34.4 %
Turbomachinery shaft power	MW	362.3	51.9 %
Turbomachinery mechanical loss	MW	-0.8	-0.1 %
Turbomachinery generator loss	MW	-3.2	-0.5 %
Turbomachinery generator terminal output	**MW**	**358.3**	**51.4 %**
Plant auxiliary power		-3.1	-0.4 %
Net plant power island output	**MW**	**355.2**	**50.9 %**
Work CO_2 compression	MW	-6.2	-0.9 %
Net Plant power output	**MW**	**349.0**	**50.0 %**

The stream data for the CLCCC-ER at the condition of PR=10 and TIT=1200°C are included in Appendix B.

The cycle configuration is simpler compared to the base-case cycle, due to the absence of CO_2 turbine, yet quite efficient. Nonetheless, it achieves a lower efficiency compared to the base-case cycle, which is due to the limitations associated with the heat transfer in the air and fuel preheater. The reduction in overall heat integration resulting in exergy destruction causes the efficiency to drop. Quite obviously, the higher the air and fuel inlet temperature the better will be the plant efficiency. For the design purpose, the air preheater is specified by the minimum cold end temperature difference, mainly due to the large difference in the flow rates of the hot and the cold fluids. The fuel preheater specification is the minimum hot end temperature difference. Hence, the preheaters design is vital in this regard as they influence the degree of heat utilisation in the cycle.

6.6.2 CLC Combined Cycle with Exhaust Recuperation and Steam Generation (CLCCC-ERS)

Figure 6.9 presents another variant of the CLC-combined cycle where exhaust is used for not only air and fuel preheating but also to generate steam that is further utilised in the bottoming steam cycle together with the steam generated in HRSG.

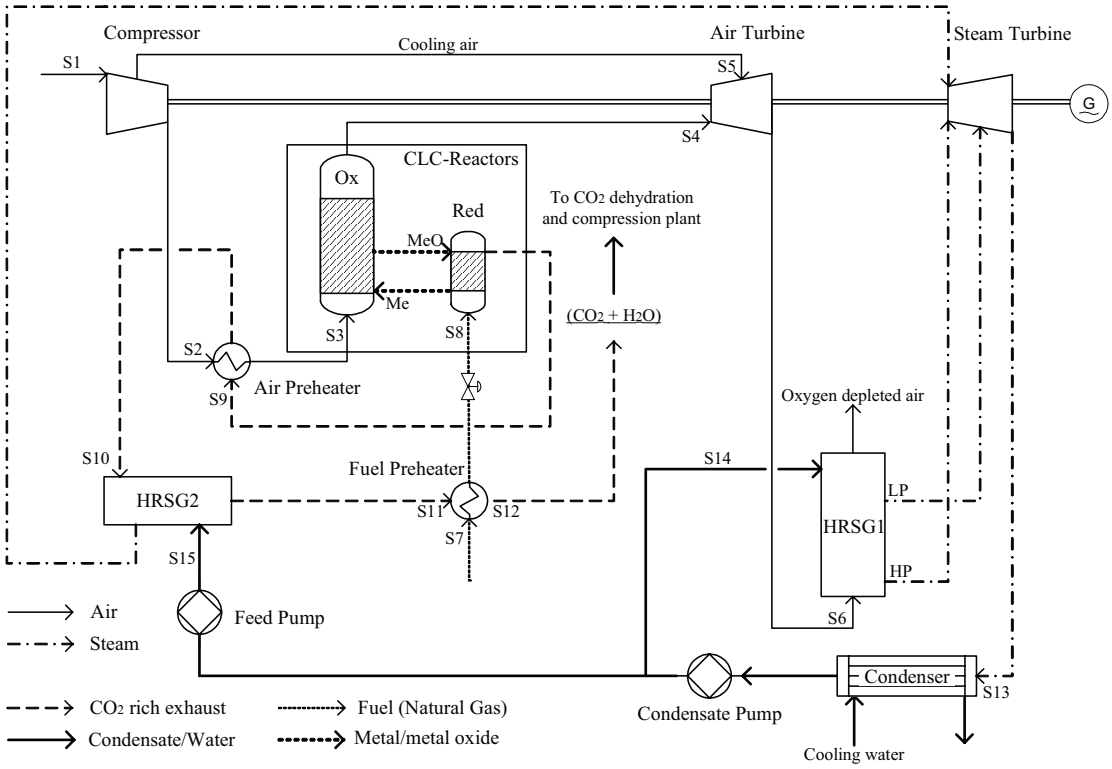

Figure 6.9 CLC-combined cycle with recuperation and steam generation (CLCCC-RS)

The cycle is quite similar to the previously presented combined cycle with exhaust recuperation (CLCCC-ER) except for introduction of a secondary heat recovery steam generator (HRSG2) downstream of the air preheater and upstream of the fuel preheater. One reason for adopting this approach is the temperature limitation in the fuel preheater. At

higher compressor pressure ratios, the exhaust temperature at the air preheater outlet is fairly high, while the preheater is specified by the cold end temperature difference. Although natural gas can be preheated to fairly high temperatures (600°C or above) before it starts to dissociate; but in order to avoid any risk, fuel temperature can be kept at moderate levels with the current cycle configuration while maintaining a fairly high degree of heat integration.

The major steam production is in the hot air heat recovery steam generator (HRSG1), while HRSG2 produces additional steam. The steam pressure in HRSG2 is the same as that of high pressure steam (HP) in HRSG1. Due to relatively low temperature of the CO_2-rich exhaust at the inlet of HRSG2, the degree of superheat is not very high. Hence, there is a temperature loss at the inlet of the steam turbine due to the mixing of the two streams. The total steam expands through the steam turbine to the pressure level of low pressure steam (LP). The condensed steam is split in two streams, the minor being fed to HRSG2. The CO_2-rich exhaust at the HRSG2 outlet is goes to the fuel preheater and consequently to the CO_2 dehydration and compression plant. Since the CO_2 stream is not expanded, it is available at a higher pressure and thus the CO_2 compression work is reduced compared to that for CO_2 compression from atmospheric pressure to the end pressure.

Cycle Sensitivity Study Results

Figure 6.10 presents the sensitivity study results for the cycle in terms of specific work and net plant efficiency.

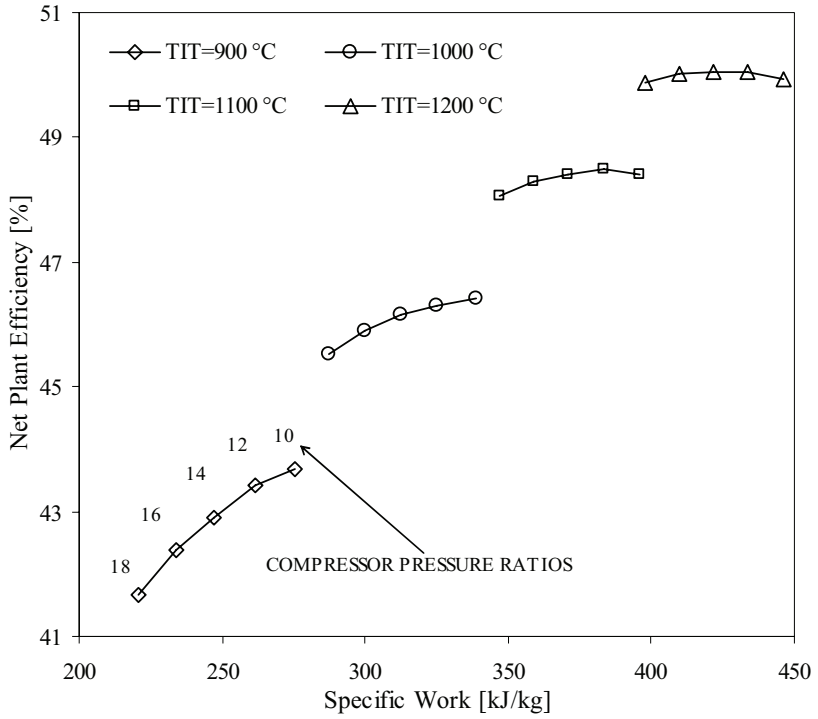

Figure 6.10 Net plant efficiency of CLCCC-ERS as a function of specific work

The cycle behaviour is almost the same as that of the CLC-combined cycle with exhaust recuperation (CLCCC-ER); because the cycle under study is an extended version of CLCCC-ER with an additional HRSG. The cycle does not show a strong dependency on the compressor pressure ratio due to the same causes explained in the results section of CLCCC-ER description. The degree of utilisation is improved in the cycle due to the additional HRSG utilising the CO_2-rich exhaust as the hot fluid; nevertheless the overall efficiency remains almost the same as in CLCCC-ER. The analysis of the mass and energy flows suggests that despite additional steam generation there is not a considerable increase in the work output from the steam turbine. The steam turbine specific work (kJ/kg steam) does in fact decrease due to the design choice of mixing of the two steam streams. The steam produced in the additional HRSG does not match the degree of superheat of the mainstream steam produced in the air turbine-HRSG due to the lower temperature of the CO_2-stream entering HRSG2. Therefore, the mixing of the two steam streams at the inlet of the steam turbine results in temperature loss and therefore results in lower steam turbine specific work compared to other cycles, for instance CLCCC-ER.

Figure 6.10 also shows that although the maximum efficiency is achieved at the lowest pressure ratio i.e. 10 (over the chosen range of PR) for the TIT values of 900 and 1000°C, the maximum efficiency at 1100 and 1200°C is achieved at a pressure ratio of 12. The results data for these conditions shows that the same gross output work is achieved at PR of 10 and 12 as the increase in the air turbine work is balanced out by reduction in the steam turbine work, going from 10 to 12 pressure ratio. But the CO_2 compression work is slightly lower at the pressure ratio of 12, which results in an overall net work output greater than that at a pressure ratio of 10. A further increase in PR results in declining net plant efficiency based on the same reasoning as given in the explanation of CLCCC-ER results. Another effect of the additional HRSG is the variation in air flow rate compared to that in CLCCC-ER, assuming a constant fuel flow.

The fuel inlet temperature has a little impact on the air flow rate; based on the results presented for the adiabatic reactors, in chapter 5. This effect is due to the enthalpy in the solid stream entering the oxidation reactor. The steam production in HRSG2 leaves very little heat available in the CO_2-stream that preheats the fuel only a few degrees. Therefore, the fuel inlet temperature is much lower as compared to that in CLCCC-ER, which causes a lower air flow rate through the cycle and air turbine produces lesser work. The steam production in the air turbine HRSG (HRSG1) is also affected, however it is made up by the additional steam produced in HRSG2. The mixing of the two streams although results in some losses, but nevertheless, the net work extraction from the cycle remains the same as in CLCCC-ER. The specific work does however change due to the variation in the air flow rate which is lower compared to the CLC combined cycle with only air and fuel preheater (CLCCC-ER).

Power and Energy Balance for the Optimum Condition

Table 6-4 presents the power and energy balance for CLCCC-ERS.

Table 6-4 Power and energy balance for CLCCC-ERS: CPR=12, TIT=1200°C

Fuel flow	kg/s	15	Share of LHV
Fuel LHV	MW	697.5	100.0 %
Air Turbine work	MW	493.3	70.7 %
Steam Turbine work	MW	142.5	20.4 %
Compressor work	MW	-273.7	-39.2 %
Turbomachinery shaft power	MW	362.1	51.9 %
Turbomachinery mechanical loss	MW	-0.9	-0.1 %
Turbomachinery generator loss	MW	-3.3	-0.5 %
Turbomachinery generator terminal output	**MW**	**357.9**	**51.3 %**
Plant auxiliary power		-3.2	-0.5 %
Net plant power island output	**MW**	**354.7**	**50.9 %**
Work CO_2 compression	MW	-5.6	-0.8 %
Net Plant power output	**MW**	**349.1**	**50.1 %**

The stream data for the CLCCC-ERS at the condition of PR=12 and TIT=1200°C are included in Appendix B.

The cycle is complex compared to the cycle with only air and fuel preheating (CLCCC-ER), yet it may be considered simpler than the base-case cycle (CLCCC) comparing the operational complexity associated with an additional HRSG and that with a CO_2-turbine. However, the cycle shows no significant efficiency improvement compared to CLCCC-ER despite a design effort to improve the heat integration in the cycle.

6.7 Temperature Limitations in CLC

In CLC, oxidation reactor exit temperature is the parameter of paramount significance. The higher the oxidation temperature, the higher is the turbine inlet temperature (TIT) and hence the higher is the net plant efficiency. While the modern gas turbines can operate at TIT values of 1400°C or above, there exist limitations associated with the temperature inside the oxidation reactor of CLC. There are basically two constraints as regards the temperature; the oxidation reactor material and the oxygen carrier particles. The reduction reactor can however, not be overlooked in this regard. As the temperatures in the two reactors are interdependent, elevated oxidation temperatures will result in fairly high reduction temperatures as well. Therefore, the limitations associated with the material of reduction reactor should also be taken into account. Nevertheless, the material limitations cannot be considered as major hindrance in achieving high temperatures. The inner walls of the two reactors can be equipped with lining of high-temperature resistant ceramic bricks that protect the reactors' material. However such bricks should also possess adequate resilient strength to withstand high pressures. In addition the bricks material ought to be inert so that it does not affect the chemical reactions. Where the conventional circulating fluidised bed reactors can be modified according to the CLC-specific requirements, at the same time the metal oxide particles still pose the difficulties and complexities associated with the high temperatures. It is speculated that the oxygen carrier particles are prone to sintering at a temperature as high as 1200°C, followed by the agglomeration phenomenon. As the oxygen

carrier development research continues it can be expected that oxygen carriers will be developed in long term that are able to withstand high temperatures. However, it is beneficial to explore other possibilities, in the meantime, that would result in efficient CLC-combined cycles operating on relatively lower and thus safer temperatures. At the current developmental stage of CLC, considering the available experimental data, it may well be stated that an oxidation temperature of 1000°C lies under the safe temperature limit. The discussion in the following section will address the issue of efficient CLC-combined cycles operating at safer oxidation temperatures.

6.8 Multi-CLC-Reactors for Reheat Air Turbine Combined Cycles

The temperature limitations associated with CLC were discussed in the previous section. Such limitations call for the need to investigate alternative power cycles in conjunction with CLC that can achieve a reasonably high efficiency at moderate oxidation temperatures or TIT values. The significance of turbine inlet temperature is evident from the Carnot efficiency that can be written as follows:

$$\eta_c = 1 - \frac{T_c}{T_H}$$

In the above equation, T_H is the temperature at which heat is supplied to the system and T_C is the temperature at which heat is rejected; with an assumption that the two temperatures are fixed or constant. Hence, the higher the T_H the higher is the efficiency and vice-versa., but Tc has a certain limit. Therefore, T_H is the primary temperature that determines the work extraction potential of a cycle. However, the temperature at which heat is supplied to a cycle can also be expressed in terms of entropy change and enthalpy change, as given by the following equation.

$$T_H = \frac{\Delta h}{\Delta s}$$

At a constant T_H, a cycle can ideally achieve efficiency close to the Carnot efficiency if an infinite number of heat additions are made to the cycle. This results in a continuously decreasing pressure through successive heat addition and expansion, and heat rejection at the cold side. In a combined cycle, this can be done through introducing reheat to the gas turbine. Figure 6.11 elaborates the principle of reheat by comparing the expansion path of two gas turbines on a T-s diagram; a gas turbine with no reheat and one with single reheat. The T-S diagram shown in Figure 6.11 reveals two changes of supreme interest that are the result of reheat introduction. First of all, the total enthalpy drop in the two turbine sections of the reheat turbine operating at relatively lower TIT is comparable to that with a single non-reheat turbine. If the reheat turbine operated on the same TIT as the non-reheat turbine, the total specific work from the two turbine sections would be higher than the specific work from the non-reheat turbine. The second interesting fact is the turbine exhaust temperature (TET) that increases with the number of reheats, when the exhaust pressure is kept constant. In this way, there is more heat available for the bottoming steam cycle. The net result is a higher work from the steam turbine as compared to that produced in the non-reheat gas turbine combined cycle. If a CLC-combined cycle operates at a certain oxidation temperature, introducing reheat will result in an increased overall efficiency at the same oxidation temperature. However, if reheat is introduced at a relatively low and safe

oxidation temperature, it will result in efficiency comparable to that of a higher oxidation temperature without reheat. In CLC, reheat can be applied to the can be done by employing more than one CLC-reactor and thereby employing a reheat air turbine.

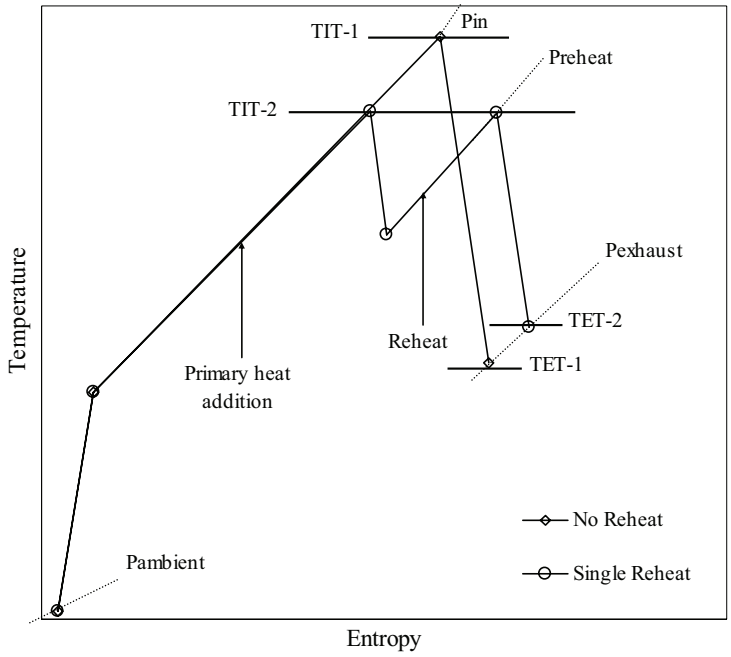

Figure 6.11 Comparison of non-reheat and single reheat gas turbine expansion path on T-s diagram of a gas turbine

Different CLC combined cycle configurations based on the reheat principle will be discussed in the following sections. The presented cycles are however, also analysed at oxidation temperatures higher than 1000°C in order to compare the efficiency of reheat cycles with the non-reheat cycles at the same oxidation reactor exit temperature.

6.8.1 Single Reheat CLC-Combined Cycle (SR-CLCCC)

Figure 6.12 presents the schematics of a CLC-combined cycle with single reheat air turbine and 2-pressure-level CO_2-turbine. The two CLC-reactors can be designated according to the pressure and be graded as high pressure (HP-CLC-Reactors) and low pressure (LP-CLC-Reactors) reactor, respectively. AT1 and AT2 are the high pressure and low pressure air turbines. Air from compressor exit enters air reactor (Ox) of the high pressure CLC-reactor. The hot pressurised oxygen depleted air at the oxidation reactor exit enters the high pressure air turbine (AT1). The turbine is cooled by the cooling air drawn from the air compressor. Air expands in AT1 down to the reheat pressure and enters the oxidation reactor (Ox) of the low pressure CLC-reactor and is reheated up to the oxidation reactor exit temperature. More oxygen is consumed in the low pressure oxidation reactor and the air at outlet enters the low pressure air turbine (AT2), which is also cooled by the cooling air drawn from the air compressor. Air after expansion through AT2 passes through the heat recovery steam generator (HRSG) to produce steam at 2-pressure levels i.e. 60 bar and 5 bar. Exhaust from both reduction reactors (Red) comprises of CO_2 and steam. Exhaust from the first reduction reactor is admitted to the CO_2 turbine and expands to the pressure corresponding to the

pressure of the exhaust stream from the LP-CLC-reactors. The resulting exhaust then expands down to the atmospheric pressure (considering pressure drop in the fuel preheater).

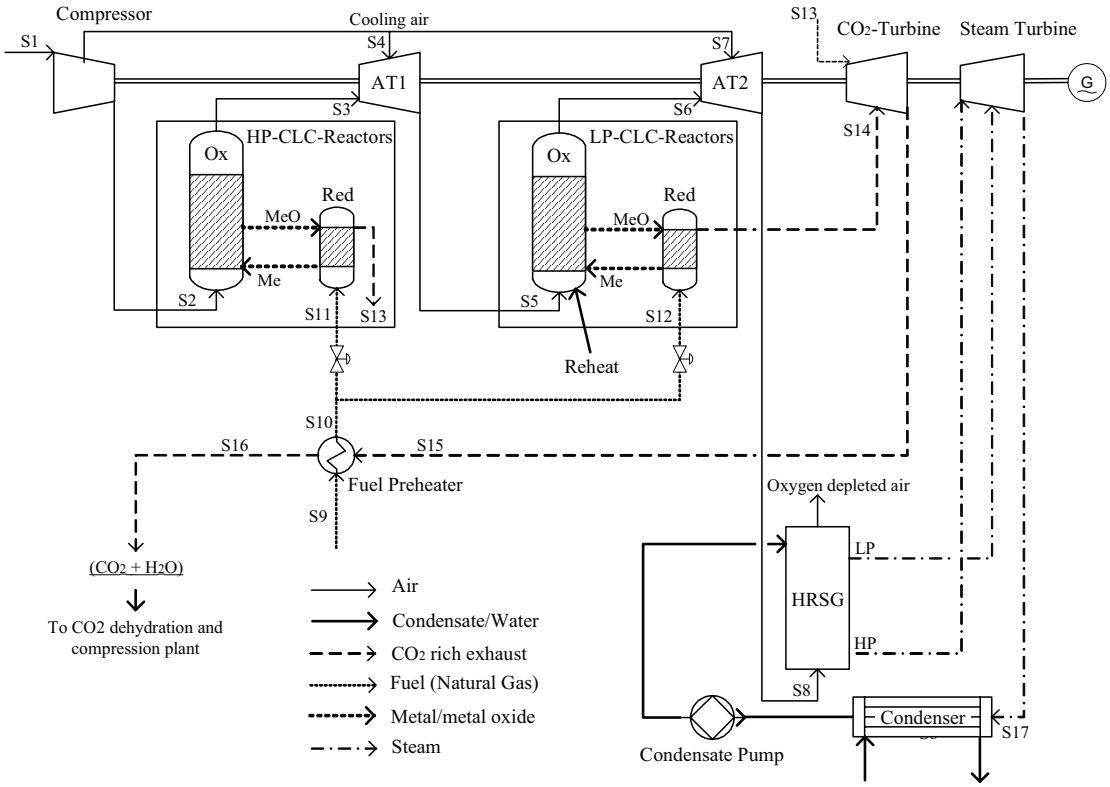

Figure 6.12 Schematics of single reheat CLC-combined cycle (SR-CLCCC)

The CO_2 turbine exhaust is used in the fuel preheater to pre-heat the fuel. Natural gas is available at a high pressure and is preheated in the fuel preheater prior to a split into two streams. As the fuel inlet pressure in both reduction reactors differs, the pressure control valves are used to reduce the fuel pressure accordingly. The CO_2 rich exhaust then goes to the CO_2 dehydration and recompression plant.

Cycle Sensitivity Study Results

The cycle configuration suggests that unlike the non-reheat combined cycles, in addition to compressor pressure ratio and oxidation temperature, the single reheat cycle is also sensitive to the pressure ratios of the two air turbines. Therefore, in order to accomplish a realistic sensitivity analysis, it is a rational approach to determine the optimum pressure ratios of the two turbine sections for each condition of compressor pressure ratio and oxidation temperature. This was done through optimisation of the cycle with respect to the pressure ratio in the two turbine sections.

Optimum Pressure Split Ratio of the Air Turbine

The cycle under study, does however consists of the two air turbines and the selection of the optimum pressure ratio for both the turbines is an important task during the process of cycle efficiency estimation. In the cycle under study, the pressure ratios of AT1 and AT2 are

interdependent. At a fixed turbine inlet temperature, pressure ratio of either AT1 or AT2 can be varied at different compressor pressure ratios. The split ratio for the air turbine can be defined as a function of the overall turbine pressure ratio. The overall air turbine pressure ratio is a function of compressor pressure ratio and is defined by the following equation:

$$PR = CPR \cdot \left(1 - \sum_{i=1}^{n} \Delta P \right) \text{ (i=number of oxidation reactors)}$$

In the above equation, PR is the air turbine overall pressure ratio, ΔP is the percent pressure drop occurring from the air compressor exit to the air turbine inlet, while CPR is the air compressor pressure ratio.

At the optimum split ratio, maximum work will be extracted from both the air turbine and the steam turbine. It is common practice to split the pressure equally between the two turbines in a single reheat cycle. In this case, both the sections have the same pressure ratio as given by the following equation.

$$PR_i = \sqrt{PR} \text{ (i= turbine section number)}$$

So that; $PR_1 = PR_2$

The split ratio determined by the above equation is not necessarily at the optimum value as the optimum value of the split ratio is different for each condition of CPR and TIT. Therefore, this work treats the air turbine in such a way that the pressure ratio of the two air turbine sections may differ from each other. The pressure ratio of a turbine can hence be defined according to the following equation:

$$PR_i = PR^{\lambda}$$

In the above equation, the exponent λ is the split ratio and is between 0 and 1. The subscript i corresponds to the turbine i.e. i=1 for the first turbine. The air turbine split ratio is thus calculated according to the following equation:

$$\lambda = \frac{\ln\left(PR_i\right)}{\ln\left(PR\right)} \text{ (i=1 for single reheat)}$$

Regardless of the features of the above equation that helps determining a more realistic split ratio, the real optimum split ratio determination is not a trivial task and requires the cycle optimisation, which is discussed briefly in the following.

Objective Function: The objective function is the gross plant work i.e. Total work from the air turbine and steam turbine. The objective function is to be maximised.

Variable: The optimisation study is done by varying only the split ratio.

Constraint: The only constraint is the air turbine exit temperature (TET), which may be quite high (above 645°C) at low compressor pressure ratios and high TIT values, compared.

At such a condition, if the design is based on a fixed hot-side temperature difference in HRSG, it will result in very high temperatures of steam. Since, the design choice in the current work has been to specify the hot-side temperature difference in the superheater of HRSG; the split ratio can be optimised while remaining within the imposed constraint on the TET. Therefore, the air turbine exit temperature is limited to 645°C and with the minimum hot-end temperature difference specification; the maximum allowable steam temperature becomes 620°C.

The optimisation is carried out over a range of compressor pressure ratios and TIT, assuming the same temperature conditions in both the CLC-reactors. The air turbine and steam turbine work varies with the split ratio. The CO_2 turbine work also varies accordingly, as it depends on the pressures at the exit of the reduction reactors in the two CLC-reactors which again are a function of the inlet pressure at the two air turbines. The CO_2 compression work, on the other hand, is independent of the pressures in the reactors due to the constant fuel flow and the expansion of the CO_2-stream down to atmospheric pressure in the low pressure air turbine. The results of the optimisation are presented in Figure 6.13 in terms of net plant efficiency as a function of the split ratio at different TIT and CPR values. It can be seen in Figure 6.13 that for each compressor pressure ratio and TIT, there is one optimum value of split ratio that gives the maximum net plant efficiency. The split ratio at that point corresponds to a certain pressure ratio of the first air turbine (AT1). An increase in the split ratio beyond that value results in declination of the net plant efficiency.

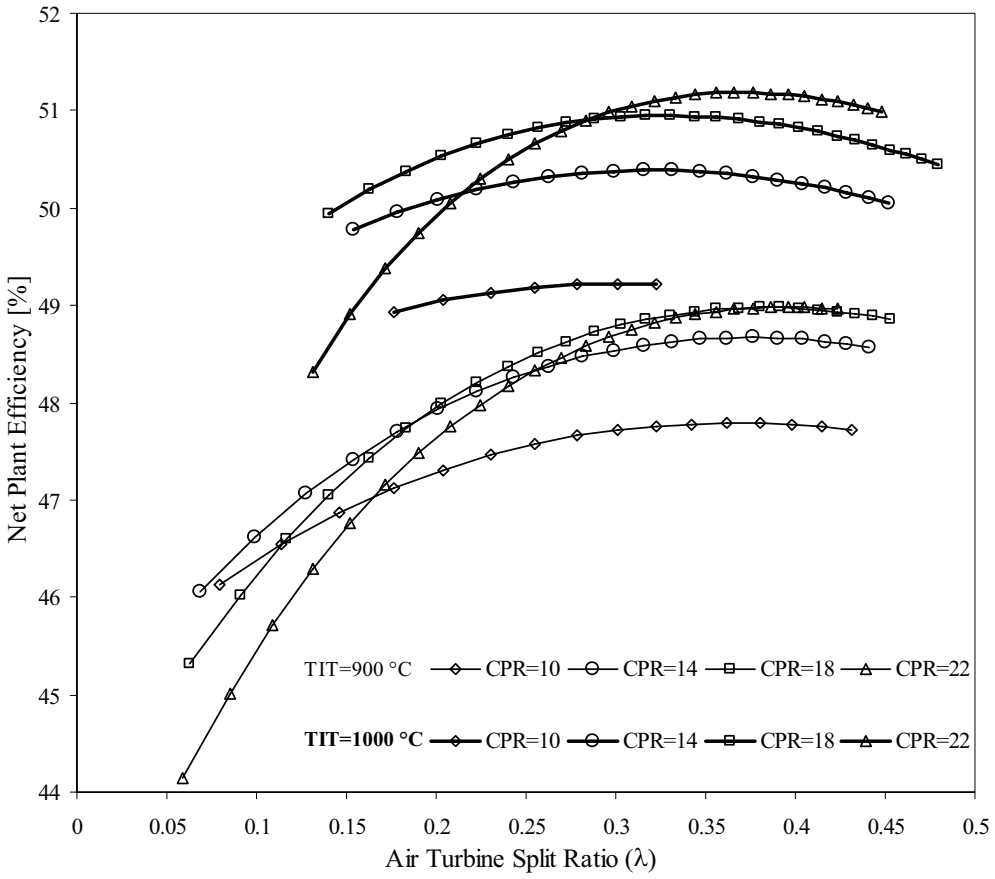

Figure 6.13 The optimisation results for single reheat combined cycle (SR-CLCCC)

The optimisation results shown in Figure 6.13 present the net plant efficiency trends only for TIT values of 900 and 1000°C, in order to elaborate the optimisation. Nevertheless, a complete overview of the cycle optimisation shows that over the TIT range of 900-1200°C and CPR range of 10-22, the optimum value of λ lies between 0.24 and 0.36.

The results for each compressor pressure ratio and TIT can also be presented in the form of net plant efficiency as a function of specific work, where each efficiency point represents the optimum point, as shown in Figure 6.14.

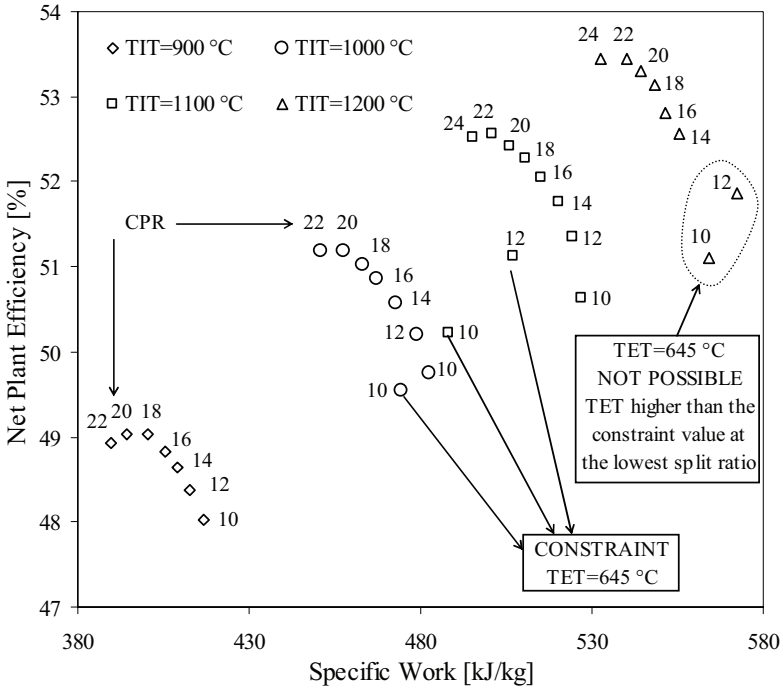

Figure 6.14 Net plant efficiency of SR-CLCCC as a function of specific work
[Each efficiency point corresponds to the optimum pressure ratios of the two air turbines that are different for different compressor pressure ratios.]

The cycle has a strong sensitivity with respect to the oxidation temperature and the efficiency rise is very prominent with increase in TIT. The cycle also has quite a strong dependency on the compressor pressure ratio that is reflected by rather steep trend of the efficiency points on Figure 6.14. The efficiency points show a consistent trend at all the compressor pressure ratios at TIT=900°C. On the other hand, at the higher oxidation temperatures the cycle has a lower specific work that makes it not in consistency with the trend of rest of the efficiency points. This effect is a consequence of the constraint imposed on the cycle performance. The cycle has been analysed at both the conditions; no TET constraint and with a TET constraint of 645°C. At the lower compressor pressure ratios and the higher TIT, the turbine exhaust temperature is very high. Due to the constraint, the pressure ratio of the turbines is varied in such a way that it does not exceed the upper limit of the turbine exhaust temperature. The higher the pressure ratio (or the split ratio) of the first air turbine, for the same TIT for both the air turbines, the higher is the AT2 exhaust temperature. At a constant fuel flow, the first air turbine pressure ratio also determines the inlet temperature to the second oxidation reactor, which in turn affects the air flow rate

required by the system. With the imposed constraint, the pressure ratio of the first turbine is lower than the real optimum value, leaving high temperature air to enter the second reactor and hence reducing the air flow rate required by the second oxidation reactor. The net effect is an overall lower air flow rate through the cycle as compared to that what would be without any constraint. Also, if there was no constraint applied, the turbine exit temperature would be much higher and so would be the steam temperature and thus the steam turbine work output. However, in case of imposed constraint, the point of efficiency does not reveal the full potential of the work that could be extracted from the cycle. Despite a lower air flowrate the specific work is lesser as compared to higher compressor pressure ratios because of the less work extraction both from the air and steam turbine. As the compressor pressure ratio increases, the turbine exit temperature decreases until a certain value of the air turbine pressure ratio is reached where the exit temperature is at or within the upper limit. From that point onwards the optimisation results reveal the true value of the heat converted into work. The imposed constraint therefore results in lower efficiency and lower specific work than that would be if there was no constraint of turbine exit temperature. At the TIT 1200°C and compressor pressure ratios 10 and 12, as it can be seen on Figure 6.14, it is not possible to impose the desired constraint of TET=645°C, because the TIT is too high to achieve this temperature at the exit of the last air turbine i.e. AT2, while forcing the first air turbine (AT1) to its minimum possible pressure ratio. Even so, the points of lower compressor pressure ratio are not of interest in the cycle design procedure as they result in very low efficiency. The design point will be selected from one of the higher compressor pressure ratios through a trade-off between efficiency and economics i.e. specific work.

Power and Energy Balance for the Optimum Condition

Table 6-5 presents the power and energy balance for SR-CLCCC.

Table 6-5 Power and energy balance for SR-CLCCC: CPR=22, TIT=1200°C

Fuel flow	kg/s	15	Share of LHV
Fuel LHV	MW	697.5	100.0 %
High-pressure Air Turbine (AT1) work	MW	144.6	20.7 %
Air turbine split ratio (λ)		0.24	
Low-pressure Air Turbine (AT2) work	MW	397.9	57.0 %
CO_2 Turbine work	MW	53.0	7.6 %
Steam Turbine work	MW	124.4	17.8 %
Compressor work	MW	-324.2	-46.5 %
Turbomachinery shaft power	MW	395.7	56.7 %
Turbomachinery mechanical loss	MW	-1.1	-0.2 %
Turbomachinery generator loss	MW	-4.1	-0.6 %
Turbomachinery generator terminal output	**MW**	**390.6**	**56.0 %**
Plant auxiliary power		-4.0	-0.6 %
Net plant power island output	**MW**	**386.6**	**55.4 %**
Work CO_2 compression	MW	-13.9	-2.0 %
Net Plant power output	**MW**	**372.7**	**53.4 %**

The stream data for the SR-CLCCC at the condition of PR=22 and TIT=1200°C is included in Appendix B.

The cycle shows very promising net plant efficiency with CO_2 capture. The cycle is relatively more complex compared to the non-reheat CLC-cycles due to the introduction of second turbine and reactor system. Nevertheless, it can be argued that if single CLC-reactor system can be realised in combined cycle then multiple-reactors can also be implemented. This statement opens up the window of possibility to employ three CLC-reactor systems to configure a double reheat CLC-combined cycle, described in the following section.

6.8.2 Double Reheat CLCCC (DR-CLCCC)

Figure 6.15 presents the schematics of a CLC-combined cycle with double reheat air turbine and 3-pressure-level CO_2-turbine.

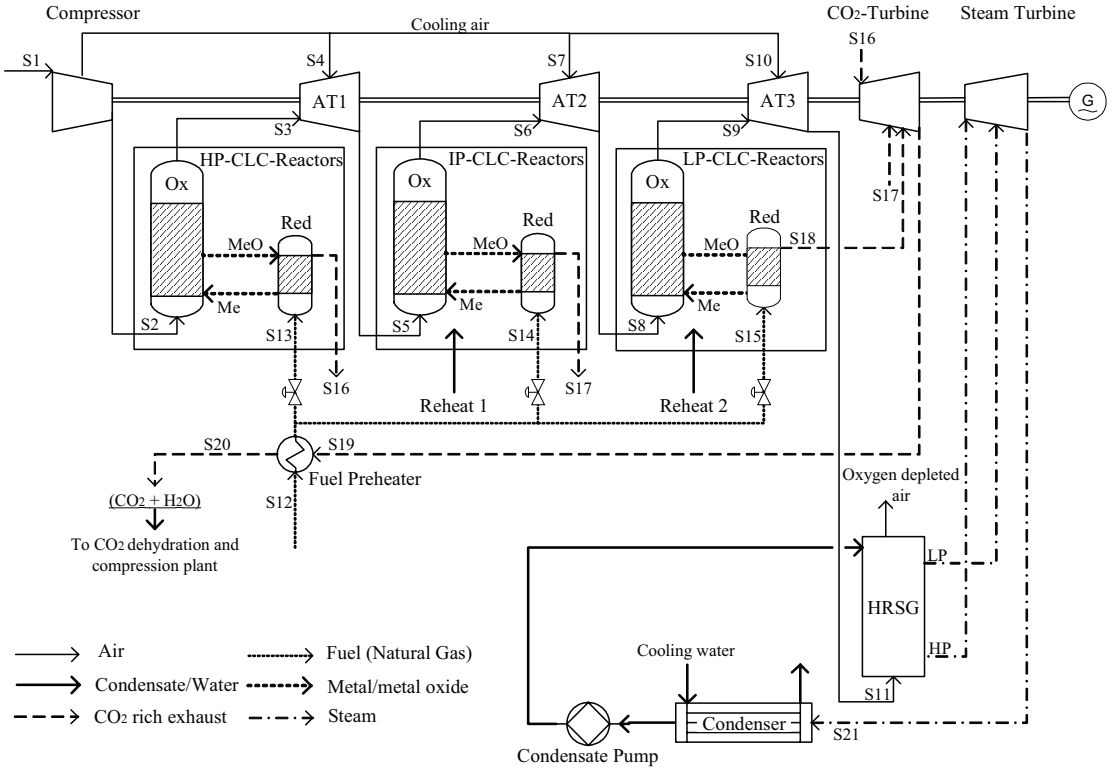

Figure 6.15 Schematics of double reheat CLC-combined cycle (DR-CLCCC)

The three CLC-reactors can be designated according to the pressure levels and are named as high pressure (HP-CLC), intermediate pressure (IP-CLC) and low pressure (LP-CLC) reactors. AT1, AT2 and AT3 are the high pressure, intermediate pressure and low pressure sections of the air turbine, respectively. Air from the air compressor exit enters the oxidation reactor (Ox) of the high pressure CLC-reactor. The hot pressurised oxygen depleted air at the air reactor exit enters the first section of air turbine i.e. AT1. The first air turbine is cooled with the cooling air drawn from the air compressor. Air expands in AT1 down to the first reheat pressure and enters the oxidation reactor (Ox) of the intermediate pressure CLC-reactor, more oxygen is consumed and the air is reheated up to the oxidation temperature. The air at the exit of the oxidation reactor in the IP-CLC-reactors enters AT2, which is also

cooled with the cooling air drawn from the air compressor. Air expands in AT2 down to the second reheat pressure and enters the oxidation reactor (Ox) of the low pressure CLC-reactor and is reheated up to the oxidation temperature. Even more oxygen is consumed in the low pressure air reactor and the air at outlet enters AT3, which is also cooled with the cooling air drawn from the air compressor. Air after expansion through AT3 passes through the heat recovery steam generator (HRSG) to produce steam at 2-pressure levels i.e. 60 bar and 5 bar. Exhaust from the high pressure reactor is admitted to the CO_2-turbine and it expands to the pressure corresponding to the pressure of the exhaust stream from the intermediate pressure reactor. The mixed exhaust then expands down to the pressure corresponding to the pressure of the exhaust stream from the low pressure reactor. Total exhaust then expands down to the atmospheric pressure (considering pressure drop in the fuel recuperator). The CO_2 turbine exhaust is used in the fuel preheater to pre-heat the fuel. Natural gas is assumed available at a high pressure and is preheated in the fuel preheater prior to its splitting into three streams. As the fuel inlet pressure in the three fuel reactors differs, the pressure control valves are used to reduce the fuel pressure accordingly. The CO_2 rich exhaust is then goes to the CO_2 dehydration and compression plant.

The Optimum Air Turbine Split Ratios

In the single reheat cycle discussed in the previous section, the determination of the optimum pressure ratios of the two turbines was based on the split ratio. The same approach is adopted for the double reheat cycle. However in case of three turbines, there are two split ratios that need to be defined; the split ratio between the first two turbines and the split ratio between the first two turbines and the last turbine by treating the first two turbines as one turbine. The overall pressure ratio of the air turbine is defined by the following equation:

$$PR = CPR \cdot \left(1 - \sum_{i=1}^{n} \Delta P \right) \quad \text{(i=number of oxidation reactors)}$$

In the above equation, PR is the air turbine overall pressure ratio, ΔP is the percent pressure drop occurring from the air compressor exit to the air turbine inlet, while CPR is the air compressor pressure ratio. One approach of defining the split ratio is to equally distribute the pressure ratio across all the turbines, so that the pressure ratio of each turbine becomes:

$$PR_i = \left(PR \right)^{\frac{1}{3}}$$

In order to find the optimum pressure ratio, turbine split ratios λ_1 and λ_2 have been defined. Treating the first two turbines in the same way as in the single reheat cycle and considering the total pressure ratio across the first two turbines, the first split ratio (λ_1) can be defined by the following equation:

$$PR_1 = PR^{\lambda_1}$$

In the above equation, PR_1 is the pressure ratio of the first air turbine, while PR is the overall pressure ratio across the first two air turbines. The second split ratio (λ_2) is between the first two air turbines (AT1 and AT2) and the last air turbine (AT3) and can be defined as per the following equation:

$$PR_1 * PR_2 = (PR)^{\lambda_2}$$

In the above equations, PR is the overall pressure ratio of the air turbine, while PR_1 and PR_2 are the pressure ratios of the first air turbine (AT1) and the second air turbine (AT2), respectively. The optimisation is carried out with respect to one objective function and two variables, i.e. λ_1 and λ_2. The same way as in SR-CLCCC, where the objective function (gross work) is maximised at the same time a constraint of 645°C is also imposed on the turbine exit temperature.

The cycle optimisation results show that over a TIT range of 900-1200°C and a CPR range of 10-26, the optimum value of λ_1 lies between 0.25 and 0.47; while the optimum value of λ_2 lies between 0.29 and 0.4.

Cycle Sensitivity Study Result

The sensitivity study results for DR-CLCCC are shown in Figure 6.16. Each efficiency point represents the optimum split ratios at the corresponding value of CPR and TIT.

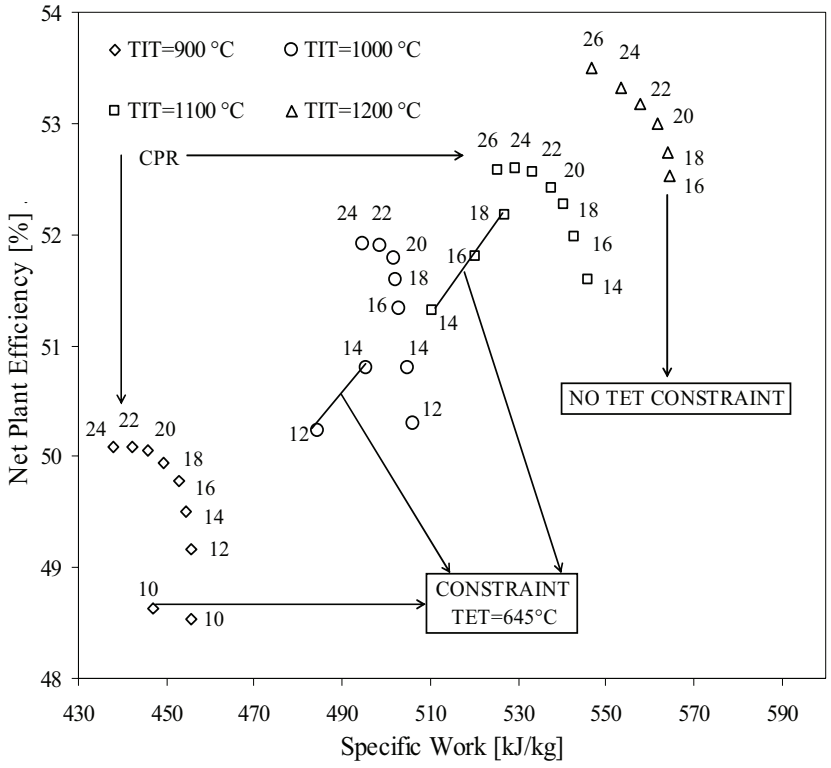

Figure 6.16 Net plant efficiency of DR-CLCCC as a function of specific work

The constraint imposed during the turbines pressure ratio optimisation procedure has the similar effect as in SR-CLCCC. In the current cycle however, the turbine exhaust temperature exceeds the imposed upper limit even at a relatively low TIT i.e. 900°C and low compressor pressure ratios. Therefore, the efficiency point at TIT=900°C and CPR=10 lies outside the mainstream trend of the efficiency/specific work points. At a higher heat

addition temperature i.e. TIT=1000°C, this effect is rather more prominent and over a range of compressor pressure ratio the turbine exhaust temperature needs to be restricted to the upper limit through variation in the turbine sections pressure ratio. Otherwise, optimum pressure ratios of the air turbines will although result in maximum work extraction, but will exceed the temperatures feasible in the HRSG. That is why the efficiency point at compressor pressure ratio of 14 is still influenced by the imposing of the constraint and does not reflect the optimum work extraction through maximum heat utilisation in the cycle. The higher the TIT the more prominent is this effect even at higher CPR values, for instance at TIT=1100°C this effect can be seen until CPR=18. The results at TIT=1200°C are presented for the efficiency optimised with respect to only the air turbine split ratio in the absence of any constraint. However, for TIT=1200°C, at the CPR values higher than 20, the results are the same with and without constraint due to the TET values lower than 645°C.

Power and energy balance for SR-CLCCC

Table 6-6 Power and energy balance for DR-CLCCC: CPR=26, TIT=1200°C

Fuel flow	kg/s	15	Share of LHV
Fuel LHV	MW	697.5	100.0 %
High-pressure Air Turbine (AT1) work	MW	46.2	6.6 %
First split ratio ($\lambda_{1)}$		0.25	
Intermediate-pressure Air Turbine (AT2) work	MW	131.8	18.9 %
Second split ratio (λ_1)		0.29	
Low-pressure Air Turbine (AT3) work	MW	382.4	54.8 %
CO_2 Turbine work	MW	54.2	7.8 %
Steam Turbine work	MW	129.5	18.6 %
Compressor work	MW	-348.0	-49.9 %
Turbomachinery shaft power	MW	396.1	56.8 %
Turbomachinery mechanical loss	MW	-1.1	-0.2 %
Turbomachinery generator loss	MW	-4.0	-0.6 %
Turbomachinery generator terminal output	**MW**	**391.1**	**56.1 %**
Plant auxiliary power		-3.9	-0.6 %
Net plant power island output	**MW**	**387.1**	**55.5 %**
Work CO_2 compression	MW	-13.9	-2.0 %
Net Plant power output	**MW**	**373.2**	**53.5 %**

The stream data at the above-mentioned operating conditions of DR-CLCCC are included in Appendix B.

Remarks on the Reheat Cycles Design and Performance

One of the most significant features of the reheat cycles is the air turbine exit temperature that is higher than that of a non-reheat air turbine. The reasons for imposing a constraint on TET have been mentioned during the discussion on reheat cycles in the previous sections.

The fact to be realised here is that CLC is a novel concept of power generation and is believed to be realised in rather a long term perspective. Therefore, no matter how difficult it may appear to deal with elevated steam temperatures, at this stage of CLC development; it should not hinder one to estimate the complete potential of a CLC-combined cycle free of any such constraints. There are continuous efforts to develop turbomachinery and power plant equipment that can handle ultra-supercritical steam even at a temperature as high as 700°C or above. Hence, it can be expected that by the time CLC is implemented in real applications, high temperature steam cycles will pose no troubles to CLC-combined cycles. The advantages of introducing reheat to a gas turbine have previously been discussed in detail. In order to analyse the impact of reheat introduction it is of interest to present the comparison of the expansion paths of non-reheat and reheat-air turbines on T-s diagram. Figure 6.17 presents this comparison where the reheat air turbines operate at the same TIT as that of the non-reheat air turbine in CLC-combined cycles. It can be seen that the reheat turbines have comparatively higher pressure losses compared to the non-reheat turbine. This is due to the pressure drops occurring in the oxidation reactors of the CLC-reactor systems. This can also be inferred from the above figure that the high pressure CLC-reactor system has considerably larger duty as compared to low pressure reactor in case of single reheat; and the intermediate and low-pressure reactors in case of double reheat.

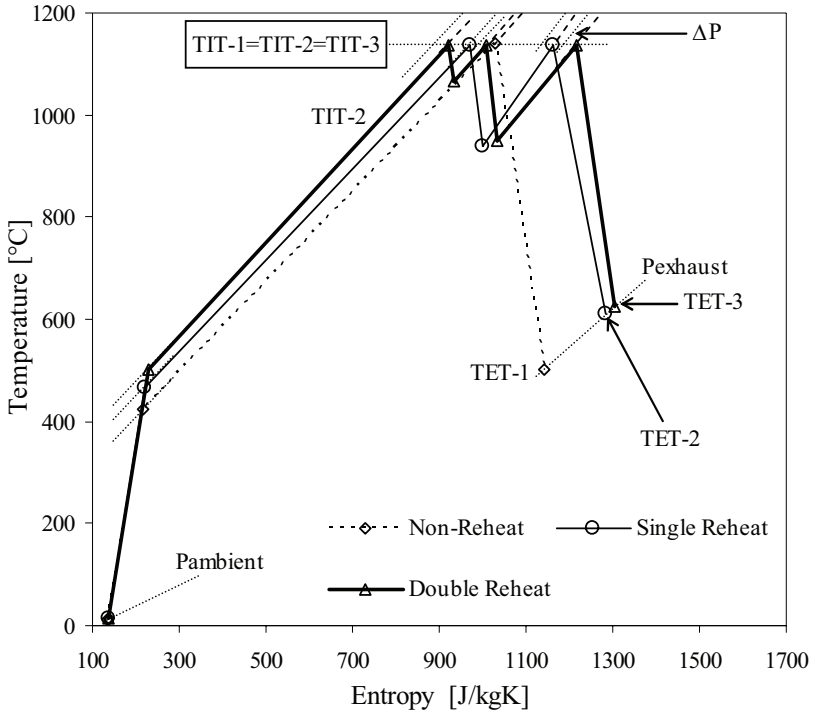

Figure 6.17 Comparison of the expansion path of non-reheat and reheat air turbines
[Non-Reheat: CPR=18, Single Reheat: CPR=22, Double Reheat: CPR=26]

The reheat air turbines total work is higher than that of the non-reheat air turbine. The turbine exit temperature (TET) is the highest in case of the double reheat air turbine, and hence the steam turbine work should also be higher in case of double reheat. The heat balance of the system results in lower air flowrate with increasing number of reheats and TIT values. Although, this effect results in higher specific work but it can be deduced that declining air flowrate with increase in number of reheats may have the consequence that the

efficiency gain is not very prominent with each heat addition. This is because not only the air turbine work is the working fluid flowrate dependent but also the quantity of steam raised in HRSG depends on the amount of air available at the exhaust of the air turbine. Examination path of the double reheat air turbine also reveals an interesting fact that the optimum pressure ratio of the first turbine section is very low. The results show that not only at the condition of CPR=26 but also other CPR values, this ratio is very low. This means that the presence of the first turbine section does not make any significant difference and points out that an additional section of turbine is not explicitly beneficial. This fact is also reflected by the efficiency gain by introducing double reheat, which is incremental at the TIT=1200°C and only 0.1% efficiency improvement is observed compared to single reheat cycle. At lower TIT values however, the efficiency improvement is slightly higher and at TIT=900°C, the double reheat cycle exhibits about 1% efficiency improvement compared to the single reheat cycle. The introduction of reheat also affects the performance of the CO_2-turbine in a positive way. Due to the availability of multiple exhaust streams at different pressure levels but the same temperature (as the oxidation temperature is the same in all the CLC-reactors). Figure 6.18 compares the expansion path of the CO_2 turbine in the base-case CLCCC and the reheat CLC-combined cycles. The term TIT in the following figure refers to the CO_2-turbine inlet temperature i.e. the exhaust temperature at the reduction reactor exit.

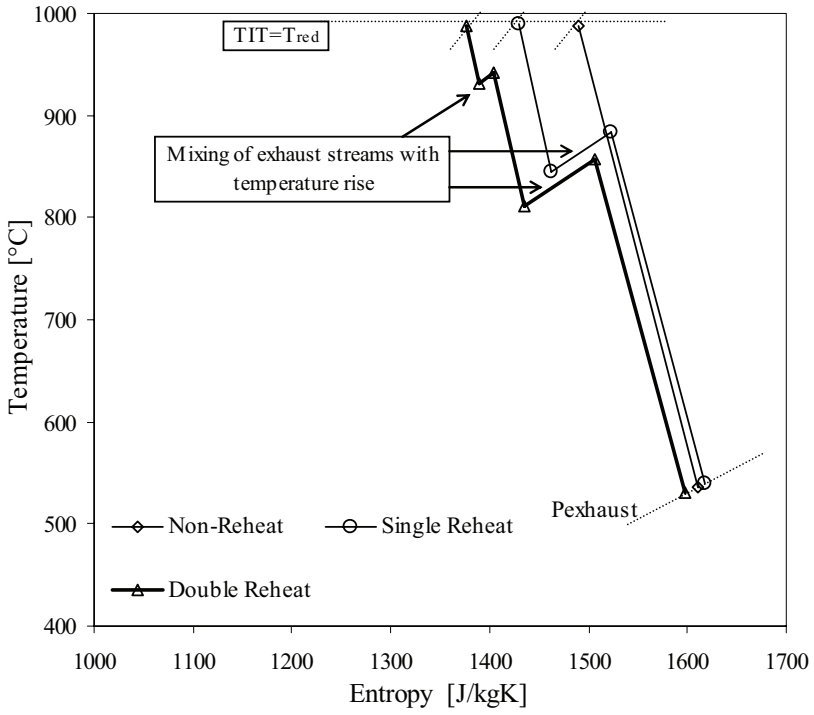

Figure 6.18 Comparison of the expansion path of non-reheat and reheat CO2-turbines
[Non-Reheat: CPR=18, Single Reheat: CPR=22, Double Reheat: CPR=26]

It can be seen that, as in the reheat air turbines, despite the same TIT, reheat results in a higher total work extraction from the CO_2-turbine. Another factor is the gradually increasing flowrate of the working fluid through the sections of the reheat CO_2-turbine, which does not appear on the T-s diagram. The flowrate of the working fluid (exhaust) in each section is higher than that in the preceding section due to the admission of the CO_2-stream from the corresponding reduction reactor. Unlike the air turbine, turbine exit temperature of the

double reheat CO_2-turbine is lower than that in the single reheat and non-reheat cycle. This is a consequence of mixing of exhaust streams that occurs twice in the double reheat cycle. The mixing of streams does not result in sufficiently high temperature of the gas at the admission of the second and the third turbine section. The pressure drop is more prominent in the double reheat cycle due to three reduction reactors and mixing of streams twice. The result is that the pressure at the admission of the last section of the double reheat CO_2-turbine is lower than that of the last section in single reheat cycle. The lower TIT for the last section together with a lower pressure at the admission results in a lower TET. A very low optimum pressure ratio of the first expansion section in the CO_2-turbine of the double reheat cycle also indicates that its presence does not lead to a significant improvement in the cycle.

The reheat cycles presented so far employ the CO_2-turbine which is left uncooled in this work for the sake of simplicity. The issues concerning the CO_2-turbine cooling and the additional operational complexity due to its presence in the combined cycle have previously been discussed briefly. In reheat cycles however, the exhaust recuperation can be performed in order to preheat the air and the fuel. This approach is quite similar to that presented in CLCCC-ER and CLCCC-ERS. In the following a single reheat CLC-combined cycle with exhaust recuperation will be presented. The cycle can be looked upon as a modification to the CLCCC-ER by introducing additional reheat.

6.8.3 Single Reheat CLCCC with Exhaust Recuperation (SRCLC-ER)

Figure 6.19 presents the schematics of a single reheat CLC-combined cycle without the CO_2-turbine whereas the CO_2-rich exhaust is used for preheating air and fuel.

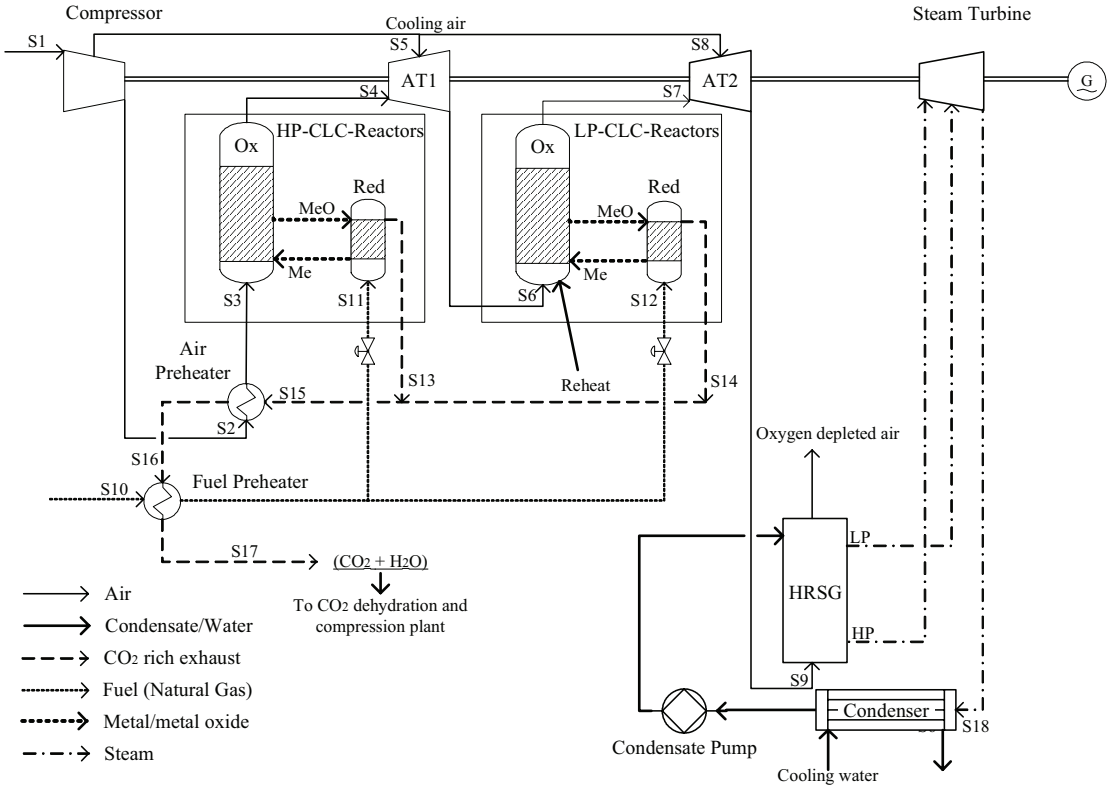

Figure 6.19 Single reheat CLCCC with exhaust recuperation (SRCLC-ER)

The cycle is quite similar to the single reheat CLC-combined cycle, except for the way in which heat in the CO_2-rich exhaust is utilised. The exhaust from the two reduction reactors are mixed, instead of expanding through the turbine at different pressure levels. The mixing of the two streams inevitably results in pressure drop, and the mixing pressure is assumed to be equal to the pressure of the stream at lower pressure i.e. the exhaust from the LP-reactor. The exhaust is then passed on to the air preheater where it preheats the high pressure air from the compressor discharge. Due to a large difference in the flowrates of the cold fluid (compressed air) and the hot fluid (exhaust), the recuperator specification is based on the cold end temperature difference. The exhaust at the air recuperator exit is available at a sufficiently high temperature to pre-heat the fuel in the fuel recuperator. The CO_2-rich exhaust at the fuel preheater exit is fed to the dehydration and compression plant. Since the CO_2 stream is not expanded, it is available at a pressure higher than atmospheric pressure and hence the CO_2 compression work is lower compared to atmospheric compression.

Optimum Air Turbine Split Ratio

The air turbine split ratio has been defined in the same way as for the single reheat CLC-combined cycle. The cycle optimisation is carried out to find out the optimum split ratio. However, unlike the single reheat combined cycle (SR-CLCCC), the net plant efficiency of the cycle under discussion does not solely depend on the split ratio. The configuration of the cycle is such that the first turbine pressure ratio also determines the pressure of the CO_2 stream to the inlet of the dehydration and compression plant. The exhaust from the two reduction reactors mix and as per assumption, the pressure of the product stream is the same as that of the stream with lower pressure. The air turbine split ratio (or the first air turbine pressure ratio) also determines the pressure at the inlet of the second air turbine section i.e. pressure at the low-pressure oxidation reactor exit. This pressure is inevitably equal to the pressure at the low-pressure reduction reactor exit, which is the pressure at which the CO_2 stream is available at the inlet to the CO_2 dehydration and compression plant. It has already been presented that the CO_2 compression work increases with reduction in the pressure at the inlet of the CO_2 dehydration and compression plant. Therefore, the maximum net plant efficiency does not necessarily occur at the split ratio which gives maximum work extraction from the air turbine and the steam turbine. Therefore, the CO_2 compression work must also be considered during the procedure of the optimum air turbine split ratio determination. For this purpose an additional parameter R_{WCG} is defined here, which is the ratio between CO_2 compression work and the plant gross work, given in the following:

$$R_{WCG} = \frac{W_{CO_2,comp}}{W_{gross,plant}}$$

The aforesaid inferring about the CO_2 compression work is supported by Figure 6.20 that presents the optimisation results at TIT=1000°C and three different compressor pressure ratios (CPR), in the form of efficiency as a function of split ratio and R_{WCG}.

It can be seen in Figure 6.20 that the maximum efficiency is not achieved at the point where the CO_2 compression work is at the minimum. The results shown in Figure 6.20 do not include any TET constraints. Also, the figure does not present the whole range of TIT and CPR values for which the sensitivity study is carried out. Nevertheless, the figure serves as an indicator of the interdependency between the air turbine split ratio, CO_2 compression work and efficiency.

Sensitivity Study Results

Figure 6.20 explains the optimisation procedure to spot the optimum points at various values of TIT and CPR where the maximum efficiency is achieved. A series of such points over a range of TIT and CPR was calculated to find the optimum split ratio for each condition.

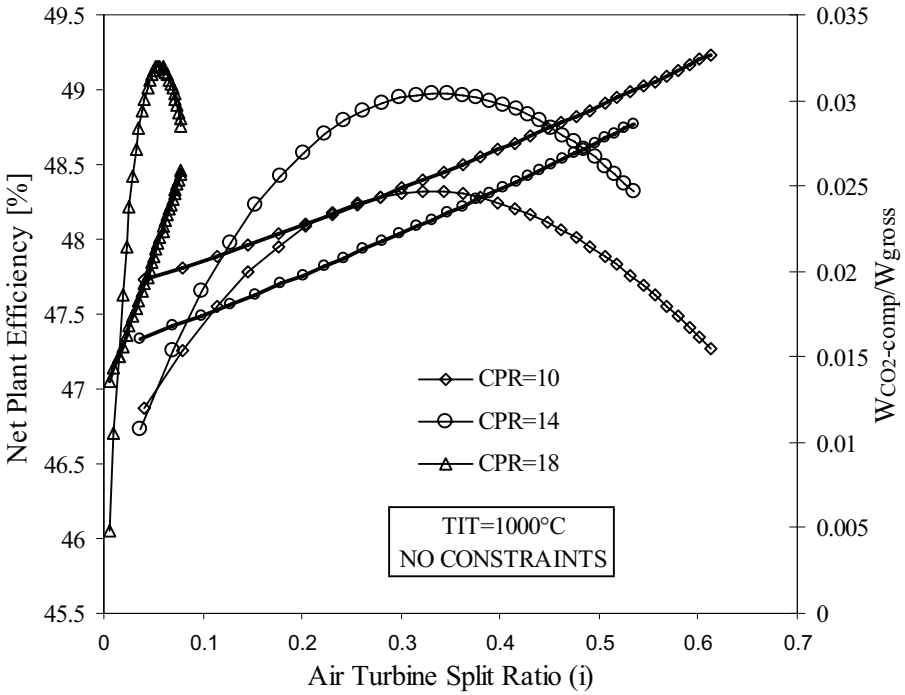

Figure 6.20 The optimisation results for single reheat CLC-combined cycle with exhaust recuperation (SRCLC-ER) [Thick lines represent $W_{CO2\text{-}comp}/W_{gross}$]

The optimisation results for SRCLC-ER show that for the TIT range of 900-1200°C and CPR range of 10-20; the optimum air turbine split ratio lies in the range of 0.24-0.39.

Figure 6.21 presents the sensitivity study results for the single reheat CLC combined cycle with exhaust recuperation. Each efficiency point corresponds to the optimum pressure ratios of the two air turbine sections that are different for different compressor pressure ratios. It can be seen that the imposed TET constraint also affects the cycle behaviour, as the design choice has been to fix the hot-end temperature difference in the HRSG superheater. Although, it can be expected to achieve steam temperatures higher than 625°C in HRSG, in a long-term perspective; nevertheless the cycle shows reasonably high efficiency at higher CPR values where the results are the similar with and without the TET constraint. In Considering the CLC-development in long-term, the SRCLC-Er design point has been selected to be at the TIT=1200°C and CPR=18, where the net plant efficiency is 51.3%, as shown in Figure 6.21.

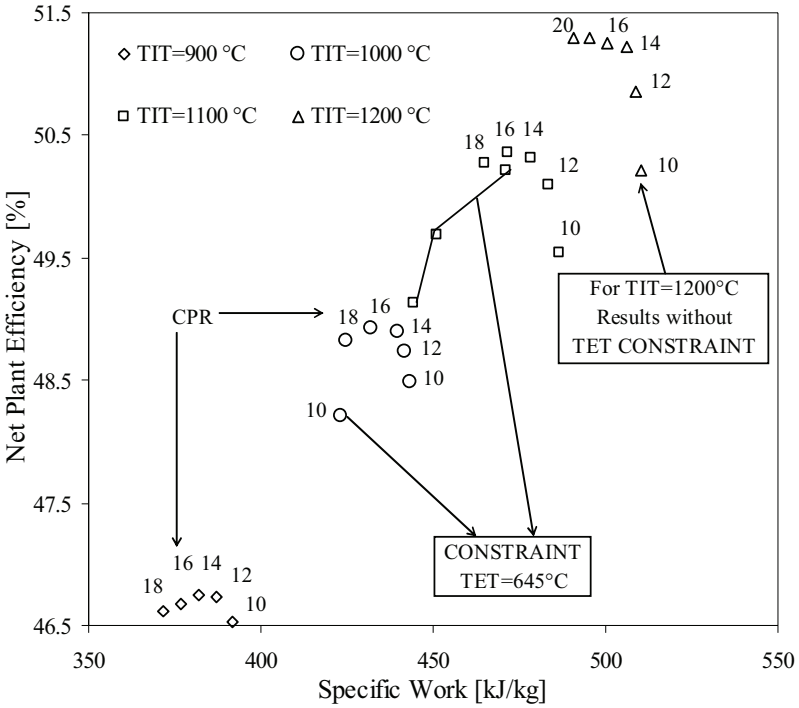

Figure 6.21 Net plant efficiency of SRCLC-ER as a function of specific work

Remarks on the Cycle Design and Performance

The cycle shows promising efficiency at all the oxidation temperature values. If the cycle were to be employed in near term and at lower and safer oxidation temperatures, a temperature of 1000°C would be a reasonable choice and the cycle would achieve a net plant efficiency of about 49%. Nevertheless, the cycle has not been optimised with respect to all the vital parameters and such optimisation may result in higher net plant efficiency. Another significant feature is the mixing of two exhaust streams coming from the two reduction reactors. It results in an unnecessary loss of exergy and the consequence is higher penalty for CO_2 compression. This can be improved by employing heat exchangers in series where the two exhaust streams are not mixed and heat up the cold fluids i.e. air and fuel in separate sections of heat exchangers. It necessarily demands for a different or modified CO_2 dehydration and compression plant. The lower pressure exhaust stream can be passed on directly to the same dehydration and compression plant as employed throughout this work. However, the higher pressure exhaust stream can be introduced downstream of the first compression stage at a pressure level that matches its pressure. Where the approach of multiple section preheaters and modified compression plant would result in a better efficiency, at the same time it will increase the cost of the plant as well. Since the economic analysis is not the main objective of this work, neither has it been carried out; the efficiency-cost trade-off is beyond the scope of this work and therefore is not further discussed here.

Power and Energy Balance for the Optimum Condition

Table 6-7 presents the energy and power balance for the cycle.

Table 6-7 Power and energy balance for SRCLC-ER: CPR=18, TIT=1200°C

Fuel flow	kg/s	15	Share of LHV
Fuel LHV	MW	697.5	100.0 %
High-pressure Air Turbine (AT1) work	MW	143.6	20.6 %
Low-pressure Air Turbine (AT2) work	MW	388.0	55.6 %
Steam Turbine work	MW	147.0	21.1 %
Compressor work	MW	-306.4	-43.9 %
Turbomachinery shaft power	MW	372.2	53.4 %
Turbomachinery mechanical loss	MW	-0.9	-0.1 %
Turbomachinery generator loss	MW	-3.4	-0.5 %
Turbomachinery generator terminal output	**MW**	**367.9**	**52.8 %**
Power island gross power output	MW	367.9	52.8 %
Plant auxiliary power		-3.3	-0.5 %
Net plant power island output	**MW**	**364.6**	**52.3 %**
Work CO_2 compression	MW	-6.7	-1.0 %
Net Plant power output	**MW**	**357.9**	**51.3 %**

The stream data for the cycle at the selected design point is included in Appendix B.

6.9 Comparison of Cycles

The thermodynamic analysis of various CLC-combined cycle options presented so far in this chapter suggest that all the cycles have a high potential of efficient power generation with CO_2 capture. It must be mentioned here that CLC-combined cycles can be configured in numerous forms, apart from those presented in this chapter. Nevertheless, the selected cycles very much represent the major types of possible combined cycle configurations. For the sake of benchmarking, this section compares the selected cycles with the reference conventional combined cycle. Since the foremost objective of this work is efficiency estimation of CLC-combined cycles, net plant efficiency of the CLC-cycles are compared with one another as well as with the reference conventional combined cycle with and without CO_2 capture. An important parameter in this regard is TIT, which is the oxidation temperature in case of CLC-cycles, and the combustor exit temperature in case of the conventional reference combined cycle. It is a rational approach to associate the efficiency of a cycle with its corresponding TIT, as shown in Figure 6.22. It can be seen that the reheat cycles, not surprisingly, show the highest efficiencies; yet the selection of number of reheats is an issue of discussion. It is quite evident from the above figure that all the CLC-cycles have higher net plant efficiency than the conventional natural gas-fired combined cycles that suffer an 8% efficiency drop due to CO_2 capture penalty. Thanks to the inherent CO_2 separation, the CLC-cycles have to undergo an efficiency drop associated solely with CO_2 compression, which is about 2%, and therefore the CLC-cycles exhibit a better efficiency than the conventional cycle with CO_2 capture.

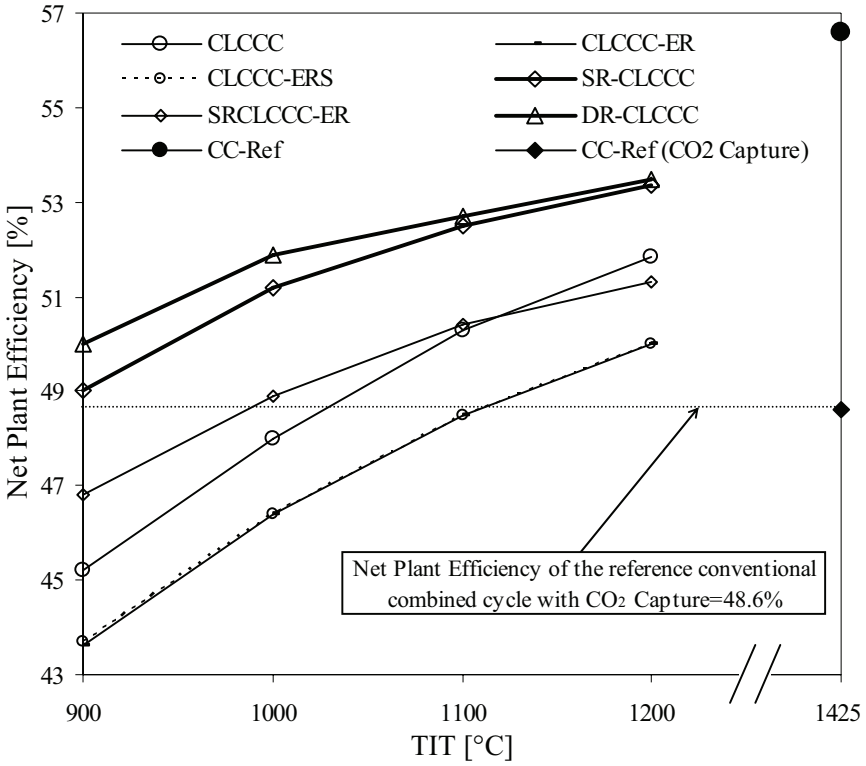

Figure 6.22 Comparison of cycles; maximum efficiency at the corresponding TIT

Considering the comparison of the CLC-cycles with one another, the CLCCC-ER and CLCCC-ERS have the same efficiency at all the TIT values and therefore they are graded as the competitors. The CLCCC-ER cycle however has an advantage over CLCCC-ERS as it does not involve any HRSG and steam generation that makes a plant bulky as well as adds value to the overall cost.

Figure 6.22 leaves no ambiguity in the argument that single reheat cycles has an edge over the double reheat cycles. It can be seen that DR-CLCCC has very little efficiency improvement at high TIT values (above 1000°C) as compared to SR-CLCCC, and at the cost of one extra CLC-reactor system as well as enhanced operational complexity. Hence, it can be suggested that if reheat were to be introduced in the air turbine of a CLC-combined cycle, single reheat is a feasible approach. The single reheat cycle with exhaust recuperation (SRCLC-ER) however, has the same efficiency as the base-case CLCCCC at TIT 1100°C and it tends to decline at higher TIT values. This is because of the increased CO_2 compression work at higher TIT values, because of the reduced CO_2-rich exhaust pressure. Nevertheless, the comparison of this cycle with CLCCC-ER and CLCCC-ERS would be more appropriate as all three cycles have the same basic configuration i.e. no CO_2 turbine. And SRCLC-ER has a prominently higher efficiency than these two cycles.

The performance of all the cycles can also be summarised in the form of CO_2 production per MJ of electricity (MJ_{el}). Figure 6.23 presents such a comparison, where the negative values present the CO_2 release and the positive values represent the CO_2 captured. Since the CLC-cycles are assumed to capture above 99% CO_2, they can be considered at near-to-zero emissions level. The DR-CLCCC and SR-CLCCC have almost the same value of (CO_2

kg/MJel), which is the similar to that of the reference cycle with CO_2 capture. However, the efficiencies of the CLC-cycles are much higher than the reference cycle with CO_2 capture. Reheat cycles however do have another edge over other CLC-combined cycles that they result in higher specific work that is advantageous concerning the cost of a plant.

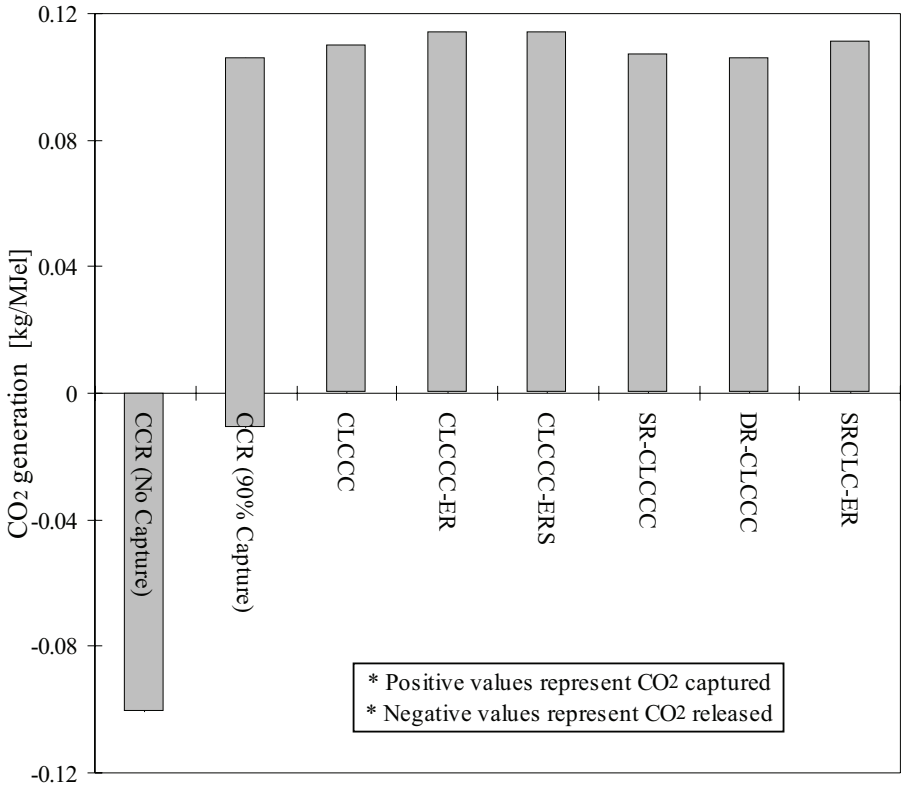

Figure 6.23 Cycles comparison in the form of CO2 generation and capture

6.10 Environmental Behaviour of NiO in CLC Applications

In CLC, nickel oxide (NiO) is believed to be the most promising metal. The experiments [Brandvoll, 2005] have shown that NiO exhibits better mechanical strength, conversion with fuel and heat carrying capacity as compared to other metal oxides. That is why this thesis uses NiO supported on $NiAl_2O_4$ as the oxygen carrier. However, there may be concerns about the environmental behaviour of nickel, which is formed as a result of NiO reduction with fuel in the reduction reactor of a CLC-reactor. During the reduction reaction, CO could be formed which can further react with reduced nickel to form nickel carbonyl, which is a hazardous gas. Regardless of the probability of nickel carbonyl formation in CLC, this can be a rather paradoxical situation if a power plant captures a greenhouse gas like CO_2 but produces a fatal gas like nickel carbonyl. In order to analyse the risk of nickel carbonyl formation and its consequences in CLC, it is inevitable to look into the phenomenon of nickel carbonyl formation, the temperature and pressure conditions at which it is formed and its physical properties. The chemical reaction of nickel with CO is given by the following equation:

$$Ni + 4CO \rightarrow Ni(CO)_4$$

In this reaction, nickel metal is reacting with carbon monoxide to produce $Ni(CO)_4$ (nickel carbonyl). This reaction takes place below 200°C and favourably at around 75°C [Goldberger and Othmer, 1963]. Although the reaction itself is a heterogeneous, nickel carbonyl is released in the gaseous phase and is highly carcinogenic. Reaction conditions for Ni and CO to produce $Ni(CO)_4$ range from almost 4 bar to 14 bar CO overpressure at a temperature of 75°C. When the gaseous nickel tetracarbonyl comes into contact with a heated surface, a nickel coating is the result of the decomposition of the nickel tetracarbonyl. This is given by the following reaction:

$$\mathrm{Ni(CO)_4 + heat \rightarrow Ni(metal) + 4CO}$$

This decomposition occurs between 35°C and 300°C, with optimal results at 175°C or greater, when coating forms [Goldberger and Othmer, 1963]. As in other equilibria reactions, the temperature of the nickel tetracarbonyl decomposition is increased with increasing carbon monoxide overpressure. Nickel carbonyl quickly evaporates to a gas if released as a liquid. It will oxidise in the air to form nickel oxide and carbon dioxide. The primary sources of nickel carbonyl are the industries that manufacture it or use it in production, such as nickel mining and refining, chemical industries, glass and metal plating.

As regards Chemical Looping Combustion, the temperature in the reduction reactor is far above those mentioned earlier, at which Nickel carbonyl is formed and decomposed. Therefore, it can be stated that at the temperatures above 600°C (which occur in the reduction reactor), considering the chemical equilibrium of the reactions, the nickel carbonyl decomposition reaction will be more favoured as compared to its formation. Therefore, the risk of nickel carbonyl formation is very slim even in case of pressurised CLC-reactors, as in a CLC-combined cycle, in which CO is available at the pressures in the range of 4 and 14 bar. Also, in the case of atmospheric CLC-reactors, which are not discussed in this chapter, the pressure and the temperature in the reduction reactor are not favourable for nickel carbonyl formation. The nickel oxide entering the reduction reactor is at high temperatures and reacts with the fuel entering at fairly high temperature as a result of the fuel preheating. Therefore, the risk of nickel carbonyl formation during the continuous operation of CLC is low. However, special considerations are needed for the plant start-up and shut-down. A cold start may result in nickel carbonyl formation; however, the reactor can be heated by some external source in this case, in order to provide an internal environment which is not favourable for such a reaction to take place. During the plant shut-down on the other hand, nickel carbonyl is more likely to be produced. This problem can be dealt with by flushing the gas out of the reactor followed by heat addition. This would result in decomposition of nickel carbonyl and recuperation of nickel metal.

Another aspect of significance is the stoichiometry of the nickel carbonyl formation reaction. Four moles of CO are required for each mole of nickel to form one mole of $Ni(CO)_4$. The large amount of nickel present in the reduction reactor together with very little amounts of CO will have two consequences; (1) assuming the formation of nickel carbonyl, the loss of nickel will be negligible, (2) amounts of produced nickel carbonyl will be very low. Nevertheless, even minute amounts of this gas can be fatal and lethal if exposed to the living beings. This issue has not yet been addressed sufficiently by the researchers who have carried out experiments on the nickel-based oxygen carriers for CLC, and must be considered in the future experiments.

6.11 Challenges in Applying Conventional Technology in CLCCC

The results presented in this chapter suggest that CLC has high potential for efficient power generation with CO_2 capture. This statement opens up the door to further research and development that may lead to successful realisation of CLC in power cycles. There are a lot more to investigate in each of the CLC-power cycle options i.e. off-design behaviour and transient analysis. The off-design analysis of some selected CLC-combined cycles will be presented in chapter 7. Nevertheless, the discussion on challenges in implementing conventional technology in CLC-combined cycles is presented here. This is an attempt to identify the difficulties associated with practical realisation of CLC and to assess the possibilities of using state-of-the-art turbomachinery and other components in a CLC-combined cycle.

The present work is based on idealised behaviour of the oxygen carrier particles and the CLC-reactors. The reactor system and oxygen carrier together form the most vital component of a CLC-power plant. Although the CLC-concept is still in the incipient phase of its development, there is a growing interest in CLC and the research on development of suitable oxygen carriers is going on in several parts of the world. This can be expected that suitable solid substances for CLC-applications will be available in future. On the other hand, the CLC-reactor system is assumed to be a circulating fluidised bed (CFB) system, which is a proven and widely used technology. Nevertheless, pressurised CFB reactors are not so widely commercially available and need further research and development before they can be adapted for CLC-applications. Another issue of concern is the successful circulation of solids within the reactor system. It can be stated that the circulation of solids in fluidised beds is not problematic as long as the particles have enough resilience strength. The pressure drop in the oxidation reactor can lead to reduced efficiency and this problem can be dealt with by employing compressed air fan or booster. This fan can make up for the pressure drop across the reactor without influencing the compressor pressure ratio and thereby increasing the compression work that could result in efficiency drop.

In traditional gas turbine units, the turbine and compressor are generally present in the form of single unit and are connected with each other by the shaft and surrounded by the combustion chamber. However, this is not the case in CLC where the so-called combustion takes place externally. This means that the shaft rotating the compressor will be exposed to two different temperatures, and essentially quite high. The turbine end of the shaft, which can also be called as the ‘hot end’ would necessarily have to be exposed to the oxidation temperature as certain length of the shaft will be present in the duct through which hot oxygen-depleted air is admitted to the air turbine. The compressor end, which can be called as the ‘cold end’ would be exposed to the hot air at the compressor exit. Despite that there is a temperature gradient along the axis of the shaft; there are some examples of external combustion implemented in conventional gas turbines. Therefore, this feature of CLC-combined cycles does not pose any major trouble concerning the plant layout and operational stability.

The industrial gas turbines operate on certain air and fuel flowrates and a flue gas composition that is very different from the oxygen-depleted air. The conventional turbines can however be operated on the oxygen-depleted air and the CLC-combined cycles can be scaled up in order to match with the gas flowrate of the conventional turbines. One major issue regarding the air turbine performance can be the escape of particulate matter out of the reactor system. A gas turbine is an intricate piece of engineering that cannot tolerate any

coarse particles. If particles are coarse enough they might get stuck in the annulus of the turbine. Although the escape of CLC-solid particles can be minimised by designing effective cyclone separation system, there always is a chance that some fines may not be collected. In order to avoid this problem, high temperature membrane can be applied prior to hot air admission to the turbine. Nonetheless, the conventional high temperature membranes cannot stand temperatures as high as 1000°C or above. Hence, further research is needed on this very aspect of CLC-combined cycles.

The CO_2-turbine is not commercially available yet, and therefore if manufactured, it can be custom-made for the CLC-applications.

The air and fuel preheaters are gas-to-gas heat exchangers, which are also a mature technology. The heat exchangers can be of the plate-fin type used in process industry for gas-to-gas heat transfer. The exchangers can also be of rotating Ljungström type. Also, the heat exchangers do not have to be essentially available off the shelf and can be manufactured as per CLC-requirements.

7 Off-design Evaluation of CLC-Combined Cycles

This chapter presents off-design evaluation of selected CLC-combined cycles. The design point data for the selected cycles is established on the basis of sensitivity study results obtained in chapter 6. There are two combined cycle configurations selected for off-design performance analysis; one cycle being designated as the base-case combined cycle. The base-case cycle is analysed in part-load mode as well as for the ambient temperature variations while the other cycle is analysed only at the part-load conditions. Comparison of part-load behaviour of both the CLC-combined cycles is presented with that of two state-of-the-art combined cycles with and without post-combustion CO_2 capture.

7.1 Methodology and Scope of the Off-design Evaluation

Off-design evaluation is an essential and vital step during the development process of a power cycle. A power plant is designed and built for its maximum capacity or full-load when it is operating at STP i.e. standard ambient temperature and pressure. However, in real applications, a power plant generally operates at off-design during most of its lifetime. A power plant operates not only under load varying conditions but also undergoes ambient temperature variations during different seasons of the year. Therefore, the off-design evaluation becomes necessary to analyse the plant behaviour under load- and ambient temperature-varying conditions. The off-design evaluation not only provides the information regarding the efficiency and flow conditions at different operating points but also indicates the operational problems that may be encountered by the plant under certain conditions. The control strategies for the plant are adopted in order to cope with those problems while maintaining the net plant efficiency as high as possible. Each power plant has specific requirements that have to be met at all the time regardless of the load and ambient temperature conditions.

The CLC-research carried out across the world so far, does not yet include any investigation of the off-design behaviour of a CLC-cycle. The objective of this chapter is to provide an insight into the off-design performance of selected CLC-combined cycles, address the operating limitations and devise control strategies. A number of CLC-combined cycle configurations were presented in Chapter 6. Two cycle configurations have been selected for the purpose of off-design evaluation. In chapter 6, one CLC-combined cycle was designated as the base-case cycle (CLCCC) and therefore it has been selected for the off-design evaluation. The cycle employs an air turbine, a CO_2-turbine and a steam turbine. In order to evaluate a cycle that does not employ any CO_2-turbine, the second selected cycle is the CLC-combined cycle with exhaust recuperation (CLCCC-ER). In this way two basic types of CLC-combined cycles are compared in the off-design mode.

In order to analyse a power cycle under off-design mode, it is essential to have a reasonable thermodynamic design. Once the thermodynamic design is achieved, the key cycle components can be dimensioned for the design-point. The cycle dimensions are fixed in the off-design mode and only the load and the ambient temperature conditions are varied. Chapter 6 serves the basis for the design point establishment of each of the two studied cycles. The sensitivity study of the key cycle parameters for the two cycles was presented in Chapter 6 and a design point was proposed. Nevertheless, the cycle studies presented in Chapter 6 did not take into account the pressure drop calculations in the CLC-reactors and the pressure drops were based on the consistent assumption of 5% of the incoming stream.

For the sake of off-design evaluation, the CLC-reactors dimensioning and calculation of reactors-specific parameters is done at the design point. In order to achieve a more realistic design, the pressure drops in the two reactors were calculated. The reactors' hydrodynamic behaviour is based on the reactors model involving geometry, presented in Chapter 4.

The solids transport between the two CLC reactors is subject to changes in the air and fuel flowrates which in turn are subject to the load and ambient temperature conditions as well as the control strategy adopted. The air turbine is also a key component in CLC-combined cycles as it drives the compressor and the air flow through the cycle is largely dependent on the conditions at the air turbine inlet. In the off-design mode, the compressor pressure ratio and inlet flow are determined from the choked air turbine. The coolant fraction at different load conditions also varies. There are two major strategies for determining the coolant fraction (% of flow at compressor inlet). It can either be assumed as the same fraction of the compressor inlet air as at the design point; or it can be assumed that the coolant flow is choked. The latter approach has been adopted for the present work. The off-design behaviour of the cycles that employ CO_2-turbine operating on the reduction reactor exhaust as working fluid will be different as compared to the cycles that do not include such a turbine. The CO_2-turbine is not directly related to the compressor and is a free power turbine. But nevertheless it is related to the compressor in an indirect way through the pressure requirements at the reduction reactor exit. The CO_2-turbine determines pressure at the fuel reactor entry and its work also varies at reduced fuel flowrate (part-load). Pressure in the reduction reactor is determined by the choked CO_2-turbine in the off-design mode. The steam turbine work is dependent on the air turbine exhaust temperature and varies accordingly. This work also assumes that the CO_2 dehydration and compression supplies pure CO_2 at the final pressure of 110 bar at all the load conditions.

The results for the base-case cycle include part-load evaluation as well as evaluation under varying ambient temperature. The results present efficiency reduction at part-load and the results related to the CLC-specific parameters i.e. solids conversion, solids flowrates, solids internal recirculation, residence times as well as the pressure drops in the two reactors. The CLC-combined cycle with exhaust recuperation (CLCCC-ER) has primarily been analysed to compare the efficiency reduction at part-load with the base-case cycle and the conventional combined cycles. Therefore, ambient temperature variations have not been considered for this cycle. While the oxidation reactor pressure drop varies according to the conditions of air at its inlet, the reduction reactor pressure drop is assumed to be constant. Since, oxidation is rather a rapid phenomenon, it is assumed that all the solids exiting the oxidation reactor are fully oxidised. The reduction is on the other hand, more complicated and it is calculated on the basis of amount of fuel entering the reduction reactor and amount of solids being transported out of the reduction reactor.

In this work the part-load is defined on the basis of the load factor as given in the following equation:

$$\text{Load Factor} = \frac{W}{W_0}$$

In the above equation, W and W_0 are the net plant work output at the part-load and the design point full-load, respectively.

Since, the power plant undergoes efficiency reduction at part-load; the efficiency can be presented in the form of relative net plant efficiency. The definition of relative net plant efficiency is given as follows:

$$\eta_{rel} = \frac{\eta_{PL}}{\eta_0}$$

In the above equation, η_{PL} and η_0 are the net plant efficiency at the part-load and the design point full-load, respectively.

The plant undergoes air flow reduction at part-load, which can be presented in the form of relative air flowrate given as:

$$\text{Relative air flowrate} = \frac{\dot{m}}{\dot{m}_0}$$

In the above equation, $\dot{m}$ and $\dot{m}_0$ are the air flowrate at the compressor inlet at a certain load condition and the design point, respectively.

The air and fuel preheater duty also change with the load condition and can therefore be represented in the form of relative duty given as:

$$Q_{rel} = \frac{Q}{Q_0}$$

In the above equation Q_{rel} is the relative duty of a heat exchanger, while Q and Q_0 are the duty of the same heat exchanger at a certain operating condition and the design-point, respectively.

The definitions of 'load factor' and 'relative net plant efficiency' are valid for both the CLC-cycles and the conventional combined cycles. In order to compare the off-design performance of CLC-combined cycles with the conventional combined cycles, two commercial gas turbines are selected and applied in combined cycle configuration. The selected turbines are GE 9FA and Mitsubishi 7G. The data for these turbines was obtained by GTPRO and part load simulations were carried out in GTMASTER [Thermoflow, Inc.]. The post-combustion CO_2 capture by amine absorption is also applied to the conventional combined cycles. The same strategy as that for the post combustion CO_2 capture from the generic reference-combined cycle presented in Chapter 6, is applied here. The absorption tower pressure drop is assumed to be 150 mbar at the full load design-point for both the conventional combined cycles. This pressure drop does inevitably change in the off-design mode. Assuming a continuous flow of the flue gas and that the flue gas temperature, pressure and molecular weight remain constant at the gas turbine exit, the pressure drop in the absorption tower can be related to the flowrate of the flue gas as given in the following:

$$\frac{\Delta P}{\Delta P_0} = \left(\frac{\dot{m}}{\dot{m}_0} \right)^e$$

In the above equation, ΔP and ΔP_0 is the pressure drop in the absorption tower at a certain operating condition and at the design-point, respectively. The $\dot{m}$ and $\dot{m}_0$ are flowrate of flue gas through the absorption tower at a certain condition and at the design-point, respectively. The value of the coefficient 'e' is set to 1.8, based on the derivation of the equation for the pressure drop in the absorption tower, on the basis of the continuity equation and treating the flue gas as perfect gas. The total efficiency drop of the conventional combined cycles due to the CO_2 capture is calculated in the same way as described in Chapter 6, based on the work by Undrum and Bolland [2003].

7.2 Off-design Evaluation of the Base-case Cycle (CLCCC)

Figure 7.1 shows schematics of the CLC-combined cycle designated as the base-case.

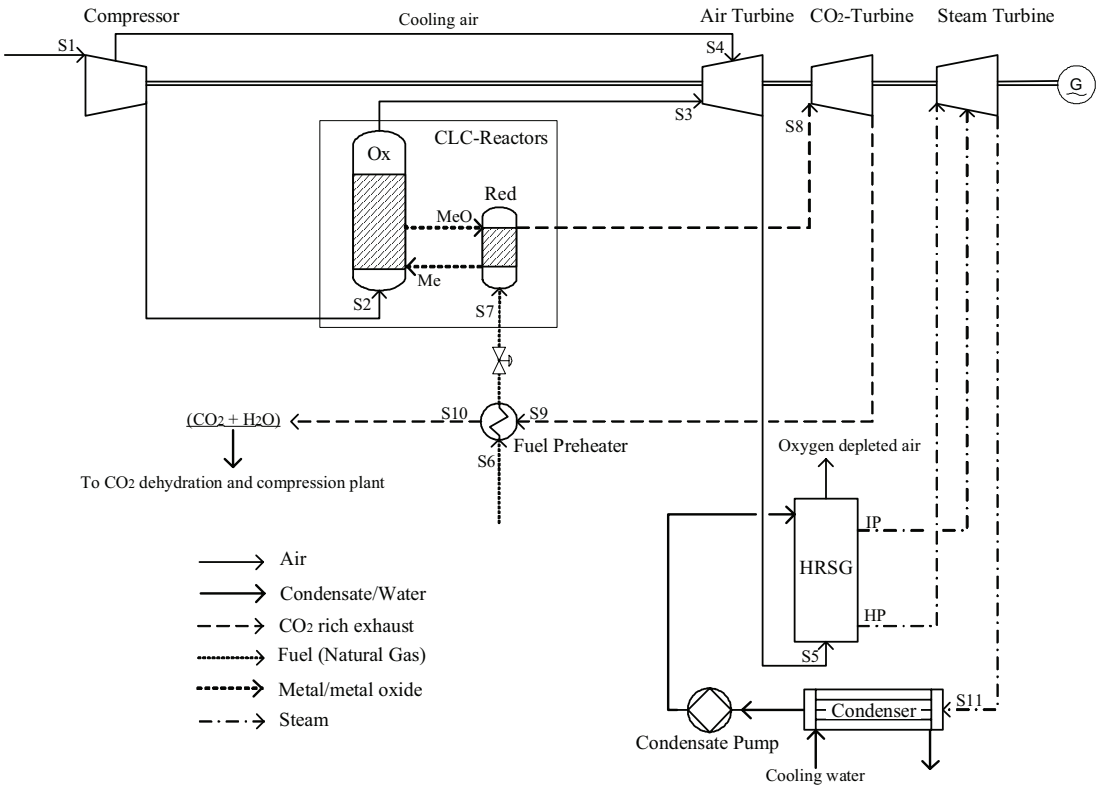

Figure 7.1 Schematics of the base-case CLC-combined cycle (CLCCC)

The cycle description was presented in detail in Chapter 6 and therefore it is not given here but the design-point data is presented.

7.2.1 Design-point Data

Table 7-1 presents the design-point data for the cycle.

Table 7-1 Design-point data for CLCCC

Compressor		
Compressor pressure ratio		18
Air flow at compressor inlet	kg/s	823
Coolant flow	kg/s	62.5
Oxidation Reactor (+Cyclone)		
Oxidation Temperature	°C	1200
Degree of oxidation (Xox)		1
Reactor diameter	m	14
Reactor height	m	30
Pressure drop	mbar	153
Solids entrainment ratio		0.254
Solids residence time	sec	47
Solids flowrate at oxidation reactor exit	kg/s	616
Reduction Reactor		
Reduction Temperature	°C	980
Degree of reduction (Xred)		0.3
Reactor diameter	m	8
Reactor height	m	2
Pressure drop	mbar	316
Solids residence time	sec	156
Solids flowrate at reduction reactor exit	kg/s	561
Fuel Preheater		
Fuel flow	kg/s	15
Preheating temperature	°C	508
Overall area of heat transfer	m^2	1227
overall heat transfer coefficient [U]	W/m^2K	150
Hot-end temperature difference		25
Air Turbine		
Pressure ratio		17.36
Flowrate at turbine inlet	kg/s	768
Turbine inlet temperature	°C	1140
Turbine exit temperature	°C	492
Net work	MW	234
CO_2-Turbine		
Pressure ratio		16.7
Flowrate at turbine inlet	kg/s	70.5
Turbine inlet temperature	°C	980
Turbine exit temperature	°C	533
Net work	MW	53.6
Steam Cycle		
Steam pressure (HP/IP)	bar	60/5
Steam temperature (HP/IP)	°C	467/258
Steam flow (HP/IP)	kg/s	77.5/21.8
Steam turbine net work	MW	101.5
CO_2 compression plant work	MW	13.9
Net plant work	MW	365.5
Net plant efficiency	%	52.4

Note: *The design-point data for the cycle is the same as that presented in Paper II except for the CO_2 compression work. The papers are based on the assumption of CO_2 final pressure of 200 bar while the presented work assumes 110 bar delivery pressure. Therefore, the CO_2 compression work in the present work is lower than that in the papers and the net plant efficiency at the design-point is slightly higher.*

7.2.2 The Off-design Scenario

As soon as a power plant deviates from the design point during its operation, a number of changes occur simultaneously in the cycle. In order to meet with the load demand and to fulfil certain plant criteria, different off-design strategies can be adopted. It is important to identify the most important plant criteria to be satisfied before any control strategy can be devised. The most critical criterion is to achieve the same pressure at the exit of the two CLC-reactors.

Pressure at Reactors' Exit

It is of utmost importance to maintain the same pressure of the gases in the ducting that connects the CLC-reactors for solids transport. This duct is necessarily the one, through which the solids separated from the oxygen-depleted air in the cyclone system, fall down to the fuel reactor. In case of any pressure difference occurring in the ducting, gas may leak between the two reactors. Such conditions are highly undesirable because the main idea behind the Chemical Looping Combustion is to keep the air and the fuel streams separated from each other. The proposed reactor system consists of the air reactor essentially being a pneumatic transport reactor with air as the oxidising agent. The fuel reactor is the bubbling fluidised bed with natural gas as the reducing agent. Due to its pneumatic transport nature, the air reactor has a lower pressure drop compared to the fuel reactor. The power plant is configured in such a way that the oxygen-depleted air at the air reactor exit and the CO_2-rich exhaust at the fuel reactor outlet are at the same pressure at the design point. As soon as the plant operates off design, a pressure difference will occur at the reactors exit unless a control strategy is adopted. The occurrence of this pressure gradient is the consequence of the presence of the presence of two turbines; the air turbine and the CO_2-turbine, both resulting in different inlet pressures at part-load. Since the turbines are assumed choked, the pressure requirements at the inlet of the two turbines differ. Since the reduction reactor has a larger pressure drop, the CO_2-turbine inlet pressure will be lower than the air turbine inlet pressure. The plant then needs to be controlled in such a way that the pressure at the air turbine inlet becomes equal to that at the CO_2-turbine inlet. If uncontrolled, the oxygen-depleted air will entrap into the fuel reactor coming in direct contact with the fuel, thereby upsetting the stoichiometric reactions and resulting in undesired dilution of the CO_2 with nitrogen and oxygen. In order to cope with this problem, the present work employs a compressor with variable inlet guide vanes (VGVs). At a certain off-design operating point, the variable guide vanes are closing by a certain degree. This changes the compressor geometry and reduces the air flowrate through it. The result is a reduced air turbine inlet pressure in accordance with the CO_2-turbine inlet pressure.

The Off-design Strategy

The off-design strategies may vary under different load and ambient temperature conditions. When at part-load, the control strategy for the present work focuses on two major issues:

fuel cut in order to meet the load requirements; and use of variable guide vane angles at the compressor inlet (VGVs) in order to reduce the air flowrate, influencing the pressure through the system thereby achieving the same pressure at the two reactors exits. In case of ambient temperature variations, a fall in ambient temperature results in increased air density and the air flowrate at the compressor inlet increases. The variable guide vanes then perform their function to control the air flowrate for the pressure matching at the reactors' exits. Conversely, the air flowrate decreases at the compressor inlet with the ambient temperature rise. Under such condition the fuel cut is appreciable as well as the variable guide vanes are used to match the air requirements in accordance with the fuel flow and the desired pressure at the oxidation reactor outlet. Therefore, quite contrary to the conventional combined cycle power plants, the control strategy does not emphasise on maintaining a constant turbine inlet temperature or turbine exit temperature and can be referred to as 'sliding TIT' strategy.

The plant can be sub-divided into two parts; the upstream of CLC-reactors consisting of the fuel preheater and the compressor, and the downstream of the CLC-reactors comprising of the turbines. The plant is controlled with respect to the lowest pressure occurring in the downstream part of the cycle, which is at the CO_2-turbine inlet. This pressure is the lowest due to the higher pressure drop in the bubbling bed reduction reactor. The reduction reactor exit pressure should be equal to the pressure at the oxidation reactor exit. Since the streams at both the reactors' exit are led directly to the turbines, therefore the two turbines' inlet pressure must be the same. In other words, when the turbines are choked, the CO_2-turbine not only demands for a certain inlet pressure but also influences the inlet pressure of the air turbine. At part-load, the VGVs at the air compressor inlet can be closed down to a certain degree. The air flowrate influences the pressure through the system and can be reduced to the extent at which the pressure requirements downstream of the reactor system are satisfied. The reduced air flowrate together with a reduced TIT result in the reduced steam turbine work as well. At the same time, the reduced airflow means that fewer particles are transported out of the oxidation reactor. In case of part-load operation, the fuel flow reduction also occurs in conjunction with the load requirements and reduced air flow. Therefore, the exhaust flow out of the reduction reactor also decreases together with the reduced pressure at the reduction reactor exit, i.e. the CO_2-turbine work decreases. The operation of the fuel preheater is also affected because the percent reduction in the hot fluid (exhaust) flowrate is more prominent than the percent reduction in the cold fluid (fuel). The ambient temperature variations result in the same interactions but to a different extent.

7.2.3 Part-load Behaviour

In this section, the cycle's part-load behaviour at the design-point ambient temperature will be presented in the form of relative net plant efficiency and air flow reduction.

Relative Net Plant Efficiency

The part-load analysis of the base-case CLC-combined cycle (CLCCC) shows that by reducing the load down to 60%, net plant efficiency of the CLC-combined cycle drops by 2.6%-points. This work however emphasises on the part-load behaviour of the CLC combined cycle and its comparison with the conventional combined cycles. Therefore, it is appropriate to present the part-load performance in terms of the relative net plant efficiency. Figure 7.2 compares the relative net plant efficiency of the base-case CLC-combined cycle with two conventional combined cycles at various values of load factor. The relative net plant efficiency of the CLC combined cycle at part-load is better in comparison with

conventional combined cycles. Under part-load, the plant is controlled by reducing the airflow at the compressor inlet which results in pressure reduction at the air turbine inlet. This strategy is adopted for controlling the plant in order to match with the lowest pressure occurring in downstream of the oxidation and the reduction reactors. Therefore, the pressure at the air turbine inlet is controlled according to the pressure at the CO_2-turbine inlet which is the lower of the two. The pressure reduction results in a reduced air flowrate through the cycle which has to be met with the fuel flow reduction at the reduction reactor inlet. At the same time, the oxidation reactor must fulfil the requirement of the essential solids transport in conjunction with the fuel supply. The net effect is a relatively higher reduction in fuel flow at part-load compared to the selected conventional combined cycles, resulting in more promising net plant efficiency of the CLCCC at part-load. The relative net plant efficiency of the CLC-combined cycle at 60% load is about 0.95, which is very promising in comparison with the conventional combined cycles that achieve relative net plant efficiency of about 0.91at 60% load.

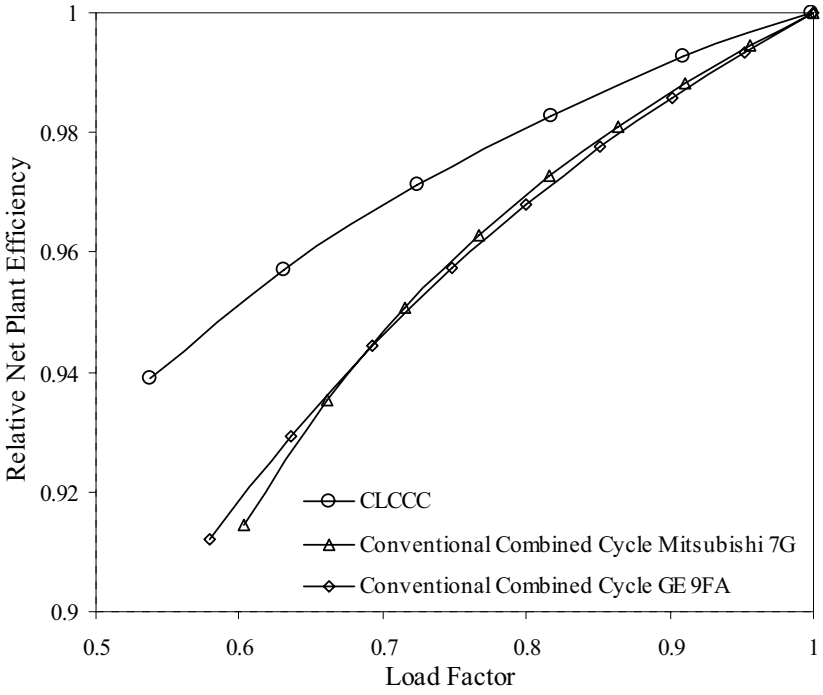

Figure 7.2 Relative net plant efficiency at varying load

Air Flow Reduction at Part-load

Figure 7.3 presents the relative air flow as a function of load factor for the base-case CLCCC at the design point ambient temperature. It can be seen that decreasing the load down to 56% results in 60% air flow reduction. Modern compressors are equipped with VGVs that can reduce the flowrate from 100% to typically 60%, as mentioned by the 'VGV LIMIT LINE'. Therefore, according to Figure 7.3, the plant cannot be controlled with the proposed control strategy below part-load of 56% when air flow reduction is limited to 60%. This implies that this strategy is not valid for the plant start-up and shut-down as well. The results shown in Figure 7.3 call the need to investigate alternative control strategies for the cycle, which will be discussed in the section '7.2.5- Alternative Control Strategies'.

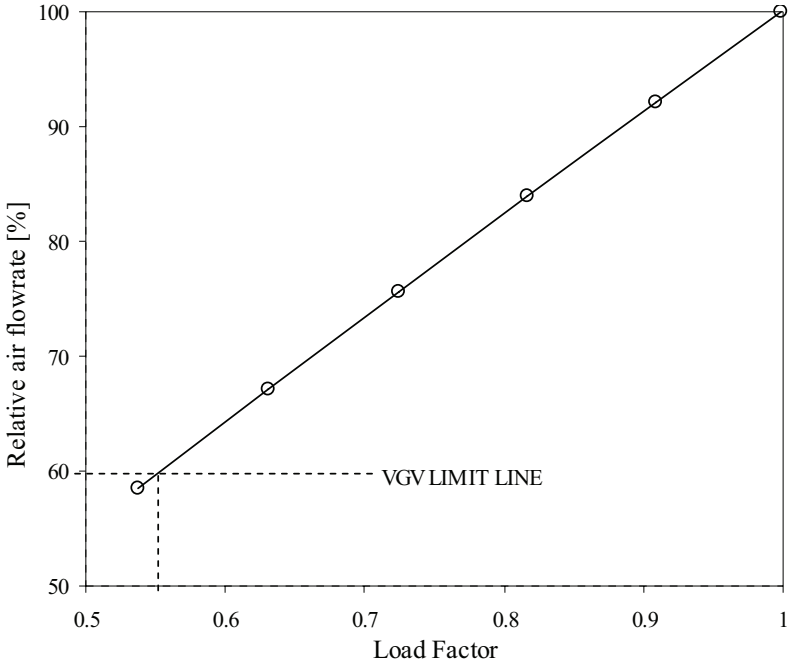

Figure 7.3 Air flow reduction as a function of load factor
[The base-case CLCCC at the design point ambient temperature]

Air Turbine Exit Temperature (TET)

Figure 7.4 presents the air turbine exit temperature (TET) as a function of load factor. The air flow reduction also results in the reduced compressor pressure ratio thereby affecting the turbine inlet temperature as well as turbine exit temperature. It can be seen in Figure 7.4 that the load reduction results in the increase of the air turbine exit temperature. This implies that the work extraction from the air turbine, which has the highest share in the net plant work, is decreased by virtue of lower enthalpy drop due to the reduction in TIT and increase in TET. Hence, the adopted control strategy can be named as the 'increasing TET' strategy that results in a better part-load efficiency compared to the selected conventional combined cycles while satisfying the vital plant criteria. The CLC-combined cycle part-load performance can be explained with the help of an overall analysis of the cycle key parameters at relative load, as given in Table 7-2. When the plant operates at part-load, two main changes take place simultaneously; the air flow reduction at the compressor inlet for balancing the CLC-reactor pressures, and the fuel flowrate reduction to reduce the air turbine inlet temperature (TIT) for fulfilling the load demand. The part-load analysis of the CLC combined cycle presented in Table 7-2 shows that despite the reduction in the air turbine inlet temperature, the turbine exit temperature increases at part-load. This effect is due to the successive reduction in the compressor pressure ratio in order to match with the pressure requirements in the CLC-reactors. This implies that the steam cycle work is not reduced to the same extent as that of the air turbine and the CO_2-turbine at part-load.

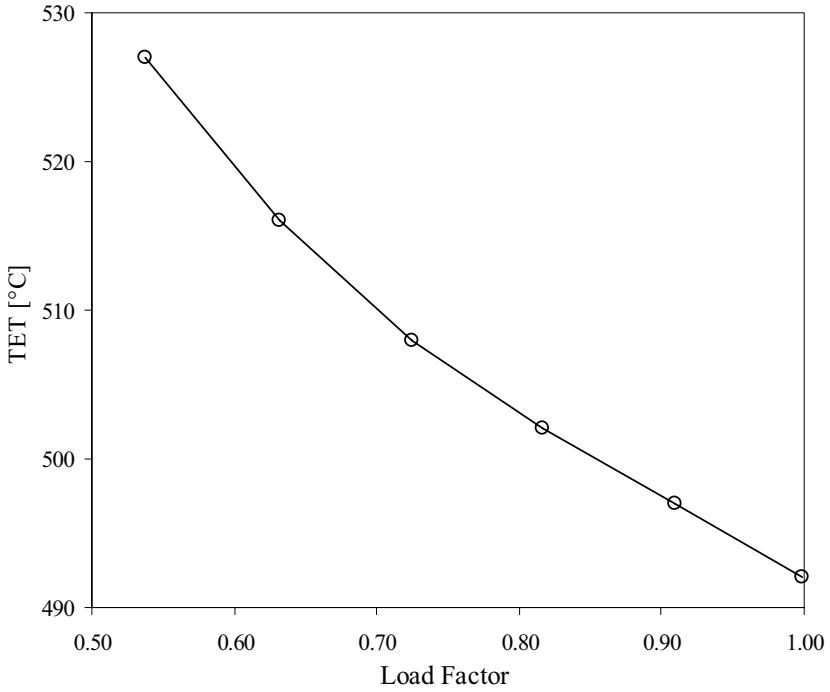

Figure 7.4 The air turbine exit temperature as a function of load factor

The steam cycle part-load performance is hence better compared to the air turbine and the CO_2-turbine. Therefore, due to the comparatively better performance of the steam cycle, the relative net plant efficiency of the CLC combined cycle is better as compared to the conventional combined cycles. It can be seen that despite a reduced flue gas flowrate to the HRSG, the reduction in the HP and LP steam production does not drop appreciably and hence the steam cycle relative power output is higher at part-load. The air turbine and CO_2-turbine power output, on the other hand, decrease more rapidly at part-load compared to the steam turbine work. A comparison of the relative power of the three turbines reveals that at a certain part-load, the steam turbine has the highest relative power followed by the air turbine, while CO_2-turbine has the lowest relative power. Since, the fuel flow is reduced at part-load; the CO_2-production also decreases thus resulting in relatively lower power demand for the CO_2 compression process. The CO_2 compression plant relative power is slightly lower than that of the steam turbine, at different values of relative load. The CO_2-turbine exit temperature, like that of the air turbine, also increases with decrease in load. Since, the CO_2-turbine exhaust preheats the fuel; the consequence is that the fuel preheating temperature increases at part-load, as shown in Table 7-2.

Another factor that has a slightly positive impact on the part-load performance of the CLC combined cycle is the fuel flowrate at part-load. The results show that reduction in the fuel flowrate at part-load is slightly greater in the CLC combined cycle compared to that in the conventional cycles; which also contributes towards the better relative part-load efficiency.

Table 7-2 Key parameters of CLCCC at various values of relative load

Relative Load		1	0.91	0.82	0.72	0.63	0.54
Compressor							
Compressor pressure ratio		18	16.3	14.7	13.1	11.6	10
Air flow at compressor inlet	kg/s	823	754	685	615	545	473.4
Coolant flow	kg/s	62.5	47.1	37	26.7	19.6	13
Air Reactor (+Cyclone)							
Oxidation Temperature	°C	1200	1171	1146	1119	1092	1063
Pressure drop	mbar	153	159	165	173	184	199
u0-uT		0.63	0.61	0.59	0.57	0.54	0.5
Solids entrainment ratio		0.25	0.24	0.23	0.22	0.21	0.19
Fuel Reactor							
Fuel flow	kg/s	15	13.7	12.5	11.2	9.9	8.6
Reduction Temperature	°C	980	973	962	948	934	917
Degree of reduction (Xred)		0.3	0.34	0.37	0.41	0.45	0.48
Pressure drop	mbar	316	316	316	316	316	316
Fuel Preheater							
Preheating temperature	°C	508	513	521	528	538	548
Air Turbine							
Tiurbine inlet temperature	°C	1140	1120	1101	1080	1057	1033
Turbine exit temperature	°C	492	497	502	508	516	527
Relative power		1.00	0.90	0.80	0.70	0.60	0.50
CO2-Turbine							
Pressure ratio		16.7	15.2	13.7	12.2	10.8	9.3
Flowrate at turbine inlet	kg/s	70.5	64.5	58.5	52.5	46.4	40.2
Tiurbine inlet temperature	°C	980	973	962	948	934	917
Turbine exit temperature	°C	533	534	536	542	547	563
Relative power		1	0.88	0.77	0.66	0.55	0.44
Steam Turbine							
HP steam flow	kg/s	77.3	73.5	69.4	65.3	60.5	55.3
LP steam flow	kg/s	21.7	19.1	16.7	14.2	11.8	9.8
Relative power		1.00	0.94	0.88	0.82	0.75	0.67
CO2 compression-relative power		1.00	0.93	0.84	0.76	0.67	0.58

7.2.4 Ambient Temperature Variation

The part-load performance presented in the preceding section of this chapter takes into account only the load reduction and is based on the design point ambient temperature. In order to achieve a broader overview of the plant behaviour it is devisable to analyse the plant simultaneously at varying load and varying ambient temperature. Where the load variations impose certain changes in the flowrates and demand for certain control strategies, the temperature variations also have significant impacts on the air flowrates and the fuel requirements, depending on the control strategy.

The ambient temperature variation at the part-load can either enhance the same effect as occurring due to the load change or quite contrarily have a very different impact on the cycle as compared to the load variation. Such changes need to be predicted before further

development of a new concept can be done. Therefore, this section deals with the ambient and load variations occurring in the cycle under study. Since the CLC-reactors are the key components in the cycle and all the efforts are made to achieve the desired transport of materials between the two reactors; the control strategies in the off-design mode are adopted with the emphasis on fulfilling this requirement together with the key requirement of the similar pressure at the reactors' exit. The ambient temperature variation affects the net plant efficiency of a combined cycle to a less extent. With increase in the ambient temperature, the compressor efficiency decreases and hence the work extraction from the air turbine also decreases. But the consequence is a higher air turbine exit temperature. The steam turbine work hence balances out the reduction in the air turbine work. Therefore, the efficiency variation is not of much significance with respect to ambient temperature variation.

The CLC-specific parameters are sensitive to these variations because they are to a large extent dependant on the flow conditions at the reactors inlet. The flow conditions at the compressor inlet vary with part-load as well as ambient temperature. With drop in ambient temperature, air at the compressor inlet is cooler and denser. As a result, mass flow at the compressor inlet and hence the compressor pressure ratio increase. On the contrary, as the temperature of air at the compressor inlet increases, the air density decreases and mass flow and pressure ratio decrease. The ambient variations are thus closely linked with the conditions at the CLC-oxidation reactor inlet, which is fed with the compressed air. Figure 7.5 presents the relative air flow as at varying load for variations in the ambient temperature.

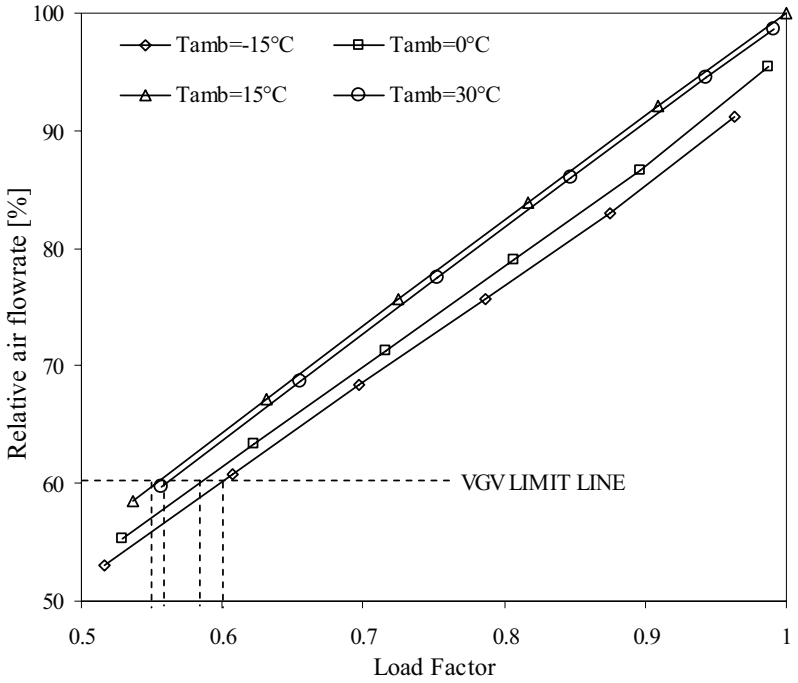

Figure 7.5 Air flow reduction as a function of load factor and ambient temperature

It can be seen in Figure 7.5 that at high part-loads (above 95%) ambient temperature variations may result in reduced air flowrates as compared to the design point ambient temperature. The airflow reduction is the consequence of the fulfilment of the criterion to achieve the similar pressure at the oxidation and the reduction reactor outlets as well as fulfilling the requirement of the solids transport. The air flow reduction at these load

conditions can be as low as that the plant cannot be operated at full-load because there is not enough air available at the oxidation reactor inlet in order to transport the desired amount of solids required by the fuel. This can be regarded as the design-limitation of the cycle. But nevertheless this problem can be dealt with by either employing a compressor with VGVs that not only close down but also open up and hence changing the compressor geometry and draw in more air when the ambient temperature is higher than the design point ambient temperature at full-load. Another solution to this problem can be cooling of air prior to its entry into the compressor. Air cooling is common in gas turbine units operating in hot and dry climate. This increases the density of air at the compressor inlet and more air is drawn in. This technique can help achieving the desired air flowrate that can fulfil the vital cycle criteria.

Degrees of Solids Conversion

The present work is based on the complete conversion of solids in the oxidation reactor and hence the degree of oxidation is always 100% (Xox=1) regardless of the operating condition. The degree of reduction (Xred) does however vary with the operating conditions. Figure 7.6 presents the degree of reduction of solids (Xred) as a function of load factor and ambient temperature.

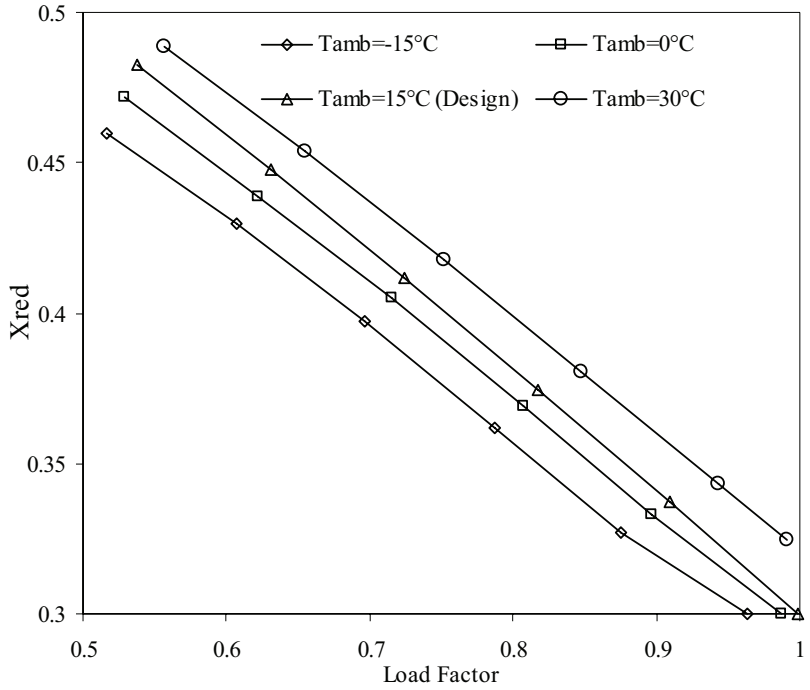

Figure 7.6 Degree of reduction (Xred) as a function of load factor
[Xred=0 means 100% reduction, Xred=1 means no reduction at all)

The results show that the solids conversion in the reduction reactor goes on decreasing at part-load because the solids transport out of the reduction reactor decreases at part-load due to the fuel flow reduction as well as fall in the pressure in the reduction reactor. When the ambient temperature rises above the design-point ambient temperature, the degree of reduction is comparably lower even at very high load factor values as compared to that at

the design-point. This is due to the fuel-cut and pressure reduction in the reduction reactor in order to match with the reduced compressor pressure ratio at part-load and reduced air flowrate due to the increased ambient temperature.

Solids Internal Recirculation/ Entrainment Ratio in the Oxidation Reactor

The internal recirculation of solids or the amount of solids entrained out of the oxidation reactor is a function of air flowrate and air pressure in the oxidation reactor which keeps varying with the operating conditions. Figure 7.7 presents the solids entrainment ratio at different load-varying conditions.

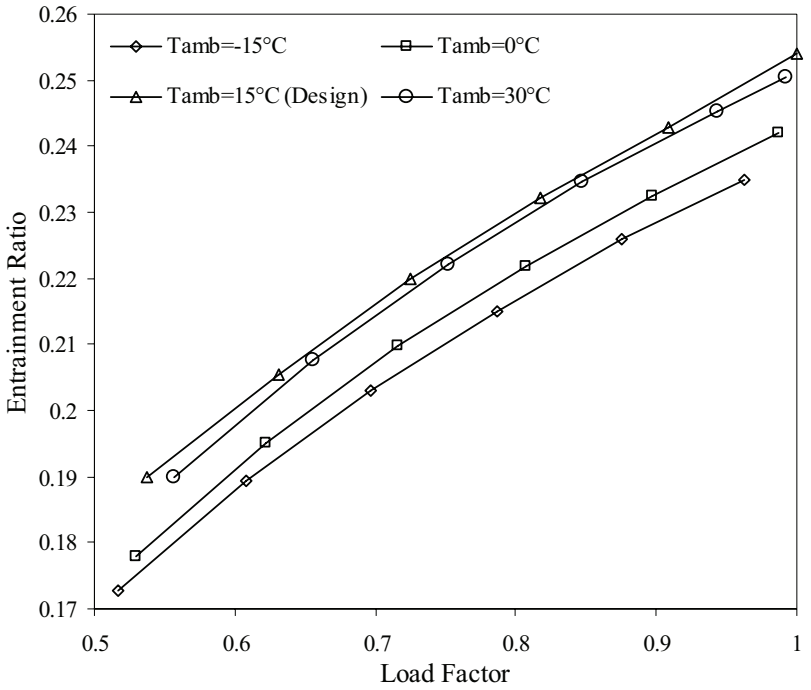

Figure 7.7 Solids entrainment ratio at load- and ambient temperature varying conditions

It can be seen in Figure 7.7 that the solids entrainment ratio goes on decreasing with load reduction. The ambient temperature variation also affects the solids entrainment ratio but the impact of ambient temperature change is not as profound as that of the load change.

The part-load necessarily results in reduced air flowrates and air pressure into the oxidation reactor. The plant also undergoes the fuel-cut at part-load. Thereby the necessary supply of oxygen to the fuel in the form of solid particles decreases. The plant is controlled in such a way that only the accurate solids supply is maintained which is lower than that at the design-point. Therefore, the superficial air velocity at the oxidation reactor inlet reduces with the air pressure and air flowrate, resulting in a lower difference between the superficial air velocity and the terminal falling velocity of the solids.

Figure 7.7 shows the consequence of the reduced air flowrate, which results in lesser and lesser amounts of solids being transported out of the oxidation reactor, at part-load. The

lower the entrainment ratio the higher is the amount of solids circulating internally in the oxidation reactor, thereby increasing the internal recirculation ratio as shown in Figure 7.8

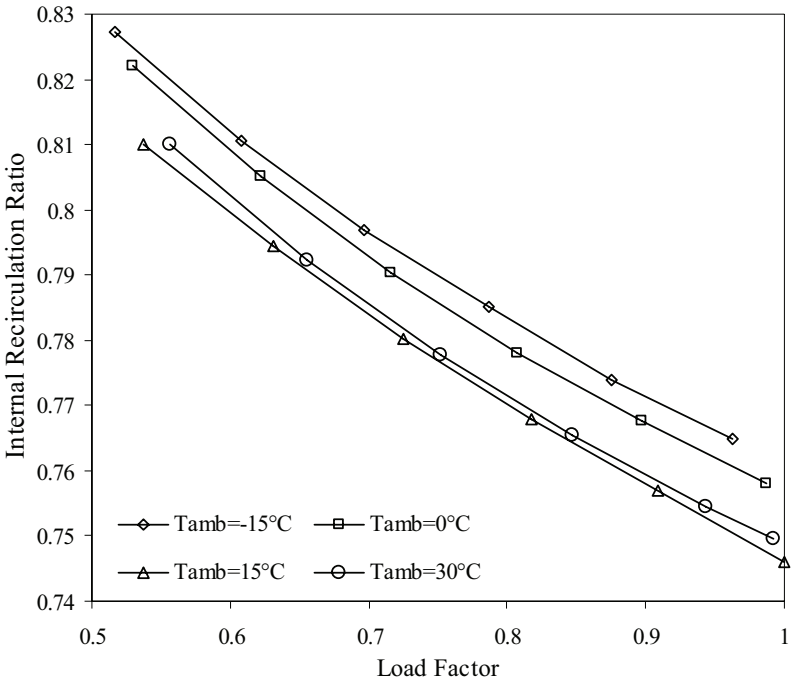

Figure 7.8 Internal recirculation ratio at load- and ambient temperature varying conditions

Solids Residence Time

The solids entrainment ratio and the solids internal recirculation are directly linked with the amounts of solids being transported out of the oxidation reactor as well. Hence, it can be stated that the solids residence time is a function of the solids entrainment ratio. The solids entrainment ratio, internal recirculation, the air flowrate and air pressure at the oxidation reactor are all interwoven quantities. Therefore, variation in one inevitably leads to variation in the other. In the off-design mode, the effect of load reduction on the air flowrate and related quantities has been discussed in the preceding sections.

It was shown in Figure 7.7 and Figure 7.8 that at the part-load more and more solids internally recirculated. This means that the hold up of the particles in the oxidation reactor increases. In other words, the solids residence time in the oxidation reactor goes on increasing with load reduction. Figure 7.9 presents the solids residence time in the oxidation reactor as a function of load factor, for different values of ambient temperature. It can be seen in Figure 7.9 that the solids residence time strongly depends on the load conditions. The simultaneous ambient temperature and load variation result in different demands of air and fuel flowrate at different operating points, which has a direct effect on the amount of solids transported out of the reactors. Therefore, the residence time of solids in the reduction reactor also increases.

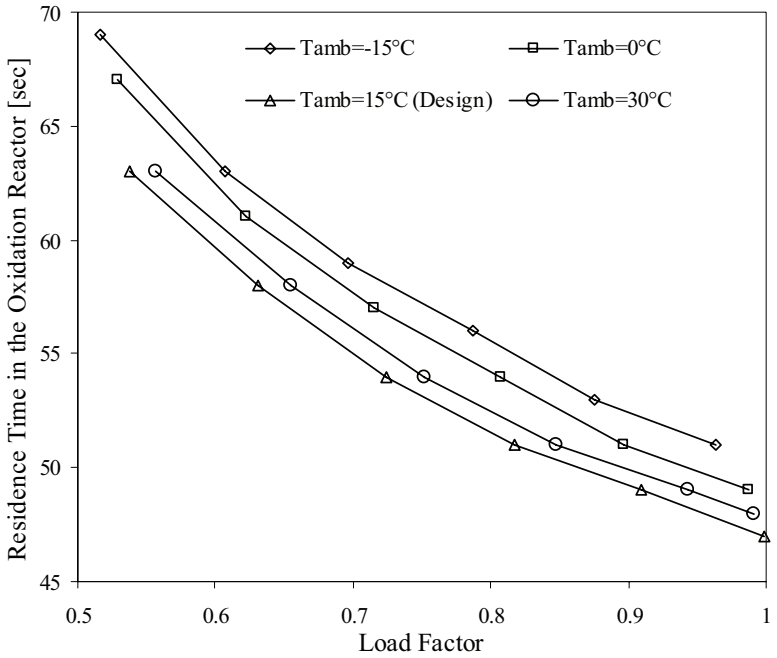

Figure 7.9 Solids residence time in the oxidation reactor as a function of load factor

Figure 7.10 presents the solids residence time in the reduction reactor as a function of load factor, for different values of ambient temperature.

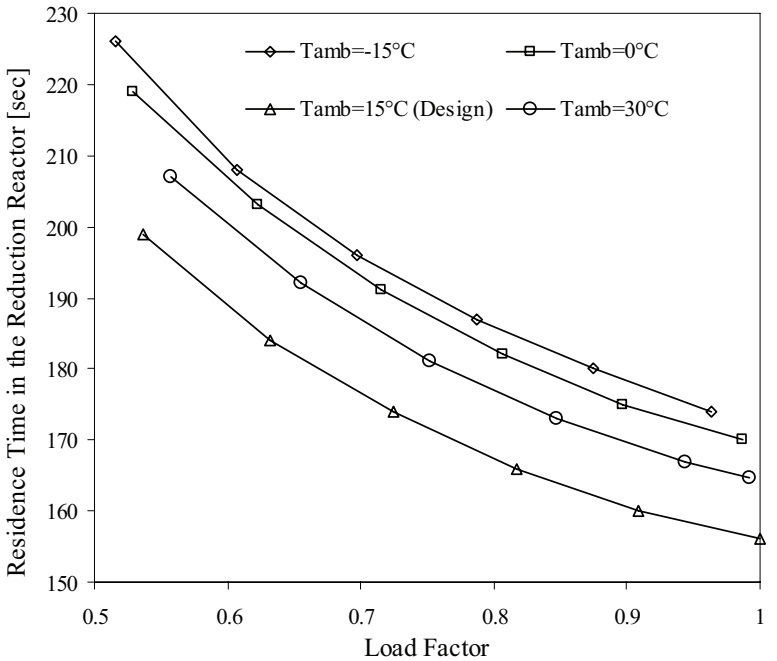

Figure 7.10 Solids residence time in the reduction reactor as a function of load factor

It can be seen that the solids residence time in the reduction reactor is much larger as compared to that in the oxidation reactor. This is due to the nature of the reduction reactor,

which is a bubbling fluidised bed type reactor. The increase in the solids residence time in the reduction reactor is surely beneficial because the reduction reaction is less rapid as compared to the oxidation reaction and an increased residence time may result in better solids conversion. Although the increased residence time can be considered to be beneficial because it results in better conversion of solids; but nevertheless it also results in increased pressure drop. This effect will be discussed in the following section.

Reactors' Pressure Drop

The oxidation reactor pressure drop increases at part-load due to the air flow reduction and the increased solids internal recirculation. The ambient temperature variation also results in increased pressure drop because the VGVS operate at all the operating points away from the design-point and the plant undergoes reduction in the air flowrate. Figure 7.11 presents the oxidation reactor pressure drop as a function of load factor over a range of ambient temperature. The pressure drop includes a constant cyclone pressure drop of 20 mbar.

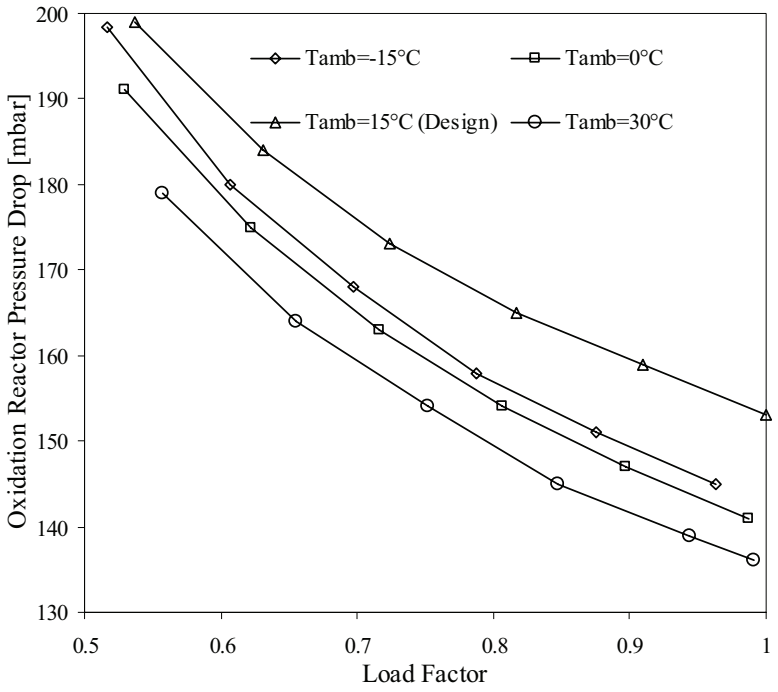

Figure 7.11 Oxidation reactor pressure drop as a function of load factor

The solids hold-up in the reduction reactor increases at the off-design and hence the residence time also increases. In principle, this should result in an increased pressure drop over the fluidised bed reduction reactor. Recalling the reactors' hydrodynamic model involving the reactors' geometry presented in Chapter 4, the current work is based on the assumption of a constant average solids fraction (ε_f=0.4) in the reduction reactor. This assumption was made for the sake of simplicity and ease of the calculation procedure for the reduction reactor behaviour estimation. This assumption necessarily maintains the condition that the reduction reactor remains fluidised at all the operating conditions. The solids hold-up is a function of the reactor dimensions, the solids density and the average solids fraction. Since the reactors' dimensions are fixed and the average solids density remains constant as

well, a consistent solids fraction in the reduction reactor results in a constant solids hold-up regardless of the operating conditions. The average solids residence time is calculated in the basis of the hold-up and the average of the solids flowrates entering and exiting the reduction reactor. In spite of the constant hold-up the residence time of solids changes because the amount of solids entering and leaving the reactor changes in accordance with the air and the fuel flowrate. But nevertheless, the reduction reactor pressure drop is a function of the reactor dimensions, acceleration due to gravity and solids hold-up, all three quantities being constant at all the points and thereby resulting in a constant pressure drop of 316 mbar under all the operating conditions.

7.2.5 Alternate Control Strategies

The off-design results for the base-case CLC-combined cycle (CLCCC) presented in this work are based on one basic off-design strategy that implies the use of VGVs for pressure balancing at the two reactors' exits and fuel-cut to match with the load requirements. As mentioned earlier, this strategy is not applicable under the conditions of part-load below 56% i.e. also at the plant start-up and shut-down. Also, this strategy is not the only strategy to be applied for controlling the power plant under study. There can be a range of diverse control strategies, which may be applied alone or in combination with one another at different load conditions.

One alternate control strategy can be a combination of variable guide vanes and air bleed off at several points down the compression path. Under the load conditions where VGVS cannot be closed down further, air bleeds can be blown off the compressor at certain points along the compression path. These bleeds are not recovered and hence the net result is the air flow reduction at the compressor discharge. The amount of air being bled off can be controlled with the help of control valves according to the air flow requirement at the compressor discharge in correspondence with the pressure requirements at the oxidation reactor outlet.

The air flowrate can also be controlled by throttling the compressed air at the compressor discharge. The air flowrate reduction by virtue of throttling downstream of the compressor may however have some limit and thus throttling in combination with air bleed-off can be an option to achieve the desired air flowrate.

While the major focus of the afore-mentioned schemes is controlling the air-side of the plant, there is certain degree of freedom to manipulate with the fuel/exhaust-side. Exhaust from the reduction reactor does not have a high flowrate and can thus be easily throttled. In this way the pressure at the CO_2-turbine inlet can be controlled.

An innovative control strategy can be to introduce VGVs at CO_2-turbine inlet. By equipping the CO_2-turbine with the variable guide vanes, the geometry of the turbine at the inlet can be changed. The VGVs can open up when required, thereby increasing the flowrate of at the air inlet and hence increasing the pressure at the turbine inlet.

A simpler CLC-combined cycle compared to the base-case CLCCC will undoubtedly pose less operational complexity and will therefore be relatively easy to operate by conventional control techniques. The off-design evaluation of a simpler CLC-power plant that does not include a CO_2-turbine is presented in the following section.

7.3 Off-design Evaluation of CLCCC-ER

Figure 7.12 presents schematics of the CLC-combined cycle with exhaust recuperation (CLCCC-ER).

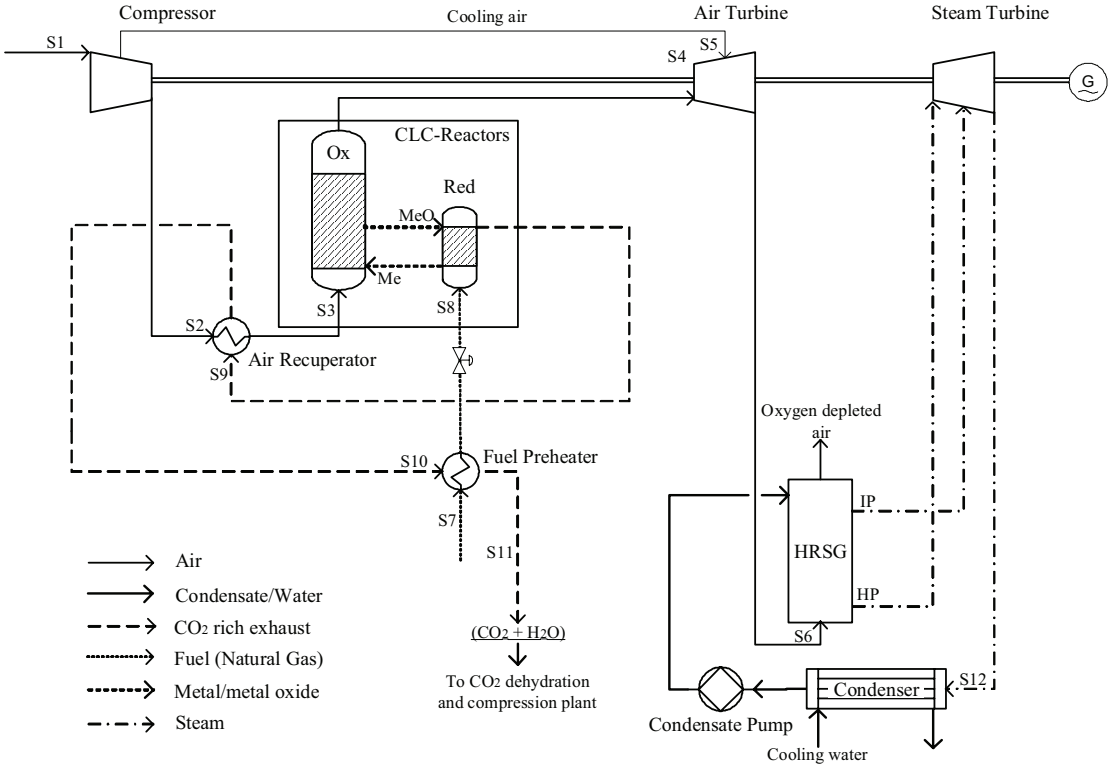

Figure 7.12 Schematic sketch of the CLC-combined cycle with exhaust recuperation CLCCC-ER)

The cycle description is not presented here, since it was given in detail in chapter 6. However, the design-point data is presented in the following section.

7.3.1 Design-point Data

Table 7-3 presents the design-point data for the CLCCC-ER.

Table 7-3 Design-point data for the CLCCC-ER

Compressor		
Compressor pressure ratio		10
Air flow at compressor inlet	kg/s	786
Coolant flow	kg/s	49.2
Oxidation Reactor (+Cyclone)		
Oxidation Temperature	°C	1200
Degree of oxidation (Xox)		1
Reactor diameter	m	21.5
Reactor height	m	20
Pressure drop	mbar	250
Solids entrainment ratio		0.1
Solids residence time	s	80
Solids flowrate at oxidation reactor exit	kg/s	616
Reduction Reactor		
Reduction Temperature	°C	980
Degree of reduction (Xred)		0.3
Reactor diameter	m	6
Reactor height	m	3
Pressure drop	mbar	474
Solids residence time	s	138
Solids flowrate at reduction reactor exit	kg/s	561
Air Preheater		
Air flow	kg/s	736
Air temperature rise	°C	94
Overall area of heat transfer	m^2	1605
overall heat transfer coefficient [U]	W/m^2K	150
Cold-end temperature difference		25
Duty	MW	73.8
Fuel Preheater		
Fuel flow	kg/s	15
Preheating temperature	°C	311
Overall area of heat transfer	m^2	681
overall heat transfer coefficient [U]	W/m^2K	150
Hot-end temperature difference		25
Duty	MW	11.5
Air Turbine		
Pressure ratio		8.97
Flowrate at turbine inlet	kg/s	730
Turbine inlet temperature	°C	1140
Turbine exit temperature	°C	617
Net work	MW	216.3
Steam Cycle		
Steam pressure (HP/IP)	bar	60/5
Steam temperature (HP/IP)	°C	592/258
Steam flow (HP/IP)	kg/s	106.6/12.3
Steam turbine net work	MW	146.7
CO_2 compression plant work	MW	6
Net plant work	MW	349.7
Net plant efficiency	%	50.2

7.3.2 The Part-load Strategy

The cycle can be looked upon as a conventional combined cycle as regards the configuration of the air turbine and compressor. The air turbine, which is the only turbine in the gas turbine cycle, drives the compressor. Therefore, at part-load the plant is operated according to the matching between the compressor and the choked air turbine. However, the presence of the oxidation reactor upstream of the air turbine is also taken into account when devising the control strategy for the plant. The oxidation reactor must satisfy the condition of transporting the desired amounts of solids to the reduction reactor in accordance with the oxygen required by the fuel whose flowrate changes in the off-design mode. Since, the compressed air at the oxidation reactor inlet is the means of solids transport; the compressor is equipped with variable guide vanes in order to control the air flowrate to achieve the required solids transport. The load reduction is achieved by adopting the constant TET strategy i.e. maintaining the same turbine exit temperature at all the load conditions. This can be achieved by simultaneous reduction in fuel flow and air flow reduction by means of VGVs to a certain degree at which the desired amount of solids are transported out of the oxidation reactor. At part-load, the air flow reduction together with the drop in the compressor pressure ratio results in a lower turbine inlet temperature and reduced turbine pressure ratio while the turbine exit temperature is constant. The net effect is reduction in the net turbine work. At the same time, in the HRSG the steam production is reduced due to the decreased air flowrate at the air turbine exit resulting in reduced steam turbine load.

7.3.3 Part-load Behaviour

The part-load behaviour of the cycle is presented only for the design-point ambient temperature in the form of relative net plant efficiency, air flow reduction and the air and fuel preheater performance. The definitions of relative net plant efficiency and relative air flowrate are the same as used for the base-case CLCCC.

Relative Net Plant Efficiency

Figure 7.13 compares the relative net plant efficiency of the studied cycle with the two conventional combined cycles as well as the previously studied CLCCC at various values of load factor. The results show that by reducing the load down to 60% the net plant efficiency drops by 2.9%- points, hence making the relative net plant efficiency drop down to about 0.94 at 60% of the full-load. The relative net plant efficiency of the CLCCC-ER at part-load decreases more rapidly in comparison with the base case CLCCC that includes the CO_2-turbine. On the other hand, the relative net plant efficiency of CLCCC-ER decreases less rapidly as compared to the selected conventional combined cycles. Since the plant is controlled according to the constant TET strategy, the fuel flowrate at part-load is higher as compared to the CLCCC, hence achieving a relatively higher TIT as compared to the base-case CLCCC, in order to maintain the constant TET, which is 621°C. Consequently, the part-load efficiency of CLCCC-ER is relatively lower. The relatively lower fuel flowrate at part-load in case of CLCCC-Er results in a more promising efficiency compared to the selected conventional combined cycles. The comparatively lower fuel flowrate at part-load is a consequence of the air flowrate reduction in order to satisfy the required solids transport. The air flowrate and fuel flowrate are linked with each other according to the stoichiometry of the reactions in the CLC-reactor system as well as the heat balance. It is therefore, of interest to present the air flowrate reduction at part-load.

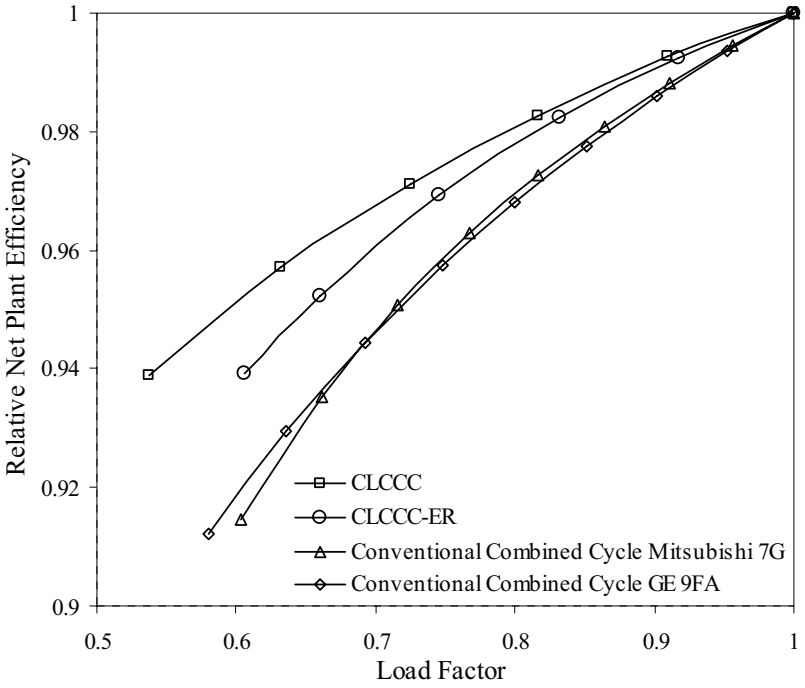

Figure 7.13 Relative net plant efficiency at varying load

Air Flow Reduction at Part-load

Figure 7.14 presents the comparison of relative air flowrate for CLCCC-ER and CLCCC.

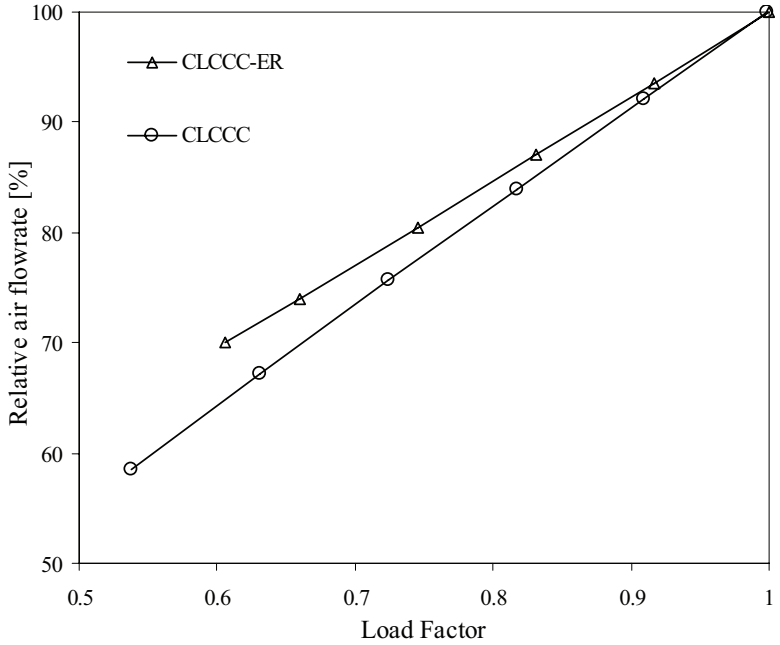

Figure 7.14 Air flow reduction as a function of load factor
[CLCCC-ER, design point ambient temperature]

It can be seen in Figure 7.14 that the air flowrate reduction at part-load in case of CLCCC-ER is less rapid as compared to the CLCCC. This is due to the absence of the CO_2-turbine in the cycle under study. Since the air flowrate is controlled solely for the purpose of achieving the desired solids transport out of the oxidation reactor; no additional air flow reduction is experienced by the cycle for balancing the pressure at the reactors' exit. The same pressure at the two reactors' exit is achieved by controlling the pressure of the fuel at the reduction reactor inlet. Considering the trend of the air flow reduction at part-load and the fact that the plant is expected to operate at high loads, it can be stated that the devised part-load strategy does not have any limitations associated with the use of VGVs.

Air- and Fuel-Preheaters Performance at Part-load

Figure 7.15 shows the relative duty of the air and fuel preheaters as a function of load factor.

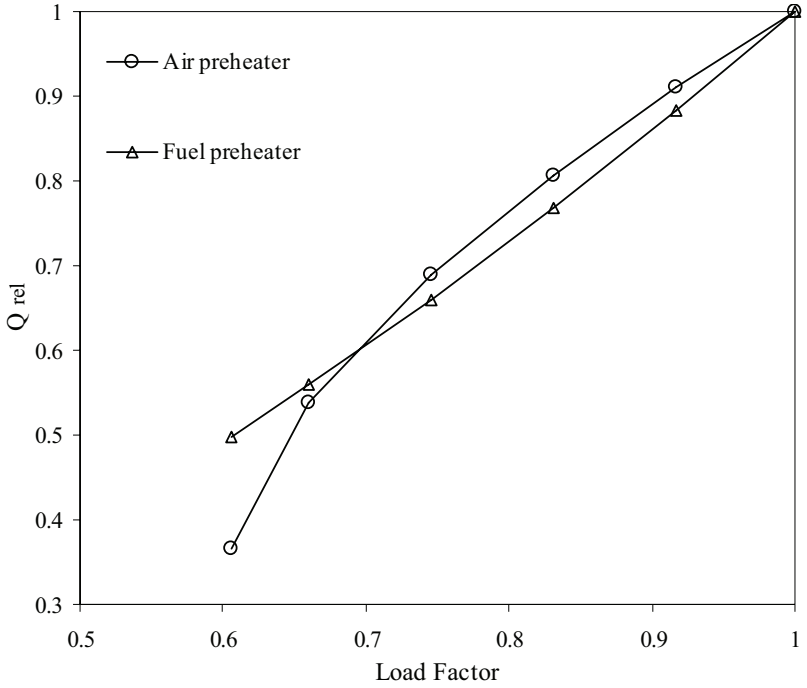

Figure 7.15 Relative duty of air and fuel preheater at load varying conditions

7.4 Remarks on the CLC-Reactors Off-design Performance

The off-design evaluation procedure of the CLC-combined cycles is based on certain assumptions of the CLC-reactor system. However, there are some features of the CLC-reactor system off-design model that can be improved. The solids internal recirculation in the oxidation reactor has been assumed to be a linear function of the relative velocity between the air and the solids. This should be determined on the basis of empirical formulations for a pressurised circulating fluidised bed system. The solids conversion rates in the oxidation and reduction reactors need to be determined on the basis of residence times of particles. The solids fraction in the fuel reactor needs also to be determined by taking into account the fuel flowrate together with residence time of particles. The reduction reactor is assumed to remain fluidised no matter what the load and eventually flow conditions may be.

This is due to the assumption of a constant overall solids fraction. This assumption can be regarded as one limitation of the off-design model presented in this work. In reality, the solids fraction will change according to the flow conditions and must be accounted for the changes and determined at different conditions. The changing solids fraction in the bubbling bed reduction reactor implies that during the part-load operation a condition may occur when the bed will tend to defluidise. This means that the reactor will start behaving like a fixed bed and there will be no more transport of solids out of the reactor. In other words, the system will collapse. This problem can be dealt with by adopting control techniques at the fuel/exhaust side of the CLC-reactor system.

7.4.1 Comparison of the Cycles' Off-design Performance

All the results presented so far can be collected to present a true picture of the part-load scenario of different cycles for the sake of comparison. Figure 7.16 presents the comparison of relative net plant efficiency for the CLC-combined cycles and the conventional combined cycles with and without CO_2 capture.

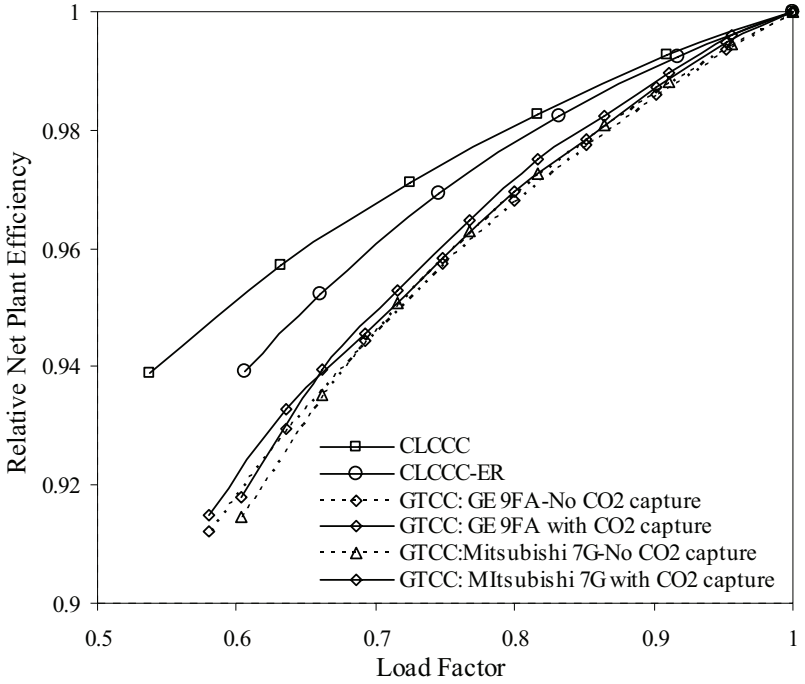

Figure 7.16 Comparison of the cycles' relative net plant efficiency at part-load [Design-point ambient temperature]

Figure 7.16 indicates that the CLC-combined cycles regardless of the cycle configuration, have a better part-load performance as compared to the conventional combined cycles with and without CO_2 capture. This is due to the nature of the CLC-combined cycles; where the air flowrate and fuel flowrate are in accordance with the solids supply thereby resulting in higher fuel-cut as compared to the conventional combined cycles. This has been discussed in detail in the previous sections. As regards the conventional combined cycles with 90% post-combustion CO_2 capture, the relative net plant efficiency is slightly lower as compared to the same cycles without CO_2 capture. This is due to the part-load inefficiencies associated with the post-combustion capture plant. But nevertheless, those efficiency penalties are not

so prominent at high part-load conditions. Although the total net energy penalty for CO_2 capture decreases with load reduction due to the reduced amounts of carbon being fed in the form of fuel; but the energy penalty per MW of net electricity production increases at part-load. This effect is very prominent at low part-load values. Since, the off-design evaluation of conventional combined cycles with post-combustion CO_2 capture is not the focus of this thesis and has been carried out for the sake of comparison with CLC-combined cycles; further discussion on this topic is not presented here.

In order to further comprehend the better part-load efficiency of the CLC-combined cycles compared to the conventional combined cycles, the changes in the heat rate at part-load can be considered. The heat rate reflects the amount of fuel being used at a certain load condition and is represented in the form of kJ/kWh of electricity produced. If a certain cycle has a higher heat rate compared to the other, it means that the cycle has a more fuel input in order to generate the same kWh of electricity compared to the other cycle. The relative net plant efficiency of a cycle can be linked to the heat rate of the cycle.

Figure 7.17 presents the comparison of the relative heat rate as a function of load factor for the CLC-combined cycles and the conventional combined cycles.

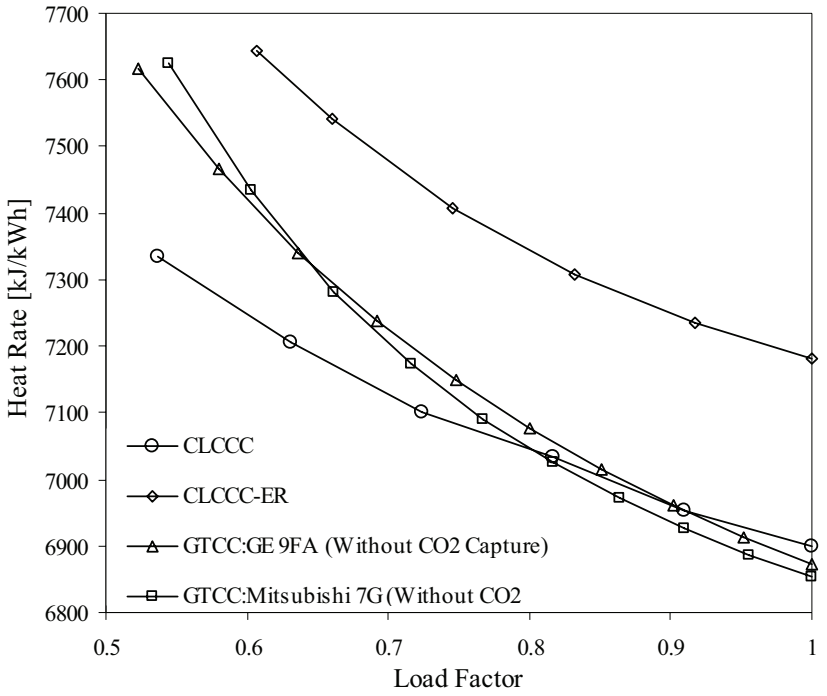

Figure 7.17 Relative heat rate at load varying conditions

It can be seen in Figure 7.17 that the relative heat rate of the conventional combined cycles is higher at part-load as compared to the CLC-combined cycles. Also, in case of the CLCCC-ER, the relative heat rate is higher compared to the CLCCC. The higher the value of relative heat rate the lower is the amount of fuel-cut at part-load. Therefore CLCCC, which has the lowest relative heat rate as shown in Figure 7.17, has the highest relative net plant efficiency, as shown previously in Figure 7.16.

The potential of power generation with CO_2 capture from a CLC-combined cycle operating at part-load is also of interest. Therefore, the absolute numbers of net plant efficiency at part-load of the CLC-combined cycles with the conventional combined cycles should be presented. Figure 7.18 presents such a comparison. Figure 7.18 clearly suggests that at part-load the CLC-combined cycles have an edge over the conventional combined cycles with post combustion CO_2 capture. Figure 7.18 shows that the efficiency drop due to the post combustion CO_2 capture does not vary to a large extent at part-load. Both the CLC-combined cycles under study have higher efficiency at part-load as compared to the conventional combined cycles with 90% CO_2 capture. The main reason behind this is that even at the full-load design-point the conventional cycles with CO_2 capture achieve a lower net plant efficiency as compared to the CLC-combined cycles.

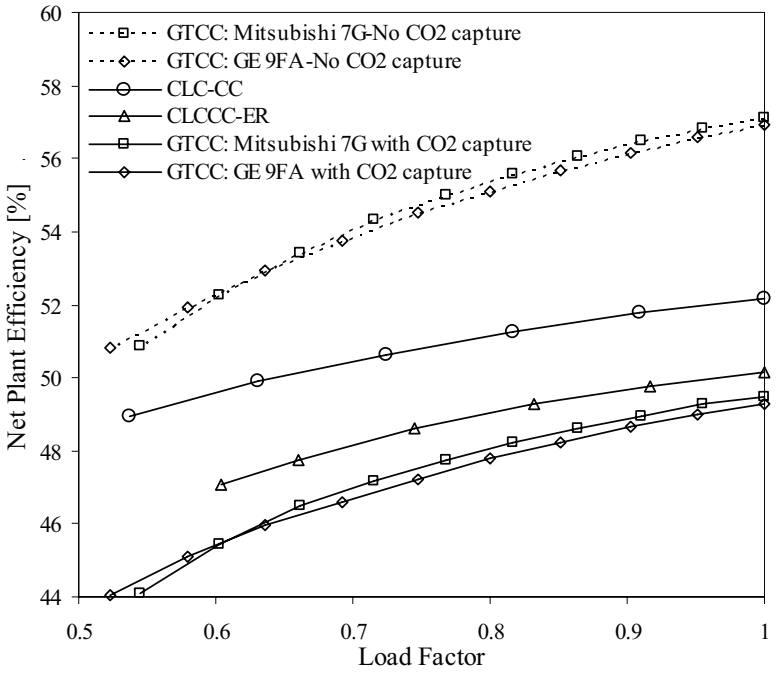

Figure 7.18 Comparison of the cycles' net plant efficiency at part-load

It was also shown previously that the relative net plant efficiency of CLC-combined cycles is higher at part-load compared to the conventional combined cycles. Therefore, the efficiency reduction at part-load is even more prominent for the conventional combined cycles with CO_2 capture as compared to the CLC-combined cycles. Although, an ideal operating condition for a power plant is the full-load condition at which it exhibits its maximum net plant efficiency. However, in real applications, a combined cycle is more likely to operate at part-load and hence the CLC-combined cycles are more attractive than the conventional combined cycles with CO_2 capture in terms of part-load efficiency.

8 CLC Application in Steam Cycles

This chapter presents CLC application in steam cycles. In a CLC-steam cycle, atmospheric CLC-reactors are based on the conventional circulating fluidised bed technology and steam is assumed to be generated inside the oxidation reactor. The chapter presents two natural gas-fired CLC-steam cycle configurations; single reheat cycle and double reheat cycle. The cycle operating parameters have been selected based on the sensitivity analysis of non-adiabatic reactors presented in chapter 5. Power and energy balance at the design point is presented for both the cycles. Challenges in implementing conventional steam power plants technology in CLC-steam cycles are also comprehensively discussed.

8.1 Scope of Cycles' Studies

This chapter addresses implementation of Chemical Looping Combustion in a Rankine cycle. The CLC application in combined cycles was discussed previously in chapter 6. Also, the temperature limitations of CLC in combined cycles were discussed. In a combined cycle, a reasonable thermodynamic efficiency is achieved at high turbine inlet temperatures and pressures. Therefore, when applied in a combined cycle, the CLC-reactors will have to be operated at high temperatures and pressures that will affect not only the performance of the solid particles but the reactors as well. Since, the pressurised CLC-reactors involve complex control strategies and the solids have their own limitations to temperatures and pressure; it is of interest to investigate other power cycles with which a reasonable thermodynamic efficiency may be achieved at relatively lower oxidation temperatures and pressures. One concept of interest is natural gas-fired CLC-steam cycle where the CLC-reactors operate on atmospheric pressure with the oxidation reactor being the steam generator. The oxidation temperature in such cycles can be fixed at one appropriate safe value and the present work is based on an oxidation temperature of 850°C.

Traditionally, natural gas is used in combined cycle power plants which are the most efficient, while steam power plants are generally coal-fired. However, there are examples of natural gas fired steam power plants with the major objective of achieving a fair energy-mix by utilising diversity of fuels (including biomass); thereby providing energy security as well as the economic benefit of using alternate fuels during the seasons when natural gas prices are high. These objectives however, do not play a significant role in the concept of a natural gas fired CLC-steam cycle. The foremost objective of this work is to evaluate a CLC-power plant with CO_2 capture, achieving a reasonable thermodynamic efficiency at low reactors temperatures and atmospheric pressure. The difficulties and complexities associated with pressurised fluidised bed (PFB) reactors, which are inevitable to be employed in case of pressurised CLC-reactors in a combined cycle, make the atmospheric reactors a practical and reasonable choice at the current developmental stage of CLC-technology. In the CLC-steam cycle non-adiabatic/atmospheric reactors are applied which can be based on the classical circulating fluidised bed (CFB) reactors technology; this is a well-established and proven concept and is being extensively used in the industry. In a CLC-steam cycle, the oxidation reactor is the main source of steam production. This reactor is essentially a pneumatic transport type reactor and its interior ideally maintains an atmosphere of well-mixed solids and hot air. Such an atmosphere provides excellent conditions under which heat can be transferred from the reactor interior to the water flowing inside the tubes of heat

exchangers placed in the walls of the reactor. In this way, the oxidation reactor can replace boiler in a conventional steam cycle.

The work presented in this chapter evaluates two ultra-supercritical CLC-steam cycle configurations; single reheat and double reheat cycle. A steam cycle is commonly considered ultra-supercritical if it operates at supercritical pressure above 250 bar and temperature above 600°C. The major focus of the work presented in the following sections is to achieve the most reasonable cycle configurations with maximum possible heat integration. The cycles' sensitivity study is not presented in the results section, because the sensitivity study of non-adiabatic reactors has already been presented in chapter 5; and the cycle is configured in accordance with the findings of that study. However, the results for individual components and sub-systems of the single reheat cycle are presented. The double reheat cycle is studied solely for the purpose of estimating the efficiency improvement by introducing double reheat. The results for double reheat cycle contain mainly the efficiency and power balance. The challenges associated with tailoring CLC-steam cycles to state-of-the-art technology are briefly discussed at the end of the chapter.

8.2 Single Reheat CLC-Steam Cycle (SRCLC-SC)

Figure 8.1 shows schematics of the ultra-supercritical single reheat CLC-Steam cycle.

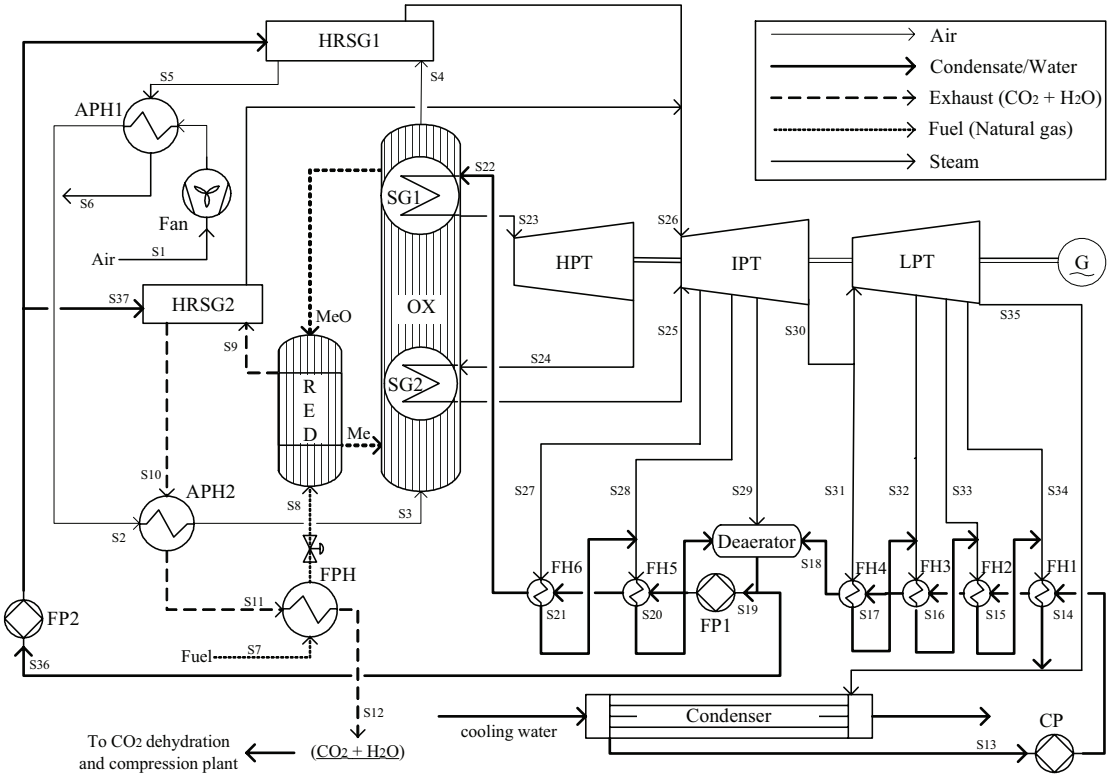

Figure 8.1 Schematics of the ultra-supercritical single reheat CLC-steam cycle

The cycle can be looked upon as consisting of two sub-systems; the CLC system and the steam/water system where the heat generated in the former is given off to the later. As far as the steam/water system is concerned, it is the same as in a conventional supercritical steam cycle. The unique feature of the proposed cycle is the availability of the hot oxygen depleted

air and the CO_2-rich exhaust that provide additional heat in addition to that available in the oxidation reactor. Atmospheric air is drawn into the cycle at the inlet of the oxidation reactor. A booster fan can be employed in order to overcome the pressure drop in the oxidation reactor. The air flow rate and oxidation temperature selection is based on the sensitivity analysis of the non-adiabatic reactors presented in chapter 5. The study suggested that the lower the air flowrate the more is the heat given off to steam production. Therefore, a minimum possible air flowrate is selected. The reaction of the air with the solid particles is a continuous cyclic process and at a given air flowrate any selected oxidation temperature can be maintained thanks to the large heat carrying capacity of the solid particles. The large heat flow inside the air reactor is balanced by taking away a major portion of heat in two steam generators. SG1 is the supercritical steam generator that also serves as the primary steam source, while SG2 is the reheater.

The air and the fuel preheaters are significant components providing heat integration to a maximum possible level in the cycle. The air preheating influences the heat balance around the air reactor leading to a better efficiency as compared to no air preheating. The higher the air temperature at the air reactor inlet, the higher is the heat given off to the steam generators thereby resulting in a higher steam flow and eventually a higher net plant work and efficiency. However, there are limitations to the air temperature prior to its entry into the air reactor. The two air preheaters can be designated as the low-temperature preheater (APH1) that utilises the oxygen-depleted air available at the exit of HRSG1 as the hot fluid, and the high-temperature preheater (APH2) that utilises the CO_2-rich exhaust available at the exit of HRSG2 as the hot fluid. APH1 has a larger duty as compared to the preheater APH2. That is because the former has a larger flow of the hot fluid, which is the oxygen depleted air, as compared to APH2 hot fluid flowrate that is the CO_2-rich exhaust. APH2 heats the air up to the final air temperature prior to its entry into the oxidation reactor. The hot fluids in both the air preheaters, due to their compositions, temperatures and pressure, leave no risk of condensation occurring at the design point. The high temperature preheater employs pure air, except for the decreased concentration of oxygen, while the low temperature preheater employs CO_2/vapour mixture at the atmospheric pressure. Therefore, it may result in condensation at the cold end of the preheater, if the fluid approaches the saturation dew point. This can be avoided by selecting appropriate temperature levels so that there is no risk of any condensation in the preheaters, at the design point. The exhaust stream at the high temperature air preheater (APH2) exit is further utilised in the fuel preheater to heat the natural gas prior to its admission into the reduction reactor. In this preheater, due to an appreciably larger flowrate of the hot fluid as compared to the fuel, the hot fluid does not undergo a large temperature drop and leaves no risk for condensation, pertaining to the proper temperature selection in the preceding high temperature air preheater (APH2).

The preheated air and fuel react with their respective solid streams in the oxidation and reduction reactor of CLC thereby making two hot streams available at high temperature; oxygen depleted air and CO_2-rich exhaust. The major portion of heat generated in the oxidation reactor goes to steam production in the internal steam generators; the ultra-supercritical steam generator (SG1) and the reheater (SG2). The supercritical steam generator is very similar to a conventional steam generator except for in thermodynamic terms that there is no saturation point reached and no evaporation occurs. However, the steam generator can be divided in three sections for the sake of heat transfer and thermodynamic loss minimisation. In the present work, the pressure losses for SG1 are included for the three heat exchanger sections. The ultra-supercritical steam from SG1 available at 280 bar and 600°C is admitted to the HP turbine and expands down to

somewhat above the IP turbine inlet temperature (considering the pressure drop in steam lines and SG2) that is the reheat pressure. The choice of an appropriate reheat pressure is significant for two reasons; optimum maximum possible efficiency, and steam quality at the exit of LP turbine. The higher the reheat pressure, the lower is the steam quality at the LP exit, which must be above approximately 0.87. The 60 bar reheat pressure is common in supercritical steam power plants with single reheat. A higher reheat pressure may result in a small increase in efficiency at the cost of additional material requirements. Besides that the steam quality has to be considered. At 60 bar, the steam quality at LP turbine exit is just above 0.87 and hence leaving no risk for droplets formation on the turbine blades that can result in corrosion and erosion of the turbine blades. The reheater (SG2) heats the steam up to 620°C at 60 bar. The steam entering in the reheater is already in a superheated condition and therefore the reheater just increases the degree of superheat. The reheater can therefore be treated as a superheater. Additional steam is raised in heat recovery steam generators (HRSG1 and HRSG2). The oxygen-depleted air at the oxidation reactor exit is led to the HRSG1 to generate steam at 620°C. In case, the air temperature (oxidation temperature) is substantially higher than the steam temperature, there will be an undesired exergy loss due to a large hot end temperature difference in the HRSG1. However, under such condition, this loss is inevitable if the current cycle configuration is applied. The high temperature oxygen-depleted air could also be used to preheat air or fuel, but the hot end temperature differences would be even higher in that case owing to the heat transfer area and temperature limitations in the heat exchangers. Therefore, the current configuration can be regarded as suitable despite the undesirably higher exergy destruction in HRSG1, in the case of high oxidation temperatures. The CO_2-rich exhaust at the reduction reactor exit is led to the HRSG2 where it generates superheated steam. Both the HRSGs operate at one pressure level corresponding to the IP turbine inlet pressure; and are fed with the preheated feedwater available after the deaerator. Due to the admission of preheated feedwater at the economisers of the two HRSGs, the hot streams leaving the HRSGs still contain enough heat to preheat air in APH1 and APH2 and thus the degree of heat integration in the cycle is also improved leading to a better efficiency. Without feedwater preheating, the hot fluids at the exit of the HRSGs will not be available at sufficiently high temperatures and there will be no more room left for heat integration. Both the heat recovery steam generators can be looked upon as a conventional HRSG employed in combined cycles. In HRSG1 and HRSG2, the hot fluids are available at slightly above atmospheric pressure (considering the pressure drop across the HRSGs) and leave the HRSGs at atmospheric pressure and temperatures comparable to those in a conventional combined cycle HRSG. The pressure level in HRSG1 and HRSG2 matches the inlet pressure of the IP steam turbine and the streams are mixed with the steam available from the reheater (SG2). The total steam i.e. reheated steam from SG2, superheated steam from HRSG1 and HRSG2 is then admitted to the IP steam turbine and it expands down to the pressure of the LPT where it finally expands down to the condenser pressure. There are steam extractions from IPT and LPT for feedwater preheating.

The condensate pump (CP) pumps the condensate to the deaerator pressure and it flows through a series of feedwater preheaters. There are 5 low pressure condensate preheaters (FW1 through deaerator) and 2 high pressure feedwater preheaters (FH5 and FH6). All the heaters are closed preheaters except the deaerator which is a direct contact low pressure preheater and also serves as the storage tank for the hot water supplied to the steam generators via the feed pump. The last condensate preheater (FH4) and the first three preheaters (FH1 to FH3) are supplied with the steam tapped off at the IP turbine exit and from the LP turbine, respectively. The deaerator and the two high pressure feedwater

preheaters are supplied with the steam tapped off from the IP steam turbine. Since one of the objectives of this work is tailoring the CLC technology towards state-of-the-art technology, therefore the steam extraction pressures are chosen to be similar as commonly used in supercritical steam power plants. All the preheaters (except for FH1) are equipped with desuperheater. In order to minimise the thermodynamic losses due to large cold end temperature differences, FH4, FH5 and FH6 are equipped with subcooler as well. Feedwater is split up into two streams at the deaerator outlet; a smaller portion of feedwater is fed to the two HRSGs while the major portion goes to the oxidation reactor. The HRSGs are fed by the light duty feedwater delivery pump (FP2). The larger flow of feedwater is pumped up to the oxidation reactor via the delivery pump FP1. The feedwater passes through FP5 and FP6 and heated up to the final preheating temperature of 265°C prior to its entry into the SG1 in the oxidation reactor.

8.2.1 Assumptions

It is important to discuss the computational assumptions before the cycles are presented. The main set of assumptions is included in Appendix A. However, some of the CLC-specific assumptions used throughout the simulations are given here. The CLC-reactors are assumed to be adiabatic with isothermal and homogenous mixing of solids with gases. The simulations are based on idealised behaviour of solid particles circulating between the two reactors. The pressure drop in each reactor is assumed to be 5% of the incoming stream pressure. The present work uses NiO supported on $NiAl_2O_4$ (60% NiO by mass) as oxygen carrier with natural gas as fuel. The theoretical thermodynamic limit of NiO to convert fuel is 99.5% [Lyngfelt et al., 2004]. However, 100% fuel conversion was assumed for the present work. Degree of oxidation is assumed 100 % (Xox=1.0) which means that all Ni entering the air reactor undergoes a complete oxidation. Degree of reduction in the fuel reactor is assumed 70% (Xred=0.3) which means that 70% of NiO entering the fuel reactor is converted into Ni. All the results are based on the assumption of complete stoichiometric conversion of fuel, for instance 1 mole of methane reacts with 2 moles of oxygen to form 1 mole of CO_2 and 2 moles of H_2O and the same holds for other components of natural gas. Definitions of all the parameters are in accordance with chapter 4.

8.2.2 Cycle Study Results

The results are presented in the form of overall energy and power balance for the cycle. As far as the individual components and sub-systems of the cycle are concerned, which mainly consist of the air and fuel preheaters and heat recovery steam generators; the results related to those are of no significant interest during the procedure of efficiency assessment of the cycle. These components are standard heat exchangers which are specified as per the hot-end or the cold-end temperature difference. However, the feedwater preheating system can be of interest in the context of this particular cycle, as it affects the performance of the steam cycle and contributes to the overall efficiency improvement. In the following, feedwater preheating system will be discussed, followed by the plant energy and power balance.

Feedwater System

Figure 8.2 presents the temperature profile of the feedwater along the feedwater heaters. The temperature profile of the feedwater is independent of the gases temperatures and flow rates in the CLC-system.

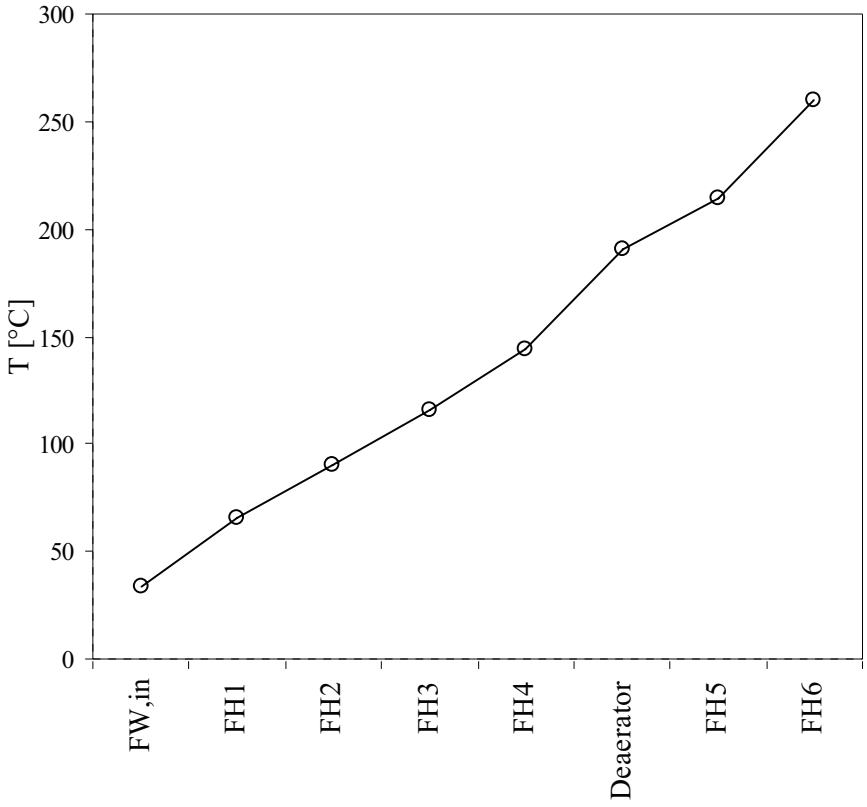

Figure 8.2 Feedwater temperature profile along the feed heaters

It can be seen in Figure 8.2 that the maximum heat given off to the feedwater occurs in the deaerator while final feedwater preheater (FH6) has the largest duty. This is reflected in the form of temperature rise in FH6 in order to achieve the final preheating temperature of 265°C. Both the FH5 and FH6 have larger duties as compared to the condensate preheaters. FH1 has a larger duty as compared to FH2 and FH3 as it has to heat up the condensate from the condenser temperature up to a temperature approaching the steam condensation temperature at 0.3 bar. At the same time, FH4 has a larger duty as compared to FH2 and FH3, since it has to heat up the condensate to the saturation temperature at the deaerator pressure, while maintaining the terminal temperature difference.

Power and Energy Balance

Table 8-1 presents the efficiency and power balance for the single reheat CLC-steam cycle at the deign point.

Table 8-1 Power and energy balance for the single reheat CLC-steam cycle (SRCLC-SC) [Oxidation Temperature=850°C]

Fuel flow	kg/s	15	Share of LHV
Fuel LHV	MW	697.5	100.0 %
High pressure turbine (HPT) work	MW	68.2	9.8 %
Intermediate pressure turbine (IPT) work	MW	150.6	21.6 %
Low pressure turbine (LPT) work	MW	116.5	16.7 %
Condensate Pump (CP) work	MW	-0.4	-0.1 %
Feedwater Delivery Pump 1 (FP1) work	MW	-8.9	-1.3 %
Feedwater Delivery Pump 2 (FP2) work	MW	-0.5	-0.1 %
Turbomachinery shaft power	MW	325.5	46.7 %
Turbomachinery mechanical loss	MW	-1.3	-0.2 %
Turbomachinery generator loss	MW	-4.9	-0.7 %
Turbomachinery generator terminal output	**MW**	**319.3**	45.8 %
Cooling Water Pump work	MW	-1.5	-0.2 %
Plant auxiliary power	MW	-4.8	-0.7 %
Work CO2 compression	MW	-13.9	-2.0 %
Net Plant power output	**MW**	**299.1**	**42.9 %**
CO_2 generation (>99% capture)	**kg/MJel**	**0.133**	

The stream data for the cycle at the design point is included in Appendix B.

The cycle has a net plant efficiency of 42.9% including CO_2 capture. This efficiency can be considered as very promising and comparable to a conventional natural gas fired steam cycle without CO_2 capture, achieving an efficiency of approximately 47%.

Note: *Paper I also presents results for a CLC-steam cycle but with a different fuel composition and different computational assumptions especially those related to the CO_2 dehydration and compression plant. Also the plant configuration is different from those presented here. Moreover, the paper presented the CLC-steam cycle concept for the first time and is a typical 'proof of concept' study and therefore its result do not necessarily reflect the potential of a CLC-steam as presented in this chapter.*

8.3 Double Reheat CLC-Steam Cycle (DRCLC-SC)

Figure 8.3 shows schematics of the ultra-supercritical double reheat CLC-Steam cycle. The cycle is not very different from the single reheat CLC-steam cycle (SRCLC-SC) except for some features. Since the double reheat is required, the portion of the heat generated in the oxidation reactor that is given off for steam generation is distributed amongst the three steam generators namely; SG1 (the supercritical steam generator), SG2 (the first reheater) and SG3 (the second reheater). The selection of air flowrate and the oxidation temperature is based on the sensitivity study of the non-adiabatic CLC-reactors previously presented in chapter 5. Due to the additional reheat as compared to the single reheat cycle, an additional

intermediate pressure steam turbine (IPT2) is employed. The feedwater preheating system consists of the same number of preheaters as in SRCLC-SC but with different steam extraction pressure levels. The final feedwater preheating temperature is 295°C. The final feedwater heater (FW6) is fed with the steam tapped off from the steam line at the exit of the high pressure turbine (HPT) by splitting up the exhaust in two streams, where the larger steam fraction is fed to the first reheater (SG2).

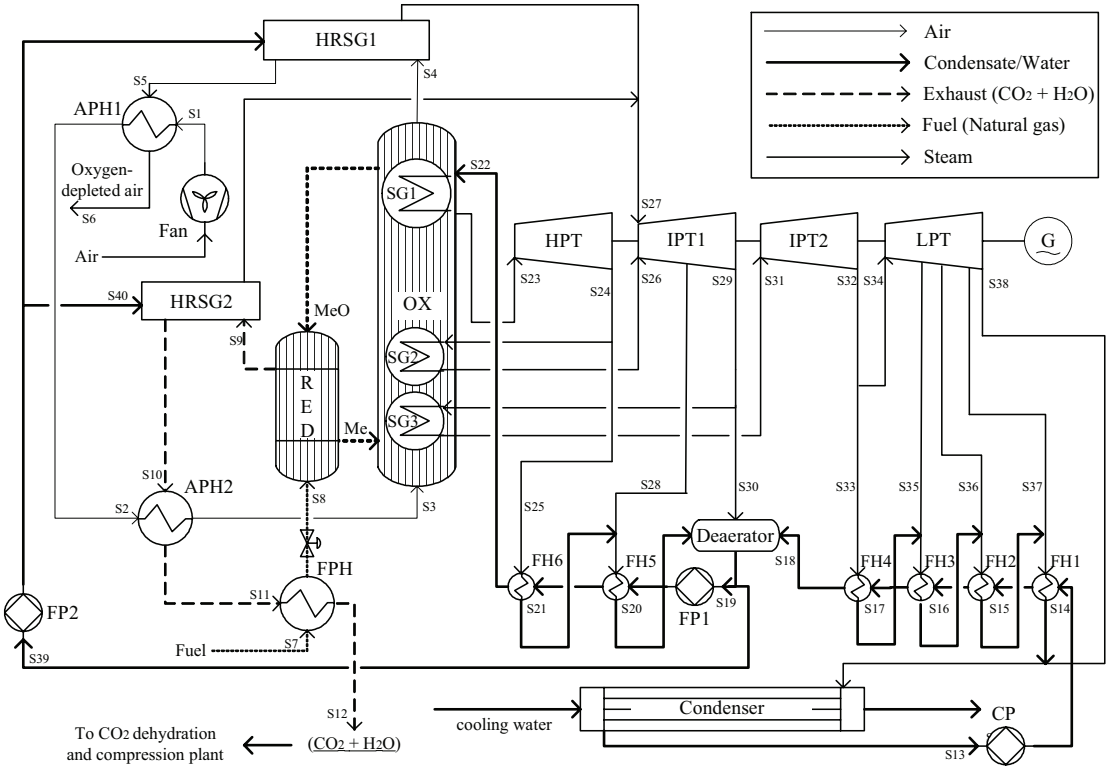

Figure 8.3 Schematics of the ultra-supercritical double reheat CLC-steam cycle

The first intermediate pressure turbine (IPT1) is equipped with one extraction point while its exhaust is split up into two streams; the smaller fraction feeding the deaerator while the larger fraction is led to the second reheater (SG3). The second intermediate pressure turbine (IPT2) has no steam extractions along its expansion path but its exhaust is split up into two streams where the smaller fraction feeds the last condensate preheater (FH4) while the larger fraction is admitted to the low pressure steam turbine (LPT). The low pressure turbine has essentially the same features as that in the SRCLC-SG except that the steam pressure at its inlet is relatively higher due to the double reheat as compared to that in the single reheat. The steam extraction pressures along the expansion path of LPT are the same as those in the single reheat cycle. The CLC-system and its corresponding heat recovery steam generators (HRSG1 and HRSG2) as well as the air and fuel preheater are configured in the same way as those in the SRCLC-SG. The air flowrate and the oxidation temperature are selected in the light of the sensitivity study of SRCLC-SG presented in the previous section, as the steam cycle is solely dependent on the heat generation in the CLC-system and affects the current cycle in the same way as it affects the single reheat cycle.

8.3.1 Cycle Study Results

The sensitivity study of the single reheat steam cycle (SRCLC-SG) is the indicator of the significant parameters in a CLC-steam cycle regardless of the number of reheats. Therefore, as stated previously, sensitivity study of the double reheat cycle is not presented in this chapter. But the cycle work and efficiency is presented at the selected air flowrate and oxidation temperature, which are the same as those in the single reheat cycle.

Power and Energy Balance

Table 8-2 presents the efficiency and power balance for the single reheat CLC-steam cycle at the deign point.

Table 8-2 Efficiency and power balance for double reheat CLC-steam cycle
[Oxidation Temperature=850°C]

Fuel flow	kg/s	15	Share of LHV
Fuel LHV	MW	697.5	100.0 %
High pressure turbine (HPT) work	MW	53.5	7.7 %
First intermediate pressure turbine (IPT1) work	MW	79.9	11.5 %
Second intermediate pressure turbine (IPT2) work	MW	86.2	12.4 %
Low pressure turbine (LPT) work	MW	123.5	17.7 %
Condensate Pump (CP) work	MW	-0.6	-0.1 %
Feedwater Delivery Pump 1 (FP1) work	MW	-8.2	-1.2 %
Feedwater Delivery Pump 2 (FP2) work	MW	-0.7	-0.1 %
Turbomachinery shaft power	MW	333.6	47.8 %
Turbomachinery mechanical loss	MW	-1.3	-0.2 %
Turbomachinery generator loss	MW	-5.0	-0.7 %
Turbomachinery generator terminal output	**MW**	**327.3**	46.9 %
Cooling Water Pump work	MW	-1.5	-0.2 %
Plant auxiliary power	MW	-4.9	-0.7 %
Work CO2 compression	MW	-13.9	-2.0 %
Net Plant power output	**MW**	**306.9**	**44.0 %**
CO_2 generation (>99% capture)	**kg/MJel**	**0.129**	

The stream data for the cycle at the design point is included in Appendix B.

The efficiency improvement by introducing an additional reheat is 1.1% and the double reheat cycle can achieve a net plant efficiency of 44% with 100% CO_2 capture. The cycle exhibits very promising potential of power generation with CO_2 capture, nevertheless the trade-off between efficiency and cost is a matter of concern because additional reheat necessarily implies extra cost. But such a trade-off is not presented in this work.

8.4 Comparison of Cycles

The steam cycles presented in this chapter do not represent the cycles on which the mainstream traditional steam power plants are operated. One feature of distinction is the fuel which is natural gas in the cycles presented int his work. Therefore, it is a reasonable approach to compare these natural gas fired steam cycles with the natural gas fired combined cycles. Figure 8.4 compares the CLC-steam cycles with the CLC-combined cycle concepts as well as the reference conventional combined cycle with and without CO_2 capture. The results for the CLC-combined cycles and the reference cycle are taken from chapter 6. The term TIT used in Figure 8.4 corresponds to the combustor exit temperature in case of the reference cycle, while it means the oxidation temperature in case of the CLC-combined cycles and CLC-steam cycles.

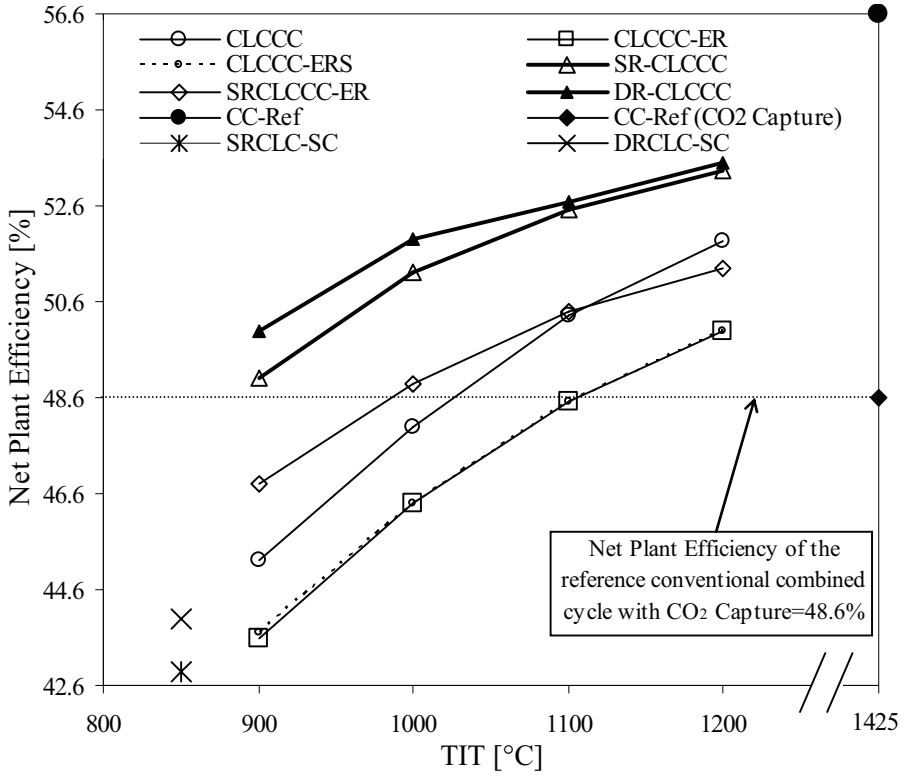

Figure 8.4 An efficiency overview of CLC-steam and combined cycles compared to the reference conventional combined cycle

It can be seen in the figure that quite contrary to their competitor cycles, the CLC-steam cycles exhibit higher efficiencies at the lower supply temperatures i.e. oxidation temperature in the CLC. This feature makes them quite unique as well as attractive in terms of material requirements and the solid particles performance in CLC. The temperature of 650°C can be regarded as safe temperature and there is no risk of sintering and agglomeration of solid particles in CLC-reactors.

The selection of number of reheats is a matter of cost as stated previously, but nevertheless whether single reheat or double reheat, both CLC-steam cycles are competitive even with the combined cycles in terms of efficiency. If the conventional combined cycle with CO_2

capture is operated on part load it will have even lower net plant efficiency which is 48.6% at full-load design point. On the other hand, the CLC-steam cycles, like many other conventional steam cycles are recommended to be operated as base-load plants and will have an edge over the conventional combined cycles with CO_2 capture unless they are also operated on base-load. However, the CLC-combined cycles are also recommended to operate as the base-load plants, mainly due to the slow transient response of the CLC-reactors, and therefore the natural gas-fired CLC-steam cycles do not have any advantage over the CLC-combined cycles in terms of efficiency. However, the CLC-steam cycles presented in this work can be an attractive solution in the short term, considering the temperature limitations concerned with the solid particles in CLC.

8.5 Challenges in applying conventional technology in CLC-SC

A CLC-steam cycle has advantage over CLC-combined cycle that there is no sensitive turbomachinery like a gas turbine involved that is sensitive to particulate matter, i.e. fine particles escaping from the cyclone separation system of the CLC-reactors. The feedwater/steam system is state-of-the-art technology and the assumptions for the work presented in this chapter have been based on the real data available for steam power plants. A CLC-steam power plant concept is attractive in the sense that steam flowrates and the steam extraction pressure levels can be selected in such a way that they match with those of the steam power plants machinery that is available off the shelf. Therefore, there should be no concerns regarding tailoring of steam turbines used in such a cycle to the state-of-the-art turbines used in modern steam power plants.

The CLC-reactors, and of course the oxygen carrier particles, are the only components that pose quite a few hindrances regarding successful realisation of CLC in steam cycles. However, one major advantage of atmospheric reactors over the pressurised reactors as those that may be used in CLC-combined cycles, is that pressure balancing of the two reactors exit is not a very complicated procedure here. Also the particulate matter can be easily recovered. The atmospheric CFB reactors have been in operation for decades and the only challenge is the operation and behaviour of the oxygen carrier particles in CFB reactor system. The CLC-novelty requires the reactors to be custom-made.

The air and fuel preheaters operate at rather low temperatures and can be easily manufactured. The only concern is the hot fluid composition in the heat exchangers that use CO_2/H_2O mixture as the hot fluid. One choice of the air preheater type can be the regenerative Ljungström air preheater. The Ljungström type heat exchangers used in coal fired power plants to preheat the air prior to its entry into the boiler. The same type of heat exchangers can be applied for the preheaters used in a CLC-steam power plant. The steam generators are vital components in the cycle that need to be built inside the walls of the oxidation reactor. But again this is based on the same technology as boilers. However, the reactor system design and manufacturing would require a start-from-scratch procedure in order to adapt the CFB technology according to the CLC-specific requirements. The heat recovery steam generators can be looked upon as the conventional HRSG used in combined cycle. However, the optimisation of these components, which is not presented in this work, must be carried out to find out the most optimum HRSG designs.

Although a CLC-steam cycle cannot be considered the ‘ultimate solution’ to the CO_2 problem; it is rational to regard it as the ‘bridging technology’ for power generation with CO_2 capture in a short term perspective until the CLC-reactors and the oxygen carriers have

been evaluated for high temperatures and pressures. Like most of the steam power plants a CLC-steam power plant can also be operated as a base-load power plant. No matter how efficient a natural gas fired CLC-steam cycle is, it will always be regarded as a short-term alternative for power generation with CO_2 capture; simply because of the argument that natural gas must be used for more efficient power plants i.e. combined cycle. At the same time, the modern highly efficient coal fired steam power plants are the major competitors for a CLC-steam power plant. One step forward towards successful realisation of CLC in steam cycles would be to analyse a coal fired CLC-steam cycle where the oxygen carrier particles are mixed with pulverised coal. Such a plant can be a ground breaking technology in a long-term perspective, since coal is predicted to attain a major share in world's primary energy sources in the future. However, reactivity of solid oxides with coal and examination of solids circulation in a pulverised-coal CFB reactor system still remains an issue of detailed experimental analysis.

9 Conclusions and Recommendations

In the preceding chapters, results for the CLC-reactor system and oxygen carriers, CLC-combined cycles and CLC-steam cycles have been presented. This chapter summarises the results and the achieved objectives of this thesis. Based on the findings of this work, recommendations for the future work are also made.

9.1 Conclusions

9.1.1 Oxygen Carrier and Reactor System

Oxygen Carriers

Ni-, Fe-, and Cu-based oxygen carriers have been analysed in this work. The Fe-based oxygen carrier results in significantly large amounts of solids flow in the reactor system, while Cu-based oxygen carriers can't stand high temperatures that are likely to occur in CLC-power cycles. Based on the experimental work found in the literature and the outcome of the analysis carried out in this work, it is suggested that NiO supported on $NiAl_2O_4$ is the most suitable oxygen carrier for realising a conceivable CLC-reactor system. In order to achieve a conceivable reactor system, the solids flowrates should be as low as possible. Low solid flowrates can be achieved by providing high degrees of conversion in the two reactors. The oxygen carrier ought to be able to withstand high temperatures and pressures. In order to be successfully applicable in CLC-combined cycle, the oxygen carrier must be able to sustain a temperature of at least 1000°C. For a given fuel flow, the oxidation temperature and air inlet temperature are the two parameters that strongly influence the air to fuel ratio through the reactor system. The higher the oxidation temperature, the lower is the air to fuel ratio. On the other hand, the higher the air inlet temperature to the oxidation reactor, the higher is the air to fuel ratio. The solids temperature in the two reactors is interdependent as well as dependent on the degree of reduction. In case of the endothermic reduction of Ni-based oxygen carriers, the solids temperature at the reduction reactor exit increases with decrease in degree of reduction of solids in the reduction reactor and vice-versa.

CLC-Reactor System

Various CLC-power cycles were evaluated with the assumption of CLC being applied in the conventional circulating fluidised bed reactors. In the CLC-combined cycles, a pressurised circulating fluidised bed reactor system is applied; while for the steam cycles it is atmospheric circulating fluidised bed technology. The oxidation reactor is essentially a pneumatic transport reactor while the reduction reactor is a bubbling fluidised bed reactor.

Based on the results for the combined cycles, it is concluded that the pressurised CLC-reactor system should be able to sustain pressures in the range of 10 bar to 26 bar, depending on the nature of the combined cycle configuration. In addition, there should be no pressure difference occurring between the two reactors' exits in order to avoid any gas leakages between the two reactors. The reactor system should also be designed in such a way that the desired amounts of oxygen carrier are transported between the two reactors at different operating conditions, to fulfil the oxygen requirements depending on fuel flow.

In case of the atmospheric CLC-reactors, the reactor system should be designed to withstand a minimum temperature of 850°C, which is a safe temperature regarding the limitations associated with oxygen carriers. Also, the oxidation reactor layout should be flexible in such a way that steam generators can be accommodated at its interior without causing any obstruction to the upwards solids flow.

9.1.2 CLC-Combined Cycles

Cycle Design

A number of natural gas-fired CLC-combined cycle configurations have been analysed and the results show that CLC-combined cycles have potential of producing electricity with relatively high efficiency and CO_2 capture. The single CLC-reactor system combined cycles in different configurations can achieve a net plant efficiency of more than 50% at the oxidation temperature of 1200°C. The comparable efficiency of a conventional combined cycle with CO_2 capture from the exhaust using absorption by amines is 48.6%. The efficiency can be further improved by applying multi-reactor CLC so that reheat is introduced to the air turbine of the combined cycle. With reheat cycles a net plant efficiency of about 50% can be achieved at the oxidation temperatures below 1000°C. At the oxidation temperature of 1200°C, the reheat cycles, which also include a CO_2 turbine, can achieve net plant efficiency higher than 53%. A single reheat cycle without CO_2 turbine can achieve net plant efficiency higher than 51% at an oxidation temperature of 1200°C. It was found that single reheat results in substantial efficiency improvement and double reheat results in incremental efficiency improvement. Since these net plant efficiencies include the energy penalty for very close to 100% CO_2 capture; it can be stated that the CLC-combined cycle is promising for highly efficient power generation with CO_2 capture, compared to the competing technologies for CO_2-capture from power plants.

Off-design Performance

The off-design evaluation has been performed for two CLC-combined cycle configurations; a CLC-combined cycle including a CO_2-turbine and the other without the CO_2-turbine. In CLC-combined cycles, the two major objectives to be met at all the operating conditions are: (1) maintaining equal pressure at the two reactors' exit to avoid gas leakages and (2) to maintain solids transport between the two reactors. The cycles including the CO_2-turbine pose operational complexities and demand for highly sophisticated control strategies. Even the cycles without the CO_2-turbine demand for a combination of control strategies. One viable strategy can be to employ a compressor with variable guide vanes to control the air flow for maintaining the pressure at the reactors' exit. The plant start-up and shut-down may however need a combination of different control techniques. The CLC-combined cycles have better relative net plant efficiency at part-load as compared to the conventional combined cycles with and without CO_2 capture. Also, the CLC-combined cycles have higher efficiency at part-load as compared to conventional combined cycles with CO_2 capture. The reactor system off-design behaviour analysis shows that the solids internal recirculation in the oxidation reactor increases at part-load resulting in increased residence time of particles and increased pressure drop. The solids residence time also increases the reduction reactor at part-load. Although the CLC-combined cycles, due to the presence of the unconventional reactor system, demand for advanced control strategies; but nevertheless part-load performance of the cycles is very promising.

9.1.3 CLC-Steam Cycles

The natural gas-fired CLC-steam cycles can prove to be efficient power plants with CO_2 capture in the short-term perspective. A single reheat ultra supercritical CLC-steam cycle can achieve a net plant efficiency of about 43%. Increasing the number of reheats to two results in 1% efficiency improvement and the cycle has a net plant efficiency of 44%. This efficiency includes the energy penalty for 100% CO_2 capture. Therefore, the CLC-steam cycles show a promising potential of CO_2-free power generation with high efficiency as compared to the conventional steam cycles, in a short-term until the CLC-reactor system and oxygen carriers are developed for high temperatures and pressures.

9.2 Recommendations

The conclusions given in the previous section clearly indicate that Chemical Looping Combustion can prove to be a ground breaking technology for highly efficient power generation with CO_2 capture. However, alongside the promising features of CLC, there also exist a number of technological barriers that must be overcome before a CLC-power plant can be built. The recommendations given in this section will help the CLC-community in identifying challenges associated with CLC.

9.2.1 Oxygen Carrier and Reactor System

Oxygen Carriers

The oxygen carrier performance must be evaluated on long-term experimental basis, both in the atmospheric and pressurised reactors. In order to achieve a clear picture of the oxygen carrier performance in a reactor system close to reality, small-scale circulating fluidised bed reactor system should be built; and the oxygen carrier particles should be circulated between the reactors. In future, research must also be focussed on developing the oxygen carriers that can tolerate temperatures as high as 1200°C or above in a pressurised atmosphere.

CLC-Reactor System

The energy and mass balance model of the CLC-reactor system in this work has been based on the complete conversion of fuel to CO_2 and H_2O without taking into account the side reactions. In future, CLC-reactor model including thermodynamic equilibrium should be implemented that considers all the possible reactions taking place in the reduction reactor. When using nickel oxide as oxygen carrier, there is a risk of nickel carbonyl formation, which is a poisonous gas. Hence, the environmental behaviour of nickel oxide should be experimentally investigated.

The reactor system models in this work did not include oxygen carrier behaviour in different regions of the oxidation and reduction reactors. The simplified model included only the average solids fraction and internal recirculation variations in the pneumatic transport oxidation reactor. In the future, a more detailed reactor system model could be developed that includes the analysis of gases and solids flow in a circulating fluidised bed reactor system. Such a model should also incorporate the different fluidisation regimes occurring along the height of the two reactors. Also, the mean solids fraction in the reduction reactor has been assumed to be constant in this work. This must be calculated on the basis of the

solids and gas flow in the reduction reactor and hence the pressure drop variations must be calculated.

The implementation of CLC in power cycles inevitably demands for the dynamic behaviour of CLC in connection with the rest of the cycle components. Therefore the reactors' dynamics should also be incorporated in the CLC-reactor system model. The dynamic model could be based on the formulations that include solids internal recirculation in the oxidation reactor, solids residence time in both the reactors and solids conversion based on the residence time. The empirical data must be incorporated in to the reactor system model as much as possible depending on the data availability.

A pressurised CLC-reactor system is an absolute necessity in the future to implement CLC in combined cycles with sufficiently high enough efficiency. So far, there has been no report of any demonstration of such a reactor system. A laboratory-scale pressurised CLC-reactor system should be developed in the near future and analysed under long-term operation.

The future research could also consider the alternate reactor systems for CLC applications; for instance rotary CLC and CLC in monolith structures based on the idea of immobilised oxygen carrier. Advanced mathematical modelling should be done for both of these concepts followed by the experimental validation.

9.2.2 CLC-Combined Cycles

A range of CLC-combined cycle configurations have been presented in this work. However, there is a variety of configurations that can be assessed. Especially, considering the set of reactions occurring in the reduction reactor as a result of the reaction between fuel and oxygen carrier, a power cycle with hydrogen production can be of interest. Such a cycle can also include a hydrogen-fuelled gas turbine alongside the air turbine and/or the CO_2 turbine.

The PCFB technology can be applied in combined cycles in such a way that steam is internally generated in the oxidation reactor and admitted to the steam turbine of the bottoming cycle in addition to the steam generated in the HRSG of the air turbine. The temperatures in the reactor system can thus be limited up to a safe level in such a system. This system should be analysed for both natural gas and coal.

The CLC-combined cycles presented in this work, have not been fully optimised. The design point has been selected mainly on the basis of TIT and compressor pressure ratio. The steam cycle parameters have also not been optimised. Therefore, in the future, each of the cycles must be optimised with respect to all the key parameters, in the gas turbine as well as steam turbine, at the design point.

In the present work, off-design evaluation of only two CLC-combined cycles has been carried out. In future, off-design behaviour of each combined cycle configuration should be analysed.

This work does not include dynamic behaviour analysis of CLC. One step forward towards the direction of CLC-development would be to carry out dynamic simulations of CLC-combined cycles in order to analyse transient response of CLC.

In the future, for the most promising CLC-combined cycle concepts, exergy analysis of the whole cycle should be carried out in order to assess the potential of further exergy loss minimisation in the cycles.

9.2.3 CLC-Steam Cycles

Although the natural-gas based CLC-steam cycles can achieve a reasonably high efficiency with CO_2 capture; however, a CLC-steam cycle can be a very attractive option if applied in conjunction with coal as fuel. This work is based on a simple energy and mass balance for the non-adiabatic CLC-reactors. In future, a more advanced model could be developed that takes into account the energy balance of the individual steam generators located in the CLC-oxidation reactor.

References

Adánez J., García-Labiano F., de Diego L.F., Plata A., Celaya J., Gayán P., Abad A., **2003**, "Optimizing the Fuel Reactor for Chemical-Looping Combustion", Proceedings of FBC2003, FBC2003-063, 17th International Fluidized Bed Combustion Conference, May 18-21, Jacksonville, Florida

Adánez J., García-Labiano F., de Diego L.F., Gayán P., Abad A., **2004a,** "Selection of Oxygen Carriers for Chemical-Looping Combustion", Energy and Fuels, vol. 18, p. 371-377

Adánez J., García-Labiano F., de Diego L.F., Gayán P., Celaya J., Abad A., **2004b,** "Characterization of oxygen carriers for Chemical-Looping Combustion", Proceedings of the 7th International Conference on Greenhouse Gas Control Technologies, Vancouver, Canada

Anderson R., Brandt H., Doyle S., Pronske K., Viteri F., **2003**; "Power generation with 100% carbon capture and sequestration", 2nd Annual Conference on Carbon Sequestration, Alexandria, VA., May 5-7

Anheden M, **2000**, "Analysis of gas turbine systems for sustainable energy conversion", PhD Thesis, Department of Chemical Engineering and Technology Energy Processes, Royal institute of Technology, Stockholm, Sweden

Anheden M., Näsholm A. S., Svedberg G., **1995**, "Chemical-looping combustion - Efficient conversion of chemical energy in fuels into work", Intersociety Energy Conversion Engineering Conference, vol. 30, p. 75-81

Anheden M., Svedberg G., **1996**, "Chemical-looping combustion in combination with integrated coal gasification", Intersociety Energy Conversion Engineering conference, vol. 31, p. 2045-50

Anheden M., Svedberg G., **1998**, "Exergy Analysis of Chemical-Looping Combustion Systems", Energy Conversion and Management, vol. 39, no. 16-18, p. 1967-1980

Barin I., **1995**, "Thermochemical data of pure substances", 3rd Edition, VCH Verlagsgesellschaft

Barrow G.M., "Physical chemistry", McGraw-Hill, 5th ed., **1988**

Black and Veatch, **1996**, "Power Plant Engineering", New York: Chapman & Hall, 1996, ISBN 0-412-06401-4

Bolland O., **2003**, "Lecture Notes: Thermal Power Cycles and Cogeneration", EP8103, Department of Energy and Process Engineering, Norwegian University of Science and Technology, Trondheim

Bolland O., Stadaas J.F., **1995**, "Comparative evaluation of combined cycles and gas turbine systems with water injection, steam injection and recuperation", Journal of Engineering for Gas Turbines and Power, vol. 28

Brandvoll Ø., **2005**, "Chemical Looping Combustion-Fuel conversion with inherent CO_2 Capture", PhD Thesis, Norwegian University of Science and Technology (NTNU), Trondheim

Brandvoll Ø., Bolland O., **2004**, "Inherent CO_2 Capture Using Chemical Looping Combustion in a Natural Gas Fired Power Cycle", Journal of Engineering for Gas Turbines and Power, vol. 126, p. 316-321

Brandvoll Ø., Olsen N., Bolland O., **2003**,"Chemical Looping Combustion – Reduction of nickel oxide/nickel aluminate with hydrogen", Chemical Engineering Transactions, vol. 3, p 105-110

Carberry, J. and Varma, A., **1986**, "Chemical Reaction and Reactor Engineering", Dekker, New York, USA, ISBN: 0-8247-7543-0

Cho P., Mattisson T., Lyngfelt A., **2002**, "Reactivity of Iron Oxide with Methane in a Laboratory Fluidized Bed – Application of Chemical-Looping Combustion", Proceedings of the 7th International Conference on circulating Fluidized Beds, Niagara Falls, Ontario, Canada, p. 599-606

Cho P., Mattisson T., Lyngfelt A., **2005a**, "Carbon formation on nickel and iron oxide-containing oxygen-carriers for chemical-looping combustion", Industrial and Engineering Chemistry Research, vol. 44, p. 668-676

Cho P., Mattisson T., Lyngfelt A., **2005b**, "Defluidization Conditions for Fluidized-bed of Iron, Nickel, and Manganese oxide-Containing Oxygen-Carriers for Chemical-Looping Combustion", submitted for publication

Cho P., **2005c**, "Development and Characterisation of Oxygen-Carrier Materials for Chemical-Looping Combustion", PhD Thesis, Chalmers University of Technology, Göteborg, Sweden

Copeland R.J., Alptekin G., Cesario M., Gershanovich Y., **2002**, "Sorbent energy transfer system (SETS) for CO_2 separation with high efficiency", Presented on the 27th International Conference on Coal utilization & Fuel Systems, Clearwater, Florida

Corbella B.M., de Diego L.F., García-Labiano F., Adánez J., Palacios J.M., **2005**, "The Performance in a Fixed Reactor of Copper-based Oxides on Titania as oxygen Carriers for Chemical Looping Combustion of Methane", Energy and Fuels, vol. 19, p. 433-441

Çengel Y.A., Boles M.A., **2005**, "Thermodynamics: An Engineering Approach", 5th Edition, McGraw-Hill Science/Engineering/Math, ISBN: 0073107689

de Diego L.F., García-Labiano F., Adánez J., Gayán P., Abad A., Corbella B.M., Palacios J.M., **2004**, "Development of Cu-based oxygen carriers for chemical-looping combustion", Fuel, vol. 83, p. 1749-1757

Gale J., **2002**, "Overview of CO_2 emission sources, potential, transport and geographical distribution of storage possibilities", Proceedings of IPCC Workshop for Carbon Capture and Storage 2002

García-Labiano F., de Diego L.F., Adánez J., Abad A., Gayán P., **2004**, "Reduction and Oxidation kinetics of a copper-based oxygen carrier prepared by impregnation for Chemical-Looping Combustion", Industrial and Engineering Chemistry research, vol. 43, p. 8168-8177

García-Labiano F., de Diego L.F., Adánez J., Abad A., Gayán P., **2005**, "Temperature variations in the oxygen carrier particles during their reduction and oxidation in a chemical-looping combustion system", Chemical Engineering Science, vol. 60, p. 851-862

Goldberger W.M. and Othmer D.F., **1963**, "The Kinetics of Nickel Carbonyl Formation", Polytechnic Institute of Brooklyn, N.Y. I&EC Process Design and Development, vol. 2, No. 3, July 1963, p. 202-209

gPROMS® ModelBuilder 2.3.3, Copyright © **1997-2004**, Process Systems Enterprise Limited

Griffin T., Bill A., Marion J.L., Nsalaka N., **2002**, "CO_2 Control technologies. Alstom Power Approach", The 6th International Conference on Greenhouse Gas Control Technologies, Kyoto, Japan

GTPRO/GTMASTER, Version 11.0.2, Copyright © **1987-2004**, Thermoflow, Inc. 29 Hudson Road Sudbury, MA 01776, USA

Harvey S.P., Richter H. J., **1994**, "A high efficiency gas turbine power generation cycle with solid oxide fuel cell technology and chemical looping combustion", AES-vol. 33, Thermodynamics and the Design, Analysis and improvement of energy systems ASME, p. 65-76

Hatanaka T., Matsuda S., Hatano H., **1997**, "A new-concept gas-solid combustion system "MERIT" for high combustion efficiency and low emissions", Proceedings of the 32nd Intersociety Energy Conversion Engineering Conference, p. 944-947

Heitmer F., Jericha H., **2003**, "Graz cycle-an optimized power plant concept for CO_2 retention", First International Conference on Industrial GT Technologies, RTD Framework Programme of the European Union, July 2003, Brussels, Belgium

Hou K., Hughes R., **2001**, "The kinetics of steam methane reforming over a Ni/α-Al_2O catalyst", Chemical Engineering Journal, vol. 82, p. 311-328

Howard, J.R., **1989,** "Fluidized Bed Technology - Principles and Application", Adam Hilger, Bristol, UK.

Ishida M., Jin H., **1994a,** "A novel combustor based on chemical-looping reactions and its reaction kinetics", Journal of Chemical Engineering of Japan, vol. 27, No. 3, p. 296-301

Ishida M., Jin H., **1994b**, "A new advanced power-generation system using chemical-looping combustion", Energy, vol. 19, No. 4, p. 415-422

Ishida M., Jin H., **1996**, "A novel Chemical-Looping Combustor without NOx Formation", Research Notes, Industrial and Engineering Chemistry, vol. 35, 2469-2472

Ishida M., Jin H., **1997**, "CO_2 recovery in a power plant with chemical looping combustion", Energy Conversion and Management, vol. 38, Suppl., p. 187-192

Ishida M., Jin H., **1999**, "Greenhouse gas control by a novel combustion: No energy penalty and no CO_2 separation equipment", Greenhouse Gas Control Technologies, Proceedings of the 4th International conference on Greenhouse Gas Control Technologies, 30 Aug – 2 Sep 1998, Interlaken, Switzerland, p. 627-632

Ishida M., Jin H., Okamoto T., **1996**, "A fundamental study of a new kind of medium material for chemical-looping combustion", Energy & Fuels, vol. 10, p. 923-963

Ishida M., Jin H., Okamoto T., **1998a**, "Development of a novel chemical-looping combustion: Synthesis of a looping material with a double metal oxide of CoO-NiO", Energy & Fuels, vol. 12, p. 1272-1277

Ishida M., Jin H., Okamoto T., **1998b**, "Kinetic behavior of solid particle in chemical-looping combustion: Suppressing Carbon deposition in reduction", Energy & Fuels, vol. 12, p. 223-229

Ishida M., Yamamoto M., Ohba T., **2002**, "Experimental results of chemical-looping combustion with NiO/NiAl$_2$O4 particle circulation at 1200°C", Energy Conversion and Management, vol. 43, p. 1469-1478

Ishida M., Zheng D., Akehata T., **1987**, "Evaluation of a chemical-looping-combustion power-generation system by graphic exergy analysis", Energy, vol. 12, p. 147-154

Jeong J.H., Park J.W., Yoon W.L., **2003**, "Redox Characteristics of CoOx/$CoAl_2O_4$ as a Oxygen carrier for Chemical-Looping Combustion", Journal of Korean Industrial and Engineering Chemistry, written in Korean, vol. 14, p. 411-417

Jin H., Ishida M., **2000,** "A novel gas turbine cycle with hydrogen-fueled chemical-looping combustion", International Journal of Hydrogen Energy, vol 25, no 12, p 1209-1215

Jin H., Ishida M., **2001**, "Reactivity study on a novel hydrogen fueled chemical-looping combustion", International Journal of Hydrogen Energy, vol. 26, p 889-894

Jin H., Ishida M., **2002**, "Reactivity study on natural-gas-fueled chemical-looping combustion by a fixed-bed reactor", Industrial and Engineering Chemistry Research, vol. 41, no. 16, Aug 7, p 4004-4007

Jin H., Ishida M., **2004**, "A new type of coal gas fueled chemical-looping combustion", Fuel, vol. 83, p. 2411-2417

Jin H., Okamoto T., Ishida M., **1999**, "Development of a novel chemical-looping combustion: Synthesis of a Solid looping material NiO/$NiAl_2O_4$", Industrial and Engineering Chemistry Research, vol. 38, p. 126-132

Johansson E., **2005**, "Fluidized-Bed Reactor Systems for Chemical-Looping Combustion with Inherent Separation of CO_2", PhD Thesis, Chalmers University of Technology, Göteborg, Sweden

Johansson E., Lyngfelt A, Mattisson T., Johnsson F., **2003**, "Gas leakage measurements in a cold model of an interconnected fluidized bed for chemical-looping combustion", Powder Technology 134, p. 210-217

Johansson M., Mattisson T., Lyngfelt A., **2004**, "Investigation of Fe_2O_3 with $MgAl_2O_4$ for chemical-looping combustion", Industrial and Engineering Chemistry Research, vol. 43, p. 6968-6987

Jukkola G., Levasseur A., Turek D., Teigen B., Suresh J., Thibeault P., **2003**, "Performance results with ALSTOM's circulating moving bed combustor", Proceedings of FBC2003, 17th Fluidized Bed Conference, p. 99-105

Knache O., Kubaschewski O., Hesselmann K., **1991**, "Thermochemical Properties of Inorganic Substances", 2nd Edition, Springer-Verlag Inc.

Kronberger B., Lyngfelt A., Löffler G., Hofbauer H., **2005**, "Design and fluid Dynamic Analysis of a Bench-Scale Combustion System with CO_2 Separation - Chemical-Looping Combustion", Industrial and Engineering Chemistry, vol. 44, p.546-556

Kronberger B., Löffler G., Hofbauer H., **2005**, "Simulations of Mass and Energy Balances of a Chemical-Looping Combustion System", Clean Air, vol. 6, p. 1-14

Kunii D., Levenspiel O., **1991**, "Fluidization Engineering", 2nd Edition, Butterworth-Heinemann, USA, ISBN 0-409-90233-0

Lee J.B., Song Y.W., Choi S.I., Park C.S., Kim Y.H., Yang H.S., **2005**, "Redox Characteristics of Various Kinds of Oxygen Carriers for Hydrogen Fueled Chemical-Looping Combustion", Journal of Industrial Engineering Chemistry, vol. 11, p. 96-102

Lyngfelt A., Leckner B., Mattisson T., **2001**, A fluidized-bed combustion process with inherent CO_2 separation, Chemical Engineering Science, vol. 56, no. 10, p. 3101-3113

Lyngfelt A., Kronberger B., Adánez J., Morin J.X., Hust P., **2004**, "The GRACE Project. Development of oxygen carrier particles for chemical-looping combustion. Design and operation of a 10kW chemical-looping combustor", Proceedings of the 7th International Conference on Greenhouse Gas Control Technologies, Vancouver, Canada

Lødeng R., De Chen, Jakobsen C.K., Holmen A., **2000**, "A study of coke formation kinetics by a conventional and an oscillating microbalance on steam reforming catalysts", Studies in Surface Science and Catalysis, vol. 130, p. 3639-3644

Mathieu P., **2003**, "Mitigation of CO_2 emissions using low and near zero CO_2 emission power plants", International Journal on Energy for a Clean Environment, vol. 4, p. 1-14

Mattisson T., Johansson M., Lyngfelt A., **2006**, "The use of NiO as an oxygen carrier in chemical-looping combustion", Fuel, vol. 85, p. 736-747

Mattisson T., Järdnäs A., Lyngfelt A., **2003**, "Reactivity of some metal oxides supported on alumina with alternating methane and oxygen-application for Chemical-Looping combustion", Energy & Fuels, v 17, p 643-651

Mattisson T., Lyngfelt A., Cho P., **2001**, "The use of iron oxide as an oxygen carrier in chemical-looping combustion of methane with inherent separation of CO_2", Fuel, vol. 80, no. 13, p. 1953-1962

Nakano Y., Iwamoto S., Maeda T., Ishida M., Akehata T., **1986**, "Characteristics of Reduction and Oxidation Cycle Process by Use of a Fe_2O_3 Medium", ISIJ International 72, p. 1521-1528

Naqvi R., Bolland O., Brandvoll O., Helle K., **2004**,"Chemical Looping Combustion, Analysis of natural gas fired power cycle with inherent CO_2 capture", Proceedings of ASME Turbo Expo 2004, GT2004-53359, 14-17 June, Vienna, Austria

Naqvi R., Bolland O., Wolf J., **2006**, "Part-load Analysis of a Chemical Looping Combustion (CLC) Combined Cycle with CO_2 Capture", Energy- The International Journal, Article in press

Naqvi R., Bolland O., **2006**, "Multi-stage Chemical Looping Combustion for Combined Cycles with CO_2 Capture", Proceedings of GHGT8, June 19-22, Trondheim-Norway

OECD/IEA, **2005a**, "World Energy Outlook 2004"

OECD/IEA, **2005b**, "Prospects for CO_2 Capture and Storage"

Olafsen A., **1999**, "Structure and Stability of Rare Earth Oxide Carbonates. Properties of Nd-based Ruddlesden-Popper Type Oxides", PhD Thesis, Faculty of Mathematics and Natural Science, University of Oslo, Norway

Pavone D., **2005**, "CO_2 capture by means of chemical looping combustion", presented at Conference FEMLAB 2005, 15 November, Paris

PRO/II 6.0, © **1994-2002**, Simulation Sciences, Inc.

Richter H.J., Knoche K., **1983,** "Reversibility of Combustion processes", Efficiency and Costing – Second Law Analysis of Processes, ACS Symposium series 235, p. 71-85

Rydén M., Lyngfelt A., **2006a**, "Using steam reforming to produce hydrogen with carbon dioxide capture by chemical-looping combustion", International Journal of Hydrogen Energy, Article in Press

Rydén M., Lyngfelt A., Mattisson T., **2006b**, "Synthesis gas generation by chemical-looping reforming in a continuously operating laboratory reactor", Fuel, Article in Press

Ryu H.J., Bae D.H., Han K.H., Lee S.Y., Jin G.T., Choi J.H., **2001**, "Oxidation and reduction characteristics of oxygen carrier particles and reaction kinetics by unreacted core model", Korean Journal of Chemical Engineering, vol. 18, no. 6, p. 831-837

Saravanamuttoo H.I.H., Rogers G.F.C., Cohen H., **2001**, "Gas turbine theory", 5th Edition, Pearson education Ltd., ISBN 0130-15847-X

Shimomura, Y., **2003**, "The CO_2 wheel: a revolutionary approach to carbon dioxide capture", Modern Power Systems p.15-17

Song K.S., Seo Y.S., Yoon H.K., June C.S., **2003**, "Characteristics of the NiO/Hexaaluminate for Chemical-Looping Combustion", Korean Journal of Chemical Engineering, vol. 20, p. 471-475

Undrum, H. and Bolland, O., **2003**, "A novel methodology for comparing CO_2 capture options for natural gas-fired combined cycle plants, Advances in Environmental Research", vol. 7, p. 901-911

Villa R., Cristiani C., Groppi G., Lietti L., Forzatti P., Cornaro U., Rossini S., **2003**, "Ni based mixed oxide materials for CH4 oxidation under redox cycle conditions", Journal of Molecular Catalysis A-Chemical, vol. 204, p. 637-646

Wolf J., **2004**, "CO_2 Mitigation in Advanced Power Cycles- Chemical Looping Combustion and Steam-Based Gasification", PhD Thesis, Royal Institute of Technology (KTH), Stockholm, Sweden

Wolf J., Anheden M., Yan J., **2001**, "Performance of Power Generation Processes with Chemical Looping Combustion for CO_2 Removal – Requirements for the Oxidation and Reduction Reactors", Proceedings of International Pittsburgh Coal Conference, Newcastle, New South Wales, Australia, December 3-7

Wolf J., Anheden M., Yan J., **2005**, "Comparison of nickel- and iron-based oxygen carriers in chemical looping combustion for CO_2 capture in power generation", Fuel, vol. 84, Issues 7-8, p. 993-1006

Wolf J., Yan J., **2004**, "Cogeneration of hydrogen and electrical power in an extended chemical-looping combustion", Proceedings of ECOS 2004, July 7-9, Mexico

Zafar Q., Mattisson T., Gevert B., **2005a**, "Integrated Hydrogen and Power Production with CO_2 Capture Using Chemical-Looping Reforming-Redox Reactivity of Particles of CuO, Mn_2O_3, NiO, and Fe_2O_3 Using SiO_2 as a Support", Industrial and Engineering Chemistry Research, vol. 44, p. 3485-3496

Zafar Q., Mattisson T., Gevert B., **2005b**, "Redox investigation of some oxides of transition state metals Ni, Cu, Fe and Mn supported on SiO_2 and $MgAl_2O_4$", submitted for publication

Zafar Q., **2005c**, "Investigation of Oxygen carrier Materials for Chemical-Looping Reforming", Licentiate of Engineering Thesis, Chalmers University of Technology, Göteborg, Sweden

APPENDIX A

(Computational Assumptions)

Computational Assumptions

Reference state

The condition at the reference state is as follows:
$T_0 = 25°C$
$P_0 = 1$ bar

Fuel

Natural gas
Pressure and temperature
P = 70 bar
T = 10°C

Composition (mole %):
N_2 = 0.89
CO_2 = 2.0
C1 = 89.0
C2 = 7.0
C3 = 1.0
C4 = 0.05
C5 = 0.05

Lower Heating Value-LHV [kJ/kg] = 46503
Molecular weight [kg/kmole] = 18.02
Density [kg/Sm^3] = 0.76212

Ambient Conditions

Ambient Air
Relative humidity: 60%

Pressure and temperature
P = 1.01325 bar
T = 15°C
Composition (mole %):
N_2 = 77.39
O_2 = 20.74
CO_2 = 0.03
H_2O = 1.01
Ar = 0.92

CLC Reactor System

Mean particle diameter = 150 μm
Average particle density = 2400 kg/m^3
Pressure drop (cycle design simulations):
Oxidation reactor + cyclone = 5% of incoming stream pressure
Reduction reactor = 5% of incoming stream pressure
Off-design calculation:
Cyclone pressure drop (constant) = 20mbar

Efficiency calculation

Mechanical efficiency: η_m = 99.6%
Generator efficiency: η_G = 98.5%
Natural gas fired: η_{aux} = 98.5%

Combined Cycles

Air Compressor
Inlet filter pressure drop = 10 mbar
Polytropic efficiency = 91.5%

Air turbine/CO_2-turbine
Polytropic efficiency = 86.2%
Exhaust pressure drop:
HRSG = 40 mbar
No HRSG = 10 mbar

Steam cycles

Single reheat: 280 bar, 600°C/620°C
Double reheat: 280 bar, 600°C/620°C/620°C
Pressure losses:
Δp_{cold} = 3% for each heat exchanger
$\Delta p_{reheat,\ cold,\ tot}$ = 10%
$\Delta p_{\text{"steam pipe + valve"}}$ = 7%
Temperature losses:
From superheater/reheater to turbine = 2K
Temperature differences:
$\Delta T_{steam/gas}$ = 25K
$\Delta T_{gas/liquid}$ = 10K
$\Delta T_{approach,\ ECO}$ = 5K
Natural circulation
Blowdown = 0%
Fan work (combustion air, flue gases) = included in auxiliary power

HRSG

Conventional Combined Cycle
Triple pressure, single reheat, 125 bar/30 bar/4.5 bar, 560°C/560°C
Reheat: mix superheated IP steam with cold reheat steam before reheat
η_{HRSG} = 99.7% (heat losses)
Pressure losses:
$\Delta p_{HRSG,\ hot}$ = 4 kPa
Δp_{cold} = 3% for each heat exchanger
$\Delta p_{reheat,\ cold,\ tot}$ = 10%
$\Delta p_{\text{"steam pipe + valve"}}$:
HP = 7%
IP = 9% (when steam flows directly to IP turbine)
IP = 9% for Reheat/IP-steam mixing (assuming pressure loss of 2% from HP turbine exit to HRSG, 3% in HRSG Reheater, and 5% from HRSG to IP turbine inlet)
LP = 12%

Temperature losses:

From superheater/reheater to turbine = 1 kJ/kg (approximately 0.5 K)

Temperature differences:

$\Delta T_{steam/gas}$ = 25K

$\Delta T_{pinch\ point,\ gas/boiling\ liquid}$ = 10K

$\Delta T_{gas/liquid}$ = 10K

$\Delta T_{approach,\ ECO}$ = 5K

Natural circulation

Blowdown = 0%

Condenser - pure steam

Water cooling

Condenser pressure: P_{cond} = 0.048 bar (T_{sat} = 32.2 °C => ΔT_{min} = 7K)

Cooling water pump work = 0.5% of steam turbine power

Cooling water pressure = 2-2.5 bara

Limitations on cooling water outlet temperature: Maximum $T_{cw\ out}$ = 25°C ($T_{cw\ in}$ = 15°C)

Saturated condensate at condenser outlet

Condenser – steam mixed with non-condensable gases

Steam Cycle

Steam Turbines

Isentropic efficiency, dependency on pressure:

η_{HP} = 90%

η_{IP} = 92%

η_{LP} = 88%

HP steam turbine admission temperature = 600°C

Reheat steam temperature = 620 °C

The total isentropic efficiency for HPT, IPT and LPT is the same regardless of number of steam extraction points

Minimum steam quality = 0.87 (kg steam/kg steam + liquid water)

Pressure losses for steam extraction:

IP-extraction pipe + preheater, Δp = 3%

LP-extraction pipe + preheater, Δp = 5%

$\Delta p_{\text{“steam pipe + valve”}}$ = 7%

Pumps

Total efficiency = 70%

Feedwater preheating

Single Reheat CLC-Steam Cycle

2 feedwater preheaters + 1 deaerator + 4 condensate preheaters

Deaerator:

Saturated liquid at outlet

Pressure = 12.5 bar

Extraction pressures: 51 / 26 / 13 / 5 / 1.9 / 0.8 / 0.3 bara

Final preheating temperature = 265°C

Double Reheat CLC-Steam Cycle

2 feedwater preheaters + 1 deaerator + 4 condensate preheaters

Deaerator:
Saturated liquid at outlet
Pressure = 12.5 bar
Extraction pressures: 84.3 / 51 / 24 / 5.37 / 1.9 / 0.8 / 0.3 bara
Final preheating temperature = 295°C

Conventional Combined cycle
No feedwater preheating with turbine steam extraction
Feedwater preheating with exhaust gas heat to T_{H2O} = 95°C
Deaerator:
Saturated liquid at outlet
Pressure = 1.2 bar (T_{sat} = 105°C)
Closed feedwater heater:
Δp_{cold} = 1%
Δp_{hot} = 1%
Terminal temperature difference ($T_{sat.\ steam}$-$T_{condensate\ out}$) = 3°C
Drain cooler approach ($T_{condensed\ steam}$ - $T_{condensate\ in}$) = 6°C
Condensed steam sent to feedwater heater at lower pressure or deaerator

Heat exchangers

Pinch points:
Gas/Gas = 25 Kelvin
Gas/Boiling or liquid phase = 10 Kelvin
Liquid/Liquid = 10 Kelvin
Condensing/Liquid = 4 Kelvin
Heat Loss:
Economiser, Evaporator and Superheater = 0.3%
All other heat exchangers; No heat loss
Pressure drop Gas/Gas:
Cold side = 3%
Hot side = 5%
Pressure drop Gas/steam:
Cold side = 3%
Hot side (absolute) = Economiser: 0.04 bar, Evaporator and superheater: 0
Pressure drop steam/water (Feed water heaters and condenser):
Cold side = 1%
Hot side = 1%, (condenser: 0)

CO_2 compression

Polytropic efficiency (stage 1, 2, 3) (%): 85, 80, 75
Heat exchanger pressure drop (stage 1, 2, 3): 0.15, 1.5, 2.4 bar
Cold utility (water) inlet/outlet temperature: 15°C/24°C
Adiabatic efficiency CO_2 pump: 75%
Compressor intercooler exit temperature: 30°C

Post-combustion CO_2 capture plant

90% CO_2 capture
Absorption tower pressure drop: 150 mbar
Heat demand for CO_2 stripper: 3.8 MJ/kg CO_2 captured
CO_2 end pressure: 110 bar

APPENDIX B

(Stream Data)

Stream data: Base-case CLC Combined Cycle (CLCCC)
CPR=18, Tox=1200°C
(Reference Flowsheet: Figure 6.3)

Stream		S1	S2	S3	S5	S7	S8	S10	S11
Phase	Unit	Gas	Gas	Gas	Gas	Gas	G/V	G/V	St
MW	kg/kmol	28.85	28.85	28.62	28.65	18.02	27.05	27.05	18.02
Pressure	bar	1.01	18.24	17.32	1.04	18.24	17.32	1.05	0.04
Temperature	°C	15	423	1200	501	511	988	336	29
Temperature	K	288	696	1473	774	784	1261	609	302
Flow rate	kg/s	823.0	760.0	704.0	767.0	15.0	70.5	70.5	101.2
Flow rate	kmol/s	28.53	26.34	24.60	26.77	0.83	2.61	2.61	5.62
CO_2	vol-%	0.03	0.03	0.03	0.03	2.00	34.66	34.66	0.00
O_2	vol-%	20.74	20.74	15.20	15.20	0.00	0.00	0.00	0.00
N_2	vol-%	77.30	77.30	82.70	82.70	0.89	0.28	0.28	0.00
Ar	vol-%	0.92	0.92	0.98	0.98	0.00	0.00	0.00	0.00
H_2O	vol-%	1.01	1.01	1.08	1.08	0.00	65.06	65.06	1.00
C_1H_4	vol-%	0.00	0.00	0.00	0.00	89.00	0.00	0.00	0.00
C_2H_6	vol-%	0.00	0.00	0.00	0.00	7.00	0.00	0.00	0.00
C3H8	vol-%	0.00	0.00	0.00	0.00	1.00	0.00	0.00	0.00
C_4H_{10}-i	vol-%	0.00	0.00	0.00	0.00	0.05	0.00	0.00	0.00
C_4H_{10}-n	vol-%	0.00	0.00	0.00	0.00	0.05	0.00	0.00	0.00
C_5H_{12}-i	vol-%	0.00	0.00	0.00	0.00	0.005	0.00	0.00	0.00
C_5H_{12}-n	vol-%	0.00	0.00	0.00	0.00	0.004	0.00	0.00	0.00
C_6H_{14}	vol-%	0.00	0.00	0.00	0.00	0.001	0.00	0.00	0.00

- G/V = Gas/Vapour
- St = Steam

Stream data: CLC Combined Cycle with Exhaust Recuperation (CLCCC-ER)
CPR=10, Tox=1200°C
(Reference Flowsheet: Figure 6.7)

Stream		S1	S2	S3	S4	S6	S8	S9	S10	S11	S12
Phase	Unit	Gas	Gas	Gas	Gas	Gas	Gas	G/V	G/V	G/V	St
MW	kg/kmol	28.85	28.85	28.85	28.62	28.65	18.02	27.05	27.05	27.05	18.02
Pressure	bar	1.01	10.13	9.62	9.14	1.04	9.62	9.14	8.79	8.46	0.04
Temperature	°C	15	312	406	1200	621	312	973	337	226	29
Temperature	K	288	585	679	1473	894	585	1246	610	499	302
Flow rate	kg/s	786.0	736.0	736.0	681.0	731.0	15.0	70.5	70.5	101.2	119.8
Flow rate	kmol/s	27.2	25.5	25.5	23.8	25.5	0.8	2.6	2.6	3.7	6.6
CO_2	vol-%	0.03	0.03	0.03	0.03	0.03	2.00	34.66	34.66	34.66	0.00
O_2	vol-%	20.74	20.74	20.74	14.96	15.20	0.00	0.00	0.00	0.00	0.00
N_2	vol-%	77.30	77.30	77.30	82.93	82.70	0.89	0.28	0.28	0.28	0.00
Ar	vol-%	0.92	0.92	0.92	0.99	0.98	0.00	0.00	0.00	0.00	0.00
H_2O	vol-%	1.01	1.01	1.01	1.08	1.08	0.00	65.06	65.06	65.06	1.00
C_1H_4	vol-%	0.00	0.00	0.00	0.00	0.00	89.00	0.00	0.00	0.00	0.00
C_2H_6	vol-%	0.00	0.00	0.00	0.00	0.00	7.00	0.00	0.00	0.00	0.00
C3H8	vol-%	0.00	0.00	0.00	0.00	0.00	1.00	0.00	0.00	0.00	0.00
C_4H_{10}-i	vol-%	0.00	0.00	0.00	0.00	0.00	0.05	0.00	0.00	0.00	0.00
C_4H_{10}-n	vol-%	0.00	0.00	0.00	0.00	0.00	0.05	0.00	0.00	0.00	0.00
C_5H_{12}-i	vol-%	0.00	0.00	0.00	0.00	0.00	0.005	0.00	0.00	0.00	0.00
C_5H_{12}-n	vol-%	0.00	0.00	0.00	0.00	0.00	0.004	0.00	0.00	0.00	0.00
C_6H_{14}	vol-%	0.00	0.00	0.00	0.00	0.00	0.001	0.00	0.00	0.00	0.00

- G/V = Gas/Vapour
- St = Steam

Stream data: CLC Combined Cycle with Exhaust Recuperation and Steam Generation (CLCCC-ERS)
CPR=12, Tox=1200°C
(Reference Flowsheet: Figure 6.10)

Stream		S1	S2	S3	S4	S6	S8	S9	S10	S11	S12	S13
Phase	Unit	Gas	Gas	Gas	Gas	Gas	Gas	G/V	G/V	G/V	G/V	St
MW	kg/kmol	28.85	28.85	28.85	28.62	28.65	18.02	27.05	27.05	27.05	27.05	18.02
Pressure	bar	1.01	12.16	11.55	10.97	1.04	11.55	10.97	10.56	10.54	10.14	0.04
Temperature	°C	15	345	430	1200	585	121	961	369	236	200	29
Temperature	K	288	618	703	1473	858	394	1234	642	509	473	302
Flow rate	kg/s	804.0	751.0	751.0	695.0	749.0	15.0	70.5	70.5	70.5	70.5	121.0
Flow rate	kmol/s	27.9	26.0	26.0	24.3	26.1	0.8	2.6	2.6	2.6	2.6	6.7
CO_2	vol-%	0.03	0.03	0.03	0.03	0.03	2.00	34.66	34.66	34.66	34.66	0.00
O_2	vol-%	20.74	20.74	20.74	14.96	15.20	0.00	0.00	0.00	0.00	0.00	0.00
N_2	vol-%	77.30	77.30	77.30	82.93	82.70	0.89	0.28	0.28	0.28	0.28	0.00
Ar	vol-%	0.92	0.92	0.92	0.99	0.98	0.00	0.00	0.00	0.00	0.00	0.00
H_2O	vol-%	1.01	1.01	1.01	1.08	1.08	0.00	65.06	65.06	65.06	65.06	1.00
C_1H_4	vol-%	0.00	0.00	0.00	0.00	0.00	89.00	0.00	0.00	0.00	0.00	0.00
C_2H_6	vol-%	0.00	0.00	0.00	0.00	0.00	7.00	0.00	0.00	0.00	0.00	0.00
C3H8	vol-%	0.00	0.00	0.00	0.00	0.00	1.00	0.00	0.00	0.00	0.00	0.00
C_4H_{10}-i	vol-%	0.00	0.00	0.00	0.00	0.00	0.05	0.00	0.00	0.00	0.00	0.00
C_4H_{10}-n	vol-%	0.00	0.00	0.00	0.00	0.00	0.05	0.00	0.00	0.00	0.00	0.00
C_5H_{12}-i	vol-%	0.00	0.00	0.00	0.00	0.00	0.005	0.00	0.00	0.00	0.00	0.00
C_5H_{12}-n	vol-%	0.00	0.00	0.00	0.00	0.00	0.004	0.00	0.00	0.00	0.00	0.00
C_6H_{14}	vol-%	0.00	0.00	0.00	0.00	0.00	0.001	0.00	0.00	0.00	0.00	0.00

- G/V = Gas/Vapour
- St = Steam

Stream data: Single Reheat CLC Combined Cycle (SR-CLCCC)
CPR=18, $T_{oxidation}$=1200°C
(Reference Flowsheet: Figure 6.13)

Stream		S1	S2	S3	S5	S6	S8	S11	S12	S15	S16	S17
Phase	Unit	Gas	Gas	Gas	Gas	Gas	Gas	Gas	Gas	G/V	G/V	St
MW	kg/kmol	28.85	28.85	28.64	28.66	28.58	28.60	18.02	18.02	27.05	27.05	18.02
Pressure	bar	1.01	22.29	21.17	10.08	9.57	1.04	22.29	10.08	1.05	1.01	0.04
Temperature	°C	15	465	1200	939	1200	609	515	515	540	332	29
Temperature	K	288	738	1473	1212	1473	882	788	788	813	605	302
Flow rate	kg/s	689	689	541	593	578	633	10.9	4.12	70.5	70.5	102
Flow rate	kmol/s	23.89	23.88	18.89	20.69	20.22	22.13	0.60	0.23	2.61	2.61	5.66
CO_2	vol-%	0.03	0.03	0.03	0.03	0.03	0.03	2.00	2.00	34.66	34.66	0.00
O_2	vol-%	20.74	20.74	15.46	15.92	13.94	13.97	0.00	0.00	0.00	0.00	0.00
N_2	vol-%	77.30	77.30	82.40	81.99	83.90	83.87	0.89	0.89	0.28	0.28	0.00
Ar	vol-%	0.92	0.92	0.98	0.98	1.00	1.00	0.00	0.00	0.00	0.00	0.00
H_2O	vol-%	1.01	1.01	1.07	1.07	1.10	1.10	0.00	0.00	65.06	65.06	1.00
C_1H_4	vol-%	0.00	0.00	0.00	0.00	0.00	0.00	89.00	89.00	0.00	0.00	0.00
C_2H_6	vol-%	0.00	0.00	0.00	0.00	0.00	0.00	7.00	7.00	0.00	0.00	0.00
C3H8	vol-%	0.00	0.00	0.00	0.00	0.00	0.00	1.00	1.00	0.00	0.00	0.00
C_4H_{10}-i	vol-%	0.00	0.00	0.00	0.00	0.00	0.00	0.05	0.05	0.00	0.00	0.00
C_4H_{10}-n	vol-%	0.00	0.00	0.00	0.00	0.00	0.00	0.05	0.05	0.00	0.00	0.00
C_5H_{12}-i	vol-%	0.00	0.00	0.00	0.00	0.00	0.00	0.005	0.005	0.00	0.00	0.00
C_5H_{12}-n	vol-%	0.00	0.00	0.00	0.00	0.00	0.00	0.004	0.004	0.00	0.00	0.00
C_6H_{14}	vol-%	0.00	0.00	0.00	0.00	0.00	0.00	0.001	0.001	0.00	0.00	0.00

- G/V = Gas/Vapour
- St = Steam

Stream data: Double Reheat CLC Combined Cycle (DR-CLCCC)
CPR=18, $T_{oxidation}$=1200°C
(Reference Flowsheet: Figure 6.16)

Stream		S1	S2	S3	S5	S6	S8	S9	S11	S13	S14	S15	S19	S20	S21
Phase	Unit	Gas	Gas	Gas	Gas	Gas	Gas	Gas	Gas	Gas	Gas	Gas	G/V	G/V	St
MW	kg/kmol	28.9	28.9	28.7	28.7	28.6	28.7	28.6	29	18	18	18	27	27	18
Pressure	bar	1.01	26.3	25	19.5	18.5	9.32	8.85	1	26.3	19.5	8.85	1	1	0
Temperature	°C	15	501	1200	1067	1200	951	1200	623	504	504	504	530	327	29
Temperature	K	288	774	1473	1340	1473	1224	1473	896	777	777	777	803	600	302
Flow rate	kg/s	682	518	484	534	527	582	568	627	9.25	1.9	3.85	71	71	103
Flow rate	kmol/s	23.6	18	16.9	18.6	18.4	20.3	19.9	22	0.51	0.11	0.21	2.6	2.6	5.7
CO_2	vol-%	0.03	0.03	0.03	0.03	0.03	0.03	0.03	0	2	2	2	35	35	0
O_2	vol-%	20.7	20.7	15.7	16.2	15.2	15.7	13.8	14	0	0	0	0	0	0
N_2	vol-%	77.3	77.3	82.2	81.7	82.7	82.2	84	84	0.89	0.89	0.89	0.3	0.3	0
Ar	vol-%	0.92	0.92	0.98	0.97	0.98	0.98	1	1	0	0	0	0	0	0
H_2O	vol-%	1.01	1.01	1.07	1.07	1.08	1.07	1.1	1.1	0	0	0	65	65	1
C_1H_4	vol-%	0	0	0	0	0	0	0	0	89	89	89	0	0	0
C_2H_6	vol-%	0	0	0	0	0	0	0	0	7	7	7	0	0	0
C3H8	vol-%	0	0	0	0	0	0	0	0	1	1	1	0	0	0
C_4H_{10}-i	vol-%	0	0	0	0	0	0	0	0	0.05	0.05	0.05	0	0	0
C_4H_{10}-n	vol-%	0	0	0	0	0	0	0	0	0.05	0.05	0.05	0	0	0
C_5H_{12}-i	vol-%	0	0	0	0	0	0	0	0	0.005	0.005	0.005	0	0	0
C_5H_{12}-n	vol-%	0	0	0	0	0	0	0	0	0.004	0.004	0.004	0	0	0
C_6H_{14}	vol-%	0	0	0	0	0	0	0	0	0.001	0.001	0.001	0	0	0

- G/V = Gas/Vapour
- St = Steam

Stream data: Single Reheat CLC Combined Cycle with Exhaust Recuperation (SRCLC-ER)
CPR=18, $T_{oxidation}$=1200°C
(Reference Flowsheet: Figure 6.20)

Stream		S1	S2	S3	S4	S6	S7	S9	S11	S12	S15	S16	S17	S18
Phase	Unit	Gas	Gas	Gas	Gas	Gas	Gas	Gas	Gas	Gas	G/V	G/V	G/V	St
MW	kg/kmol	28.9	28.9	28.9	28.7	28.7	28.6	28.6	18	18	27.1	27.1	27.1	18
Pressure	bar	1.01	18.2	17.3	16.5	8.23	7.82	1.04	17.3	8.23	7.82	7.52	7.24	0.04
Temperature	°C	15	423	516	1200	952	1200	645	422	422	981	448	283	29
Temperature	K	288	696	789	1473	1225	1473	918	695	695	1254	721	556	302
Flow rate	kg/s	722	722	616	576	627	612	666	10.9	4.15	70.5	70.5	70.5	113
Flow rate	kmol/s	25	25	21.4	20.1	21.9	21.4	23.3	0.6	0.23	2.61	2.61	2.61	6.27
CO_2	vol-%	0.03	0.03	0.03	0.03	0.03	0.03	0.03	2	2	34.7	34.7	34.7	0
O_2	vol-%	20.7	20.7	15.5	15.8	16.2	14.3	14.4	0	0	0	0	0	0
N_2	vol-%	77.3	77.3	82.4	82.1	81.7	83.6	83.2	0.89	0.89	0.28	0.28	0.28	0
Ar	vol-%	0.92	0.92	0.98	0.98	0.97	1	1	0	0	0	0	0	0
H_2O	vol-%	1.01	1.01	1.07	1.07	1.07	1.09	1.09	0	0	65.1	65.1	65.1	1
C_1H_4	vol-%	0	0	0	0	0	0	0	89	89	0	0	0	0
C_2H_6	vol-%	0	0	0	0	0	0	0	7	7	0	0	0	0
C3H8	vol-%	0	0	0	0	0	0	0	1	1	0	0	0	0
C_4H_{10}-i	vol-%	0	0	0	0	0	0	0	0.05	0.05	0	0	0	0
C_4H_{10}-n	vol-%	0	0	0	0	0	0	0	0.05	0.05	0	0	0	0
C_5H_{12}-i	vol-%	0	0	0	0	0	0	0	0.005	0.005	0	0	0	0
C_5H_{12}-n	vol-%	0	0	0	0	0	0	0	0.004	0.004	0	0	0	0
C_6H_{14}	vol-%	0	0	0	0	0	0	0	0.001	0.001	0	0	0	0

- G/V = Gas/Vapour
- St = Steam

Stream data: Single Reheat CLC Steam Cycle (SR-CLCSC)
$T_{oxidation}$=850°C
(Reference Flowsheet: Figure 8.1)

Stream		S1	S2	S3	S4	S5	S6	S7	S8	S9	S10	S11	S12
Phase	Unit	Gas	Gas	Gas	Gas	Gas	Gas	Gas	Gas	G/V	G/V	G/V	G/V
MW	kg/kmol	28.85	28.85	28.85	28.03	28.03	28.03	18.02	18.02	27.05	27.05	27.05	27.05
Pressure	bar	1.32	1.25	1.19	1.13	1.09	1.01	1.25	1.19	1.13	1.09	1.05	1.01
Temperature	°C	15	138	166	850	195	40	10	138	609	233	163	119
Temperature	K	288	411	439	1123	468	313	283	411	882	506	436	392
Flow rate	kg/s	242	242	242	186	186	186	15	15	70.5	70.5	70.5	70.5
Flow rate	kmol/s	8.39	8.39	8.39	6.64	6.64	6.64	0.83	0.83	2.61	2.61	2.61	2.61
CO_2	vol-%	0.03	0.03	0.03	0.03	0.03	0.03	2.00	2.00	34.66	34.66	34.66	34.66
O_2	vol-%	20.74	20.74	20.74	0.09	0.09	0.09	0.00	0.00	0.00	0.00	0.00	0.00
N_2	vol-%	77.30	77.30	77.30	97.40	97.40	97.40	89.00	89.00	0.28	0.28	0.28	0.28
Ar	vol-%	0.92	0.92	0.92	1.16	1.16	1.16	0.00	0.00	0.00	0.00	0.00	0.00
H_2O	vol-%	1.01	1.01	1.01	1.27	1.27	1.27	0.00	0.00	65.06	65.06	65.06	65.06
C_1H_4	vol-%	0.00	0.00	0.00	0.00	0.00	0.00	7.00	7.00	0.00	0.00	0.00	0.00
C_2H_6	vol-%	0.00	0.00	0.00	0.00	0.00	0.00	1.00	1.00	0.00	0.00	0.00	0.00
C3H8	vol-%	0.00	0.00	0.00	0.00	0.00	0.00	0.05	0.05	0.00	0.00	0.00	0.00
C_4H_{10}-i	vol-%	0.00	0.00	0.00	0.00	0.00	0.00	0.05	0.05	0.00	0.00	0.00	0.00
C_4H_{10}-n	vol-%	0.00	0.00	0.00	0.00	0.00	0.00	0.005	0.005	0.00	0.00	0.00	0.00
C_5H_{12}-i	vol-%	0.00	0.00	0.00	0.00	0.00	0.00	0.005	0.005	0.00	0.00	0.00	0.00
C_5H_{12}-n	vol-%	0.00	0.00	0.00	0.00	0.00	0.00	0.004	0.004	0.00	0.00	0.00	0.00
C_6H_{14}	vol-%	0.00	0.00	0.00	0.00	0.00	0.00	0.001	0.001	0.00	0.00	0.00	0.00

Steam/Water Stream		S13	S14	S15	S16	S17	S18	S19	S20	S21	S22	S23	S24
Pressure	bar	0.0	13.3	13.1	13.0	12.9	12.7	12.7	326.8	323.5	320.3	280.0	64.5
Temperature	°C	32	32	66	89	114	147	190	190	222	265	600	365
Temperature	K	305	305	339	362	387	420	463	463	495	538	873	638
Flow rate	kg/s	200	200	200	200	200	200	236	174.5	174.5	174.5	174.5	175

Steam/Water Stream		S25	S26	S27	S28	S29	S30	S31	S32	S33	S34	S35	S36	S37
Pressure	bar	60.0	60.0	51.0	26.0	13.0	5.0	4.8	1.9	0.8	0.3	0.0	12.7	63.8
Temperature	°C	620	602	589	483	385	265	264	172	100	69	32	190	190
Temperature	K	893	875	862	756	658	538	537	445	373	342	305	463	463
Flow rate	kg/s	175	61.5	13.7	8.63	14.3	200	11.9	8.3	7.72	11.1	161	61.5	61.5

Stream data: Double Reheat CLC Steam Cycle (DR-CLCSC)
$T_{oxidation}$=850°C
(Reference Flowsheet: Figure 8.3)

Stream		S1	S2	S3	S4	S5	S6	S7	S8	S9	S10	S11	S12
Phase	Unit	Gas	Gas	Gas	Gas	Gas	Gas	Gas	Gas	G/V	G/V	G/V	G/V
MW	kg/kmol	28.85	28.85	28.85	28.03	28.03	28.03	18.02	18.02	27.05	27.05	27.05	27.05
Pressure	bar	1.32	1.25	1.19	1.13	1.09	1.01	1.25	1.19	1.13	1.09	1.05	1.01
Temperature	°C	15	159	188	850	221	40	10	159	610	257	184	132
Temperature	K	288	432	461	1123	494	313	283	432	883	530	457	405
Flow rate	kg/s	242	242	242	186	186	186	15	15	70.5	70.5	70.5	70.5
Flow rate	kmol/s	8.39	8.39	8.39	6.64	6.64	6.64	0.83	0.83	2.61	2.61	2.61	2.61
CO_2	vol-%	0.03	0.03	0.03	0.03	0.03	0.03	2.00	2.00	34.66	34.66	34.66	34.66
O_2	vol-%	20.74	20.74	20.74	0.09	0.09	0.09	0.00	0.00	0.00	0.00	0.00	0.00
N_2	vol-%	77.30	77.30	77.30	97.40	97.40	97.40	89.00	89.00	0.28	0.28	0.28	0.28
Ar	vol-%	0.92	0.92	0.92	1.16	1.16	1.16	0.00	0.00	0.00	0.00	0.00	0.00
H_2O	vol-%	1.01	1.01	1.01	1.27	1.27	1.27	0.00	0.00	65.06	65.06	65.06	65.06
C_1H_4	vol-%	0.00	0.00	0.00	0.00	0.00	0.00	7.00	7.00	0.00	0.00	0.00	0.00
C_2H_6	vol-%	0.00	0.00	0.00	0.00	0.00	0.00	1.00	1.00	0.00	0.00	0.00	0.00
C3H8	vol-%	0.00	0.00	0.00	0.00	0.00	0.00	0.05	0.05	0.00	0.00	0.00	0.00
C_4H_{10}-i	vol-%	0.00	0.00	0.00	0.00	0.00	0.00	0.05	0.05	0.00	0.00	0.00	0.00
C_4H_{10}-n	vol-%	0.00	0.00	0.00	0.00	0.00	0.00	0.005	0.005	0.00	0.00	0.00	0.00
C_5H_{12}-i	vol-%	0.00	0.00	0.00	0.00	0.00	0.00	0.005	0.005	0.00	0.00	0.00	0.00
C_5H_{12}-n	vol-%	0.00	0.00	0.00	0.00	0.00	0.00	0.004	0.004	0.00	0.00	0.00	0.00
C_6H_{14}	vol-%	0.00	0.00	0.00	0.00	0.00	0.00	0.001	0.001	0.00	0.00	0.00	0.00

Steam/Water Stream		S13	S14	S15	S16	S17	S18	S19	S20	S21	S22
Pressure	bar	0.05	24.48	4.00	23.99	23.75	23.52	23.52	316.70	313.52	310.38
Temperature	°C	32	32	65	89	114	150	220	220	261	295
Temperature	K	305	305	338	362	387	423	493	493	534	568
Flow rate	kg/s	179	179	179	179	179	179	165	165.2	165.2	165.2

Steam/Water Stream		S23	S24	S25	S26	S27	S28	S29	S30	S31	S32
Pressure	bar	280	86.00	84.30	80.00	80.00	51.00	24.00	23.50	24.00	5.37
Temperature	°C	600	405	404	620	620	543	427	426	620	390
Temperature	K	873	678	677	893	893	816	700	699	893	663
Flow rate	kg/s	165.2	165	14.9	150	62.2	11.5	201	21.6	179.4	179.4

Steam/Water Stream		S33	S34	S35	S36	S37	S38	S39	S40
Pressure	bar	5.16	5.00	1.90	0.80	0.03	0.05	23.50	85.00
Temperature	°C	390	390	284	198	114	32	220	220
Temperature	K	663	663	557	471	387	305	493	493
Flow rate	kg/s	10.4	169	6.8	6.4	9.3	146	62.2	14.4

APPENDIX C

(Papers)

Paper I

CHEMICAL LOOPING COMBUSTION-ANALYSIS OF NATURAL GAAS FIRED POWER CYCLES WITH INHERENT CO_2 CAPTURE

Rehan Naqvi, Olav Bolland, Øyvind Brandvoll, Kaare Helle

Published at:

ASME TURBO EXPO 2004, Vienna, Austria, June 14-17, 2004

Paper I is not included due to copyright.

Paper II

PART-LOAD ANALYSIS OF A CHEMICAL LOOPING COMBUSTION (CLC) COMBINED CYCLE WITH CO_2 CAPTURE

Rehan Naqvi, Jens Wolf, Olav Bolland

Accepted for publication in:

Energy-The International Journal

PART-LOAD ANALYSIS OF A CHEMICAL LOOPING COMBUSTION (CLC) COMBINED CYCLE WITH CO_2 CAPTURE

Rehan Naqvi* **and Olav Bolland**
Norwegian University of Science and Technology (NTNU)
Department of Energy and Process Engineering
NO-7491 Trondheim
Norway
Jens Wolf
Vattenfall R&D Corporation
SE-16287 Stockholm
Sweden

ABSTRACT
This paper presents part-load evaluation of a natural gas-fired Chemical Looping Combustion (CLC) combined cycle with CO_2 capture. The novel combined cycle employs an air-based gas turbine, a CO_2-turbine and a steam turbine cycle. In this combined cycle, the CLC reactors replace combustion chamber of the gas turbine. The proposed combined cycle has a net plant efficiency of about 52.2% at full-load, including CO_2 compression. The part-load evaluation shows that reducing the load down to 60% results in an efficiency drop of 2.6%-points. However, the plant shows better relative part-load efficiency compared to conventional combined cycles. The pressure in CLC-reduction and -oxidation reactors is balanced by airflow control, using a compressor equipped with variable guide vanes. A combination of control strategies is discussed for plant start-up and shut-down and for part-load when airflow reduction is not practically possible with current generation of compressors. The results show that the combined cycle has a promising efficiency even at part-load; however, it requires an advanced control strategy.

INTRODUCTION

Carbon dioxide is the most prevalent of man-made emissions of greenhouse gases. Power plants combusting fossil fuels are a major source of CO_2 release. Natural gas is the cleanest of fossil fuels and its combustion in power plants results in CO_2 emissions per kWh electricity below half to that of that coal. This paper presents off-design evaluation of a natural gas fired combined cycle power plant with CO_2 capture. The plant is based on Chemical Looping Combustion instead of a conventional combustor.

Chemical Looping Combustion (CLC) was proposed by Richter and Knoche [1] in 1983 for the first time. CLC is a novel concept of power production with inherent CO_2 capture. In CLC, unlike a conventional combustion process, combustion takes place without any direct contact between air and fuel. Combustion is split up into intermediate oxidation and reduction reactions. A certain metal oxide as oxygen carrier circulates between the two reactors, as depicted in Fig. 1. In a reduction reactor (RED), fuel reacts with oxygen in the metal oxide in a stoichiometric ratio thereby reducing the metal oxide to metal. The reduction reaction is given by Eq. (1).

$$C_nH_{2n+2} + mMeO \rightarrow nCO_2 + [n+1]H_2O + mMe \quad (1)$$

*Corresponding author: Phone: +47 73596894, Fax: +47 73598390, E-mail: rehan.naqvi@ntnu.no

The reduced metal circulates to the oxidation reactor (OX), carrying with it the chemical energy in the fuel. In the oxidation reactor, oxygen in the air oxidises the metal back to metal oxide. The oxidation reaction is given by Eq. (2).

$$mMe + \left(\frac{m}{2}\right)O_2 \rightarrow mMeO \qquad (2)$$

The metal oxide circulates back into the reduction reactor, transports oxygen to the fuel through reduction as well as provides heat for the endothermic reduction reaction. Equation (3) gives the net exothermic reaction.

$$C_nH_{2n+2} + \left[\frac{3n+1}{2}\right]O_2 \rightarrow nCO_2 + [n+1]H_2O \qquad (3)$$

In Eqs. (1), (2) and (3), MeO is metal oxide, Me is a reduced metal, C_nH_{2n+2} is an alkane fuel molecule, while 'n' and 'm' are stoichiometric factors.

The oxidation of the metal is exothermic and the oxygen depleted air is available at high temperature and pressure (in case of a pressurised reactor), and can be utilised for power production. The hot CO_2-rich exhaust stream can also be utilised for power generation, either by expansion or steam generation. The CO_2-rich exhaust stream can afterwards be condensed to separate water and CO_2 is compressed. In this way the energy penalty for CO_2 separation and compression is lower than a conventional power plant where CO_2 is diluted with other combustion products [2].

The metal oxide performance is vital to the process. The metal oxide should be mixed with an inert stabiliser to provide adequate mechanical stability and improved chemical reactivity. So far, investigations have been made for iron oxide [3] and various other metal oxides [4] (Ni, Cu, Mn, Co). Out of all, nickel oxide (NiO) exhibits the most promising properties [5] and the present work uses NiO supported on $NiAl_2O_4$ (60% NiO by mass).

CYCLE DESCRIPTION

Figure 2 presents the schematics of the proposed CLC combined cycle with CO_2 capture. The cycle has a unique feature that it has two turbines in a Brayton type cycle; an air-based gas turbine and a CO_2-turbine. It is assumed that the air turbine drives the compressor. The high temperature/pressure oxygen-depleted air at the air reactor (OX) exit enters the air turbine. Cooling air for the turbine is drawn from the compressor. The air turbine exhaust is used to generate steam in a heat recovery steam generator. The high pressure (HP) and low pressure (LP) steam is expanded in a steam turbine. The CO_2-rich stream from the fuel reactor (RED) expands in the CO_2-turbine. The CO_2-turbine exhaust is used to pre-heat the fuel in the fuel preheater. The exhaust is then fed to the CO_2 dehydration and recompression process. The power plant is configured to give large power output (>300 MW) under varying conditions to achieve a reasonable thermodynamic design which can further be analysed under off-design mode. The computational assumptions used in the present work are given in the appendix.

MODELLING BACKGROUND

The steady-state generic models of the air compressor, fuel recuperator, reactor system, air turbine and the CO_2-turbine were developed and implemented in the simulation tool gPROMS [6]. The cooling penalty for the air turbine was determined by incorporating a cooling model [7]

into the air turbine model. The CO_2-turbine works at relatively lower temperatures and was assumed to be uncooled. The steam cycle was simulated in GTPRO/GTMASTER [8]. The CO_2 compression process was simulated in PRO/II [9]. The reactor system model is based on two sub-models; a mass and energy balance model [10] and a model considering the hydrodynamic behaviour of the reactors by involving reactors geometry. In off-design mode, the compressor operates according to characteristic map of a large axial compressor. The off-design behaviour of the air and CO_2-turbine is governed according to the choked nozzle equation [11], thus making their performance independent of rotational speed. Equation (4) gives the choked nozzle equation.

$$\overline{FR}^2 = \frac{\left(\overline{P_{in}}^2\right)}{\overline{TIT}} \tag{4}$$

In Eq. (4):

$\overline{FR}$ is dimensionless flowrate at the turbine inlet, given as:

$$\overline{FR} = \frac{\dot{m}}{\dot{m}_0}$$

$\overline{P_{in}}$ is the dimensionless turbine inlet pressure, given as:

$$\overline{P_{in}} = \frac{P_{in}}{P_{in0}}$$

$\overline{TIT}$ is dimensionless turbine inlet temperature, given as:

$$\overline{TIT} = \frac{TIT}{TIT_0}$$

Each dimensionless variable is defined as the ratio between the variable at a certain operating point and its value at the design point. Hence, in all the above expressions for the dimensionless variables, numerator corresponds to a certain operating point and denominator corresponds to the design point.

Reactor System

The reactors should be capable of not only transporting the required amount of solids but also providing necessary solids conversion rate. The concept of circulating fluidised bed reactor (CFBR) was proposed by Lyngfelt [12] and the present work employs the same. Figure 3 presents the schematics of the reactor system.

In this work, the CLC-reactor system design is based on certain simplifications and assumptions yet sufficient details have been maintained to predict its behaviour under load-varying conditions. It is assumed that the solids leaving the air reactor are fully oxidised, homogenously mixed and in thermal equilibrium with the air leaving the reactor [13]. The solids at the fuel reactor exit are also assumed in thermal equilibrium with the exhaust (CO_2/H_2O) stream [13]. The degree of solids reaction (X) in the air and fuel reactor is defined by Eq. (5).

$$X = \frac{m - m_{red}}{m_{ox} - m_{red}} \tag{5}$$

In Eq. (5), m_{red} is mass of metal oxide when it is fully reduced and m_{ox} is its mass when it is fully oxidised; while m stands for mass of metal oxide at a certain time. Hence, $X_{red}=0$ for complete reduction of metal oxide to metal; and $X_{ox}=1$ for complete oxidation of metal to metal oxide.

With a given air reactor diameter resulting in a certain superficial air velocity, flowrate of solids lifted from bottom of the air reactor can be calculated by Eq. (6).

$$\dot{m}_{lift} = A_a \cdot \rho_s \cdot \varepsilon \cdot \left(u_0 - u_T\right) \tag{6}$$

In Eq. (6), A_a is cross-sectional area of the air reactor, ρ_s is average density of solids and ε is average solids fraction in the air reactor; while u_0 and u_T are superficial air velocity and terminal falling velocity of solids, respectively. The superficial air velocity and terminal falling velocity of solids are calculated by Eqs. (7) and (8), respectively.

$$u_0 = \frac{\dot{m}_{air}}{A_a \cdot \rho_{air}} \tag{7}$$

$$u_T = \left[\frac{4 \cdot g \cdot d_p}{3 \cdot C_D} \cdot \left(\frac{\rho_s}{\rho_{air}} - 1\right)\right]^{1/2} \tag{8}$$

In Eq. (7), u_0 is the superficial air velocity and $\dot{m}_{air}$ is the air flow at the air reactor inlet. In Eq. (8), g is acceleration due to gravity, d_P is average diameter of solids, ρ_{air} is the air density and C_D is drag coefficient, which is calculated by Eq. (9).

$$C_D = \frac{a_1}{Re_T^{\,b}} \tag{9}$$

The constants a_1 and b were calculated according to Howard [14].

In Eq. (9), Re_T is Reynolds Number of solids at terminal falling velocity given by Eq. (10).

$$Re_T = \frac{u_T \cdot d_p \cdot \rho_{air}}{\mu} \tag{10}$$

In Eq. (10), μ is dynamic viscosity of air. In the riser (air reactor), there is a certain internal recirculation of the solids. The internal recirculation ratio (I) is given by Eq. (11).

$$I = 1 - R \tag{11}$$

In Eq. (11), R is the entrainment ratio defined as:

$$R = \frac{\dot{m}_{ox}}{\dot{m}_{lift}} \tag{12}$$

In Eq. (12), $\dot{m}_{lift}$ is flowrate of solids lifted by the air at the bottom of the air reactor while $\dot{m}_{ox}$ is flowrate of fully oxidised solids (pure NiO) and inert stabiliser. Equations (11) and (12)

suggest that internal recirculation of solids increases with decrease in the entrainment of solids out of the reactor. Internal recirculation of solids results in an increased overall solid fraction (ε in Eq. 6) in the air reactor.

This work defines the overall solids fraction in the air reactor as given by Eq. (13):

$$\varepsilon = \frac{(2 - R) \cdot \varepsilon_{se}}{R} \tag{13}$$

In Eq. (13), ε_{se} is solid fraction at exit of a pneumatic transport reactor. This is typically in the range of 0.001-0.003 and is assumed to be 0.0015. According to Eq. (12), at R=0, there is no particle entrainment and hence the reactor behaves as a steady-state fluidised bed. And when R=1, all the solids are entrained i.e. transported out of the reactor in a single pass and hence there is no internal recirculation of solids. The entrainment ratio, R is a function of the difference in superficial velocity and solids terminal velocity, say; $\Delta u = u_0 - u_T$. Entrainment ratio increases with an increase in superficial velocity until a threshold point is reached where all the solids are blown out of the reactor without any internal recirculation. The difference in the two velocities at the threshold point is denoted as Δu_{TH} and is assumed to be 2.5, which is fairly realistic for a pneumatic transport reactor. After the threshold point, an increase in superficial air velocity has no effect on internal recirculation and a continuous pneumatic transport prevails. This phenomenon is expressed in the form of Eq. (14) and Fig. 4.

$$R = \begin{cases} \dfrac{1}{\Delta u_{TH}} \Delta u & \Delta u - \Delta u_{TH} < 0 \\ 1 & \Delta u \geq \Delta u_{TH} \end{cases} \tag{14}$$

The air reactor hold-up (M_a) of solids is calculated as:

$$M_a = A_a \cdot H_a \cdot \rho_s \cdot \varepsilon \tag{15}$$

In Eq. (15), A_a and H_a are the cross-sectional area and height of the air reactor, respectively. Mean residence time of the solids in the air reactor (τ_a) is then calculated by Eq. (16).

$$\tau_a = \frac{M_a}{\dot{m}_{lift}} \tag{16}$$

Mean residence time of solids in the fuel reactor (τ_f) is calculated on the basis of average flowrate of solids entering and exiting the fuel reactor, given by Eq. (17).

$$\tau_f = \frac{2 \cdot M_f}{\dot{m}_{red} + \dot{m}_{ox}} \tag{17}$$

In Eq. (17), M_f is solids mass in the fuel reactor given as:

$$M_f = A_f \cdot H_f \cdot \rho_s \cdot \varepsilon_f \tag{18}$$

In Eq. (18), A_f and H_f are the cross-sectional area and height of the fuel reactor, respectively. ε_f is the average solids fraction in the fuel reactor and is assumed to be 0.4 which is typical for a fluidised bed reactor. The present work is based on a constant ε_f under various load and flow conditions, which means that the fuel reactor is assumed to remain fluidised regardless of the load- and eventual flow conditions.

Pressure drop in the air and fuel reactor is calculated by Eq. (19).

$$\Delta P = \Delta P_B + \Delta P_D \tag{19}$$

In Eq. (19), ΔP_B and ΔP_D are pressure drop in the fluidised bed and pressure drop caused by gas distributors, respectively. The pressure drop over the fluidised bed (ΔP_B) is calculated by using Eq. (20) which is derived from the hydrodynamics described by Carberry and Varma [15] & Kunii and Levenspiel [16].

$$\Delta P_B = 1.2 \cdot \frac{M \cdot g}{A} \tag{20}$$

In Eq. (20), M is hold-up of the solids in air or fuel reactor, g is acceleration due to gravity and A is cross-sectional area of the reactor.

Pressure drop due to the gas distributors is given as:

$$\Delta P_D = 0.4 \cdot \Delta P_B \tag{21}$$

The pressure drop in cyclones is assumed to be constant at 20 mbar.

The definitions of net plant efficiency and specific work used in the present work are given by Eqs. (22) and (23), respectively.

$$\eta_{net} = \frac{\left(\left(\dot{W}_{GT} + \dot{W}_{CO_2-T} + \dot{W}_{ST} - \dot{W}_{comp.}\right) \cdot \eta_{m+g+aux}\right) - \dot{W}_{CO_2-comp.}}{\dot{m}_{fuel} \cdot LHV} \tag{22}$$

$$w = \frac{\left(\left(\dot{W}_{GT} + \dot{W}_{CO_2-T} + \dot{W}_{ST} - \dot{W}_{comp.}\right) \cdot \eta_{m+g+aux}\right) - \dot{W}_{CO_2-comp.}}{\dot{m}_{air}} \tag{23}$$

In Eqs. (22) and (23), $\dot{W}_{GT}, \dot{W}_{CO_2-T}, \dot{W}_{ST}, \dot{W}_{comp.} \dot{W}_{CO_2-comp.}, \eta_{m+g+aux}$ are the gas turbine work, CO_2-turbine work, steam turbine work, compressor work, CO_2 compression work and the efficiency (mechanical, generator, auxiliaries), respectively.

For the sake of part-load evaluation, the terms Relative Load (L_R) and Relative Net Plant Efficiency (η_{rel}) are defined, given by Eqs. (24) and (25), respectively.

$$L_R = \frac{\dot{W}}{\dot{W}_0} \tag{24}$$

$$\eta_{rel} = \frac{\eta}{\eta_0} \quad (25)$$

In Eq. (24), $\dot{W}$ and $\dot{W}_0$ are the net plant power output of a combined cycle at part-load and full-load, respectively; whereas in Eq. (25), η and η_0 are the net plant efficiency of a combined cycle at part-load and full-load, respectively.

The definition of the relative power (W_R) for the air turbine, CO_2-turbine, steam turbine and the CO_2 compression plant is given by Eq. (26).

$$\text{Relative power} = \frac{\dot{W}_i}{\dot{W}_{i,0}} \quad \text{(i=turbine or compression plant)} \quad (26)$$

In Eq. (26), $\dot{W}_i$ and $\dot{W}_{i,0}$ are the power of a turbine or the compression plant at part-load and full-load, respectively.

In order to compare part-load performance of the CLC combined cycle with conventional combined cycles, two state-of-the-art gas turbines are selected; Mitsubishi 7G and GE 9FA, and implemented in combined cycle. The part-load results for the conventional cycles were obtained by simulations in GTMASTER [8].

This work assumes that the CO_2-dehydration and compression plant separates all the produced CO_2 from water and compresses it to the final delivery pressure at all the load conditions.

METHODOLOGY

Thermodynamic Analysis

In order to analyse a power cycle under off-design mode, it is essential to have a reasonable thermodynamic design. Once the thermodynamic design is achieved, the key cycle components are dimensioned. The cycle hardware parameters are fixed in the off-design mode and only the load condition is varied. A sensitivity study of the key cycle parameters was carried out to thermodynamically analyse the CLC combined cycle and a design point was established. Under the thermodynamic analysis, the reactor system was based on certain assumptions. Pressure drop in both the reactors was calculated in accordance with Eq. (19) for the oxidation temperature of 1200°C and compressor pressure ratio of 18. The same pressure drop percentage was used during the thermodynamic analysis under all conditions. It was also assumed that the internal solids of both the reactors are well-mixed, and the exiting solid streams are in thermal equilibrium with the corresponding outlet gaseous streams. It was assumed that 100% of the solids entering the air reactor are converted (oxidised) while only 70% of the solids entering the fuel reactor are converted (reduced). According to Lyngfelt [5], the theoretical thermodynamic limit of NiO to convert fuel is 99.5%. However, 100% fuel conversion was assumed in this work. The net plant efficiency includes CO_2 compression penalty and losses (mechanical, generator, auxiliaries), as given in Eq. (22).

Figure 5 presents the net plant efficiency as a function of specific work for different values of compressor pressure ratio (PR) and TIT values. The term TIT refers to the air reactor exit temperature. The simulation results showed that the proposed CLC combined cycle can achieve a net plant efficiency of about 52.2% at TIT=1200°C and compressor pressure ratio (PR) of 18. There is a certain air and fuel flow at the condition of TIT=1200°C and PR=18 resulting in the

design-point full load. The CLC-reactors are then dimensioned to achieve the required solids transport between the two reactors at the design-point air and fuel flow conditions. Table 1 presents the cycle summary at the full-load design point. It can be seen in Table 1 that at the full-load, solids entrainment ratio is 0.25. This means that 25% of the solids are entrained out of the air reactor, or in other words, 75% of the solids entering the air reactor are internally recirculated. The solids entrainment ratio and internal recirculation ratio at the design point are also mentioned on Fig. 4. The cycle is designed in such a way that a degree of reduction X_{red}=0.3 is achieved at full-load. This means that at the design point, the fuel reactor can convert 70% of the NiO supplied to the fuel. The solids residence time in the fuel reactor is 156 sec at full-load, which is sufficient to achieve this degree of reduction [13].

Part-load Scenario

In order to meet the load demand and to fulfil certain plant criteria, different control strategies can be adopted. It is important to identify the most important plant criteria to be satisfied before any control strategy can be devised. In the cycle under study, the most critical criterion is to achieve the same pressure at the exit of the two CLC-reactors.

Reactors exit pressures

It is of utmost importance to maintain the same pressure of the gases in the ducting that connects the CLC-reactors for solids transport. This duct is necessarily that through which the solids separated from the oxygen-depleted air in the cyclone system, fall down to the fuel reactor. In case of any pressure difference occurring in the ducting, gas may leak between the two reactors. Such conditions are highly undesirable because the main idea behind the Chemical Looping Combustion is to keep the air and the fuel streams separated from each other. The proposed reactor system consists of the air reactor essentially being a pneumatic transport reactor with air as the oxidising agent. The fuel reactor is the bubbling fluidised bed with natural gas as the reducing agent. Due to its pneumatic transport nature, the air reactor has a lower pressure drop compared to the fuel reactor. The power plant is configured in such a way that the oxygen-depleted air at the air reactor exit and the CO_2-rich exhaust at the fuel reactor outlet are at the same pressure at the design point. As soon as the plant operates off design, a pressure difference will occur at the reactors exit unless a control strategy is adopted. The occurrence of this pressure gradient is the consequence of the presence of the presence of two turbines; the air turbine and the CO_2-turbine, both resulting in different inlet pressures at part-load. Since the turbines are assumed choked, the pressure requirements at the inlet of the two turbines differ. Since the reduction reactor has a larger pressure drop, the CO_2-turbine inlet pressure will be lower than the air turbine inlet pressure. The plant then needs to be controlled in such a way that the pressure at the air turbine inlet becomes equal to that at the CO_2-turbine inlet. If uncontrolled, the oxygen-depleted air will entrap into the fuel reactor coming in direct contact with the fuel, thereby upsetting the stoichiometric reactions and resulting in undesired dilution of the CO_2 with nitrogen and oxygen. In order to cope with this problem, the present work employs a compressor with variable inlet guide vanes (VGVs). At a certain off-design operating point, the variable guide vanes are closing by a certain degree. This changes the compressor geometry and reduces the air flowrate through it. The result is a reduced air turbine inlet pressure in accordance with the CO_2-turbine inlet pressure.

The Part-load Strategy

The control strategy for the CLC combined cycle at part-load focuses on two major issues: the use of variable guide vane angles (VGV) at the compressor inlet in order to reduce the air flowrate, influencing the pressure through the air-side of the cycle to avoid pressure difference between the two reactors; and the fuel flowrate reduction in order to meet the load

requirements. Under part-load operation, the air flowrate is reduced at the compressor inlet by means of VGVs in order to fulfil the pressure balancing between the two reactors. The air flowrate reduction affects the solids transport out of the air reactor. The present work assumes complete oxidation in the air reactor regardless of the load condition; however the degree of reduction rate in the fuel reactor depends on the amount of solids eventually transported out of the air reactor and reacting with the fuel in the fuel reactor. This work assumes that all the fuel reacting with the solids is converted at any time. In parallel with the air flowrate reduction, the fuel flowrate reduction results in decrease in the oxidation temperature in the air reactor with subsequent reduction in the air turbine inlet temperature. This also results in decreased temperature in the fuel reactor with subsequent drop in the CO_2-turbine inlet temperature. Therefore, quite contrary to the conventional combined cycle power plants, the control strategy does not emphasise on maintaining a constant turbine inlet temperature or turbine exit temperature.

RESULTS AND DISCUSSION

Part-load Performance

The results show that by reducing the load down to 60%, net plant efficiency of the CLC combined cycle drops by 2.6%-points. This work however emphasises on the part-load behaviour of the CLC combined cycle and its comparison with the conventional combined cycles. Therefore, it is appropriate to present the part-load performance in terms of the relative net plant efficiency, defined in Eq. (24). Figure 6 compares the relative net plant efficiency of the proposed CLC combined cycle with two conventional combined cycles at varying relative load. The relative net plant efficiency of the CLC combined cycle at part-load is better in comparison with conventional combined cycles. This can be explained with the help of an overall analysis of the cycle key parameters at part-load. Table 2 presents the cycle summary for various values of relative load, in terms of the key cycle parameters data.

When the plant operates at part-load, two main changes take place simultaneously; the air flow reduction at the compressor inlet for balancing the CLC-reactor pressures, and the fuel flowrate reduction to reduce the air turbine inlet temperature (TIT) for fulfilling the load demand. The part-load analysis of the CLC combined cycle presented in Table 2 shows that despite the reduction in the air turbine inlet temperature, the turbine exit temperature increases at part-load. This effect is due to the successive reduction in the compressor pressure ratio in order to match with the pressure requirements in the CLC-reactors. This implies that the steam cycle work is not reduced to the same extent as that of the air turbine and the CO_2-turbine at part-load. The steam cycle part-load performance is hence better compared to the air turbine and the CO_2-turbine. Therefore, due to the comparatively better performance of the steam cycle, the relative net plant efficiency of the CLC combined cycle is better as compared to the conventional combined cycles. It can be seen that despite a reduced flue gas flowrate to the HRSG, the reduction in the HP and LP steam production does not drop appreciably and hence the steam cycle relative power output is higher at part-load. The air turbine and CO_2-turbine power output, on the other hand, decrease more rapidly at part-load compared to the steam turbine work. A comparison of the relative power of the three turbines reveals that at a certain part-load, the steam turbine has the highest relative power followed by the air turbine, while CO_2-turbine has the lowest relative power. Since, the fuel flow is reduced at part-load; the CO_2-production also decreases thus resulting in relatively lower power demand for the CO_2 compression process. The CO_2 compression plant relative power is slightly lower than that of the steam turbine, at different values of relative load. The CO_2-turbine exit temperature, like that of the air turbine, also increases with decrease in load. Since, the CO_2-turbine exhaust preheats the fuel; the consequence is that the fuel preheating temperature increases at part-load, as shown in Table 2.

Another factor that has a slightly positive impact on the part-load performance of the CLC combined cycle is the fuel flowrate at part-load. The results show that reduction in the fuel flowrate at part-load is slightly greater in the CLC combined cycle compared to that in the conventional cycles; which also contributes towards the better relative part-load efficiency.

Figure 7 presents air flowrate as a percent of the design point flowrate at varying load. It is seen in Fig. 7 that decreasing the load down to 56% results in 60% air flow reduction. Modern compressors are equipped with VGVs that can reduce the flowrate from 100% to typically 60%. Therefore, according to Fig. 7, the plant cannot be controlled with the proposed control strategy below part-load of 56% when air flow reduction is limited to 60%. This implies that this strategy is not valid for the plant start-up and shut-down as well. This conclusion calls for the need to investigate alternative control strategies. There are diverse control strategies that can be employed in combination with one another at different load conditions. The system can also be controlled from the start-up to the 56% load by using VGVs as well as taking extra bleeds from the compressor thereby reducing the flowrate through the air reactor and regulating the pressure. Another possibility is to throttle the air after the compressor exit but it may cause surge problems. While the major focus of the afore-mentioned schemes is controlling the air-side of the plant, there is certain degree of freedom to manipulate with the fuel/exhaust-side. Exhaust from the fuel reactor can be throttled and an innovative solution to the problem is to introduce VGV in the first row of the CO_2-turbine.

The cycle can also be simplified by avoiding the CO_2-turbine and generate steam in a condenser via heat recovery from the pressurised exhaust stream. This is beneficial in the terms that it is easier to control the pressure in a condenser as compared to that at a turbine inlet. The system can also utilise the exhaust stream for air preheating after the compressor prior to its entry into the air reactor.

There are a number of parameters that influence the CLC-reactors' performance. The solids entrainment ratio, internal recirculation, the air flowrate and pressure in the air reactor are all inter-dependent quantities. Therefore, it can be inferred that variation in one entity will inevitably lead to variation in the other.

This can be seen in Table 2 that reducing the load down to 54% results in a decreased entrainment ratio of 0.19 compared to that at full-load i.e. 0.25. In Table 2, the difference between superficial velocity of air and terminal velocity of particles ($\Delta u=u_0-u_T$) is also presented. This can be seen that with load reduction, this difference decreases. The superficial air velocity is a function of air flowrate that decreases at part-load, thereby resulting in a relatively lower superficial air velocity (u_0). While the solids terminal falling velocity (u_T) does not vary to a large extent, at part-load, and hence the difference between u_0 and u_T, i.e. Δu decreases with load reduction. According to the definition of solids internal recirculation ratio, presented in Fig. 4, the lower the Δu the higher is the solids internal recirculation ratio. Since, the solids entrainment ratio and the solids internal recirculation are directly linked with the amounts of solids being transported out of the air reactor; it can be stated that the solids residence time in the air reactor is also a function of the solids entrainment ratio. While the solids residence time in the fuel reactor depends on the difference between the amount of solids entering and leaving the reduction reactor. Figure 8 presents the residence time of solids in the air and fuel reactor at varying load. The solids residence time in the air reactor increases from 47 sec at full-load to 64 sec at about 54% load. The solids residence time in the fuel reactor, on the other hand, increases from 156 sec at full-load to 199 sec at 54% load. This appreciably higher solids residence time in

the fuel reactor compared to that in the air reactor is due to the bubbling fluidised bed nature of the fuel reactor.

The increased solids residence time in the air reactor results in an increased pressure drop. It can be seen in Table 2 that the air reactor pressure drop increases with the load reduction that is due to an increased residence time and hold-up of solids in the air reactor, at part-load.

However, there is a different scenario in the fuel reactor. The current work is based on the assumption of a consistent average solids fraction (ε_f=0.4) in the fuel reactor. This assumption was made for the sake of simplicity and ease of the calculation procedure for the reduction reactor behaviour estimation. This assumption necessarily maintains the condition that the reduction reactor remains fluidised at all the operating conditions. The solids hold-up is a function of the reactor dimensions, the solids density and the average solids fraction. Since the reactors' dimensions are fixed and the average solids density remains constant as well, a consistent solids fraction in the reduction reactor results in a constant solids hold-up regardless of the operating conditions. The average solids residence time is calculated in the basis of the hold-up and the average of the solids flowrates entering and exiting the fuel reactor. In spite of the constant hold-up the residence time of solids changes because the amount of solids entering and leaving the fuel reactor changes at part-load in accordance with the air and the fuel flowrate. But nevertheless, the fuel reactor pressure drop is a function of the reactor dimensions, acceleration due to gravity and solids hold-up, all three quantities being constant at all the points. Therefore, it can be seen in Table 2 that there is a constant pressure drop of 316 mbar in the fuel reactor under all the operating conditions. In reality, the solids fraction will change according to the flow conditions and must be accounted for the changes and determined at different conditions. This fact does imply that during the operation a condition may occur when the bed tends to defluidise. This means that the reactor will start behaving like a fixed bed and there will be no more transport of solids out of the reactor. In other words, the system will collapse. This problem can be dealt with by adopting control techniques at the fuel/exhaust side, as discussed previously.

This work is based on the assumption of complete oxidation of solids in the air reactor independent of the load- and flow conditions. The solids reduction in the fuel reactor is however calculated on the basis of the solids entering and leaving the fuel reactor. Table 2 also includes the results for the solids rate of reduction (X_{red}) in the fuel reactor at different values of relative load. The results show that the solids conversion in the fuel reactor decreases by 18% by decreasing the load down to 54%. At full-load X_{red}=0.3 i.e. 70% of the solids are reduced while at a load factor of 0.54, X_{red}=0.48 i.e. 52% of the solids are reduced. In this work, the reduction rate (solids conversion) is a function of the fuel supplied and the difference between the solids flowrate at the inlet and exit of the fuel reactor. Therefore, despite an increase in the residence time, the solids reduction rate decreases at part-load.

CONCLUSIONS

This work has been the very first attempt to evaluate part-load performance of a CLC combined cycle. With the proposed configuration, the CLC combined cycle can achieve a full-load design point efficiency of 52.2% including CO_2 capture. The part-load analysis of the CLC combined cycle shows that the net plant efficiency drops by 2.6%-points when reducing the load down to 60%. The relative net plant efficiency of the cycle is higher at part-load compared to a conventional combined cycle. This work suggests airflow reduction at compressor inlet in order to balance reactors exit pressure at part-load. Other strategies have also been indicated when airflow reduction alone is not applicable under plant start-up and shut-down and up to 56% of

the full-load. This work concludes that the CLC combined cycle has promising efficiency both at full-load and part-load; however, it exhibits some operational problems at part-load which are described and control strategies to cope with the problems have been suggested.

ACKNOWLEDGEMENTS
This work has been sponsored by the Norwegian Research Council CLIMIT Project.

APPENDIX
Computational Assumptions
Computational assumptions used in the present work are given below.
Ambient Air:
15°C, 1.01325 bar, 60% Relative Humidity
Composition (Mole-%):
N_2 (77.3), O_2 (20.74), CO_2 (0.03), H_2O (1.01), Ar (0.92)
Fuel:
Natural Gas: 10°C, 70 bar, LHV=46503 kJ/kg
Composition (Mole-%):
N_2 (0.89), CO_2 (0.2), CH_4 (89), C_2H_6 (9.4), C_3H_8 (4.7), C_4H_{10} (1.6), C_5H_{12} (0.7)
CLC- Reactors System:
Adiabatic reactors
Mean particle diameter: 150 μm
Average particle density: 2400 kg/m^3
Gas Turbine Cycle:
Compressor:
Polytropic efficiency 91.5%
Turbines: Polytropic efficiency: 86.2%
Air turbine back pressure: 10 mbar
Efficiency $\eta_{m+g+aux}$ (Mech. + gen. + aux.): 96.6%
Steam Cycle
HRSG: 2-Pressure levels: 60 bar, 5 bar
Hot side temperature difference: 20°C
LP temperature: 260°C, Pinch (HP, LP): 10°C
Steam turbine isentropic efficiency: 92%
CO_2 compression:
Polytropic efficiency (stage 1, 2, 3) (%): 85, 80, 75
CO_2 Pump adiabatic efficiency (%): 75
Compressor intercooler exit temperature: 30°C
CO_2 delivery pressure: 110 bar

REFERENCES

[1] Richter HJ, Knoche K. Reversibility of combustion processes, Efficiency and Costing. Second Law Analysis of Processes. In: 1983 ACS symposium, Washington D.C., vol. 235. p. 71-85.

[2] Brandvoll Ø, Bolland O. Inherent CO_2 Capture Using Chemical Looping Combustion in a Natural Gas Fired Power Cycle. Journal of Engineering for Gas Turbines and Power 2004; 126: 316-321.

[3] Mattisson T, Järdnäs A, Lyngfelt A. Reactivity of Some Metal Oxides Supported on Alumina with Alternating Methane and Oxygen-Application for Chemical-Looping Combustion. Energy and Fuels 2003; 17: 643-651.

[4] Mattisson T, Lyngfelt A, Cho P. The use of iron oxide as an oxygen carrier in chemical-looping combustion of methane with inherent separation of CO_2. Fuel 2001; 80: 1953-1962.

[5] Lyngfelt A, Kronberger B, Adánez J, Morin J-X, Hurst P. The Grace Project. Development of oxygen carrier solids for Chemical-Looping Combustion. Design and operation of a 10kW Chemical-Looping Combustor. In: 7th International Conference on Greenhouse Gas Control Technologies (GHGT7), Vancouver, Canada, 2004.

[6] gPROMS® ModelBuilder 2.3.3, ©1997-2004 Process Systems Enterprise Limited.

[7] Bolland O, Stadaas JF. Comparative evaluation of Combined Cycles and Gas Turbine Systems with Water Injection, Steam Injection and Recuperation. ASME Journal of Engineering for Gas Turbines and Power 1995; 117: 138-145

[8] GT PRO/GT MASTER, Version 11.0.2, ©1987-2004, Thermoflow Inc.

[9] PRO/II 6.0, ©1994-2002 Simulation Sciences, Inc.

[10] Naqvi R, Bolland O, Brandvoll Ø, Helle K. Chemical Looping Combustion-Analysis of Natural Gas Fired Power Cycles With Inherent CO_2 Capture. In: Proceedings of ASME Turbo-Expo 2004; Vienna, Austria, 2004; GT2004-53359.

[11] Saravanamuttoo HIH, Rogers GFC, Cohen H. Gas Turbine Theory. England: Pearson Education Limited, 2001.

[12] Lyngfelt A, Leckner B, Mattisson T. A fluidized-bed combustion process with inherent CO_2 separation-application of chemical- looping combustion, Chemical Engineering Science 2000; 56: 3101-3313.

[13] Brandvoll Ø. Chemical Looping Combustion-Fuel conversion with inherent CO_2 capture. Doctoral Thesis 2005; NTNU-Norway.

[14] Howard JR. Fluidized Bed Technology-Principles and Application. Bristol, UK: Adam Hilger, 1989.

[15] Carberry J, Varma A. Chemical Reaction and Reactor Engineering. New York: Dekker, 1986.

[16] Kunii D, Levenspiel O. Fluidization Engineering. USA: Butterworth-Heinemann, 1991.

Figures Captions

Figure 1: **The Chemical Looping Combustion principle**

Figure 2: **Schematics of the proposed CLC combined cycle with CO_2 capture**

Figure 3: **Schematic sketch of the circulating fluidised bed reactor system**

Figure 4: **Entrainment ratio and internal recirculation ratio in the air reactor**

Figure 5: **CLC combined cycle net plant efficiency as a function of specific work**

Figure 6: **Relative net plant efficiency as a function of relative load**

Figure 7: **Air flow reduction as a function of relative load**

Figure 8: **Solids residence time in the air and fuel reactor as a function of relative load**

Figure 1

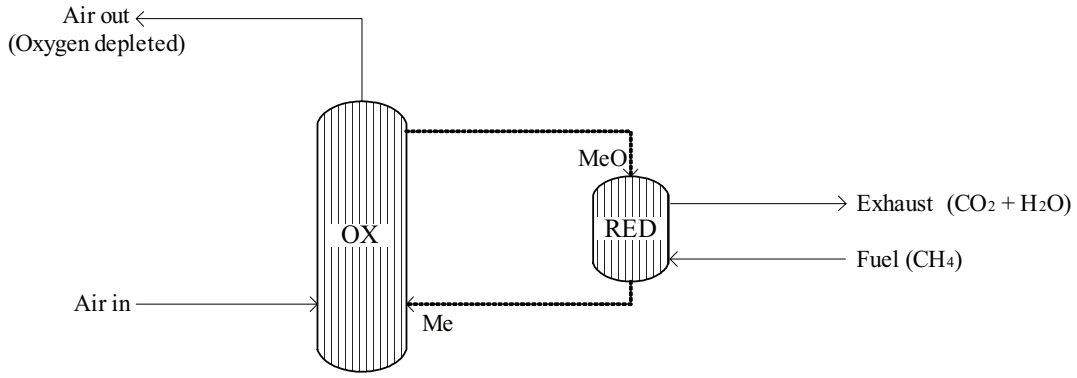

Figure 2

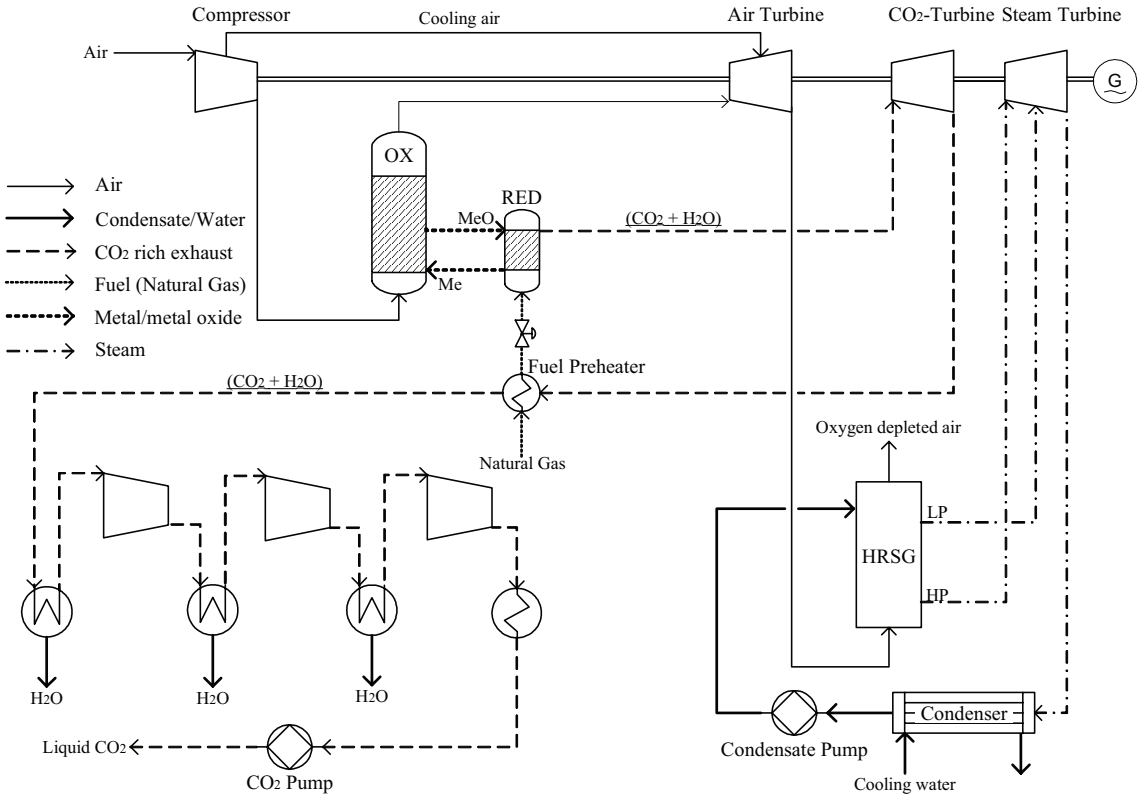

Figure 3

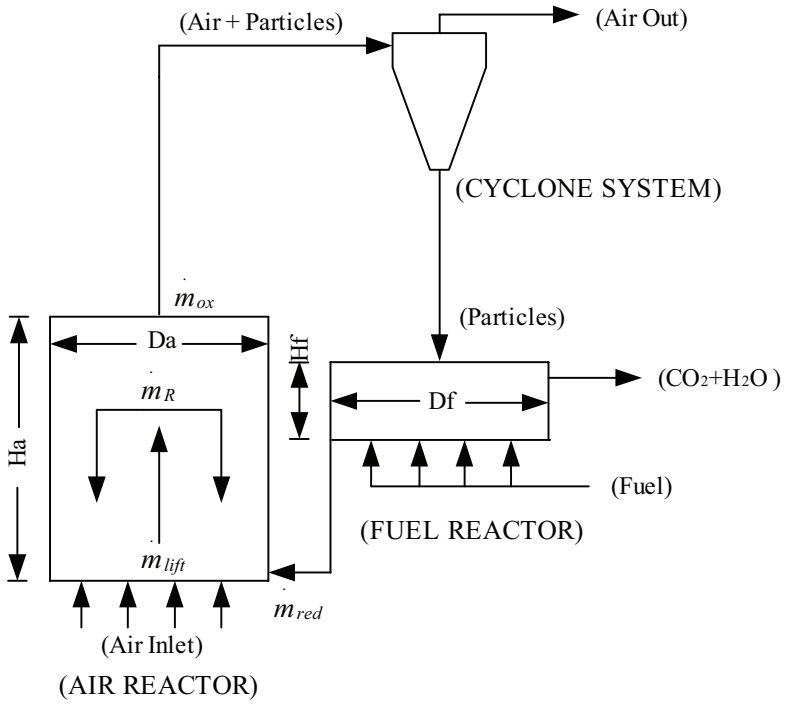

Figure 4

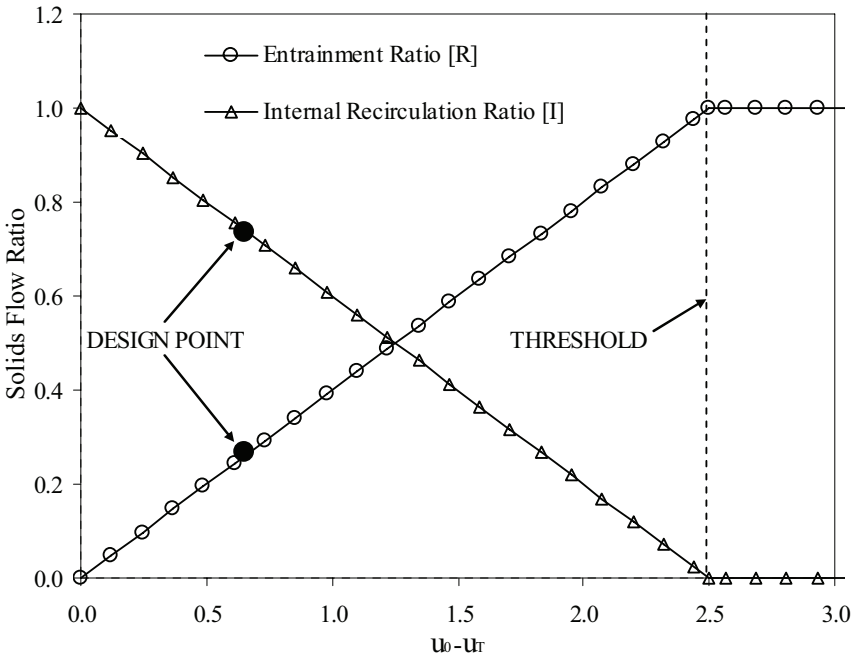

Figure 5

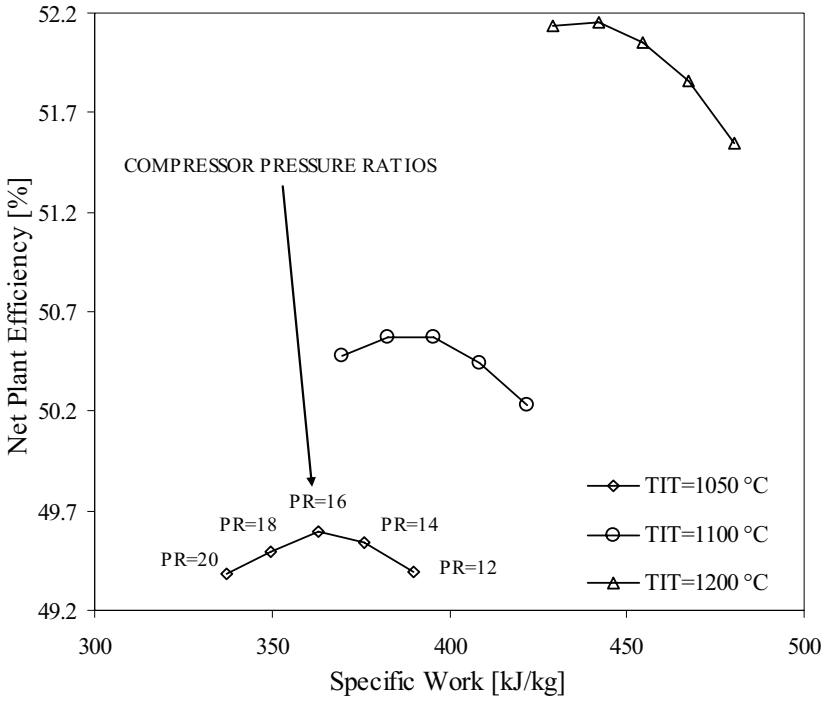

Figure 6

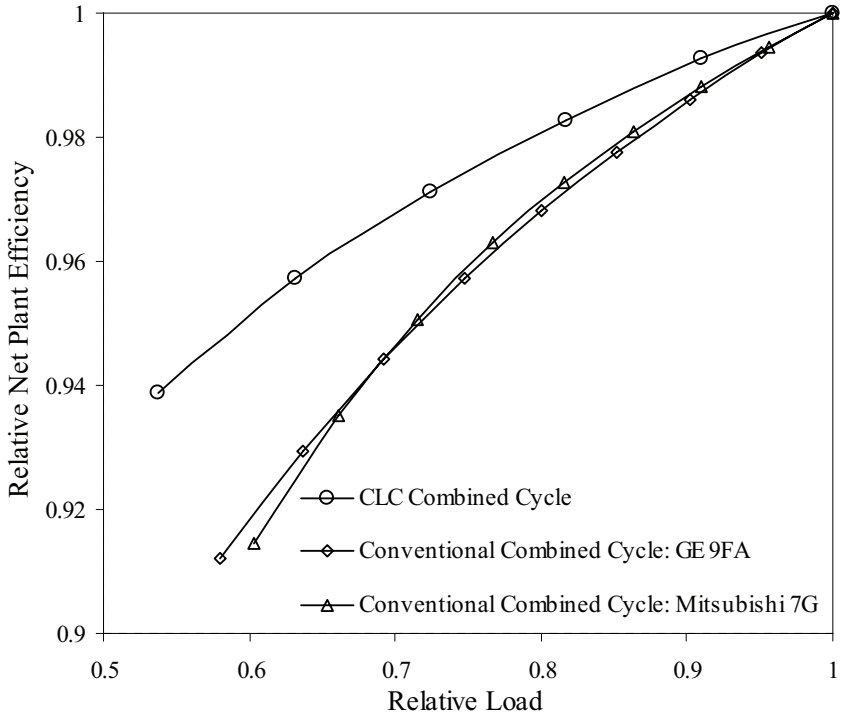

Figure 7

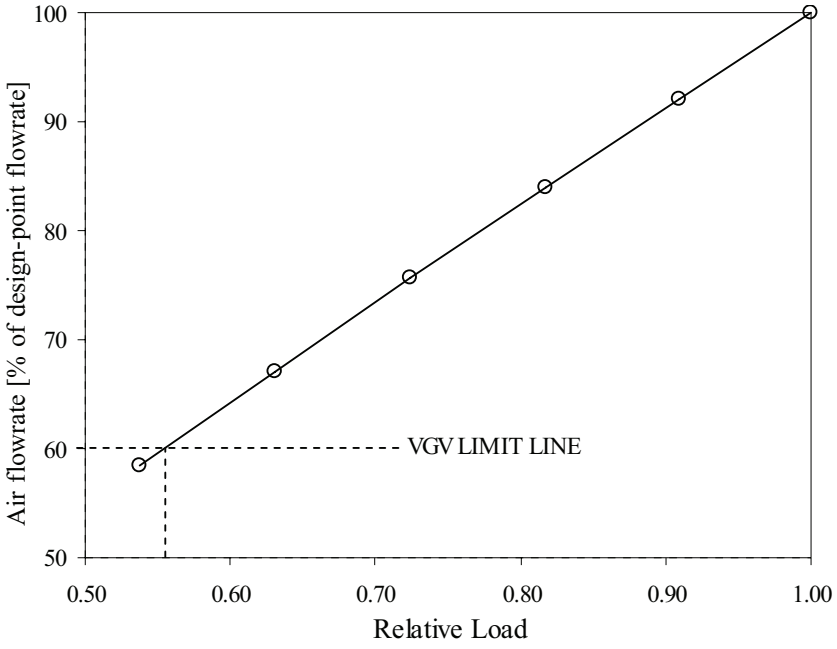

Figure 8

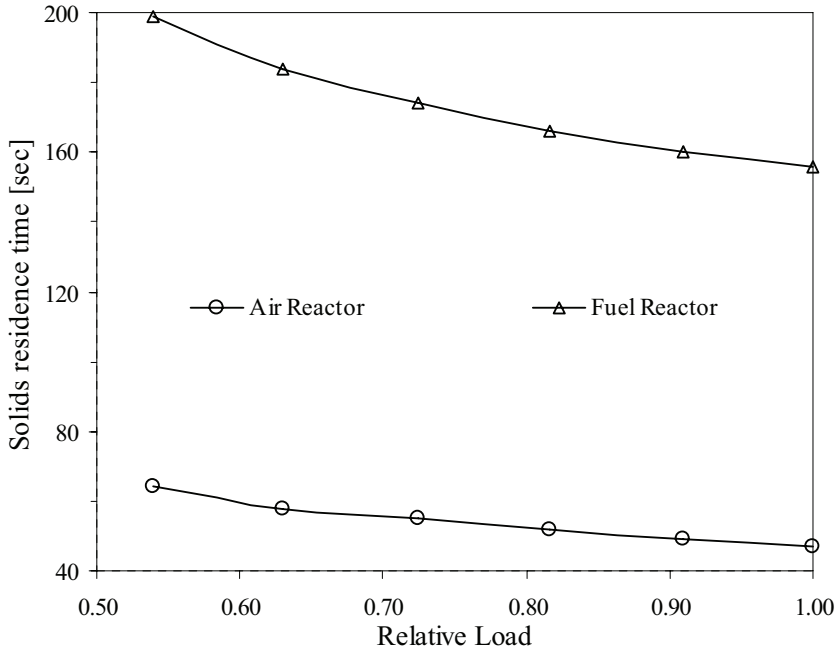

Tables

Compressor		
Compressor pressure ratio		18
Air flow at compressor inlet	kg/s	823
Coolant flow	kg/s	62.5
Air Reactor (+Cyclone)		
Oxidation Temperature	°C	1200
Degree of oxidation (Xox)		1
Reactor diameter	m	14
Reactor height	m	30
Pressure drop	mbar	153
Solids entrainment ratio		0.25
Solids residence time	sec	47
Solids flowrate at inlet	kg/s	556
Solids flowrate at exit	kg/s	616
Fuel Reactor		
Reduction Temperature	°C	980
Reactor diameter	m	8
Reactor height	m	2
Pressure drop	mbar	316
Solids residence time	sec	156
Solids flowrate at reduction reactor exit	kg/s	561
Air Turbine		
Flowrate at turbine inlet	kg/s	768
Tiurbine inlet temperature	°C	1140
Turbine exit temperature	°C	492
Power output	MW	234
Fuel Preheater		
Fuel flow	kg/s	15
Preheating temperature	°C	508
Overall area of heat transfer	m2	1227
Overall heat transfer coefficient [U]	W/m2K	150
Hot-end temperature difference		25
CO_2-Turbine		
Pressure ratio		16.7
Flowrate at turbine inlet	kg/s	70.5
Turbine inlet temperature	°C	980
Turbine exit temperature	°C	533
Power output	MW	53.6
Steam Turbine		
Steam pressure (HP/LP)	bar	60/5
Steam temperature (HP/LP)	°C	467/258
Steam flow (HP/LP)	kg/s	77.3/21.7
Power output	MW	101.5
Power for CO_2 compression	**MW**	**15.4**
Net plant power output	**MW**	**364**
Net plant efficiency	**%**	**52.2**

Table 1: Design-point data for the CLC combined cycle

Relative Load		1	0.91	0.82	0.72	0.63	0.54
Compressor							
Compressor pressure ratio		18	16.3	14.7	13.1	11.6	10
Air flow at compressor inlet	kg/s	823	754	685	615	545	473
Coolant flow	kg/s	62.5	47.1	37	26.7	19.6	13
Air Reactor (+Cyclone)							
Oxidation Temperature	°C	1200	1171	1146	1119	1092	1063
Pressure drop	mbar	153	159	165	173	184	199
u_0-u_T		0.63	0.61	0.59	0.57	0.54	0.5
Solids entrainment ratio		0.25	0.24	0.23	0.22	0.21	0.19
Fuel Reactor							
Fuel flow	kg/s	15	13.7	12.5	11.2	9.9	8.6
Reduction Temperature	°C	980	973	962	948	934	917
Degree of reduction (Xred)		0.3	0.34	0.37	0.41	0.45	0.48
Pressure drop	mbar	316	316	316	316	316	316
Fuel Preheater							
Preheating temperature	°C	508	513	521	528	538	548
Air Turbine							
Tiurbine inlet temperature	°C	1140	1120	1101	1080	1057	1033
Turbine exit temperature	°C	492	497	502	508	516	527
Relative power		1.00	0.90	0.80	0.70	0.60	0.50
CO_2-Turbine							
Pressure ratio		16.7	15.2	13.7	12.2	10.8	9.3
Flowrate at turbine inlet	kg/s	70.5	64.5	58.5	52.5	46.4	40.2
Tiurbine inlet temperature	°C	980	973	962	948	934	917
Turbine exit temperature	°C	533	534	536	542	547	563
Relative power		1	0.88	0.77	0.66	0.55	0.44
Steam Turbine							
HP steam flow	kg/s	77.3	73.5	69.4	65.3	60.5	55.3
LP steam flow	kg/s	21.7	19.1	16.7	14.2	11.8	9.8
Relative power		1.00	0.94	0.88	0.82	0.75	0.67
CO_2 compression-relative power		1.00	0.93	0.84	0.76	0.67	0.58

Table 2: Cycle key parameters at various values of relative load

Paper III

Multi-stage chemical looping combustion for combined cycles with CO_2 capture

Rehan Naqvi and Olav Bolland

Presented at:
GHGT8-The 8th International Conference on Greenhouse Gas Control Technologies, June 19-22, 2006, Trondheim-Norway

Invited for publication in:

International Journal of Greenhouse Gas Control

Multi-stage chemical looping combustion for combined cycles with CO_2 capture

Rehan Naqvi and Olav Bolland

The Norwegian University of Science and Technology (NTNU),
NO-7491 Trondheim, Norway

Abstract

This paper presents application of Chemical Looping Combustion (CLC) method in natural gas-fired combined cycles for power generation with CO_2 capture. A CLC combined cycle, consisting of single CLC-reactor system, an air turbine, a CO_2-turbine and a steam cycle has been designated as the base-case cycle. The base-case cycle can achieve net plant efficiency of 52% at an oxidation temperature of 1200°C. In order to achieve a reasonable efficiency at safer and lower oxidation temperature, reheat is introduced into the air turbine by employing multi-CLC-reactors. The results show that the reheat CLC combined cycles can achieve net plant efficiency of above 51% at oxidation temperature of 1000°C, including CO_2 compression, which is very promising.

Keywords: Chemical Looping Combustion, combined cycle, CO_2 capture, reheat air turbine

Introduction

Chemical Looping Combustion (CLC), proposed by Richter and Knoche [1983], is a novel concept of hydrocarbon fuels energy conversion with inherent CO_2 capture. In CLC, air and fuel remain in separate environments and have no direct contact with each other. The unconventional combustion can be regarded as an alternative to oxy-fuel combustion while achieving the combustion product in the form of a CO_2/steam mixture. The fuel conversion is accomplished by virtue of two intermediary reactions; oxidation and reduction. Figure 1 depicts the principle of Chemical Looping Combustion.

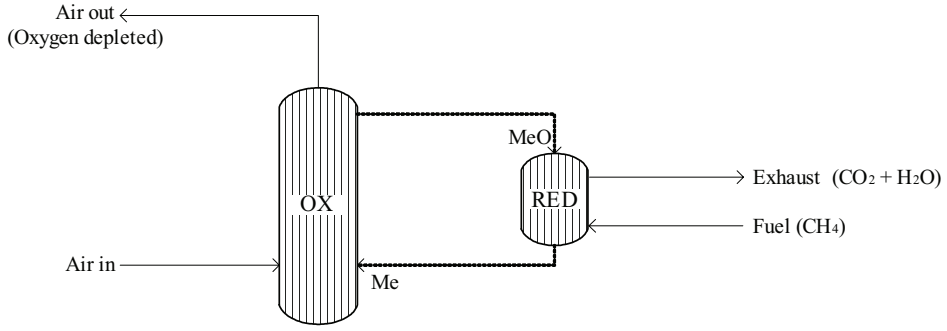

Figure 1 The Chemical Looping Combustion Principle

The oxygen needed by the fuel is supplied by employing a metal oxide (MeO) that extracts the oxygen in the air by getting oxidised in an oxidation reactor (OX). The metal oxide then flows to a reduction reactor (RED) where it reacts with the fuel. The fuel gives off its chemical energy to the metal oxide and takes up oxygen as a result of reduction reaction, thereby reducing the metal oxide to metal (Me). The reduced metal then circulates back to the oxidation reactor, transports the chemical energy in the fuel to air and gets regenerated to MeO. The oxidation of metal is exothermic and the oxygen depleted air is available at high temperature and can be utilised for power production. The hot CO_2-rich exhaust stream can also be utilised for power generation, either by expansion or steam generation. The CO_2-rich exhaust stream can afterwards be condensed to separate water and CO_2 is compressed. In this way the energy penalty for CO_2 separation and compression is lower than a conventional power plant where CO_2 is diluted with other

combustion products. There is only a low level of thermal NOx formation because of relatively lower temperatures and fuel NOx due to very low nitrogen content in case of natural gas. The metal oxide performance is vital to the process. The metal oxide should be mixed with an inert substance for providing adequate mechanical stability and improved chemical reactivity. Mattisson et al. [2001] investigated iron oxide as oxygen carrier for CLC-application. Mattisson et al. [2003] also investigated the oxides of Ni, Cu, Mn and Co. Although all these metal oxides are capable of being regenerated and transporting oxygen; however nickel oxide (NiO) exhibits the most promising properties [Lyngfelt, 2004] and the present work uses NiO supported on $NiAl_2O_4$.

Scope of this Work

This paper presents implementation of Chemical Looping Combustion (CLC) in combined cycles where the CLC-reactors replace the combustion chamber of gas turbine. A CLC-combined cycle is distinctive from a conventional gas turbine combined cycle in the way that the gas turbine cycle has two working fluids available at high temperature and pressure i.e. air and CO_2-rich exhaust. The oxygen depleted air coming out of the oxidation reactor is available at high temperature and pressure and can be used for power generation. The exhaust from the reduction reactor ideally contains a mixture of CO_2 and water vapour which is also available to be used for power generation. Different configurations of CLC-combined cycle have so far been proposed and the results in terms of efficiency have been quite promising. Naqvi et al. [2006] presented a natural gas fired CLC-combined cycle that employed an air turbine, a CO_2 turbine and a steam cycle, that can achieve net plant efficiency of above 51% with CO_2 capture and compression, at an oxidation temperature of 1200°C. As regards CLC, 1200°C is considered rather high temperature for the solid particles and the reactors. It is likely that solids will tend to sinter and agglomerate at temperatures higher than 1000°C depending on the type of material used. Therefore, it is of interest to investigate other power cycles with which a reasonable thermodynamic efficiency can be achieved at relatively lower oxidation temperatures. A cycle can ideally achieve efficiency close to the Carnot efficiency if an infinite number of heat additions to the cycle are made at a constant temperature. This results in a continuously decreasing pressure through successive expansion and heat addition. This principle can be realised by introducing reheat into a gas turbine. This approach has been adopted for the current work by employing multi-CLC-reactors in a combined cycle. If reheat is introduced to the air turbine of a CLC combined cycle at a relatively low oxidation temperature, it can result in a reasonably high efficiency compared to that at a higher oxidation temperature without any reheat.

Modelling and Simulation Background

The heat and mass balance presented by Naqvi et al. [2004] is the basis for this work. The gas turbine cycle has been simulated using the tool gPROMS [PSE, Inc.]. The SRK equation of state has been used for the physical properties calculation of gases. The steam cycle has been simulated in GTPRO [Thermoflow, Inc.]. According to Lyngfelt [2004], the theoretical thermodynamic limit of NiO to convert fuel is 99.5% but100% fuel conversion was assumed for the present work. The same cooling model is applied to the air turbine as in the work by Naqvi et al. [2006], while the CO_2-turbine is assumed uncooled. When reheat is introduced to a CLC combined cycle, the air turbine consists of more than one section. This work treats the air turbine in such a way that the pressure ratio of the air turbine sections may differ from each other. Hence, the term split ratio has been defined to determine the pressure ratio of each turbine section. Equation 1 gives split ratio for the single reheat air turbine.

$$PR_i = PR^{\lambda} \qquad (1)$$

In Equation 1, PR is the overall pressure ratio of the air turbine and the exponent λ is the split ratio that is between 0 and 1. The subscript i corresponds to the turbine section i.e. i=1 for the first air turbine section. In case of the double reheat cycle, the air turbine consists of three sections. Therefore the air turbine split ratios λ_1 and λ_2 have been defined. Treating the first two air turbines in the same way as in the single reheat cycle where PR_1 is the pressure ratio of first air turbine, and PR is the total pressure

ratio across the first two air turbine sections, the first split ratio (λ_1) is defined by Equation 2.

$$PR_1 = PR^{\lambda_1} \tag{2}$$

Equation 3 gives λ_2, which is the split ratio between the first two and the last sections of the air turbine.

$$PR_1 * PR_2 = (PR)^{\lambda_2} \tag{3}$$

In Equations 2 and 3, PR_1 and PR_2 are the pressure ratios of the first air turbine and the second air turbine, respectively; while PR is the overall pressure ratio of the air turbine.

The definition of net plant efficiency used in this work is given by Equation 4.

$$\eta_{\text{Net Plant}} = \frac{\left(W_{\text{air turbine}} + W_{CO_2-\text{turbine}} + W_{\text{steam turbine}} - W_{\text{compressor}}\right)\eta_m \eta_g \eta_{\text{aux}} - W_{CO_2-\text{compression}}}{\dot{m}_{\text{fuel}} \cdot \text{LHV}} \tag{4}$$

In Equation 4, W is the work, η is efficiency, $\dot{m}_{\text{fuel}}$ is the fuel flow rate and LHV is the lower heating value of fuel. The assumptions used in this work are in accordance with the work by Naqvi et al. [2006].

CLC Implementation in Combined Cycles

In this work, CLC has been implemented in three combined cycle configurations; the base-case cycle with and no reheat, the single and the double reheat combined cycle, described in the following.

Figure 2 presents the schematics of the base-case combined cycle with no reheat (CLCCC).

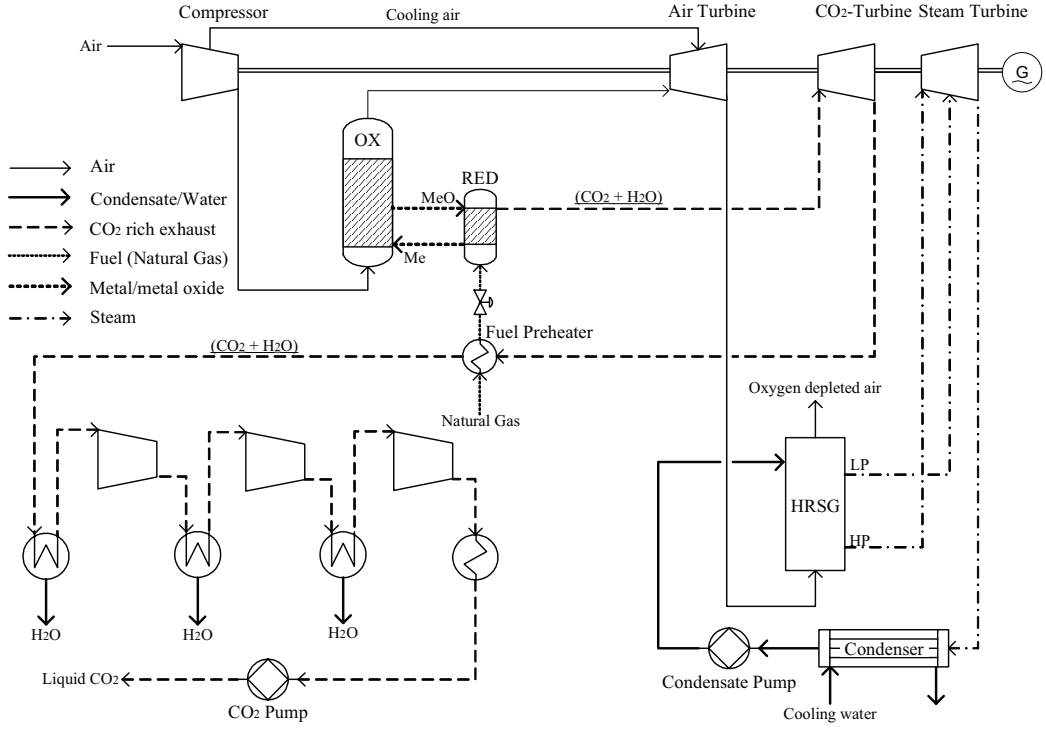

Figure 2 The base-case CLC-Combined Cycle (CLCCC)

The fuel is assumed to be pressurised, therefore no fuel compressor is included. Air at the compressor exit enters the CLC-oxidation reactor (Ox) where it reacts with the reduced metal, while fuel reacts with the metal oxide in the reduction reactor (Red) at the same time, in a continuous operation. Hot and pressurised oxygen-depleted air flowing out of the oxidation reactor enters the air turbine where it mixes with the coolant bleed drawn from the compressor. The air turbine exhaust generates steam at two pressure levels. The total steam then expands down to the condenser pressure. In the reduction reactor (Red), the reaction of fuel with metal oxide results in an exhaust comprising CO_2 and steam at the reduction reactor temperature and pressure. The exhaust after expanding in the CO_2-turbine preheats

the fuel in the fuel preheater and then goes to the CO_2 dehydration and recompression plant.

Figure 3 presents the flow sheet of the CLC-combined cycle with single reheat air turbine and 2-pressure-level CO_2-turbine. The two CLC-reactors can be designated according to the pressure as high pressure (HP-CLC-Reactors) and low pressure (LP-CLC-Reactors) with the same oxidation temperature. AT1 and AT2 are the high pressure and low pressure air turbines.

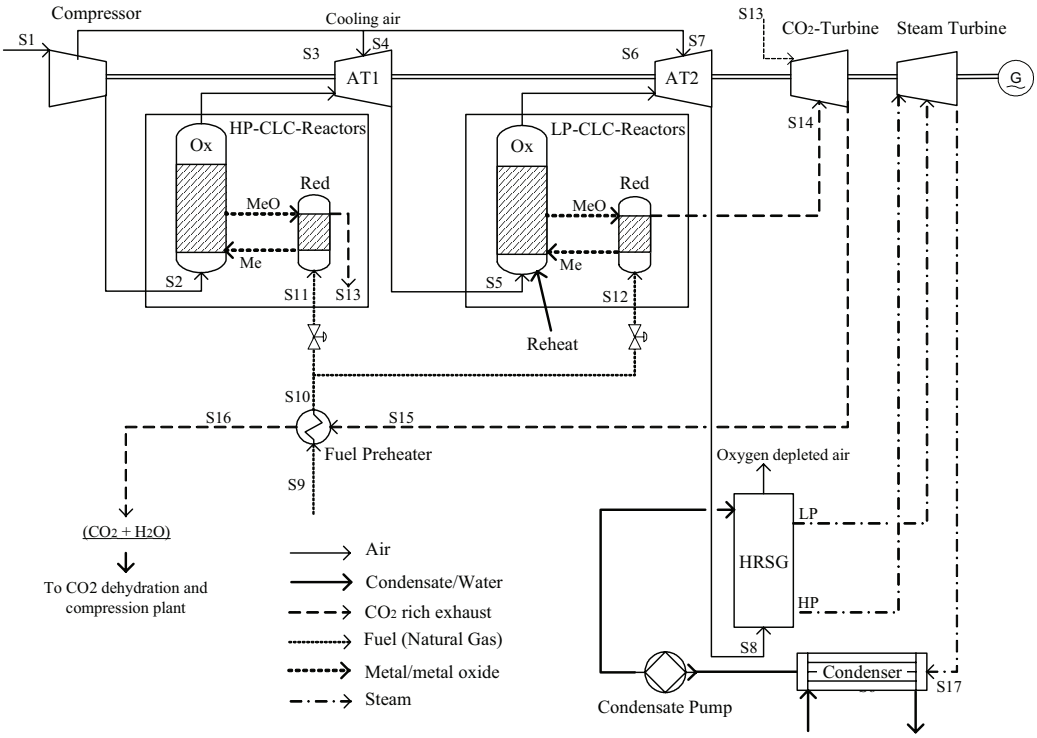

Figure 3 Single Reheat CLC-Combined Cycle (SR-CLCCC)

Air from compressor exit enters the air reactor (Ox) of the HP-CLC-Reactors. The hot pressurised oxygen depleted air at the oxidation reactor exit enters the high pressure air turbine (AT1). Air expands in AT1 down to the reheat pressure and enters the oxidation reactor (Ox) of the LP-CLC-Reactors. Reheat occurs in the low pressure oxidation reactor with more oxygen consumption and the air at the outlet of the oxidation reactor (Ox) of LP-CLC-Reactors enters the low pressure air turbine (AT2). AT2 passes through the heat recovery steam generator to raise steam at 2-pressure-levels that expands in the steam turbine. Exhaust from both reduction reactors (Red) comprises of CO_2 and steam. Exhaust from the first reduction reactor is admitted to the CO_2 turbine and expands to the pressure corresponding to the pressure of the exhaust stream from the LP-CLC-reactors. The resulting exhaust then expands down to the atmospheric pressure (considering pressure drop in the fuel preheater). The CO_2 turbine exhaust is used in the fuel preheater to preheat the fuel to a split into two streams. As the fuel inlet pressure in both reduction reactors differs, the pressure control valves are used to reduce the fuel pressure accordingly. The CO_2 rich exhaust then goes to the CO_2 dehydration and recompression plant, which is the same as in the base-case CLC combined cycle.

Figure 4 presents the flow sheet of a CLC-combined cycle with double reheat air turbine and 3-pressure-level CO_2-turbine. The cycle is an extension of the single reheat cycle with 3-CLC-reactors designated according to the pressure level i.e., high pressure (HP-CLC-Reactors), intermediate pressure (IP-CLC-Reactors) and low pressure (LP-CLC-Reactors) reactors with the same oxidation temperature. AT1, AT2 and AT3 are the high pressure, intermediate pressure and low pressure air turbine sections. The first and second reheat occur in the oxidation reactor (Ox) of IP-CLC-Reactors and LP-CLC-Reactors, respectively. The oxygen-depleted air at AT3 exit generates steam for the steam cycle.

Exhaust from the high pressure reduction reactor is admitted to the CO_2-turbine and it expands to the pressure corresponding to the pressure of the exhaust stream from the intermediate pressure reduction reactor. The mixed exhaust then expands down to the pressure corresponding to the pressure of the exhaust stream from the low pressure reduction reactor, which is further expanded and thereafter preheating fuel in the fuel preheater, goes to the CO_2 dehydration and compression plant, which is the same as in the base-case cycle and the single reheat cycle.

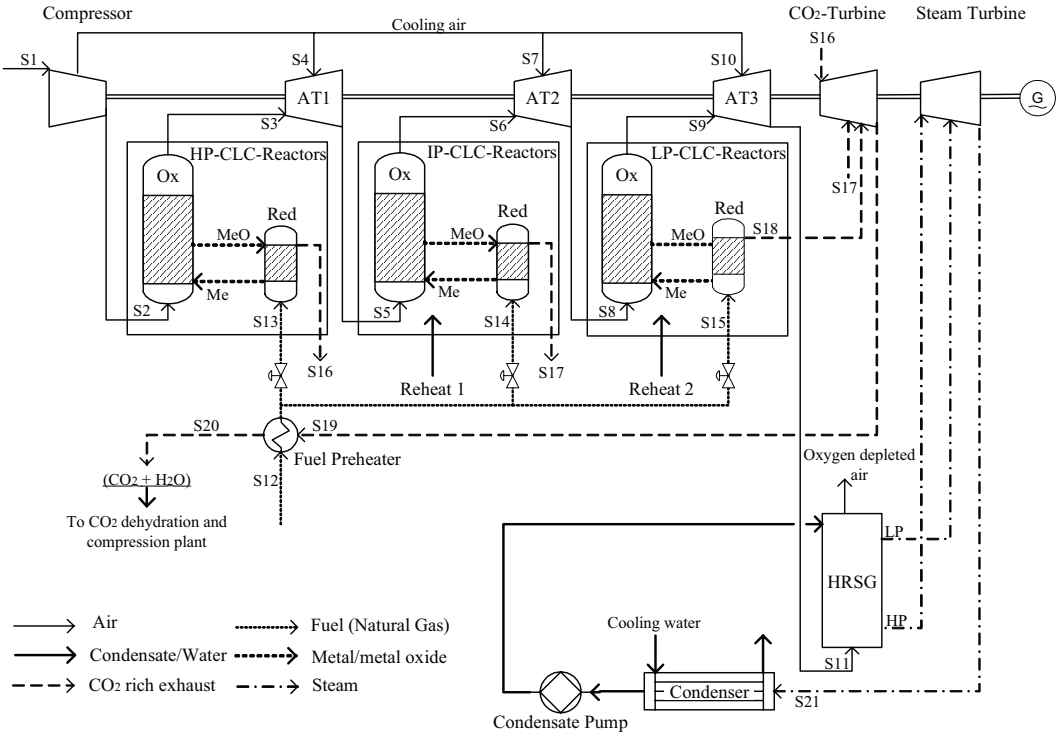

Figure 4 Double Reheat CLC-Combined Cycle (DR-CLCCC)

Methodology and Results

Sensitivity study of all the CLC-combined cycles is carried out by varying turbine inlet temperature and compressor pressure ratio. Nevertheless, in case of the reheat cycles, determination of the optimum pressure ratios of the air turbine sections is desired and hence the optimisation is carried out. Gross plant work is the objective function in both the reheat cycles under study. There is one variable i.e. the one air turbine split ratio in the SR-CLCCC, while two variables (the two split ratios) in case of DR-CLCCC. For the sake of comparison with a conventional combined cycle, a generic natural gas-fired gas turbine combined cycle model is also implemented in gPROMS. The combined cycle is based on compressor pressure ratio 17 and combustion chamber exit temperature 1425°C and a 3-pressure-level (125/30/4.5 bar), single reheat (560°C/560°C) steam turbine. The plant can achieve a net plant efficiency of 56.6% without CO_2 Capture. The post-combustion CO_2 capture with amine absorption is applied to the cycle. The assumptions for the post combustion CO_2 capture plant are on the basis of the work presented by Undrum and Bolland [2002]. At 90% CO_2 capture and the CO_2 end pressure of 110 bar the net plant efficiency drops from 56.6% to 48.6%. The results are summarised in the form of Figure 5, which presents the net plant efficiency as a function of turbine inlet temperature (TIT). Each efficiency point at a certain TIT value on Figure 5 represents the optimum condition of the air compressor pressure ratio (CPR). Apart from CPR, in case of reheat cycles, each point represents the optimum split ratios as well. The term TIT refers to the oxidation temperature in case of the CLC cycles. The single reheat cycle results in substantial efficiency improvement over the non-reheat cycle and net plant efficiency of above 51% can be achieved at oxidation temperature of 1000°C. The double reheat cycle exhibits only marginal efficiency improvement compared to the single reheat cycle, at the

expense of an extra reactor system and air turbine. All the CLC-combined cycles show promising net plant efficiency with CO_2 capture compared to a conventional combined cycle with post-combustion CO_2 capture that is 48.6% at 90% CO_2 capture.

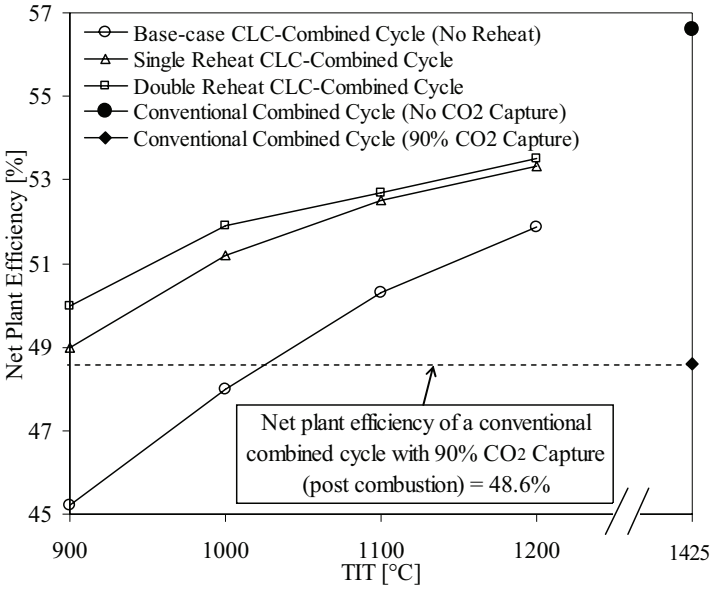

Figure 5 Comparison of the studied cycles [TIT refers to oxidation temperature in CLC cycles]

Conclusions

A CLC-combined cycle with no reheat can achieve about 52% net plant efficiency at oxidation temperature of 1200°C. Introducing single reheat to the air turbine of the CLC-combined cycle results in net plant efficiency of above 51% at oxidation temperature of 1000°C. The double reheat CLC combined cycle however, does not exhibit substantial efficiency improvement compared to the single reheat cycle. All the three CLC-combined cycles analysed in this work show high potential of efficient power generation with CO_2 capture compared to a conventional combined cycle with post-combustion CO_2 capture. However, single reheat CLC combined cycle is more interesting as it has attractive net plant efficiency at safer oxidation temperature and less number of reactors compared to double reheat.

References

[1] Richter, H. J., Knoche, K., **1983**, *Reversibility of combustion processes, Efficiency and Costing. Second Law Analysis of Processes,* ACS symposium Series 235, Washington D.C., p. 71-85

[2] Mattisson, T., Lyngfelt, A., Cho, P., **2001,** *The use of iron oxide as an oxygen carrier in chemical-looping combustion of methane with inherent separation of CO_2*, Fuel, vol. 80, p.1953-1962

[3] Mattisson, T., Järdnäs, A. and Lyngfelt, A., **2003,** *Reactivity of Some Metal Oxides Supported on Alumina with Alternating Methane and Oxygen-Application for Chemical-Looping Combustion,* Energy and Fuels, vol. 17, p. 643-651

[4] Lyngfelt A., Kronberger B., Adánez J., Morin J.-X., Hurst P., **2004**, *The Grace Project. Development of oxygen carrier particles for Chemical-Looping Combustion. Design and operation of a 10 kW Chemical-Looping Combustor,* GHG7, Vancouver, Canada, 5-9 September

[5] Naqvi, R., Bolland, O., Wolf, J., **2006**, *Part-load Analysis of a Chemical Looping Combustion (CLC) Combined Cycle with CO_2 Capture.* In press, Energy-The International Journal

[6] Naqvi et al., **2004**, *Chemical Looping Combustion-Analysis of Natural gas Fired Power Cycles with CO_2 Capture, paper no. GT2004-53359,* ASME Turbo-Expo 2004, Vienna, Austria

[7] gPROMS® ModelBuilder 2.3.3, Copyright © **1997-2004**, Process Systems Enterprise Limited

[8] GT PRO, Version 11.0.2, Copyright © **1987-2004**, Thermoflow, Inc.

[9] Undrum, H. and Bolland, O., **2003**, *A novel methodology for comparing CO_2 capture options for natural gas-fired combined cycle plants,* Advances in Environmental Research, vol. 7, p. 901-911